Cell signaling and cytoskeletal regulation in neutrophil cell migration *in vivo*

By

Pui Ying Lam

A dissertation submitted in partial fulfillment of

the requirements for the degree of

Doctor of Philosophy

(Cellular and Molecular Biology)

at the

UNIVERSITY OF WISCONSIN-MADISON

2014

Date of final oral examination: 8/21/2014

The dissertation is approved by the following members of the Final Oral Committee:

William M. Bement, Professor, Zoology

Yevgenya Grinblat, Associate Professor, Zoology

Mary Halloran, Professor, Zoology

Anna Huttenlocher, Professor, Pediatrics

David A. Wassarman, Professor, Cell and Regenerative Biology

Table of contents

Abstract

Neutrophils are the most abundant white blood cells and their recruitment to sites of injury or infection is essential for host defense. Abnormal infiltration of neutrophils is the hallmark of inflammatory disease. The activation and regulation of neutrophil chemotaxis must be precise in order to prevent abnormal situations leading to disease states. In this dissertation, I use zebrafish as an *in vivo* model to delineate the cell signaling and cytoskeletal regulation of neutrophil interstitial migration and innate immune response. In particular, I elucidate two negative regulators of neutrophil motility, the SH2-domain-containing inositol 5-phosphatase (SHIP) and microtubules. Phosphoinositide 3-kinase (PI3K), which generates the phosphatidylinositol (3,4,5)-trisphosphate [PI(3,4,5)P(3)], is necessary for neutrophil motility *in vivo*; however, the role of SHIP enzymes, which hydrolyze PI(3,4,5)P(3) to phosphatidylinositol 3,4-bisphosphate [PI(3,4)P(2)], is not well understood. In Chapter 2, I demonstrate that SHIPs control neutrophil inflammation and limit neutrophil motility by modulating PI3K signaling. The role of microtubules in regulating leukocyte migration is also not clear. In Chapter 3, I illustrate that microtubule depolymerization inhibits polarized PI3K activation at the leading edge of neutrophils, inducing PI3K independent motility but negatively impacting neutrophil directional migration. Our data also suggest that microtubules exert their effects on neutrophil polarity and motility at least in part by the negative regulation of both Rho and Rac activities. Next, in Chapter 4, I demonstrate that the routine heat shock method used for inducible gene expression in animal models with common heat shock promoters can alter neutrophil function in zebrafish. My findings suggest that caution must be taken when employing a heat shock-dependent inducible system to study the innate immune response and that data arising from such

experiments need to be carefully scrutinized. Together, my thesis research provides a better understanding of the signaling mechanisms involved in regulating neutrophil migration and function *in vivo*.

Acknowledgements

What an exciting journey towards my PhD degree! This is the perfect time for me to thank everyone that I have crossed paths with. You all have helped shape this very important milestone in my life. Being the first of my family to graduate college with a Bachelor's degree, a PhD degree seems so far-reaching. It is the inspiration, encouragement, opportunities and guidance I have received from all of you, as well as your belief in me, that has made this possible. From Dr. Andrew Miller and Dr. Sarah Ho at the Hong Kong University of Science and Technology for accepting me as an MPhil student, to Dr. Iain Drummond at the Massachusetts General Hospital for hiring me as a specialist in his lab, and to Dr. Anna Huttenlocher here at the University of Wisconsin-Madison for taking me on as a PhD student; I find myself getting closer to my once distant and far-reaching goal of obtaining a PhD degree. Perhaps more importantly, I have found my self-confidence and direction in life.

There are so many people in all of these places to thank. Expressing emotion and gratitude is not my strong suit. If you know me, I want to let you know that you are appreciated. I thank Anna in particular for her mentorship during this PhD process. Her vision in the grand scheme of things, timely support and openness to consider new ideas are not only admirable, but so highly cherished. My entire thesis committee: Dr. William Bement, Dr. Yevgenya Grinblat. Dr. Mary Halloran and Dr. David Wassarman have been a great resource in providing a different perspective, new ideas and constructive criticism throughout the course of my research. Thank you for your effort in helping me grow as a scientist.

I will also need to thank the past and current members in Anna's lab. You have made it so much fun and enjoyable around the lab. My office buddies Beth, Lindsy and Katie have proven to be a great support system. The lab management and technical support provided by Julie and David has been fantastic, facilitating the productivity we all enjoy. I must also thank all the undergrads over the years that supported and contributed to everyone's projects and were a tremendous resource for all of us. The Huttenlocher lab is truly awesome!

Last but not least, a special thank you to my family in Hong Kong for their support, even though they may not fully understand what my research is about. To my soul mate Steve, to whom I am so grateful for his love, patience and encouragement through this journey even before it began. Life is truly a journey and you all helped in making this part of it a great one.

Chapter 1

Introduction

Part of this Chapter is modified from the following published review article:

Lam P.Y. and Huttenlocher A. (2013) Interstitial leukocyte migration *in vivo*. *Current Opinion in Cell Biology*, Oct;25(5):650-8.

Inflammation

Inflammation is characterized by the infiltration of leukocytes into tissues. This process is characterized by leukocyte chemotaxis toward inflammatory mediators. Aberrant neutrophil inflammation plays a central role in the pathogenesis of many diseases, including cardiovascular disease, autoinflammatory disease and cancer (Hull et al., 2003; Huttenlocher et al., 1995; Lokuta et al., 2005). Identification of mechanisms regulating neutrophil motility and directional migration may be valuable in providing insight into potential therapeutic targets to control neutrophil-mediated tissue damage and chronic inflammation.

Leukocyte interstitial migration

The trafficking of leukocytes into peripheral tissues and lymphoid organs is critical for both innate and adaptive immune function and has been extensively reviewed (Notarangelo and Badolato, 2009; Rot and von Andrian, 2004; Stein and Nombela-Arrieta, 2005). A key step in this process is the interstitial motility of leukocytes within three-dimensional (3D) spaces, which can be either random or directed. Interstitial motility involves cycles of motility and arrest that are orchestrated by a complex hierarchy of external cues that are translated into changes in intracellular signaling. This function is evolutionarily conserved as demonstrated by the chemotactic interstitial migration of *Drosophila* hemocytes (immunosurveillance cells) to sites of tissue damage and infection (reviewed in (Fauvarque and Williams, 2011)).

Efficient leukocyte migration through interstitial tissues is a key component of the normal function of the immune system. The patrolling function of leukocytes requires cells to maneuver rapidly through complex matrix environments at speeds of up to 20-30 μm per minute. The rapid single-cell migration of leukocytes is classically known as 'amoeboid' migration. The type of protrusions formed by different leukocytes can be quite distinct, as demonstrated by neutrophils and macrophages migrating *in vivo* (Fig. 1A and B). Neutrophils project small pseudopodia that often bifurcate, while macrophages frequently extend long, thin filopodia-like protrusions in many directions as they maneuver through the interstitium toward damaged tissues within zebrafish embryos (Fig. 1C, D and E). The mechanisms that regulate the generation and maintenance of amoeboid pseudopodia and biased selection are under intense investigation both *in vitro* and *in vivo* (reviewed in (Insall, 2010; Van Haastert, 2010)).

Leukocyte amoeboid motility, in general, occurs in the absence of strong adhesive interactions with surrounding cells or tissues (reviewed in (Schmidt and Friedl, 2010)), although leukocyte arrest often requires integrin-mediated adhesion, in particular during transendothelial migration (reviewed in (Vestweber, 2012)). Integrin-mediated adhesion is essential for migration on two-dimensional surfaces. However, integrins can be dispensable for leukocyte migration in interstitial tissues (Lammermann et al., 2008) or in 3D collagen lattices (Friedl et al., 1998). The idea that movement within confined spaces can be integrin-independent was paradigm shifting and highlights the key role for adhesion in limiting leukocyte migration speed and mediating leukocyte arrest rather than an essential role in motility under many *in vivo* conditions.

Cell signaling underlying leukocyte motility

Interstitial environments contain both soluble and tissue-bound cues that help guide leukocytes to migrate or mediate cell arrest. Chemoattractants transmit signals through heterotrimeric G-protein-coupled receptors (GPCRs) (Janetopoulos et al., 2001), which activate a plethora of effectors (Bhattacharya et al., 2004; Kimmel and Parent, 2003). One of the key effectors is the class Ib phosphatydylinositol-3-kinase (PI(3)K). Although the role of PI(3)K during *in vitro* chemotaxis is controversial, PI(3)Kγ is required for cell polarity and motility *in vivo* (Hirsch et al., 2000; Sasaki et al., 2000; Yoo et al., 2010). PI(3)K promotes Rac-mediated actin polymerization at the leading edge and generates F-actin anteroposterior polarity (dynamic F-actin at the leading edge and stable F-actin at the rear). Inhibition of PI(3)K results in impaired F-actin polarity and neutrophil recruitment to both wounds and infection in zebrafish (Deng et al., 2012; Yoo et al., 2010). The importance of PI(3)K signaling is further illustrated by studies showing that the modulation of PI(3)K signaling can result in an inflammation phenotype. The PI(3)K products PI(3,4,5)P3-PI(3,4)P2 are localized to the leading edge of zebrafish neutrophils *in vivo* (Lam et al., 2012; Yoo et al., 2010) and PI(3,4,5)P3 can be hydrolyzed to PI(3,4)P2 by SH2-domain-containing inositol 5-phosphatases (SHIP). SHIP knockout mice show increased myeloid infiltration into vital organs (Helgason et al., 1998; Liu et al., 1999) and *in vitro* study suggest that SHIP regulates macrophage chemotaxis by hydrolysis of PI(3,4,5)P3 (Vedham et al., 2005). In Chapter 2, I further demonstrate that SHIP limits neutrophil motility through the modulation of PI(3)K signaling *in vivo* in zebrafish.

The role of microtubules in interstitial motility

Microtubules suppress the polarity and motility of many leukocytes *in vitro* (Niggli, 2003; Xu et al., 2005) and *in vivo* (Redd et al., 2006; Yoo et al., 2012). In macrophages, microtubule depolymerization does not affect migration speed in zebrafish, although directional migration is impaired (Redd et al., 2006). It is known that microtubules regulate Rho GTPase activity. Microtubule depolymerization can activate RhoA *in vitro,* in part through the release of microtubule associated Rho GEF (Chang et al., 2008; Krendel et al., 2002; Niggli, 2003). Both microtubule polymerization and depolymerization activate Rac *in vitro* (Waterman-Storer et al., 1999; Yoo et al., 2012). In Chapter 4, I show that depolymerization of microtubules using nocodazole enhances neutrophil polarity and motility but impairs directional migration in zebrafish. In addition, microtubule depolymerization inhibits PI(3)K activation at the leading edge of neutrophils in zebrafish. *In vitro* data suggest that the dysregulation of Rho and Rac activity upon microtubule depolymerization contributes to impaired directional motility. These observations highlight the essential role for microtubules in leukocyte directional motility *in vivo*.

Heat shock and neutrophil functions

Heat shock is a routine method used for inducible gene expression in animal models facilitated by the use of various the heat shock promoters (Halloran et al., 2000; Shoji and Sato-Maeda, 2008). However, elevated temperature increases the expression of heat shock proteins (HSPs), which play important roles in innate and adaptive

immunity (reviewed in (Colaco et al., 2013; Tsan and Gao, 2004; Tsan and Gao, 2009; Wallin et al., 2002)). Heat stress can also induce the unfolded protein response (UPR) and immune systems rely on intact UPR functions (reviewed in (Costa et al., 2011; Todd et al., 2008)). In Chapter 4, I show that this short-term heat shock method can alter neutrophil function and behavior in zebrafish. This includes an increase in neutrophil speed and number of circulating neutrophils, as well as a decrease in neutrophil recruitment to sites of wounding and infection. These findings suggest that caution should be taken when employing a heat shock-dependent inducible system to study the innate immune response and that interpreting data may be confounded by endogenous, unrelated responses to the heat stimulus.

Zebrafish as an animal model

The zebrafish, *Danio rerio*, has emerged as a powerful vertebrate model to study hematopoiesis and immunity (Kanther and Rawls, 2010). The optical transparency of zebrafish embryos allows for high-resolution live imaging at the subcellular and single cell level that is further enhanced by the generation of increasing numbers of transgenic lines. The immune systems of zebrafish and mammals are highly conserved: zebrafish develop immune cells including lymphocytes, mast cells, macrophages and neutrophils [reviewed in (de Jong and Zon, 2005; Renshaw and Trede, 2012; Trede et al., 2004)].

Introduction to the dissertation

My dissertation research has provided new insights into the regulation of neutrophil migration *in vivo*. In **Chapter 2**, my data demonstrate that the SH2-domain-containing inositol 5-phosphatase (SHIP) is a negative regulator of neutrophil motility and recruitment to wounds in zebrafish larvae. In **Chapter 3**, I show the important role of microtubules (MTs) in neutrophil polarity and migration *in vivo*. Further characterization of MT regulation of neutrophil directional migration is included in **Appendix I**. In **Chapter 4**, I demonstrate the effect of heat shock on neutrophil function. Further details concerning the current understanding of leukocyte interstitial migration through the use of *in vivo* models is contained within my co-authored publication in **Appendix II**.

High resolution *in vivo* live imaging of neutrophil undergoing interstitial migration has presented as its own challenge. The details of spinning disk microscopy setup used for neutrophil live imaging *in vivo* is included in **Appendix III**.

My interest in cell migration and cytoskeleton has also fostered another project focusing on the signaling regulation of actin rich microridges on the surface of epithelial cells. Microridges are labyrinth like actin structures found in mucosal epithelium across many animal species. My work has provided detail analysis of the formation and maintenance of microridges *in vivo*. This can be found in **Appendix IV**.

Reference

Bhattacharya, M., A.V. Babwah, and S.S. Ferguson. 2004. Small GTP-binding protein-coupled receptors. *Biochem Soc Trans*. 32:1040-4.

Chang, Y.C., P. Nalbant, J. Birkenfeld, Z.F. Chang, and G.M. Bokoch. 2008. GEF-H1 couples nocodazole-induced microtubule disassembly to cell contractility via RhoA. *Mol Biol Cell*. 19:2147-53.

Colaco, C.A., C.R. Bailey, K.B. Walker, and J. Keeble. 2013. Heat shock proteins: stimulators of innate and acquired immunity. *Biomed Res Int*. 2013:461230.

Costa, C.Z., S.E. da Rosa, and M.M. de Camargo. 2011. The unfolded protein response: how protein folding became a restrictive aspect for innate immunity and B lymphocytes. *Scand J Immunol*. 73:436-48.

de Jong, J.L., and L.I. Zon. 2005. Use of the zebrafish system to study primitive and definitive hematopoiesis. *Annu Rev Genet*. 39:481-501.

Deng, Q., E.A. Harvie, and A. Huttenlocher. 2012. Distinct signalling mechanisms mediate neutrophil attraction to bacterial infection and tissue injury. *Cell Microbiol*. 14:517-28.

Fauvarque, M.O., and M.J. Williams. 2011. Drosophila cellular immunity: a story of migration and adhesion. *J Cell Sci*. 124:1373-82.

Friedl, P., F. Entschladen, C. Conrad, B. Niggemann, and K.S. Zanker. 1998. CD4+ T lymphocytes migrating in three-dimensional collagen lattices lack focal adhesions and utilize beta1 integrin-independent strategies for polarization, interaction with collagen fibers and locomotion. *Eur J Immunol*. 28:2331-43.

Halloran, M.C., M. Sato-Maeda, J.T. Warren, F. Su, Z. Lele, P.H. Krone, J.Y. Kuwada, and W. Shoji. 2000. Laser-induced gene expression in specific cells of transgenic zebrafish. *Development*. 127:1953-60.

Helgason, C.D., J.E. Damen, P. Rosten, R. Grewal, P. Sorensen, S.M. Chappel, A. Borowski, F. Jirik, G. Krystal, and R.K. Humphries. 1998. Targeted disruption of SHIP leads to hemopoietic perturbations, lung pathology, and a shortened life span. *Genes Dev*. 12:1610-20.

Hirsch, E., V.L. Katanaev, C. Garlanda, O. Azzolino, L. Pirola, L. Silengo, S. Sozzani, A. Mantovani, F. Altruda, and M.P. Wymann. 2000. Central role for G protein-coupled phosphoinositide 3-kinase gamma in inflammation. *Science*. 287:1049-53.

Hull, K.M., N. Shoham, J.J. Chae, I. Aksentijevich, and D.L. Kastner. 2003. The expanding spectrum of systemic autoinflammatory disorders and their rheumatic manifestations. *Curr Opin Rheumatol*. 15:61-9.

Huttenlocher, A., I.J. Frieden, and H. Emery. 1995. Neonatal onset multisystem inflammatory disease. *J Rheumatol*. 22:1171-3.

Insall, R.H. 2010. Understanding eukaryotic chemotaxis: a pseudopod-centred view. *Nat Rev Mol Cell Biol*. 11:453-8.

Janetopoulos, C., T. Jin, and P. Devreotes. 2001. Receptor-mediated activation of heterotrimeric G-proteins in living cells. *Science*. 291:2408-11.

Kanther, M., and J.F. Rawls. 2010. Host-microbe interactions in the developing zebrafish. *Curr Opin Immunol*. 22:10-9.

Kimmel, A.R., and C.A. Parent. 2003. The signal to move: D. discoideum go orienteering. *Science*. 300:1525-7.

Krendel, M., F.T. Zenke, and G.M. Bokoch. 2002. Nucleotide exchange factor GEF-H1 mediates cross-talk between microtubules and the actin cytoskeleton. *Nat Cell Biol*. 4:294-301.

Lam, P.Y., S.K. Yoo, J.M. Green, and A. Huttenlocher. 2012. The SH2-domain-containing inositol 5-phosphatase (SHIP) limits the motility of neutrophils and their recruitment to wounds in zebrafish. *J Cell Sci*. 125:4973-8.

Lammermann, T., B.L. Bader, S.J. Monkley, T. Worbs, R. Wedlich-Soldner, K. Hirsch, M. Keller, R. Forster, D.R. Critchley, R. Fassler, and M. Sixt. 2008. Rapid leukocyte migration by integrin-independent flowing and squeezing. *Nature*. 453:51-5.

Liu, Q., T. Sasaki, I. Kozieradzki, A. Wakeham, A. Itie, D.J. Dumont, and J.M. Penninger. 1999. SHIP is a negative regulator of growth factor receptor-mediated PKB/Akt activation and myeloid cell survival. *Genes Dev*. 13:786-91.

Lokuta, M.A., K.M. Cooper, I. Aksentijevich, D.L. Kastner, and A. Huttenlocher. 2005. Neutrophil chemotaxis in a patient with neonatal-onset multisystem inflammatory disease and Muckle-Wells syndrome. *Ann Allergy Asthma Immunol*. 95:394-9.

Niggli, V. 2003. Microtubule-disruption-induced and chemotactic-peptide-induced migration of human neutrophils: implications for differential sets of signalling pathways. *J Cell Sci*. 116:813-22.

Notarangelo, L.D., and R. Badolato. 2009. Leukocyte trafficking in primary immunodeficiencies. *J Leukoc Biol*. 85:335-43.

Redd, M.J., G. Kelly, G. Dunn, M. Way, and P. Martin. 2006. Imaging macrophage chemotaxis in vivo: studies of microtubule function in zebrafish wound inflammation. *Cell Motil Cytoskeleton*. 63:415-22.

Renshaw, S.A., and N.S. Trede. 2012. A model 450 million years in the making: zebrafish and vertebrate immunity. *Dis Model Mech*. 5:38-47.

Rot, A., and U.H. von Andrian. 2004. Chemokines in innate and adaptive host defense: basic chemokinese grammar for immune cells. *Annu Rev Immunol*. 22:891-928.

Sasaki, T., J. Irie-Sasaki, R.G. Jones, A.J. Oliveira-dos-Santos, W.L. Stanford, B. Bolon, A. Wakeham, A. Itie, D. Bouchard, I. Kozieradzki, N. Joza, T.W. Mak, P.S. Ohashi, A. Suzuki, and J.M. Penninger. 2000. Function of PI3Kgamma in thymocyte development, T cell activation, and neutrophil migration. *Science*. 287:1040-6.

Schmidt, S., and P. Friedl. 2010. Interstitial cell migration: integrin-dependent and alternative adhesion mechanisms. *Cell Tissue Res*. 339:83-92.

Shoji, W., and M. Sato-Maeda. 2008. Application of heat shock promoter in transgenic zebrafish. *Dev Growth Differ*. 50:401-6.

Stein, J.V., and C. Nombela-Arrieta. 2005. Chemokine control of lymphocyte trafficking: a general overview. *Immunology*. 116:1-12.

Todd, D.J., A.H. Lee, and L.H. Glimcher. 2008. The endoplasmic reticulum stress response in immunity and autoimmunity. *Nat Rev Immunol*. 8:663-74.

Trede, N.S., D.M. Langenau, D. Traver, A.T. Look, and L.I. Zon. 2004. The use of zebrafish to understand immunity. *Immunity*. 20:367-79.

Tsan, M.F., and B. Gao. 2004. Heat shock protein and innate immunity. *Cell Mol Immunol*. 1:274-9.

Tsan, M.F., and B. Gao. 2009. Heat shock proteins and immune system. *J Leukoc Biol*. 85:905-10.

Van Haastert, P.J. 2010. Chemotaxis: insights from the extending pseudopod. *J Cell Sci*. 123:3031-7.

Vedham, V., H. Phee, and K.M. Coggeshall. 2005. Vav activation and function as a rac guanine nucleotide exchange factor in macrophage colony-stimulating factor-induced macrophage chemotaxis. *Mol Cell Biol*. 25:4211-20.

Vestweber, D. 2012. Novel insights into leukocyte extravasation. *Curr Opin Hematol*. 19:212-7.

Wallin, R.P., A. Lundqvist, S.H. More, A. von Bonin, R. Kiessling, and H.G. Ljunggren. 2002. Heat-shock proteins as activators of the innate immune system. *Trends Immunol*. 23:130-5.

Waterman-Storer, C.M., R.A. Worthylake, B.P. Liu, K. Burridge, and E.D. Salmon. 1999. Microtubule growth activates Rac1 to promote lamellipodial protrusion in fibroblasts. *Nat Cell Biol*. 1:45-50.

Xu, J., F. Wang, A. Van Keymeulen, M. Rentel, and H.R. Bourne. 2005. Neutrophil microtubules suppress polarity and enhance directional migration. *Proc Natl Acad Sci U S A*. 102:6884-9.

Yoo, S.K., Q. Deng, P.J. Cavnar, Y.I. Wu, K.M. Hahn, and A. Huttenlocher. 2010. Differential regulation of protrusion and polarity by PI3K during neutrophil motility in live zebrafish. *Dev Cell*. 18:226-36.

Yoo, S.K., P.Y. Lam, M.R. Eichelberg, L. Zasadil, W.M. Bement, and A. Huttenlocher. 2012. The role of microtubules in neutrophil polarity and migration in live zebrafish. *J Cell Sci*. 125:5702-10.

Fig. 1. Neutrophil and macrophage distribution, morphology and response to wounding in zebrafish embryo at 3 days post fertilization. (A) Neutrophils distribute mainly in the mesenchymal tissue in the head region (yellow box) and in the caudal hematopoietic tissue (white box). (Inset in A) A typical migrating neutrophil has multiple pseudopodia (arrow heads) and a uropod (arrow). Scale bar = 20 μm. (B) Macrophages distribute in the whole embryo with no clear tissue localization. (Inset in B) A typical migrating macrophage shows multiple spindly protrusions. Scale bar = 20 μm. (C) Time series image of neutrophils (red; lifeact-Ruby) and macrophages (green; dendra) migrate to tail fin wound. Neutrophils have arrived at the wound at 0.5 hours post wounding (hpw) and macrophages arrived at later time points. Scale bar = 50 μm. Time series image of a neutrophil (D) or a macrophage (E) migrating from left to right towards the wound. Scale bar = 20 μm.

Fig. 1

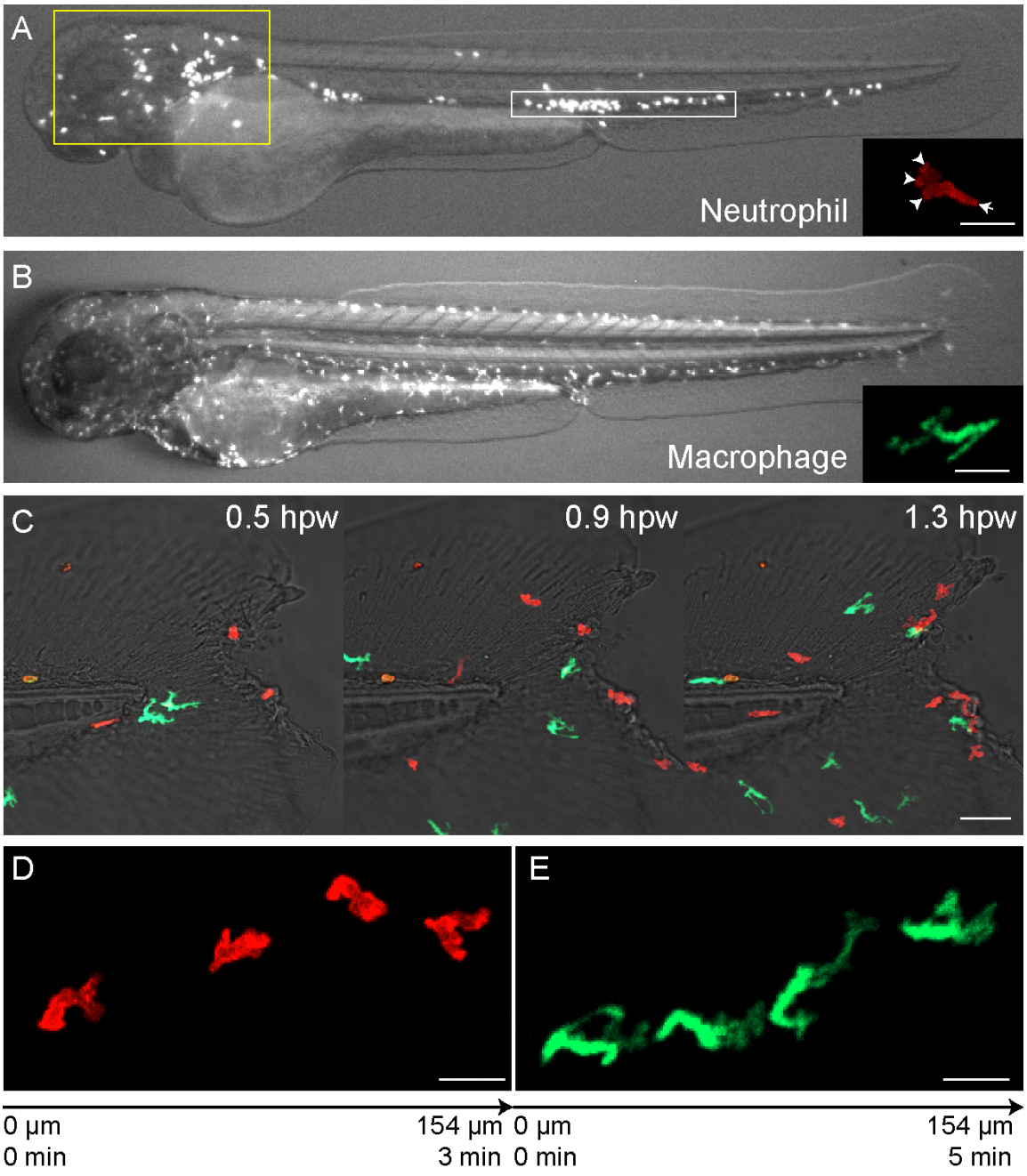
A
Neutrophil
B
Macrophage
C
0.5 hpw
0.9 hpw
1.3 hpw
D
E
0 μm
0 min
154 μm
3 min
0 μm
0 min
154 μm
5 min

Chapter 2

The SH2-domain-containing inositol 5-phosphatase (SHIP) limits the motility of neutrophils and their recruitment to wounds in zebrafish

This Chapter was published in the following journal article:

Lam P.Y., Yoo S.K., Green J.M., and Huttenlocher A. (2012) The SH2-domain-containing inositol 5-phosphatase (SHIP) limits the motility of neutrophils and their recruitment to wounds in zebrafish. *Journal of Cell Science*, Nov 1;125(Pt 21):4973-8

Summary

Neutrophil recruitment to sites of injury or infection is essential for host defense, but it needs to be tightly regulated to prevent tissue damage. Phosphoinositide 3-kinase (PI3K), which generates the phosphatidylinositol (3,4,5)-trisphosphate [$PI(3,4,5)P_3$], is necessary for neutrophil motility *in vivo*, however, the role of SH2-domain–containing 5-inositol phosphatase (SHIP) enzymes, which hydrolyze $PI(3,4,5)P_3$ to phosphatidylinositol 3,4-bisphosphate [$PI(3,4)P_2$], is not well understood. Here we show that SHIP phosphatases limit neutrophil motility in live zebrafish. Using real-time imaging of bioprobes specific for $PI(3,4,5)P_3$ and $PI(3,4)P_2$ in neutrophils, we found that $PI(3,4,5)P_3$ and $PI(3,4)P_2$ accumulate at the leading edge while $PI(3,4)P_2$ also localizes to the trailing edge of migrating neutrophils *in vivo*. Depletion of SHIP phosphatases using morpholino oligonucleotides led to increased neutrophil 3D motility and neutrophil infiltration into wounds. The increase in neutrophil wound recruitment in *SHIP* morphants was rescued by treatment with low dose PI3Kγ inhibitor, suggesting that SHIP limits neutrophil motility by modulating PI3K signaling. Moreover, overexpression of the SHIP phosphatase domain in neutrophils impaired neutrophil 3D migration. Taken together, our findings suggest that SHIP phosphatases control neutrophil inflammation by limiting neutrophil motility *in vivo*.

Introduction

Neutrophil infiltration into sites of infection or tissue injury is essential for host defense. On the other hand, tight control of neutrophil accumulation and activation is necessary to prevent tissue damage and chronic inflammation. Despite substantial progress in identifying mechanisms that initiate neutrophil wound attraction (Deng *et al.*, 2011a; McDonald *et al.*, 2010; Niethammer *et al.*, 2009; Yoo *et al.*, 2010; Yoo *et al.*, 2011), how neutrophil infiltration is regulated in live animals is not well defined.

It is well established that chemoattractant induced G protein-coupled receptor signaling induces phosphatidylinositol (3,4,5)-trisphosphate [$PI(3,4,5)P_3$]/ phosphatidylinositol 3,4-bisphosphate [$PI(3,4)P_2$] concentration at the leading edge during single cell chemotaxis *in vitro* (Parent, 2004; Servant *et al.*, 2000) and neutrophil motility *in vivo* (Yoo *et al.*, 2010). Leading edge activation of phosphoinositide 3-kinase (PI3K) results in the rapid accumulation of $PI(3,4,5)P_3$/$PI(3,4)P_2$, polarized F-actin polymerization and directed motility (Barberis and Hirsch, 2008; Hawkins and Stephens, 2007; Yoo *et al.*, 2010). The PI3K product $PI(3,4,5)P_3$ can be hydrolyzed to $PI(3,4)P_2$ by SH2-domain-containing inositol 5-phosphatase (SHIP) (Rohrschneider *et al.*, 2000). In support of an important role for SHIP in controlling inflammation, knockout mice show robust leukocyte infiltration into lungs (Helgason *et al.*, 1998). Moreover, bone marrow-derived mast cells from SHIP-deficient mice, show increased cytokine induced $PI(3,4,5)P_3$ levels and Akt activation (Liu *et al.*, 1999). By contrast, SHIP1-null neutrophils *in vitro* have impaired polarization and motility, suggesting that SHIP1 is necessary for neutrophil motility (Nishio *et al.*, 2007). These reports suggest opposite roles for SHIP in regulating neutrophil motility *in vitro* and inflammation *in vivo*,

indicating that further studies are needed to delineate the *in vivo* role of SHIP in regulating neutrophil motility.

The zebrafish, *Danio rerio*, has emerged as a powerful vertebrate model to study cell motility and immunity (Huttenlocher and Poznansky, 2008; Kanther and Rawls). The optical transparency of zebrafish embryos together with tissue specific promoter driven gene expression allow for high-resolution real time imaging at both the subcellular and single cell level in live animals. Here, we show that SHIP plays an important role in limiting leukocyte motility and infiltration in live zebrafish embryos. Depletion of SHIP 5'-phosphatases increased neutrophil wound attraction and random motility through a PI3K-dependent pathway. Moreover, ectopic expression of the SHIP1 phosphatase domain impaired neutrophil migration. Taken together, our findings suggest that SHIP phosphatases serve as a brake that limit neutrophil motility and inflammation, at least in part through their effects on PI3K signaling.

Results and Discussion

$PI(3,4,5)P_3$/$PI(3,4)P_2$ signaling in neutrophils *in vivo*

$PI(3,4,5)P_3$/$PI(3,4,)P_2$ localizes to the leading edge of neutrophils *in vitro* (Servant *et al.*, 2000). We have also demonstrated, using the PH domain of Akt/PKB (PH-Akt), that $PI(3,4,5)P_3$/$PI(3,4)P_2$ localizes to the leading edge and occasionally the tail of neutrophils migrating *in vivo* (Yoo *et al.*, 2010). The PH-Akt probe detects both $PI(3,4,5)P_3$ and $PI(3,4)P_2$ (Frech *et al.*, 1997; Gray *et al.*, 1999). To further define the endogenous dynamics and inter-conversion of these phosphoinositides *in vivo*, we used the *mpx* promoter to transiently express the $PI(3,4,5)P_3$-specific bioprobe GRP1-PH and the $PI(3,4)P_2$-specific bioprobe TAPP1-PH (Furutani *et al.*, 2006) in zebrafish neutrophils. Using ratiometric imaging of neutrophils randomly migrating in the head, we found that TAPP1-PH [detecting $PI(3,4)P_2$] concentrated both at the leading edge and the tail of motile neutrophils (Fig. 1A; supplementary material Movie 1). By contrast, GRP1-PH [detecting $PI(3,4,5)P_3$] accumulated only at the leading edge of neutrophils (Fig. 1B; supplementary material Movie 2). Accordingly, ratiometric imaging comparing the accumulation of the $PI(3,4,5)P_3$ to $PI(3,4)P_2$ probes revealed that more $PI(3,4,5)P_3$ than $PI(3,4)P_2$ accumulated at the neutrophil leading edge (Fig. 1C; supplementary material Movie 3). We have previously shown that by ratiometric imaging of the farnesylated membrane-bound probe EGFP-F, membrane signal periodically accumulated at the tail but not at the front of neutrophils (Yoo *et al.*, 2010). Therefore, the cell front signal observed is unlikely due to membrane accumulation. These findings indicate that there are local sub-cellular pools of phospholipids that can be distinguished temporally and spatially during neutrophil migration *in vivo*.

SHIP expression and localization in zebrafish leukocytes

The dynamic accumulation of $PI(3,4)P_2$ during neutrophil motility prompted us to investigate the function of SHIP phosphatases during neutrophil motility. In mammals, *SHIP1* expression is restricted to the hematopoietic lineage (Liu *et al.*, 1998) and *SHIP2* is expressed broadly (Muraille *et al.*, 1999). According to the PubMed database, zebrafish expresses one copy of SHIP1 (accession no. XP_001923007) that shares 61% identify with both human SHIP1a and SHIP1b (supplementary material Fig. S1). There are two SHIP2 paralogs in zebrafish, SHIP2a and SHIP2b. SHIP2a is most closely related to human SHIP2 (65% overall identity) and is broadly expressed in zebrafish (Jurynec and Grunwald, 2010). RT-PCR analysis using mRNA extracted from FACS-sorted leukocytes or whole zebrafish at 3 days post fertilization (dpf) using *Tg*(*mpx:dendra2*) (Mathias *et al.*, 2009; Yoo and Huttenlocher, 2011), demonstrated that zebrafish myeloid cells express *SHIP1* and *SHIP2a,* but not *SHIP2b* (Fig. 2A). Purity of the FACS-sorted myeloid cell population was confirmed by RT-PCR (Fig. 2B).

Previous studies have reported that SHIP1 and SHIP2 are localized at the leading edge in MDCK cells (Koch *et al.*, 2005). To determine where SHIP phosphatases localize in motile neutrophils, we transiently expressed human EGFP-SHIP1 in *Tg*(*mpx:mCherry*) zebrafish embryos (Yoo *et al.*, 2010), using the neutrophil specific lysozyme C (*lyz*) promoter (Kitaguchi *et al.*, 2009). Human SHIP1, like $PI(3,4)P_2$, localized both at the front and tail of motile neutrophils (Fig. 2C; supplementary material Movie 4). We further characterized the subcellular localization of zebrafish EGFP-SHIP1 and EGFP-SHIP2a in neutrophils *in vivo*. In accordance with our findings with human SHIP1, both zebrafish SHIP1 and SHIP2a transiently localize to

the cell front and at times can be seen in the tail of motile neutrophils *in vivo* (supplementary material Fig. S2; Movie 5). Neutrophil-specific protein expression using the *lyz* promoter was confirmed by crossing the transgenic line *Tg*(*lyz:TagRFP*), which we generated based on the published *lyz* promoter sequence (Kitaguchi *et al.*, 2009), with *Tg*(*mpx:dendra2*) (Yoo and Huttenlocher, 2011) (supplementary material Fig. S3).

SHIP phosphatases impair recruitment of neutrophils to wounds

To determine if SHIP phosphatases regulate neutrophil motility *in vivo*, we used SHIP-targeted splice donor blocking morpholinos (MOs) to deplete SHIP1 and SHIP2a. RT-PCR confirmed SHIP knockdown (Fig. 3A). We found that depletion of both SHIP1 and SHIP2a (Fig. 3B) but not single SHIP1/2a (data not shown) increased neutrophil wound recruitment at 0.5 and 1 hour post wound (hpw) in 2.5 dpf zebrafish. The effect of SHIP depletion was confirmed using a second set of morpholinos, which targeted *SHIP1* (*SHIP1* MO2) and *SHIP2a* (*SHIP2a* MO1) (Fig. 3C). It has been reported that there are increased total neutrophils in SHIP-deficient mice (Rauh *et al.*, 2004). By contrast, total neutrophil numbers were decreased in *SHIP* morphants (supplementary material Fig. S4**),** despite having more neutrophils infiltrate into wounds. Moreover, we also found that macrophage recruitment to wounds was increased in the *SHIP* morphants (supplementary material Fig. S5), suggesting that SHIP phosphatases limit both neutrophil and macrophage wound recruitment. After initial recruitment, neutrophils migrate repeatedly towards and away from the wound in a process called reverse migration (Mathias *et al.*, 2006; Yoo and Huttenlocher, 2011). *SHIP* morphants did not

show a significant difference in reverse migration or resolution of inflammation as compared to control (data not shown).

Previous studies have reported that depletion of SHIP1 increases $PI(3,4,5)P_3$ accumulation in leukocytes (Harris et al.; Nishio et al., 2007; Vedham et al., 2005). To test the possibility that SHIP phosphatases modulate neutrophil wound recruitment by affecting $PI(3,4,5)P_3$ levels, we inhibited $PI(3,4,5)P_3$ generation in *SHIP* morphants using low dose PI3Kγ inhibitor. It is known that PI3Kγ inhibition impairs $PI(3,4,5)P_3$/$PI(3,4)P_2$ generation and neutrophil motility *in vivo* (Yoo *et al.*, 2010). We found that treatment with low dose PI3Kγ inhibitor did not affect neutrophil wound recruitment in control zebrafish. However, low dose PI3Kγ inhibitor was sufficient to rescue neutrophil wound recruitment in *SHIP* morphants to control levels (Fig. 3D). These findings suggest that depletion of SHIP increases neutrophil recruitment through a PI3K-dependent pathway and generation of $PI(3,4,5)P_3$. However, we cannot rule out the possibility that the generation of $PI(3,4)P_2$ may also be important for SHIP effects on neutrophil wound attraction. Since PI(3)K activity and leading edge $PI(3,4,5)P_3$ is indispensable for neutrophil motility *in vivo* (Yoo *et al.*, 2010), it is interesting to speculate that SHIP hydrolyzes $PI(3,4,5)P_3$ into $PI(3,4)P_2$, particularly in the front of neutrophils, and thereby limits neutrophil motility.

SHIP phosphatases limit neutrophil motility *in vivo*

It is possible that neutrophil wound recruitment is enhanced in *SHIP* morphants due to increased neutrophil motility in *SHIP* morphants. To test this possibility, we

performed real time imaging of neutrophil random motility in the head region in control and *SHIP* morphants at 2.5 dpf. We found that there was increased neutrophil random motility in *SHIP* double morphants compared to control (Fig. 4A-C; supplementary material Movie 6).

To determine if the SHIP phosphatase activity is sufficient to alter neutrophil motility, we ectopically expressed a membrane-bound form of the human SHIP1 phosphatase domain (aa364-826) in zebrafish neutrophils (Freeburn *et al.*, 2002). Transient expression was achieved using the *lyz* promoter driving both the constitutively active SHIP1 phosphatase and EGFP expression with the viral 2A peptide system which allows multiple protein products to be expressed from a single transgene (Provost *et al.*, 2007). Transient expression of this construct in *Tg*(*mpx:mCherry*) embryos allowed for mosaic expression of the phosphatase domain labeled with EGFP and mCherry to be compared to control neutrophils that expressed mCherry alone. Live imaging of neutrophil random motility in the head of 3 dpf embryos showed that ectopic expression of the SHIP1 phosphatase domain impaired neutrophil random motility as compared to control neutrophils (Fig. 4D-E; supplementary material Movie 7). By contrast, ectopic expression of EGFP alone did not impair neutrophil motility (Fig. 4F). Further analysis demonstrated that there was no significant difference in the meandering index (displacement/track length) measured in the *SHIP* knockdown embryos and the embryos overexpressing the SHIP1 phosphatase domain (data not shown), suggesting that SHIP functions to limit neutrophil speed but not directional migration or persistence. Taken together, our findings suggest that SHIP limits neutrophil motility through the modulation of PI3K signaling. Moreover, our findings

demonstrate that the effects of ectopic expression of SHIP1 are cell autonomous, since SHIP1 expression in neutrophils alone was sufficient to impair migration.

It is well established that localized generation of $PI(3,4,5)P_3$ is critical for neutrophil motility. $PI(3,4,5)P_3$ can activate Rac through the recruitment of Rac guanine nucleotide exchange factors (Nishikimi *et al.*, 2009) and it is known that Rac2 is required for neutrophil motility *in vivo* (Deng *et al.*, 2011b). SHIP prevents $PI(3,4,5)P_3$ accumulation and it is possible that SHIP phosphatases limit neutrophil motility by affecting Rac2 activity at the leading edge. In addition to the role that SHIP plays in dampening $PI(3,4,5)P_3$ signaling, it is also possible that SHIP alters neutrophil motility through the generation of $PI(3,4)P_2$ which can act as a second messenger by binding pleckstrin homology(PH)-containing proteins such as TAPPs (Marshall *et al.*, 2002), Akt, PDK-1 and PKC family members [reviewed in (Rameh and Cantley, 1999)].

Our findings that SHIP impairs leukocyte motility are consistent with previous reports that bone marrow-derived SHIP-deficient macrophages exhibit spontaneous and enhanced migration (Vedham *et al.*, 2005) and the increase in myeloid infiltration into vital organs in $SHIP^{-/-}$ mice (Helgason *et al.*, 1998). A previous report showed that SHIP-deficient neutrophils have impaired cell polarity and migration *in vitro*, suggesting a role for SHIP in regulating neutrophil motility (Nishio *et al.*, 2007). However, this did not explain the SHIP-deficient inflammation phenotype observed *in vivo*. This discrepancy may be due to the differences between *in vitro* 2D and *in vivo* 3D motility, which sometimes yield contradictory results. For example, integrins are required for leukocyte migration on 2D surfaces but not in 3D interstitial tissues (Lammermann *et al.*, 2008). Moreover, MEK-cofilin signaling controls T-cell migration in 3D but not 2D environments

(Klemke et al.). Therefore, the use of *in vivo* model systems is crucial to increase our understanding of how specific pathways regulate leukocyte motility and inflammation in live animals.

Our findings suggest that SHIP is a key brake that limits neutrophil motility *in vivo*. An important unanswered question is how and when this "brake" is released to allow for motility. Hydrogen peroxide is generated at wounds and mediates rapid wound detection in zebrafish (Niethammer *et al.*, 2009). Moreover, we have recently shown that the Src family kinase Lyn acts as a redox sensor that can mediate leukocyte wound attraction (Yoo *et al.*, 2011). In addition to activating Lyn kinase, hydrogen peroxide can also inactivate phosphatases, such as SHIP, through the oxidation of specific cysteine residues (Paulsen and Carroll, 2010; Poole and Nelson, 2008). Although Lyn can activate SHIP under some conditions (Baran *et al.*, 2003), it is intriguing to speculate that in the presence of hydrogen peroxide, Lyn activation of SHIP phosphatases (the "brake") is prevented. A future challenge is to understand how these positive and negative regulatory pathways are coordinated and balanced to mediate proper leukocyte wound attraction and prevent untoward inflammation *in vivo*.

Material and methods

Tail fin wounding, whole-mount immunolabeling and Sudan Black staining

All animal experiments were performed according to approved guidelines. Embryos pretreated with 0.5% DMSO, AS-605240 (1 μM) for 1 hour at 2.5 dpf were anesthetized by 0.2 mg/mL tricaine and wounded at the tail fin with a 33 gauge needle. *Tg*(*mpx:dendra2*) embryos were fixed in 1.5% formaldehyde in 0.1M PIPES, 1mM $MgSO_4$, and 2mM EGTA overnight at 4°C and immunolabeled for L-plastin as previously described (Mathias *et al.*, 2009; Yoo and Huttenlocher, 2011). Wild-type embryos were fixed in 4% formaldehyde overnight at room temperature and stained with Sudan Black as described previously (Le Guyader *et al.*, 2008).

RT-PCR

RT-PCR was performed using mRNA from FACS-sorted myeloid cells using *Tg*(*mpx:dendra2*) zebrafish embryos as previously described (Mathias *et al.*, 2009; Yoo and Huttenlocher, 2011). Primers used for checking expression of different *SHIP* isoforms are as follow: *SHIP1*-RT-F: 5'-CACAGCCAATCAAATCCCACATGAC-3'; *SHIP1*-RT-R: 5'- GCTTCGTGTGATGGAAGGTCAAC-3'; *SHIP2a*-RT-F: 5'-CTGTGCAAACCTTCGAGGTGAAAC-3'; *SHIP2a*-RT-R: 5'-CCACCCATTCTTTATCGCACACAG-3'; *SHIP2b*-RT-F: 5'-GAGAATTTGAAAGGAGGCGCGTC-3'; *SHIP2b*-RT-R: 5'-CTCTGAAACTTCACCAACTGCACG-3'.

Primers used for checking MO knockdown efficiency are as follow: *SHIP1* MO1-F: 5'-GGCACCATGGCAATATCACTCGG-3'; *SHIP1* MO1-R: 5'-

CCCATTCTGGACCTGTTCTGCATC-3'; *SHIP1* MO2-F: 5'-GTCTCCTGGAGCTGGAAGACTAAG-3'; *SHIP1* MO2-R: 5'-GTCATGTGGGATTTGATTGGCTGTG-3'; *SHIP2a* MO1/MO2-F: 5'-CTTCGCCAGTGCAAAGAAAAGGG-3'; *SHIP2a* MO1/MO2-R: 5'-CTCTCTCCAGGTTCAGCTGGTC-3'.

DNA, RNA and morpholino injection

All DNA expression vectors contain either the zebrafish myeloperoxidase (*mpx*) promoter or lysozyme C (*lyz*) promoter for neutrophil expression (Kitaguchi *et al.*, 2009; Mathias *et al.*, 2006), minimal Tol2 elements for efficient integration (Urasaki *et al.*, 2006), and an SV40 polyadenylation sequence (Clontech Laboratories, Inc.). Constructs with each of the following in the backbone were constructed: TagRFP-GRP1-PH, AcGFP-TAPP1-PH (Furutani *et al.*, 2006), human EGFP-SHIP1 (accession BC113582), zebrafish EGFP-SHIP1 (accession XM_001922972), zebrafish EGFP-SHIP2a (accession DQ272661) and TM-SHIP1(aa364-826)-2A-EGFP [TM, plasma membrane targeting signal (Lyn kinase targeting sequence); human SHIP1b accession BC113582], The primers *SHIP1F*, 5'- AGCAGATCTATGTTTTCCCCCCAGCCGTG-3' and *SHIP1R*, 5'- GCTTCTAGATCACTTTAGCTGTCGACCCATCTTCAG-3' were used to amplify the full-length coding sequence of zebrafish SHIP1 from WT AB strain cDNA at 3dpf, which was then tagged with EGFP. The primers *SHIP2aF*, 5'-AGCGAATTCGTGTGAGTCTCCGCGATGGC-3' and *SHIP2aR*, 5'-GCTACTAGTGGAATTCCTCAGGTCAGATTCACCAGTGC-3' were used to subclone SHIP2a from SHIP2a cDNA and tagged with EGFP.

Expression of single construct was obtained by injection of 3 nL solution containing 12.5 ng/μL of DNA plasmid and 17.5 ng/μL *in vitro* transcribed (Ambion) Tol2 transposase mRNA into the cytoplasm of one-cell stage embryos. Expression of two constructs was obtained by mixing 6.25 ng/μL of each DNA plasmid. Two non-overlapping antisense splice-blocking morpholino oligonucleotides (MOs) of zebrafish *SHIP1* and *SHIP2a* were synthesized by Gene Tools: *SHIP1* MO1, 5'-TTGGACTGTTCAGATGTACCTGGTT-3' which corresponds to the putative exon 3/intron 3 boundary upstream of the phosphatase domain of zebrafish *SHIP1*; *SHIP1* MO2, 5'- ATGACTTAAGACATCTCACCCATGT-3' which corresponds to the putative exon 12/intron 12 region within the phosphatase domain of zebrafish *SHIP1*; *SHIP2a* MO1, 5'- TGTGTTGTTGTGTTCCTGACCGAGT-3' which corresponds to the exon 13/intron 13 of zebrafish *SHIP2a*; and *SHIP2a* MO2, 5'-CCCAGAATGCCGTGTTTCACCTGTA-3' which corresponds to the exon 15/intron 15 region within the phosphatase domain of zebrafish *SHIP2a*. Morpholinos were resuspended in Danieau buffer at a stock concentration of 1 mM. Final MO concentrations were injected into the cytoplasm of one-cell stage embryos. Individual concentrations used: 100 μM, 3nl *SHIP1* MO1; 250 μM, 3nl *SHIP1* MO2; 25 μM, 3nl *SHIP2a* MO1; 200 μM, 3nl *SHIP2a* MO2. Standard control MO from Gene Tools 5'-CCTCTTACCTCAGTTACAATTTATA-3' was used as controls. Injected embryos were cultured in E3 medium at 28.5°C.

Live imaging

Embryos at 2-3 dpf were anesthetized using 0.2 mg/mL tricaine on a glass-bottom dish for live imaging. Time-lapse fluorescence images were acquired using a

confocal microscope (FluoView FV1000, Olympus) using a NA 0.75/20x objective or a NA 1.10/60x water immersion objective. Sequential line scanning was used for each fluorescence channel. Z-stacked and ratiometric images were generated by FluoView FV1000 software (Olympus). After the ratio analysis with background subtraction was performed, a median filter was used to generate an image for visualization. For supplementary material Fig. S2 and Movie 5, a spinning disk confocal system (Yokogawa CSU-X) mounted on a Zeiss Observer Z.1 inverted microscope was used. A Photometrics Evolve EMCCD camera and a NA1.3 /60x water immersion objective was used to acquire the Z-series images with a 0.4 μm step size and 300 EM gain. Maximum intensity projection images were made using the Zen 2011 (blue edition) software (Carl Zeiss). Ratio images were generated by using the AxioVison SE64 Rel 4.8 Physiology measurement function with confidence mapping.

Statistics

Experimental results were analyzed with Prism version 4 (GraphPad Software) statistical software. Statistical significance was determined with the unpaired Student *t* test or one-way ANOVA with Dunnett post-test. The resulting *P* values are included in the figure legends for each experiment; n = the number of embryos or neutrophils quantified.

Acknowledgements

We thank Dr. David J. Grunwald and Dr. Michael J. Jurynec for the zebrafish *SHIP2a* cDNA and Dr. Toshiki Itoh for the TagRFP-GRP1-PH and AcGFP-TAPP1-PH. We thank Dr. Erwin Berthier for his help with the meandering index analysis.

Funding

This work was supported by National Institutes of Health Grants [grant number GM074827 to A.H.] and American Heart Association fellowship [number 11PRE4890041 to S.K.Y.]. Deposited in PMC for release after 12 months.

References

Baran, C.P., S. Tridandapani, C.D. Helgason, R.K. Humphries, G. Krystal, and C.B. Marsh. 2003. The inositol 5'-phosphatase SHIP-1 and the Src kinase Lyn negatively regulate macrophage colony-stimulating factor-induced Akt activity. *J Biol Chem*. 278:38628-36.

Barberis, L., and E. Hirsch. 2008. Targeting phosphoinositide 3-kinase gamma to fight inflammation and more. *Thromb Haemost*. 99:279-85.

Deng, Q., E.A. Harvie, and A. Huttenlocher. 2011a. Distinct signaling mechanisms mediate neutrophil attraction to bacterial infection and tissue injury. *Cell Microbiol*.

Deng, Q., S.K. Yoo, P.J. Cavnar, J.M. Green, and A. Huttenlocher. 2011b. Dual roles for Rac2 in neutrophil motility and active retention in zebrafish hematopoietic tissue. *Dev Cell*. 21:735-45.

Frech, M., M. Andjelkovic, E. Ingley, K.K. Reddy, J.R. Falck, and B.A. Hemmings. 1997. High affinity binding of inositol phosphates and phosphoinositides to the pleckstrin homology domain of RAC/protein kinase B and their influence on kinase activity. *J Biol Chem*. 272:8474-81.

Freeburn, R.W., K.L. Wright, S.J. Burgess, E. Astoul, D.A. Cantrell, and S.G. Ward. 2002. Evidence that SHIP-1 contributes to phosphatidylinositol 3,4,5-trisphosphate metabolism in T lymphocytes and can regulate novel phosphoinositide 3-kinase effectors. *J Immunol*. 169:5441-50.

Furutani, M., K. Tsujita, T. Itoh, T. Ijuin, and T. Takenawa. 2006. Application of phosphoinositide-binding domains for the detection and quantification of specific phosphoinositides. *Anal Biochem*. 355:8-18.

Gray, A., J. Van Der Kaay, and C.P. Downes. 1999. The pleckstrin homology domains of protein kinase B and GRP1 (general receptor for phosphoinositides-1) are sensitive and selective probes for the cellular detection of phosphatidylinositol 3,4-bisphosphate and/or phosphatidylinositol 3,4,5-trisphosphate *in vivo*. *Biochem J*. 344 Pt 3:929-36.

Harris, S.J., R.V. Parry, J.G. Foster, M.D. Blunt, A. Wang, F. Marelli-Berg, J. Westwick, and S.G. Ward. 2011. Evidence that the lipid phosphatase SHIP-1 regulates T lymphocyte morphology and motility. *J Immunol*. 186:4936-45.

Hawkins, P.T., and L.R. Stephens. 2007. PI3Kgamma is a key regulator of inflammatory responses and cardiovascular homeostasis. *Science*. 318:64-6.

Helgason, C.D., J.E. Damen, P. Rosten, R. Grewal, P. Sorensen, S.M. Chappel, A. Borowski, F. Jirik, G. Krystal, and R.K. Humphries. 1998. Targeted disruption of SHIP leads to hemopoietic perturbations, lung pathology, and a shortened life span. *Genes Dev*. 12:1610-20.

Huttenlocher, A., and M.C. Poznansky. 2008. Reverse leukocyte migration can be attractive or repulsive. *Trends Cell Biol*. 18:298-306.

Jurynec, M.J., and D.J. Grunwald. 2010. SHIP2, a factor associated with diet-induced obesity and insulin sensitivity, attenuates FGF signaling *in vivo*. *Dis Model Mech*. 3:733-42.

Kanther, M., and J.F. Rawls. 2010. Host-microbe interactions in the developing zebrafish. *Curr Opin Immunol*. 22:10-9.

Kitaguchi, T., K. Kawakami, and A. Kawahara. 2009. Transcriptional regulation of a myeloid-lineage specific gene lysozyme C during zebrafish myelopoiesis. *Mech Dev*. 126:314-23.

Klemke, M., E. Kramer, M.H. Konstandin, G.H. Wabnitz, and Y. Samstag. 2010. An MEK-cofilin signalling module controls migration of human T cells in 3D but not 2D environments. *EMBO J*. 29:2915-29.

Koch, A., A. Mancini, O. El Bounkari, and T. Tamura. 2005. The SH2-domian-containing inositol 5-phosphatase (SHIP)-2 binds to c-Met directly via tyrosine residue 1356 and involves hepatocyte growth factor (HGF)-induced lamellipodium formation, cell scattering and cell spreading. *Oncogene*. 24:3436-47.

Lammermann, T., B.L. Bader, S.J. Monkley, T. Worbs, R. Wedlich-Soldner, K. Hirsch, M. Keller, R. Forster, D.R. Critchley, R. Fassler, and M. Sixt. 2008. Rapid leukocyte migration by integrin-independent flowing and squeezing. *Nature*. 453:51-5.

Le Guyader, D., M.J. Redd, E. Colucci-Guyon, E. Murayama, K. Kissa, V. Briolat, E. Mordelet, A. Zapata, H. Shinomiya, and P. Herbomel. 2008. Origins and unconventional behavior of neutrophils in developing zebrafish. *Blood*. 111:132-41.

Liu, Q., T. Sasaki, I. Kozieradzki, A. Wakeham, A. Itie, D.J. Dumont, and J.M. Penninger. 1999. SHIP is a negative regulator of growth factor receptor-mediated PKB/Akt activation and myeloid cell survival. *Genes Dev*. 13:786-91.

Liu, Q., F. Shalaby, J. Jones, D. Bouchard, and D.J. Dumont. 1998. The SH2-containing inositol polyphosphate 5-phosphatase, ship, is expressed during hematopoiesis and spermatogenesis. *Blood*. 91:2753-9.

Marshall, A.J., A.K. Krahn, K. Ma, V. Duronio, and S. Hou. 2002. TAPP1 and TAPP2 are targets of phosphatidylinositol 3-kinase signaling in B cells: sustained plasma membrane recruitment triggered by the B-cell antigen receptor. *Mol Cell Biol*. 22:5479-91.

Mathias, J.R., M.E. Dodd, K.B. Walters, S.K. Yoo, E.A. Ranheim, and A. Huttenlocher. 2009. Characterization of zebrafish larval inflammatory macrophages. *Dev Comp Immunol*. 33:1212-7.

Mathias, J.R., B.J. Perrin, T.X. Liu, J. Kanki, A.T. Look, and A. Huttenlocher. 2006. Resolution of inflammation by retrograde chemotaxis of neutrophils in transgenic zebrafish. *J Leukoc Biol*. 80:1281-8.

McDonald, B., K. Pittman, G.B. Menezes, S.A. Hirota, I. Slaba, C.C. Waterhouse, P.L. Beck, D.A. Muruve, and P. Kubes. 2010. Intravascular danger signals guide neutrophils to sites of sterile inflammation. *Science*. 330:362-6.

Muraille, E., X. Pesesse, C. Kuntz, and C. Erneux. 1999. Distribution of the src-homology-2-domain-containing inositol 5-phosphatase SHIP-2 in both non-haemopoietic and haemopoietic cells and possible involvement of SHIP-2 in negative signalling of B-cells. *Biochem J*. 342 Pt 3:697-705.

Niethammer, P., C. Grabher, A.T. Look, and T.J. Mitchison. 2009. A tissue-scale gradient of hydrogen peroxide mediates rapid wound detection in zebrafish. *Nature*. 459:996-9.

Nishikimi, A., H. Fukuhara, W. Su, T. Hongu, S. Takasuga, H. Mihara, Q. Cao, F. Sanematsu, M. Kanai, H. Hasegawa, Y. Tanaka, M. Shibasaki, Y. Kanaho, T. Sasaki, M.A. Frohman, and Y. Fukui. 2009. Sequential regulation of DOCK2 dynamics by two phospholipids during neutrophil chemotaxis. *Science*. 324:384-7.

Nishio, M., K. Watanabe, J. Sasaki, C. Taya, S. Takasuga, R. Iizuka, T. Balla, M. Yamazaki, H. Watanabe, R. Itoh, S. Kuroda, Y. Horie, I. Forster, T.W. Mak, H. Yonekawa, J.M. Penninger, Y. Kanaho, A. Suzuki, and T. Sasaki. 2007. Control of cell polarity and motility by the PtdIns(3,4,5)P3 phosphatase SHIP1. *Nat Cell Biol*. 9:36-44.

Parent, C.A. 2004. Making all the right moves: chemotaxis in neutrophils and Dictyostelium. *Curr Opin Cell Biol*. 16:4-13.

Paulsen, C.E., and K.S. Carroll. 2010. Orchestrating redox signaling networks through regulatory cysteine switches. *ACS Chem Biol*. 5:47-62.

Poole, L.B., and K.J. Nelson. 2008. Discovering mechanisms of signaling-mediated cysteine oxidation. *Curr Opin Chem Biol*. 12:18-24.

Provost, E., J. Rhee, and S.D. Leach. 2007. Viral 2A peptides allow expression of multiple proteins from a single ORF in transgenic zebrafish embryos. *Genesis*. 45:625-9.

Rameh, L.E., and L.C. Cantley. 1999. The role of phosphoinositide 3-kinase lipid products in cell function. *J Biol Chem*. 274:8347-50.

Rauh, M.J., L.M. Sly, J. Kalesnikoff, M.R. Hughes, L.P. Cao, V. Lam, and G. Krystal. 2004. The role of SHIP1 in macrophage programming and activation. *Biochem Soc Trans*. 32:785-8.

Rohrschneider, L.R., J.F. Fuller, I. Wolf, Y. Liu, and D.M. Lucas. 2000. Structure, function, and biology of SHIP proteins. *Genes Dev*. 14:505-20.

Servant, G., O.D. Weiner, P. Herzmark, T. Balla, J.W. Sedat, and H.R. Bourne. 2000. Polarization of chemoattractant receptor signaling during neutrophil chemotaxis. *Science*. 287:1037-40.

Urasaki, A., G. Morvan, and K. Kawakami. 2006. Functional dissection of the Tol2 transposable element identified the minimal cis-sequence and a highly repetitive sequence in the subterminal region essential for transposition. *Genetics*. 174:639-49.

Vedham, V., H. Phee, and K.M. Coggeshall. 2005. Vav activation and function as a rac guanine nucleotide exchange factor in macrophage colony-stimulating factor-induced macrophage chemotaxis. *Mol Cell Biol*. 25:4211-20.

Yoo, S.K., Q. Deng, P.J. Cavnar, Y.I. Wu, K.M. Hahn, and A. Huttenlocher. 2010. Differential regulation of protrusion and polarity by PI3K during neutrophil motility in live zebrafish. *Dev Cell*. 18:226-36.

Yoo, S.K., and A. Huttenlocher. 2011. Spatiotemporal photolabeling of neutrophil trafficking during inflammation in live zebrafish. *J Leukoc Biol*. 89:661-7.

Yoo, S.K., T.W. Starnes, Q. Deng, and A. Huttenlocher. 2011. Lyn is a redox sensor that mediates leukocyte wound attraction *in vivo*. *Nature*.

Fig. 1. Ratiometric imaging of PI(3,4,5)P_3 and PI(3,4,)P_2 in motile neutrophils in zebrafish. Representative images are presented as maximum intensity projections. (A) Time lapse ratiometric imaging of PI(3,4)P_2 (TAPP1-PH/mCherry) using a 60x NA1.10 objective with 270 μm pinhole and 1.01 μm step size. (B) Time-lapse ratiometric imaging of PI(3,4,5)P_3 (GRP1-PH/dendra2) and (C) Time-lapse ratiometric imaging of PI(3,4,5)P_3 to PI(3,4)P_2 (GRP1-PH/ TAPP1-PH) or PI(3,4)P_2 to PI(3,4,5)P_3 (TAPP1-PH /GRP1-PH), using a 20x NA0.75 objective with 344 μm pinhole and 3.89 μm step size. White arrow indicates the direction of neutrophil migration. The numerical values of ratiometric analysis are shown in the scales. Scale bar, 10 μm.

Fig. 1

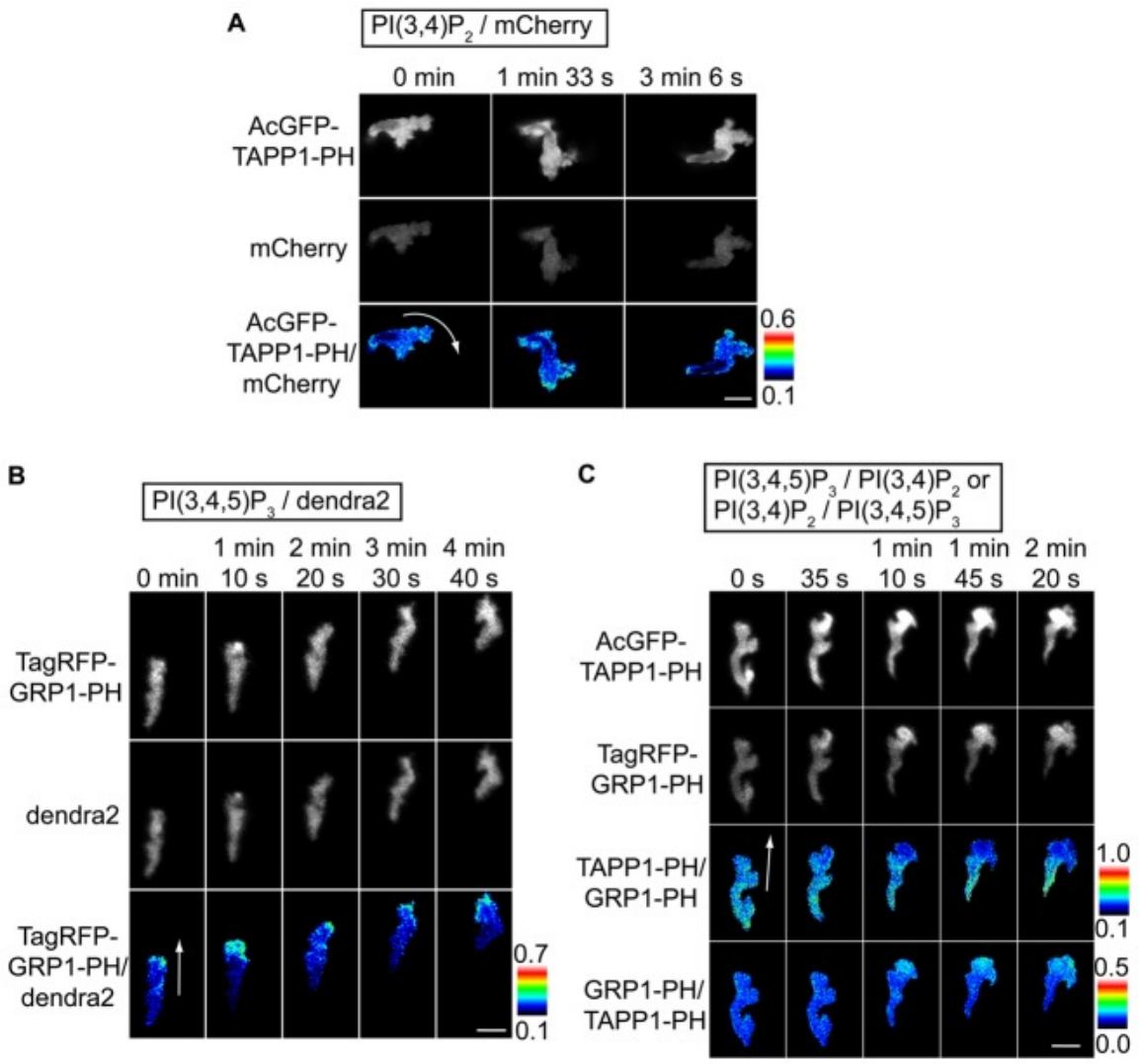
A
PI(3,4)P2 / mCherry
0 min
1 min 33 s
3 min 6 s
AcGFP-TAPP1-PH
mCherry
AcGFP-TAPP1-PH/mCherry
0.6
0.1
B
PI(3,4,5)P3 / dendra2
0 min
1 min 10 s
2 min 20 s
3 min 30 s
4 min 40 s
TagRFP-GRP1-PH
dendra2
TagRFP-GRP1-PH/dendra2
0.7
0.1
C
PI(3,4,5)P3 / PI(3,4)P2 or PI(3,4)P2 / PI(3,4,5)P3
0 s
35 s
1 min 10 s
1 min 45 s
2 min 20 s
AcGFP-TAPP1-PH
TagRFP-GRP1-PH
TAPP1-PH/GRP1-PH
GRP1-PH/TAPP1-PH
1.0
0.1
0.5
0.0

Fig. 2. Expression and localization of SHIP *in vivo*. (A) Expression of SHIP isoforms (*SHIP1*, *SHIP2a* and *SHIP2b)* from whole embryo or FACS sorted myeloid cells from *Tg*(*mpx:dendra2*) determined by RT-PCR. (B) Expression of specific markers of FACS-sorted myeloid cells from *Tg*(*mpx:dendra2*) fish by RT-PCR with markers that are expressed (*mpx, csf1r*) or not expressed *(myoD*, *p63*) in myeloid cells. (C) Time-lapse ratiometric imaging of human EGFP-SHIP1/mCherry using *lyz:EGFP-SHIP1* injected into *Tg*(*mpx:mCherry*) showing localization of SHIP1 at the front and rear of motile neutrophils. Images were acquired using a 20x NA0.75 objective with 241 μm pinhole and 2.78 μm step size; and representative images are presented as maximum intensity projections. White arrow indicates the direction of migration. The numerical value of ratiometric analysis is shown in the scale. Scale bar, 10 μm.

Fig. 2

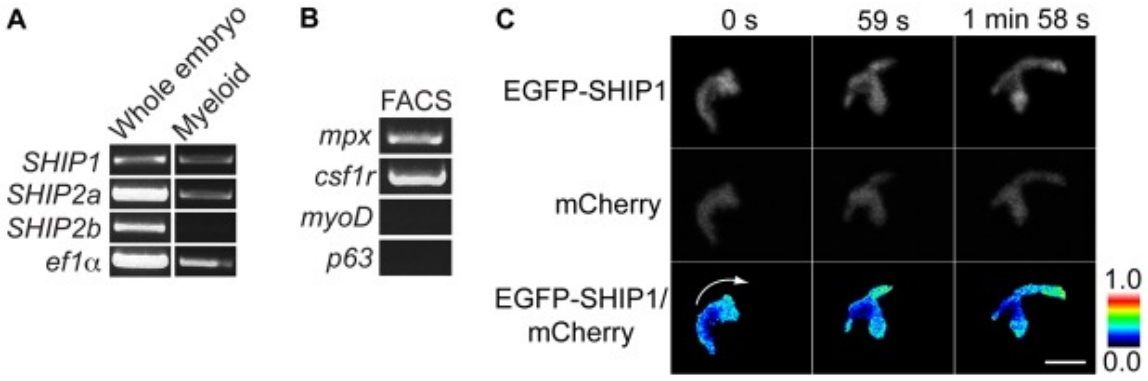
A
Whole embryo
Myeloid
SHIP1
SHIP2a
SHIP2b
ef1α
B
FACS
mpx
csf1r
myoD
p63
C
0 s
59 s
1 min 58 s
EGFP-SHIP1
mCherry
EGFP-SHIP1/
mCherry
1.0
0.0

Fig. 3. Neutrophil wound recruitment in *SHIP* morphants and rescue by PI3Kγ inhibition.

(A) RT-PCR analysis of *SHIP1* and *SHIP2a* morphants **(**B**)** Quantification of neutrophils at wounds in control and *SHIP1* (MO1) and *SHIP2a* (MO2) morphants at 0.5 and 1 hour post wounding (hpw). Data are representative of three experiments. (C) (Left panel) Quantification of neutrophils at wounds in control and *SHIP1* (MO2) and *SHIP2a* (MO1) morphants. Data are representative of at least three experiments. (Right panel**)** Representative image of Sudan Black-stained embryos. Lateral view of the tail fin of embryos at 2.5 dpf. The yellow outline indicates the area where the number of neutrophils were counted. Red arrow on control panel indicates a neutrophil after Sudan Black staining. Open arrow indicates site of wounding. n = number of embryos wounded and counted. *P<0.05, **P<0.01, ***P<0.001, (two-tailed, unpaired t test). (D) PI3Kγ inhibitor (AS-605240) (1 μM) reverses the effects of *SHIP1* and *SHIP2a* double knockdown on neutrophil recruitment. Data are representative of three experiments. n = number of embryos wounded and counted. *<0.05, **p<0.01 (one-way ANOVA with Bonferroni post-test). (Right panel**)** Representative image of Sudan Black-stained embryos used for neutrophil recruitment analysis. Lateral view of the tail fin of embryo at 2.5 dpf.

Fig. 3

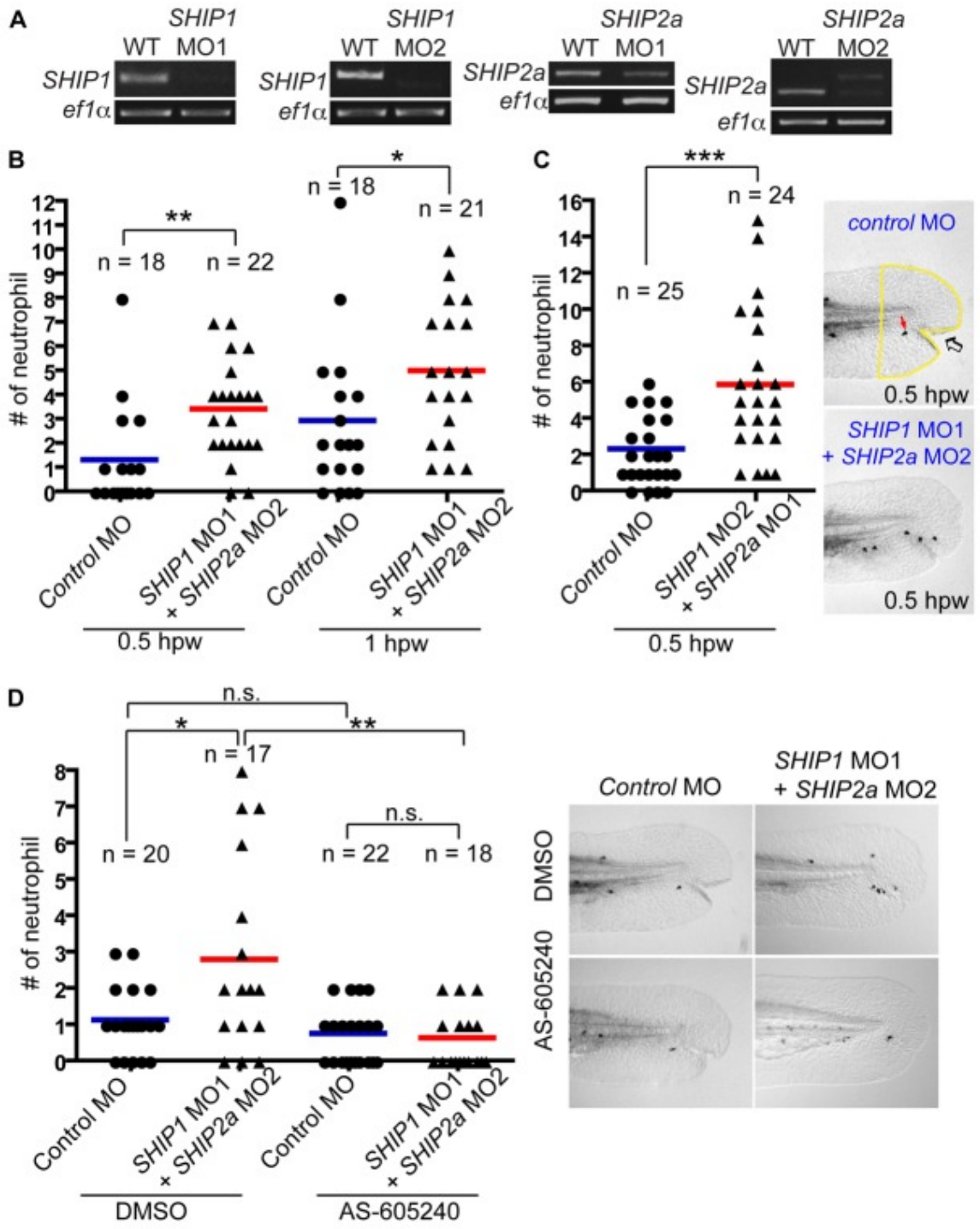
A
SHIP1
WT MO1
SHIP1
ef1α
SHIP1
WT MO2
SHIP1
ef1α
SHIP2a
WT MO1
SHIP2a
ef1α
SHIP2a
WT MO2
SHIP2a
ef1α
B
# of neutrophil
n = 18
n = 22
n = 18
n = 21
**
*
Control MO
SHIP1 MO1 + SHIP2a MO2
Control MO
SHIP1 MO1 + SHIP2a MO2
0.5 hpw
1 hpw
C
# of neutrophil
n = 25
n = 24
***
Control MO
SHIP1 MO2 + SHIP2a MO1
0.5 hpw
control MO
0.5 hpw
SHIP1 MO1 + SHIP2a MO2
0.5 hpw
D
# of neutrophil
n.s.
*
**
n = 17
n = 20
n.s.
n = 22
n = 18
Control MO
SHIP1 MO1 + SHIP2a MO2
Control MO
SHIP1 MO1 + SHIP2a MO2
DMSO
AS-605240
Control MO
SHIP1 MO1 + SHIP2a MO2
DMSO
AS-605240

Fig. 4. SHIP regulates neutrophil motility. (A) Schematic showing region (red box) where random motility was quantified. (B) Scatter plot showing the mean speed of *Tg*(*mpx:dendra2)* neutrophils from control or *SHIP* morphants at 2.5 dpf. Neutrophils were tracked in 3 dimensions (3D) using the Image J software and the MTrackJ plugin. *SHIP* morphants showed increased neutrophil speed compared with controls. Data were collected from 4 individual movies for controls and morphants. **P<0.01 (two-tailed, unpaired t-test). (C) Cell migration tracks plotted in 3D and viewed in the xy-plane (left) or the zy-plane (right). (D) Graph showing mean velocity of 3D tracked neutrophils from control or SHIP phosphatase domain [SHIP(aa364-826)-2A-EGFP] expressing neutrophils in *Tg*(*mpx:mCherry)* at 3 dpf. Data were collected from 7 individual movies. ***P<0.001 (two-tailed, unpaired t-test). (E) Similar to C, the tracks were plotted in 3D and viewed in the xy-plane (left) or the zy-plane (right). (F) As a control for (D), mean velocity of neutrophils expressing EGFP compared with neutrophils in the same embryo that do not express EGFP (Control). Data were collected from 7 individual movies. n = number of neutrophils counted.

Fig. 4

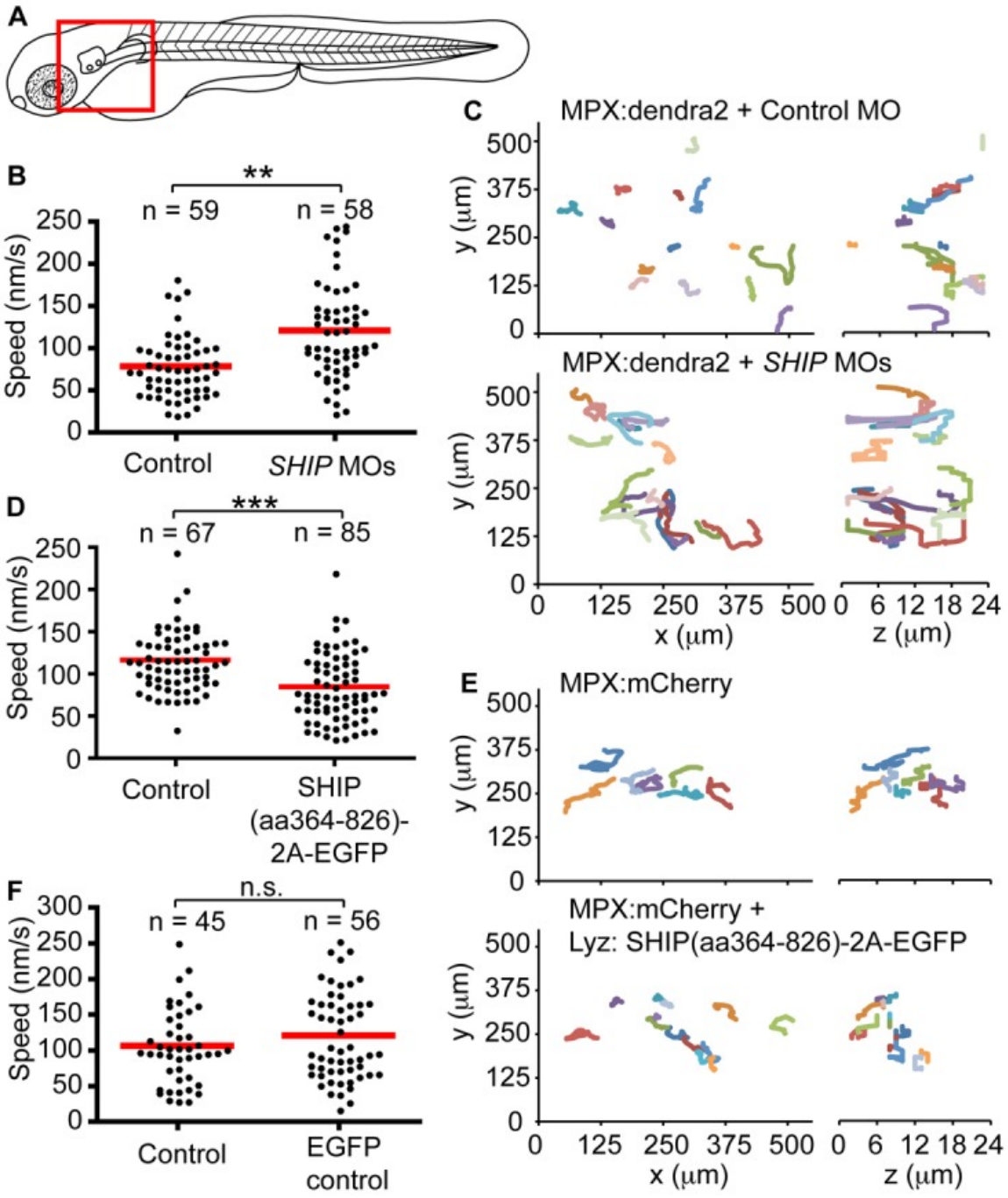
A
B
**
n = 59
n = 58
Speed (nm/s)
250
200
150
100
50
0
Control
SHIP MOs
C
MPX:dendra2 + Control MO
y (μm)
500
375
250
125
0
MPX:dendra2 + SHIP MOs
0
125
250
375
500
x (μm)
0
6
12
18
24
z (μm)
D
***
n = 67
n = 85
Control
SHIP (aa364-826)-2A-EGFP
E
MPX:mCherry
MPX:mCherry + Lyz: SHIP(aa364-826)-2A-EGFP
F
n.s.
n = 45
n = 56
300
Control
EGFP control

Fig. S1. Amino acid alignment of human SHIP1a, SHIP1b and zebrafish SHIP1. Zebrafish SHIP1 shows 61% overall identity to human SHIP1a and SHIP1b. The highest level of homology is seen within the conserved domains for SH2 (src homology 2) and IPPc (inositol polyphosphate 5-phosphatase catalytic domain).

Fig. S1

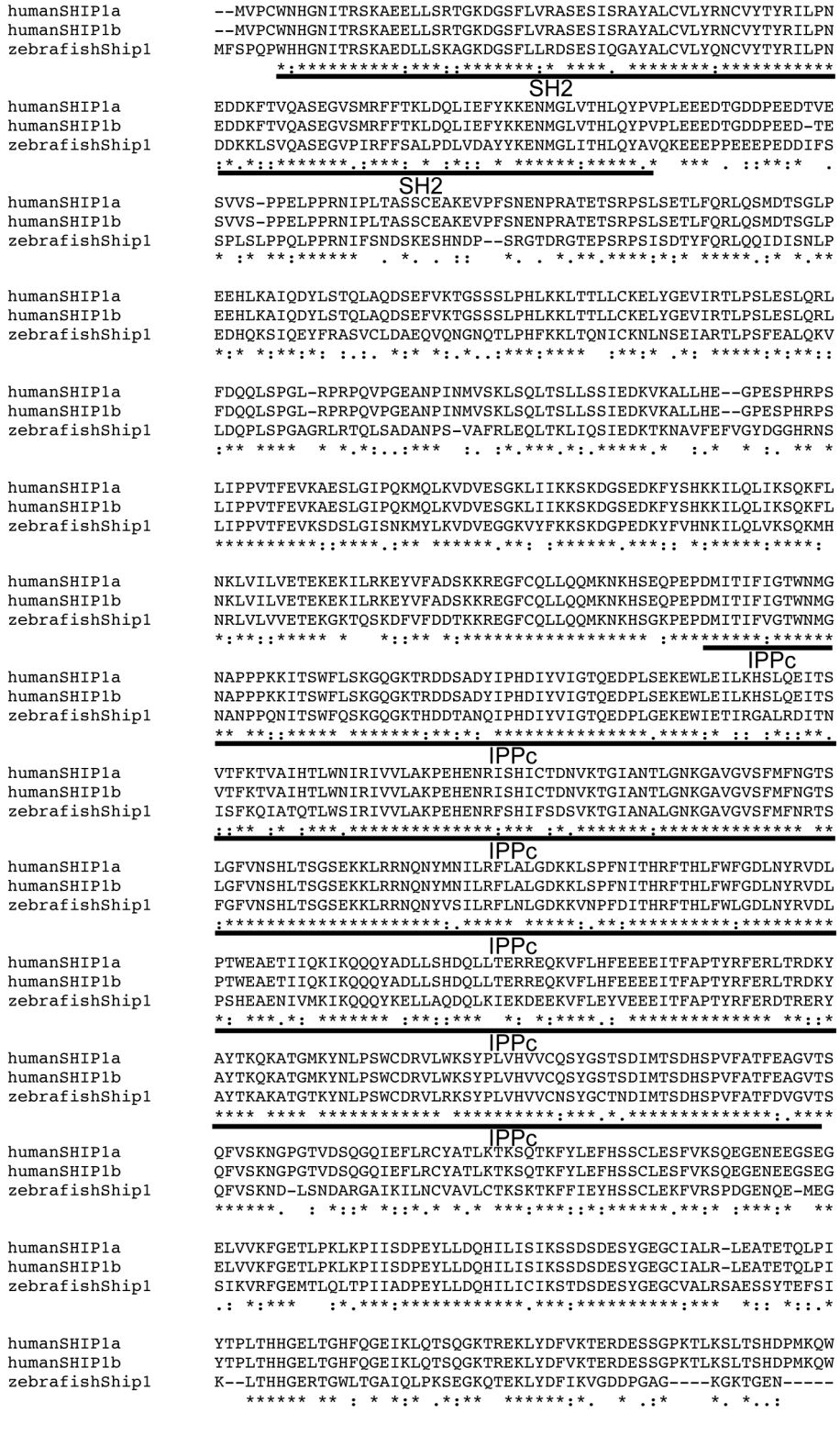

Fig. S2. Localization of zebrafish SHIP1 and SHIP2a *in vivo*.

Time-lapse ratiometric imaging of zebrafish EGFP-SHIP1/mCherry (A) and zebrafish EGFP-SHIP2a/mCherry (B) using *lyz:EGFP-SHIP1* or *lyz:EGFP-SHIP2a*, respectively, injected into *Tg*(*mpx:mCherry*) embryos. Both zebrafish SHIP1 and SHIP2a show intermittent localization at the front of motile neutrophils. Images are acquired using a NA1.3 /60x water immersion objective on a spinning disk confocal microscope equipped with a Photometrics Evolve EMCCD camera (detail in Material and Methods). Representative images are presented as maximum intensity projections. The numerical value of ratiometric analysis is shown in the scale. Scale bar, 10 μm.

Fig. S2

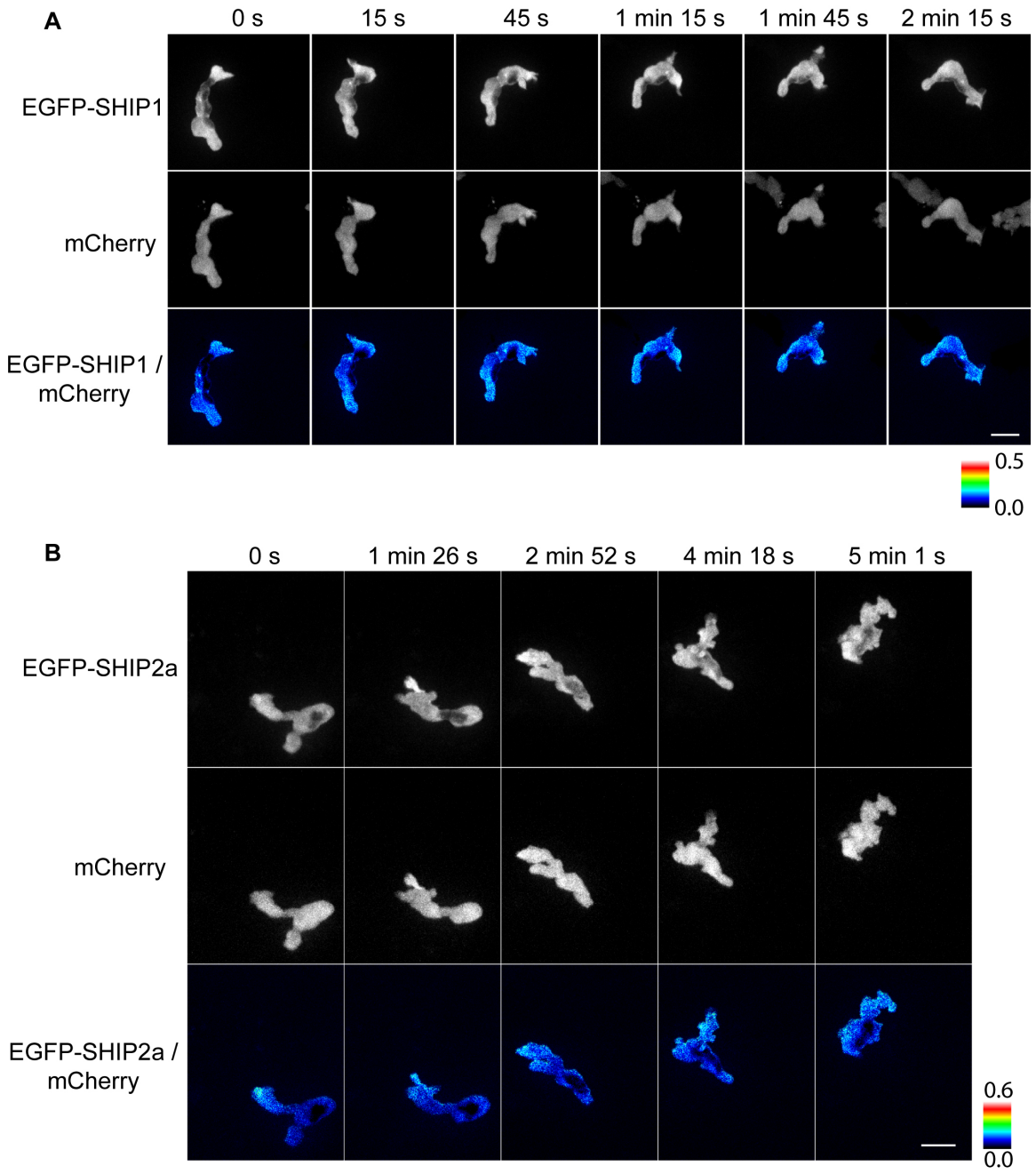
A
0 s
15 s
45 s
1 min 15 s
1 min 45 s
2 min 15 s
EGFP-SHIP1
mCherry
EGFP-SHIP1 / mCherry
0.5
0.0
B
0 s
1 min 26 s
2 min 52 s
4 min 18 s
5 min 1 s
EGFP-SHIP2a
mCherry
EGFP-SHIP2a / mCherry
0.6
0.0

Fig. S3. Overlapping expression of mpx:Dendra2 and lyz:TagRFP expression in zebrafish neutrophils.

Confocal images showing Dendra2 expressing neutrophils (left panel –green expressing cells), TagRFP expressing neutrophil (middle panel –magenta expressing cells) and overlaid image of dendra2, TagRFP signal along with the corresponding DIC image. The mpx^{+}/lyz^{+} positive cells appear white in the merged panel. Two representative embryos were selected to show neutrophils in the head (top panel) and in the caudal hematopoietic tissue (CHT) (bottom panel) at 3 dpf.

Fig. S3

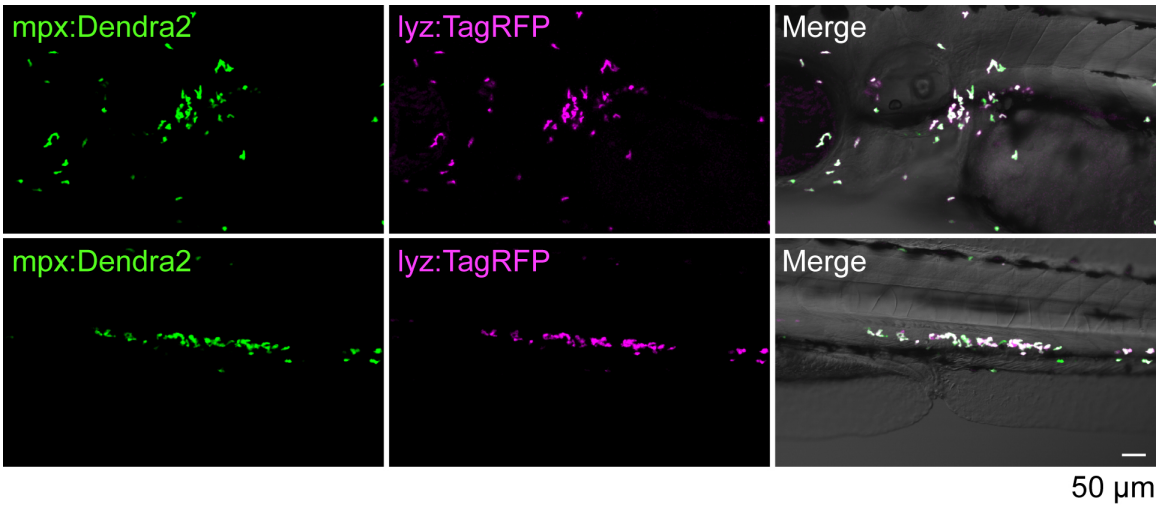
mpx:Dendra2
lyz:TagRFP
Merge
mpx:Dendra2
lyz:TagRFP
Merge
50 μm

Fig. S4. Reduced neutrophils in *SHIP* morphants.

Zebrafish embryos were injected with either control or *SHIP1* (MO1) and *SHIP2a* (MO2) MO. Embryos were fixed at 2.5 dpf and Sudan Black staining was performed to facilitate counting of total neutrophil numbers. n = number of embryo counted. ***$p<0.001$ (two-tailed, unpaired t test).

Fig. S4

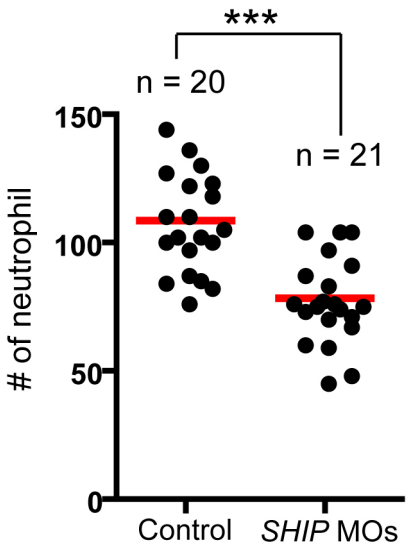

Fig. S5. Increased macrophage wound recruitment in *SHIP* morphants.

Quantification of macrophage numbers recruited to tail fin wounds in combined morpholino knockdown of *SHIP1* (MO1) and *SHIP2a* (MO2) at 0.5 hpw. Confocal imaging at wounds in control or *SHIP* MOs injected *Tg*(*mpx: dendra2*; green) embryos at 2.5 dpf immunolabeled with antibody to L-plastin (red) that labels all leukocytes. Overlapping signals are yellow indicating MPX^+, L-$plastin^+$ neutrophils while red indicates MPX^-, L-$plastin^+$ macrophages. Open arrow indicates location of the wound. n = number of embryo wounded and counted. *<0.05 (two-tailed, unpaired t test).

Fig. S5

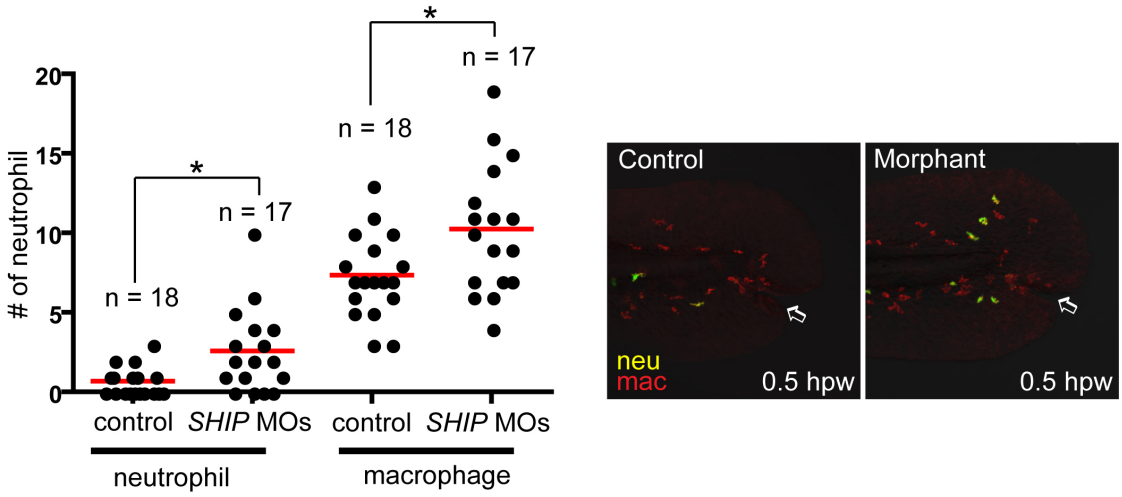
*
n = 17
n = 18
*
n = 17
n = 18
# of neutrophil
20
15
10
5
0
control
SHIP MOs
control
SHIP MOs
neutrophil
macrophage
Control
Morphant
neu
mac
0.5 hpw
0.5 hpw

Movie 1. Time-lapse ratiometric movie of migrating neutrophils showing $PI(3,4)P_2$ levels acquired by comparing the levels of TAPP1-PH versus the levels of mCherry. Expression is obtained by injecting *mpx:AcGFP-TAPP1-PH* into *Tg*(*mpx:mCherry*) embryos and imaging using confocal fluorescent microscopy. The numerical values of the ratiometric analysis are shown in the color scales.

Movie 2. Time-lapse ratiometric movie of migrating neutrophils showing $PI(3,4,5)P_3$ levels by comparing the levels of GRP1-PH versus the levels of dendra2. Expression is obtained by injecting *mpx:TagRFP-GRP1-PH* into *Tg*(*mpx:dendra2*) embryos. The numerical values of the ratiometric analysis are shown in the color scales.

Movie 3. Time-lapse ratiometric movie of migrating neutrophils showing the expression levels of $PI(3,4)P_2$ to $PI(3,4,5)P_3$ by comparing the levels of TAPP1-PH versus the levels of GRP1-PH or vice versa. Expression is obtained by injecting *mpx:AcGFP-TAPP1-PH* and *mpx:TagRFP-GRP1-PH* into wild-type embryos. The numerical values of the ratiometric analysis are shown in the color scales.

Movie 4. Time-lapse ratiometric movie of migrating neutrophils expressing human EGFP-SHIP1 and mCherry showing localization of SHIP1 at the front and tail of migrating neutrophils *in vivo.* Expression is obtained by injecting *lyz:EGFP-SHIP1* into *Tg*(*mpx:mCherry*) embryos. The numerical value of ratiometric analysis is shown in the color scale.

Movie 5. Time-lapse ratiometric movie of migrating neutrophils expressing zebrafish EGFP-SHIP1 or EGFP-SHIP2a and mCherry. Expression is obtained by injecting

lyz:EGFP-SHIP1 or *lyz:EGFP-SHIP2a* into *Tg*(*mpx:mCherry*) embryos. The numerical value of ratiometric analysis is shown in the color scale.

Movie 6. Time-lapse movie of neutrophils from the lateral side of the head of control or *ship* MO injected *Tg*(*mpx:dendra2)* embryos at 2.5 dpf.

Movie 7. Time-lapse movie of neutrophils from the lateral side of the head of a 3 dpf *Tg*(*mpx:mCherry)* embryo overexpressing SHIP phosphatase domain [SHIP(aa364-826)-2A-EGFP] specifically in neutrophils.

Chapter 3

The role of microtubules in neutrophil polarity and migration in live zebrafish

This Chapter was published in the following journal article:

Yoo S.K.*, Lam P.Y.*, Eichelberg M.R., Zasadil L., Bement W.M. and Huttenlocher A. (2012) The role of microtubules in neutrophil polarity and migration in live zebrafish. *Journal of Cell Science*, Dec 1;125(Pt 23):5702-10

* These authors contributed equally to this work.

In particular, I contributed Fig. 1E, Fig. 2, Fig. 7D, Movie 4, Movie 6, Movie 12 and part of Fig. 1A and D, Fig. 3A, B and E, Fig. 4, Fig. S1, Movie 1 and Movie 8. I also performed all the revision experiments, of which some were not shown in the final publication.

Summary

Microtubules control cell motility by positively regulating polarization in many cell types. However, how microtubules regulate leukocyte migration is not well understood, particularly in living organisms. Here we exploited the zebrafish system to study the role of microtubules in neutrophil migration *in vivo*. The localization of microtubules was visualized in motile neutrophils using various bioprobes, revealing that, in contrast to what has been seen in studies in vitro, the microtubule organizing center is positioned in front of the nucleus (relative to the direction of migration) in motile neutrophils. Microtubule disassembly impaired attraction of neutrophils to wounds but enhanced the polarity of F-actin dynamics as measured by the distribution of stable and dynamic F-actin. Microtubule depolymerization inhibited polarized phosphoinositol 3-kinase (PI(3)K) activation at the leading edge and induced rapid PI(3)K independent motility. Finally, we show that microtubules exert their effects on neutrophil polarity and motility at least in part by the negative regulation of both Rho and Rac activity. These results provide new insight into the role of microtubules in neutrophil migration in a living vertebrate and show that the motility of these professional migratory cells are subject to distinctly different rules from those established for other cell types.

Introduction

Directed cell migration is the result of a complex interplay between the actomyosin cytoskeleton, adhesion, and the microtubule network (Rodriguez et al., 2003; Small et al., 2002). More than 40 years ago, the pioneering work of Vasiliev on cultured mouse and human fibroblasts has shown that one of the major mechanisms by which microtubules contribute to cell migration is by the positive regulation of cell polarity (Vasiliev et al., 1970). Since Vasiliev's findings, it has become apparent that the microtubule cytoskeleton regulates cell migration in a cell type-dependent manner. Microtubule disassembly impairs cell migration in many types of cells such as fibroblasts, tumor cells and neurons (Etienne-Manneville, 2004; Kaverina and Straube, 2011; Mogilner and Keren, 2009; Siegrist and Doe, 2007; Small et al., 2002; Vinogradova et al., 2009; Watanabe et al., 2005; Wittmann and Waterman-Storer, 2001), whereas it promotes motility of neutrophils, but impairs their directionality (Niggli, 2003; Xu et al., 2005). In contrast, fish keratinocytes migrate directionally without microtubules (Euteneuer and Schliwa, 1984).

In addition to the context-dependent role of microtubules in cell migration, the location where microtubules nucleate and radiate during cell motility also depends on the cell type. In non-leukocyte cells, microtubules generally nucleate from the microtubule organizing center (MTOC) in front of the nucleus (relative to the direction of migration) and radiate towards the leading edge (Etienne-Manneville, 2004; Kaverina and Straube, 2011; Mogilner and Keren, 2009; Small et al., 2002; Vinogradova et al., 2009; Watanabe et al., 2005; Wittmann and Waterman-Storer, 2001). On the other hand, leukocytes are often described as having microtubules and the MTOC at the rear

of the cell (uropod) (Friedl and Weigelin, 2008; Sanchez-Madrid and del Pozo, 1999; Sanchez-Madrid and Serrador, 2009), which is in sharp contrast with other cell types. This idea is supported by multiple primary research reports using lymphocytes in vitro (Lee et al., 2004; Ratner et al., 1997; Serrador et al., 1997; Takesono et al., 2010). However, where microtubules are localized in neutrophils migrating in vitro is more controversial: several studies suggested that the MTOC is localized in front of the nucleus (Malech et al., 1977; Schliwa et al., 1982) and others suggested that microtubules nucleate between nuclear lobes (Anderson et al., 1982) or behind the nucleus (Anderson et al., 1982; Xu et al., 2005). In contrast to non-leukocyte cells where the microtubules radiate towards the leading edge, the microtubule arrays extend towards the rear in neutrophils (Eddy et al., 2002; Xu et al., 2005). Little is known about how microtubules regulate neutrophil migration in three-dimensional (3D) tissue environments *in vivo*. Evidence that the biological context matters is revealed by studies showing that what is essential for migration in vitro can be dispensable *in vivo*, or vice versa (Lammermann et al., 2008; Yoo et al., 2010).

To assess microtubule dynamics and function during neutrophil migration *in vivo*, we used zebrafish larvae, which have been an emerging tool to study immune responses and leukocyte migration in physiological contexts (Deng et al., 2012; Deng et al., 2011; Mathias et al., 2006; Niethammer et al., 2009; Trede et al., 2004; Yoo et al., 2010; Yoo and Huttenlocher, 2011; Yoo et al., 2011). Previously we have shown that phosphoinositol 3-kinase (PI(3)K) regulates neutrophil motility through both the modulation of Rac-mediated protrusion and polarity of F-actin dynamics in zebrafish (Yoo et al., 2010). Here, we investigated the role of microtubules during neutrophil 3D

motility. We demonstrate that microtubules nucleate in front of the nucleus, mainly radiating towards the uropod, and that microtubule disassembly induces neutrophil motility at least in part through the activation of both Rho and Rac in a PI(3)K-independent manner.

Results

To determine how microtubules regulate neutrophil motility *in vivo*, first we sought to visualize microtubule dynamics in neutrophils migrating rapidly in intact tissues in living zebrafish. Such imaging has not been demonstrated *in vivo*. Neutrophils migrate spontaneously and display apparent random motility in the mesenchyme of the head at 2–3 days post fertilization (dpf) by as-yet-unidentified mechanisms (Yoo et al., 2010). We used this system to study neutrophil motility as previously reported (Yoo et al., 2010). We constructed multiple bioprobes and expressed them in neutrophils by using the neutrophil-specific mpx or lyz promoter to visualize microtubule dynamics in zebrafish larvae (Kitaguchi et al., 2009; Mathias et al., 2006). We first employed GFP-tubulin, which has traditionally been used to image microtubules in live cells (Small et al., 2002). GFP-tubulin revealed a relatively bright dot in front of the nucleus (Fig. 1A; supplementary material Movie 1). This punctate dot is presumably the MTOC because the nucleation site of microtubule arrays appears as a point containing the strongest signals (Anderson et al., 1982; Eddy et al., 2002); see also below). In migrating neutrophils, the dot appeared to lead the nucleus (Fig. 1A), based on comparison of GFP-tubulin to soluble mCherry, which, unlike GFP-tubulin, is small enough to pass freely into and out of the nucleus.

In our imaging setting using rapidly migrating neutrophils in zebrafish, the GFP-tubulin failed to reveal structures likely to be individual microtubules due to high background fluorescence. Consequently, we next tried three tandem GFPs fused to the ensconsin microtubule-binding domain (EMTB-3xGFP) which was previously shown to provide higher contrast (relative to GFP-tubulin) microtubule imaging in live cultured

cells as well as echinoderm embryos (Faire et al., 1999; von Dassow et al., 2009). EMTB-3xGFP yielded more signal than GFP-tubulin, and also showed a punctate dot in front of the nucleus and some linear structures (presumably microtubules) radiating from the putative MTOC (Fig. 1B; supplementary material Movie 2). However, the EMTB probe only rarely yielded structures that could clearly be interpreted as microtubules and therefore we tried an additional probe, EB3-GFP. EB3 is a plus end-binding protein (+TIP) (Hu et al., 2008; Stepanova et al., 2003). +TIPs specifically label plus ends at low expression but labels all microtubule filaments at high expression (Stepanova et al., 2003; Stramer et al., 2010; Xu et al., 2005). Thus, +TIPs, such as CLIP170, have been used to label the whole microtubule arrays as well as plus ends (Stramer et al., 2010; Xu et al., 2005). Imaging of EB3-GFP revealed that microtubules nucleate from a MTOC positioned in front of the nucleus and mainly radiate towards the tail (Fig. 1C; supplementary material Movie 3). We also noticed that very faint microtubule filaments occasionally enter the pseudopods at the leading edge, but microtubule arrays radiating backwards were more dominant. Although the location of the nucleus was obvious due to exclusion of fluorescent signals from the nucleus (see also above), we confirmed that microtubules nucleate in front of the nucleus using a nucleus probe, mCherry-histone H2B (Fig. 1E; supplementary material Movie 4). The MTOC was mainly localized in front of the nucleus, but occasionally and transiently, it also localized on the side of the nucleus (supplementary material Fig. S1; Movie 4). We also used GFP-Tau, which is widely used to visualize microtubules in Drosophila and Xenopus *in vivo* (Brand, 1995; Kwan and Kirschner, 2005). This microtubule probe also revealed that microtubules nucleate in front of the nucleus and radiate towards the uropod (Fig. 1D; supplementary

material Movie 5). Localization of the microtubule arrays towards the uropod is consistent with previous findings in vitro (Eddy et al., 2002; Xu et al., 2005), but the MTOC localization in front of the nucleus is different from the prevailing idea that leukocytes have the MTOC at the rear of the cell (Friedl and Weigelin, 2008; Sanchez-Madrid and del Pozo, 1999; Sanchez-Madrid and Serrador, 2009). Thus, we employed γtubulin-GFP (Joshi, 1993), which labels the MTOC, to further confirm our findings and to exclude the possibility that localization of the MTOC is due to overexpression effects of the microtubule probes. Live imaging by γtubulin-GFP unambiguously showed that the MTOC is localized in front of the nucleus (Fig. 2; supplementary material Movie 6). While none of the microtubule probes employed permitted us to assay the dynamics of individual microtubules, possibly because the microtubules in these rapidly migrating cells turnover very rapidly, they nonetheless collectively indicate that microtubules nucleate in front of the nucleus and radiate towards the uropod during neutrophil motility in zebrafish. Immunostaining of zebrafish microtubules using multiple fixation conditions was also not successful, presumably due to the rapid turnover of microtubules or proteolytic enzymes in neutrophils.

We next assessed how microtubules regulate neutrophil migration *in vivo*. Microtubule depolymerization using nocodazole or colchicine impairs neutrophil directional migration but enhances neutrophil motility in vitro, presumably through Rho activation (Niggli, 2003; Xu et al., 2005). To determine whether this knowledge could be also applied to neutrophil motility *in vivo*, first we investigated the effects of microtubule depolymerization on neutrophil wound attraction, which is suitable for studying directional migration of neutrophils *in vivo* (Mathias et al., 2006; Niethammer et al.,

2009; Yoo et al., 2010; Yoo et al., 2011). We examined the effects of microtubule disassembly induced by nocodazole on neutrophil attraction to wounds at 30 minutes after wounding, a time point when neutrophil accumulation at wounds is not affected by reverse migration (Mathias et al., 2006; Niethammer et al., 2009; Yoo et al., 2010; Yoo and Huttenlocher, 2011; Yoo et al., 2011). Microtubule depolymerization impaired neutrophil directional attraction to wounds (Fig. 3A), consistent with findings in neutrophils in vitro (Xu et al., 2005) and macrophages in zebrafish (Redd et al., 2006). Next we focused on the effects of microtubule depolymerization on neutrophil random motility and F-actin polarity in the mesenchymal tissues of the head. Microtubule depolymerization with nocodazole enhanced motility and induced a more round, compact morphology (Fig. 3B–D; supplementary material Movie 7). Microtubule inhibition also enhanced polarity of F-actin dynamics (Fig. 3E), which was detected with Lifeact-Ruby (a probe for all F-actin) and GFP-UtrCH (a probe for stable F-actin) (Burkel et al., 2007; Riedl et al., 2008; Yoo et al., 2010). Nocodazole particularly emphasized tail localization of stable F-actin detected by GFP-UtrCH, presumably due to the well-established Rho-myosin activation by microtubule depolymerization (Niggli, 2003; Rodriguez et al., 2003; Wittmann and Waterman-Storer, 2001; Xu et al., 2005). Our findings are mainly consistent with findings reported for neutrophils in vitro (Xu et al., 2005), but one noticeable difference is that we did not observe decreased dynamic F-actin at the leading edge after microtubule depolymerization. This is in contrast to in vitro effects of microtubule depolymerization (Xu et al., 2005): nocodazole treatment disturbs F-actin at the leading edge of neutrophils in vitro. This implies that, in 3D tissues *in vivo*, microtubule disassembly activates ‘backness’ signals such as stable F-

actin, presumably through Rho, at the tail, but that it may also maintain ‘frontness’ signals (dynamic F-actin) during neutrophil migration.

To investigate the molecular mechanisms by which microtubules regulate neutrophil motility, we focused on PI(3)K signaling, which we recently found to regulate neutrophil motility in all contexts examined in zebrafish larvae, including wound attraction, reverse migration away from wounds, attraction to bacteria and interstitial motility in the head (Deng et al., 2012; Yoo et al., 2010). Interestingly, microtubule depolymerization-mediated neutrophil migration in vitro is independent of PI(3)K and is, in fact, inhibitory to PI(3)K signaling (Niggli, 2003; Xu et al., 2005). PHAKT-GFP (PH domain of AKT), a bioprobe for PI(3)K products PI(3,4,5)P3–PI(3,4)P2, and mCherry were expressed in neutrophils to detect PI(3)K signaling by ratiometric analysis (Yoo et al., 2010). In control, PI(3,4,5)P3–PI(3,4)P2 is localized at the leading edge as previously reported (Yoo et al., 2010), but microtubule depolymerization completely depleted PI(3,4,5)P3–PI(3,4)P2 signals at the leading edge (Fig. 4A,B; supplementary material Movie 8). This indicates that PI(3)K signaling is inhibited during nocodazole-induced neutrophil motility, suggesting that microtubule disassembly mediates neutrophil migration in a PI(3)K-independent manner. To test this hypothesis, we investigated whether microtubule depolymerization can rescue migration and F-actin polarity defects induced by PI(3)K inhibition. PI(3)K inhibition with LY294002 impairs neutrophil motility and F-actin polarity as previously reported (Fig. 5A,B) (Yoo et al., 2010). Nocodazole treatment not only reversed the effects of PI(3)K inhibition but further increased neutrophil migration and F-actin polarity compared to DMSO treatment (Fig. 5A,B; supplementary material Movie 9). Our findings indicate that microtubule

disassembly induces neutrophil motility in a PI(3)K-independent manner, in agreement with in vitro studies (Niggli, 2003; Xu et al., 2005). Moreover, the findings suggest that microtubule disruption is sufficient to rescue migration of PI(3)K inhibited cells *in vivo*, in contrast to localized Rac activation (Yoo et al., 2010).

Next we investigated how microtubule inhibition promotes neutrophil motility without PI(3)K activation. Rho was an obvious target because Rho, Rho kinase and myosin 2 are activated by microtubule disassembly in diverse cells including tumor cells, fibroblasts, Xenopus oocytes and leukoctyes (Etienne-Manneville, 2004; Kaverina and Straube, 2011; Mogilner and Keren, 2009; Rodriguez et al., 2003; Small et al., 2002; Takesono et al., 2010; Vinogradova et al., 2009; Watanabe et al., 2005; Wittmann and Waterman-Storer, 2001). Although how microtubule disassembly activates Rho pathways is not completely understood, Rho GEFs, particularly GEF-H1 and p190RhoGEF, which are activated upon release from microtubule arrays, are considered to be important for this process (Krendel et al., 2002; Ren et al., 1998; Small et al., 2002; van Horck et al., 2001). In addition, activation of Rho signaling mediates microtubule disassembly-induced neutrophil motility in vitro (Niggli, 2003; Xu et al., 2005). Thus, we examined whether Rho is also responsible for neutrophil motility induced by microtubule depolymerization *in vivo*. To specifically inhibit Rho in zebrafish neutrophils, we expressed a dominant negative RhoA T19N, which binds to GDP but not GTP, in neutrophils using the neutrophil-specific mpx promoter (Yoo et al., 2010). As previously reported, RhoA T19N inhibits neutrophil motility, inducing a rounded morphology (Fig. 6A,B) (Yoo et al., 2010). Microtubule disassembly using nocodazole slightly mobilized RhoA T19N expressing neutrophils but this effect was subtle, and

generally neutrophils with Rho inhibition did not migrate after nocodazole treatment (Fig. 6A). This is consistent with the idea that microtubules regulate cell motility through Rho. However, we found that Rho-inhibited cells protruded the leading edge extensively after nocodazole treatment (Fig. 6B; supplementary material Movie 10). In combination with the data that dynamic F-actin at the leading edge is intact after microtubule depolymerization (Fig. 3E), this suggested the possibility that microtubule disassembly may maintain or even promote frontness signals in addition to its well-known role in mediating Rho-mediated backness signals. To test this possibility, we focused on Rac2, a hematopoietic specific Rho family GTPase, which regulates neutrophil motility, promoting F-actin polymerization downstream of PI(3)K (Deng et al., 2011). As previously reported (Deng et al., 2011), Rac2 knockdown by morpholino antisense oligonucleotide inhibits neutrophil motility, making neutrophils more round and compacted than control neutrophils (Fig. 7A–C). We tested whether microtubule disassembly reverses motility arrest induced by Rac2 knockdown, as it did with PI(3)K-inhibited cells (Fig. 5B). If microtubule depolymerization induces cell motility only through enhancing Rho-mediated actomyosin tail contraction (Niggli, 2003; Xu et al., 2005), nocodazole should release the motility arrest caused by Rac2 knockdown. We found that nocodazole induced a further round, compact morphology of Rac2-deficient neutrophils, like nocodazole-treated control neutrophils, but that it did not induce neutrophil motility (Fig. 7A–C; supplementary material Movie 11). In addition, transgenic expression of dominant negative Rac2 D57N in neutrophils (Deng et al., 2011) also inhibited nocodazole-induced motility (Fig. 7D; supplementary material Movie 12). This indicates that Rac2 is necessary for microtubule depolymerization-induced motility in

addition to Rho. To further test whether microtubule depolymerization directly activates Rac as well as Rho in mammalian neutrophils in a cell autonomous manner, we purified primary human neutrophils and performed affinity precipitation assays with GST-RBD and GST-PBD, to which only the active GTP-bound forms of Rho and Rac bind respectively (Benard et al., 1999; Nishita et al., 2002; Ren et al., 1999). As shown in Fig. 7E, microtubule disassembly directly activated Rac in addition to Rho in primary human neutrophils (Fig. 7E). Taken together, our data suggest that microtubule disassembly induces neutrophil 3D motility through both Rac and Rho-dependent pathways.

Discussion

Here we investigated microtubule dynamics and function during neutrophil migration *in vivo*. In accordance with reported in vitro findings, we found that microtubule disruption impairs neutrophil directed migration to wounds but induces cell motility and polarity in a PI(3)K-independent manner. We also found that Rho mediates nocodazole-induced neutrophil motility. These findings are consistent with previous findings in vitro, but further provide a physiological context for neutrophil migration. In addition, we elucidated two previously unidentified roles of microtubules during neutrophil motility *in vivo*. First, microtubule arrays nucleate in front of the nucleus and mainly radiate towards the uropod. Second, Rac is activated by microtubule depolymerization in primary human neutrophils and is necessary for nocodazole-induced neutrophil motility *in vivo*.

Leukocytes are often described as having the microtubule cytoskeleton and MTOC behind the nucleus at the uropod (Friedl and Weigelin, 2008; Sanchez-Madrid and del Pozo, 1999; Sanchez-Madrid and Serrador, 2009). We found that microtubule arrays radiate towards the uropod, which is consistent with the idea that leukocytes have microtubules at the uropod. Microtubules visualized in zebrafish neutrophils have similar structures to those imaged in fixed human neutrophils in vitro (Eddy et al., 2002). However, our finding that microtubules nucleate from the MTOC in front of the nucleus is very different from what has been reported from in vitro studies. This suggests that we need to revise the widespread model that leukocytes have the MTOC at the rear.

Our findings that microtubule depolymerization activates Rac in addition to Rho is also different from what was previously thought. Microtubule-mediated antagonistic regulation of Rho, presumably through Rho GEFs such as GEF-H1 and p190RhoGEF, has been observed in diverse systems including tumor cells, fibroblasts, Xenopus oocytes and leukocytes (Etienne-Manneville, 2004; Kaverina and Straube, 2011; Mogilner and Keren, 2009; Rodriguez et al., 2003; Small et al., 2002; Takesono et al., 2010; Vinogradova et al., 2009; Watanabe et al., 2005; Wittmann and Waterman-Storer, 2001). On the other hand, microtubule polymerization is known to activate Rac in fibroblasts (Waterman-Storer et al., 1999; Wittmann and Waterman-Storer, 2001), suggesting a concept that microtubules regulate Rho negatively and Rac positively. However, using zebrafish neutrophils *in vivo* and primary human neutrophils in vitro, we have shown that microtubule disruption activates Rac and induces neutrophil motility in a Rac-dependent manner. The difference between our findings and previous findings are most likely due to difference in the cell types. How microtubules regulate Rac in neutrophils is not clear yet, but we speculate that two mechanisms are possible. The first possibility is that similar mechanisms to microtubule-mediated Rho regulation, such as regulation of Rac GEFs, might regulate Rac activity in neutrophils. The second possibility is that the well-known antagonistic effects of Rho on Rac activity (Small et al., 2002; Wittmann and Waterman-Storer, 2001) might occur locally in neutrophils due to the highly polarized sequestration of Rho at the tail, leading to relative activation of Rac at the leading edge and also at the whole cell level. To further elucidate the role of Rho GTPase signaling in zebrafish neutrophils would require tools that are not currently available in zebrafish including inducible or tissue specific knockdowns. Moreover, we

tried to use biosensors for Rho GTPase activation in zebrafish neutrophils but the probes had toxic effects precluding further analysis of the polarity of Rho GTPase activation in zebrafish neutrophils *in vivo* at this time.

Our current findings *in vivo*, together with previous in vitro studies (Niggli, 2003; Xu et al., 2005), suggest that microtubules regulate neutrophil directional migration positively and motility negatively. Both Rac and Rho are involved in microtubule-mediated suppression of motility, but how microtubules control directional migration remains elusive. One interesting correlation with the directional migration defects induced by microtubule disassembly is that nocodazole inhibits PI(3)K activation at the leading edge. PI(3)K regulates neutrophil motility through the regulation of both Rho and Rac (Van Keymeulen et al., 2006; Yoo et al., 2010). This implies the possibility that microtubule disassembly renders neutrophils blind to attraction signals due to inactivation of PI(3)K, which is indispensable for orchestrating cell migration upstream of Rho and Rac. In the current study, we addressed how microtubules regulate cell motility through Rho and Rac, but it is noticeable that both Rho and Rac also regulate microtubules dynamics (Palazzo et al., 2001; Takesono et al., 2010; Wittmann et al., 2004), suggesting intricate feedback systems among Rho, Rac and microtubules.

Beyond the insights of our findings to the basic mechanisms that regulate leukocyte migration, it is intriguing to note that many microtubule depolymerizing agents are clinically used as anti-inflammatory drugs to treat chronic inflammatory diseases (Cocco et al., 2010). However, the mechanisms by which microtubule depolymerizing drugs alleviate inflammatory symptoms are not known. Neutrophils from patients with autoinflammatory diseases show migration defects (Huttenlocher et al., 1995; Lokuta et

al., 2005). Further, resolution of neutrophilic inflammation is accomplished by neutrophil reverse migration away from wounded tissues in zebrafish (Mathias et al., 2006; Yoo and Huttenlocher, 2011). Neutrophil reverse migration away from injured tissues has also been observed in mice (Woodfin et al., 2011). Taken together with our current findings that microtubule disassembly induces neutrophil motility *in vivo*, this suggests an intriguing paradigm that inflammatory diseases might occur due to leukocyte migration defects or retention of leukocytes at inflammatory sites, which could be resolved by microtubule disassembly-mediated neutrophil motility.

Here, for the first time, we have visualized the dynamics of microtubules during neutrophil migration in intact tissues *in vivo*. We demonstrated that the microtubule cytoskeleton suppresses neutrophil polarity and motility through negative regulation of both Rho and Rac activity in a PI(3)K-independent manner. Together with our previous findings that PI(3)K regulates neutrophil motility through both the modulation of Rac-mediated protrusion and polarity of F-actin dynamics, we have now begun to understand the complex mechanisms that regulate 3D neutrophil migration *in vivo*. Undoubtedly, by using the genetically tractable and optically transparent vertebrate, zebrafish, we will be able to further illuminate the molecular mechanisms that orchestrate cell migration within complex tissues *in vivo*.

Materials and methods

Zebrafish maintenance and general procedures

Adult AB zebrafish and larvae were maintained as described previously (Yoo et al., 2010). For live imaging or wounding assay, larvae were anesthetized in E3 containing 0.2 mg/ml Tricaine (ethyl 3-aminobenzoate, Sigma-Aldrich). To prevent pigment formation, some larvae were maintained in E3 containing 0.2 mM N-phenylthiourea (PTU, Sigma-Aldrich). For all experiments, 2.5–3 dpf larvae were used. When drugs were used, larvae were pretreated at least for 20 minutes before experiments (0.5–2 μM nocodazole, 65 μM LY294002). Neutrophils were stained with Sudan Black as previously described (Yoo et al., 2010; Yoo and Huttenlocher, 2011).

Morpholino injection

Three nanoliters of Rac2 MO (Deng et al., 2011) at a final concentration of 100 μM was injected into 1-cell-stage embryos. Danieau buffer [58 mM NaCl, 0.7 mM KCl, 0.4 mM MgSO4, 0.6 mM Ca(NO3)2, 5.0 mM HEPES pH 7.1–7.3] was injected as a control.

Plasmid construction and injection

GFP-αtubulin was subcloned into the backbone vector with the mpx promoter (Mathias et al., 2006), minimal tol2 elements (Urasaki et al., 2006) and a SV40 polyadenylation sequence as previously described (Yoo et al., 2010). EMTB-3xGFP (Faire et al., 1999; von Dassow et al., 2009), EB3-GFP (Hu et al., 2008; Stepanova et al., 2003), GFP-Tau (human Tau: IMAGE:40007445), mCherry-histone H2B (von

Dassow et al., 2009), γtubulin-GFP or Dendra2-Rho T19N (Yoo et al., 2010) was subcloned into the backbone vector with the lyz promoter (Kitaguchi et al., 2009), minimal tol2 elements (Urasaki et al., 2006) and a SV40 polyadenylation sequence. Three nanoliters of solution containing 12.5 ng/μl DNA plasmid and 17.5 ng/μl transposase mRNA was injected into the cytoplasm of one-cell stage embryos.

Image acquisition and analysis

Except data of Fig. 2 and supplementary material Movie 6, time-lapse fluorescence images were acquired in 2–3 dpf larvae with a confocal microscope (FluoView FV1000, Olympus) using a NA 0.75/20× objective or a NA 1.10/60× water immersion objective lens as previously described (Yoo et al., 2010). For images in Fig. 2 and supplementary material Movie 6, we used a Spinning disk confocal microscope (Yokogawa CSU-X) with confocal scanhead on a Zeiss Observer Z.1 inverted microscope (NA1.3/60× water immersion objective). A Photometrics Evolve EMCCD camera was used to acquire the images. Z-series images were acquired using a 0.4 μM step size and 300 EM gain. Maximum intensity projection images were made using the Zen 2011 (blue edition) software (Carl Zeiss). Neutrophils were tracked and analyzed by using plugins MTrackj (3D tracking), Manual tracking (2D tracking) and Chemotaxis and Migration tool (ibidi) for ImageJ (NIH, Bethesda, MD). Neutrophil area and roundness were measured using ‘analyze’ function of ImageJ. To measure roundness, 4×area/π×major_axis2 was calculated. Data of time-lapse images represent at least three separate movies.

Purification of human neutrophils and affinity precipitation assays

Blood was obtained from healthy donors with informed consent. Neutrophils were purified using Polymorphprep (Nycomed Pharma AS) as previously reported (Yoo et al., 2011). Purified neutrophils were suspended in PBS at 1.5–2.5×107 cells/ml. 1×107 Cells were pretreated with DMSO or 10 μM nocodazole in a 37°C/5% CO2 incubator for 30 minutes. Affinity precipitation assays of Rho and Rac were performed as previously described (Nishita et al., 2002). Briefly, cell activation was stopped by addition of equal volume of 2×lysis/kinase buffer for 20 min on ice. After centrifugation, the supernatant was mixed with 60 μg GST-RBD or 15 μg GST-PBD bound to glutathione-Sepharose (Cytoskeleton) and incubated at 4°C for 1 h. The bead pellets were washed three times with 1×lysis/kinase buffer, suspended in 35 μl of Laemmli sample buffer, and analyzed by immunoblotting using an antibody to RhoA (Cell Signaling, 67B9) or Rac (Cell Signaling, no. 2465).

Statistics

Assuming Gaussian distribution of overall population of values, P values were derived by the following analyses. Two-tailed unpaired t-test: Fig. 3B–D. Two-tailed paired t-test: Fig. 7E. One-way ANOVA with Dunnett post-test: Fig. 3A. One-way ANOVA with Tukey post-test: Fig. 5B. One-way ANOVA with Bonferroni post-test: Fig. 7B,C.

Acknowledgements

We thank K. B. Walters for construction of tol2-mpx-GFP-tubulin plasmid, Q. Deng for construction of tol2-lyz-Dendra2-RhoT19N plasmid, E. Dent and N. Galjart for generous gift of EB3-GFP plasmid and T. W. Starnes for insightful discussion and critical reading of the manuscript.

Funding

This work was supported by a American Heart Association fellowship [number 11PRE4890041 to S.Y.]; and the National Institutes of Health [grant numbers GM052932 to W.M.B., GM074827 to A.H.]. Deposited in PMC for release after 12 months.

References

Anderson, D.C., L.J. Wible, B.J. Hughes, C.W. Smith, and B.R. Brinkley. 1982. Cytoplasmic microtubules in polymorphonuclear leukocytes: effects of chemotactic stimulation and colchicine. *Cell*. 31:719-29.

Benard, V., B.P. Bohl, and G.M. Bokoch. 1999. Characterization of rac and cdc42 activation in chemoattractant-stimulated human neutrophils using a novel assay for active GTPases. *J Biol Chem*. 274:13198-204.

Brand, A. 1995. GFP in Drosophila. *Trends Genet*. 11:324-5.

Burkel, B.M., G. von Dassow, and W.M. Bement. 2007. Versatile fluorescent probes for actin filaments based on the actin-binding domain of utrophin. *Cell Motil Cytoskeleton*. 64:822-32.

Cocco, G., D.C. Chu, and S. Pandolfi. 2010. Colchicine in clinical medicine. A guide for internists. *Eur J Intern Med*. 21:503-8.

Deng, Q., E.A. Harvie, and A. Huttenlocher. 2012. Distinct signalling mechanisms mediate neutrophil attraction to bacterial infection and tissue injury. *Cell Microbiol*. 14:517-28.

Deng, Q., S.K. Yoo, P.J. Cavnar, J.M. Green, and A. Huttenlocher. 2011. Dual roles for Rac2 in neutrophil motility and active retention in zebrafish hematopoietic tissue. *Dev Cell*. 21:735-45.

Eddy, R.J., L.M. Pierini, and F.R. Maxfield. 2002. Microtubule asymmetry during neutrophil polarization and migration. *Mol Biol Cell*. 13:4470-83.

Etienne-Manneville, S. 2004. Actin and microtubules in cell motility: which one is in control? *Traffic*. 5:470-7.

Euteneuer, U., and M. Schliwa. 1984. Persistent, directional motility of cells and cytoplasmic fragments in the absence of microtubules. *Nature*. 310:58-61.

Faire, K., C.M. Waterman-Storer, D. Gruber, D. Masson, E.D. Salmon, and J.C. Bulinski. 1999. E-MAP-115 (ensconsin) associates dynamically with microtubules *in vivo* and is not a physiological modulator of microtubule dynamics. *J Cell Sci*. 112 (Pt 23):4243-55.

Friedl, P., and B. Weigelin. 2008. Interstitial leukocyte migration and immune function. *Nat Immunol*. 9:960-9.

Hu, X., C. Viesselmann, S. Nam, E. Merriam, and E.W. Dent. 2008. Activity-dependent dynamic microtubule invasion of dendritic spines. *J Neurosci*. 28:13094-105.

Huttenlocher, A., I.J. Frieden, and H. Emery. 1995. Neonatal onset multisystem inflammatory disease. *J Rheumatol*. 22:1171-3.

Joshi, H.C. 1993. Gamma-tubulin: the hub of cellular microtubule assemblies. *Bioessays*. 15:637-43.

Kaverina, I., and A. Straube. 2011. Regulation of cell migration by dynamic microtubules. *Semin Cell Dev Biol*. 22:968-74.

Kitaguchi, T., K. Kawakami, and A. Kawahara. 2009. Transcriptional regulation of a myeloid-lineage specific gene lysozyme C during zebrafish myelopoiesis. *Mech Dev*. 126:314-23.

Krendel, M., F.T. Zenke, and G.M. Bokoch. 2002. Nucleotide exchange factor GEF-H1 mediates cross-talk between microtubules and the actin cytoskeleton. *Nat Cell Biol*. 4:294-301.

Kwan, K.M., and M.W. Kirschner. 2005. A microtubule-binding Rho-GEF controls cell morphology during convergent extension of Xenopus laevis. *Development*. 132:4599-610.

Lammermann, T., B.L. Bader, S.J. Monkley, T. Worbs, R. Wedlich-Soldner, K. Hirsch, M. Keller, R. Forster, D.R. Critchley, R. Fassler, and M. Sixt. 2008. Rapid leukocyte migration by integrin-independent flowing and squeezing. *Nature*. 453:51-5.

Lee, J.H., T. Katakai, T. Hara, H. Gonda, M. Sugai, and A. Shimizu. 2004. Roles of p-ERM and Rho-ROCK signaling in lymphocyte polarity and uropod formation. *J Cell Biol*. 167:327-37.

Lokuta, M.A., K.M. Cooper, I. Aksentijevich, D.L. Kastner, and A. Huttenlocher. 2005. Neutrophil chemotaxis in a patient with neonatal-onset multisystem inflammatory disease and Muckle-Wells syndrome. *Ann Allergy Asthma Immunol*. 95:394-9.

Malech, H.L., R.K. Root, and J.I. Gallin. 1977. Structural analysis of human neutrophil migration. Centriole, microtubule, and microfilament orientation and function during chemotaxis. *J Cell Biol*. 75:666-93.

Mathias, J.R., B.J. Perrin, T.X. Liu, J. Kanki, A.T. Look, and A. Huttenlocher. 2006. Resolution of inflammation by retrograde chemotaxis of neutrophils in transgenic zebrafish. *J Leukoc Biol*. 80:1281-8.

Mogilner, A., and K. Keren. 2009. The shape of motile cells. *Curr Biol*. 19:R762-71.

Niethammer, P., C. Grabher, A.T. Look, and T.J. Mitchison. 2009. A tissue-scale gradient of hydrogen peroxide mediates rapid wound detection in zebrafish. *Nature*. 459:996-9.

Niggli, V. 2003. Microtubule-disruption-induced and chemotactic-peptide-induced migration of human neutrophils: implications for differential sets of signalling pathways. *J Cell Sci*. 116:813-22.

Nishita, M., H. Aizawa, and K. Mizuno. 2002. Stromal cell-derived factor 1alpha activates LIM kinase 1 and induces cofilin phosphorylation for T-cell chemotaxis. *Mol Cell Biol*. 22:774-83.

Palazzo, A.F., T.A. Cook, A.S. Alberts, and G.G. Gundersen. 2001. mDia mediates Rho-regulated formation and orientation of stable microtubules. *Nat Cell Biol*. 3:723-9.

Ratner, S., W.S. Sherrod, and D. Lichlyter. 1997. Microtubule retraction into the uropod and its role in T cell polarization and motility. *J Immunol*. 159:1063-7.

Redd, M.J., G. Kelly, G. Dunn, M. Way, and P. Martin. 2006. Imaging macrophage chemotaxis *in vivo*: studies of microtubule function in zebrafish wound inflammation. *Cell Motil Cytoskeleton*. 63:415-22.

Ren, X.D., W.B. Kiosses, and M.A. Schwartz. 1999. Regulation of the small GTP-binding protein Rho by cell adhesion and the cytoskeleton. *EMBO J*. 18:578-85.

Ren, Y., R. Li, Y. Zheng, and H. Busch. 1998. Cloning and characterization of GEF-H1, a microtubule-associated guanine nucleotide exchange factor for Rac and Rho GTPases. *J Biol Chem*. 273:34954-60.

Riedl, J., A.H. Crevenna, K. Kessenbrock, J.H. Yu, D. Neukirchen, M. Bista, F. Bradke, D. Jenne, T.A. Holak, Z. Werb, M. Sixt, and R. Wedlich-Soldner. 2008. Lifeact: a versatile marker to visualize F-actin. *Nat Methods*. 5:605-7.

Rodriguez, O.C., A.W. Schaefer, C.A. Mandato, P. Forscher, W.M. Bement, and C.M. Waterman-Storer. 2003. Conserved microtubule-actin interactions in cell movement and morphogenesis. *Nat Cell Biol*. 5:599-609.

Sanchez-Madrid, F., and M.A. del Pozo. 1999. Leukocyte polarization in cell migration and immune interactions. *EMBO J*. 18:501-11.

Sanchez-Madrid, F., and J.M. Serrador. 2009. Bringing up the rear: defining the roles of the uropod. *Nat Rev Mol Cell Biol*. 10:353-9.

Schliwa, M., K.B. Pryzwansky, and U. Euteneuer. 1982. Centrosome splitting in neutrophils: an unusual phenomenon related to cell activation and motility. *Cell*. 31:705-17.

Serrador, J.M., J.L. Alonso-Lebrero, M.A. del Pozo, H. Furthmayr, R. Schwartz-Albiez, J. Calvo, F. Lozano, and F. Sanchez-Madrid. 1997. Moesin interacts with the cytoplasmic region of intercellular adhesion molecule-3 and is redistributed to the uropod of T lymphocytes during cell polarization. *J Cell Biol*. 138:1409-23.

Siegrist, S.E., and C.Q. Doe. 2007. Microtubule-induced cortical cell polarity. *Genes Dev*. 21:483-96.

Small, J.V., B. Geiger, I. Kaverina, and A. Bershadsky. 2002. How do microtubules guide migrating cells? *Nat Rev Mol Cell Biol*. 3:957-64.

Stepanova, T., J. Slemmer, C.C. Hoogenraad, G. Lansbergen, B. Dortland, C.I. De Zeeuw, F. Grosveld, G. van Cappellen, A. Akhmanova, and N. Galjart. 2003. Visualization of microtubule growth in cultured neurons via the use of EB3-GFP (end-binding protein 3-green fluorescent protein). *J Neurosci*. 23:2655-64.

Stramer, B., S. Moreira, T. Millard, I. Evans, C.Y. Huang, O. Sabet, M. Milner, G. Dunn, P. Martin, and W. Wood. 2010. Clasp-mediated microtubule bundling regulates persistent motility and contact repulsion in Drosophila macrophages *in vivo*. *J Cell Biol*. 189:681-9.

Takesono, A., S.J. Heasman, B. Wojciak-Stothard, R. Garg, and A.J. Ridley. 2010. Microtubules regulate migratory polarity through Rho/ROCK signaling in T cells. *PLoS One*. 5:e8774.

Trede, N.S., D.M. Langenau, D. Traver, A.T. Look, and L.I. Zon. 2004. The use of zebrafish to understand immunity. *Immunity*. 20:367-79.

Urasaki, A., G. Morvan, and K. Kawakami. 2006. Functional dissection of the Tol2 transposable element identified the minimal cis-sequence and a highly repetitive sequence in the subterminal region essential for transposition. *Genetics*. 174:639-49.

van Horck, F.P., M.R. Ahmadian, L.C. Haeusler, W.H. Moolenaar, and O. Kranenburg. 2001. Characterization of p190RhoGEF, a RhoA-specific guanine nucleotide exchange factor that interacts with microtubules. *J Biol Chem*. 276:4948-56.

Van Keymeulen, A., K. Wong, Z.A. Knight, C. Govaerts, K.M. Hahn, K.M. Shokat, and H.R. Bourne. 2006. To stabilize neutrophil polarity, PIP3 and Cdc42 augment RhoA activity at the back as well as signals at the front. *J Cell Biol*. 174:437-45.

Vasiliev, J.M., I.M. Gelfand, L.V. Domnina, O.Y. Ivanova, S.G. Komm, and L.V. Olshevskaja. 1970. Effect of colcemid on the locomotory behaviour of fibroblasts. *J Embryol Exp Morphol*. 24:625-40.

Vinogradova, T., P.M. Miller, and I. Kaverina. 2009. Microtubule network asymmetry in motile cells: role of Golgi-derived array. *Cell Cycle*. 8:2168-74.

von Dassow, G., K.J. Verbrugghe, A.L. Miller, J.R. Sider, and W.M. Bement. 2009. Action at a distance during cytokinesis. *J Cell Biol*. 187:831-45.

Watanabe, T., J. Noritake, and K. Kaibuchi. 2005. Regulation of microtubules in cell migration. *Trends Cell Biol*. 15:76-83.

Waterman-Storer, C.M., R.A. Worthylake, B.P. Liu, K. Burridge, and E.D. Salmon. 1999. Microtubule growth activates Rac1 to promote lamellipodial protrusion in fibroblasts. *Nat Cell Biol*. 1:45-50.

Wittmann, T., G.M. Bokoch, and C.M. Waterman-Storer. 2004. Regulation of microtubule destabilizing activity of Op18/stathmin downstream of Rac1. *J Biol Chem*. 279:6196-203.

Wittmann, T., and C.M. Waterman-Storer. 2001. Cell motility: can Rho GTPases and microtubules point the way? *J Cell Sci*. 114:3795-803.

Woodfin, A., M.B. Voisin, M. Beyrau, B. Colom, D. Caille, F.M. Diapouli, G.B. Nash, T. Chavakis, S.M. Albelda, G.E. Rainger, P. Meda, B.A. Imhof, and S. Nourshargh. 2011. The junctional adhesion molecule JAM-C regulates polarized transendothelial migration of neutrophils *in vivo*. *Nat Immunol*. 12:761-9.

Xu, J., F. Wang, A. Van Keymeulen, M. Rentel, and H.R. Bourne. 2005. Neutrophil microtubules suppress polarity and enhance directional migration. *Proc Natl Acad Sci U S A*. 102:6884-9.

Yoo, S.K., Q. Deng, P.J. Cavnar, Y.I. Wu, K.M. Hahn, and A. Huttenlocher. 2010. Differential regulation of protrusion and polarity by PI3K during neutrophil motility in live zebrafish. *Dev Cell*. 18:226-36.

Yoo, S.K., and A. Huttenlocher. 2011. Spatiotemporal photolabeling of neutrophil trafficking during inflammation in live zebrafish. *J Leukoc Biol*. 89:661-7.

Yoo, S.K., T.W. Starnes, Q. Deng, and A. Huttenlocher. 2011. Lyn is a redox sensor that mediates leukocyte wound attraction *in vivo*. *Nature*.

Fig. 1. Localization of microtubules during neutrophil motility in live zebrafish. (A) Time-lapse imaging of a neutrophil expressing GFP-tubulin and mCherry. Arrows indicate a punctate dot in front of the nucleus. Note that fluorescent signals of GFP-tubulin are excluded from the nucleus. (B) Time-lapse imaging of a neutrophil expressing EMTB-3xGFP. A punctate dot, presumably the MTOC, is indicated by arrows. Arrowheads indicate linear structures (presumably microtubules) extending to the leading edge (magenta) and to the uropod (white). (C) Time-lapse imaging of a neutrophil expressing EB3-GFP. An arrow indicates the MTOC and arrowheads indicate microtubules extending to the leading edge (magenta) and to the uropod (white). (D) Time-lapse imaging of a neutrophil expressing GFP-Tau. An arrow indicates the MTOC and arrowheads indicate microtubules extending to the leading edge (magenta) and to the uropod (white). (E) Time-lapse imaging of a neutrophil expressing EB3-GFP and a nucleus probe mCherry-histone H2B. Data are representative of more than three separate time-lapse movies. Scale bars: 10 μm. (Note: I contributed Fig. 1E and part of Fig. 1A and D where I performed spinning disk confocal imaging of GFP-Tubulin and GFP-Tau to further characterize MTs in neutrophils *in vivo.* I also cloned the *lyz:GFP-Tau* construct and generated the *Tg(mpx:GFP-Tau)* transgenic line.)

Fig. 1

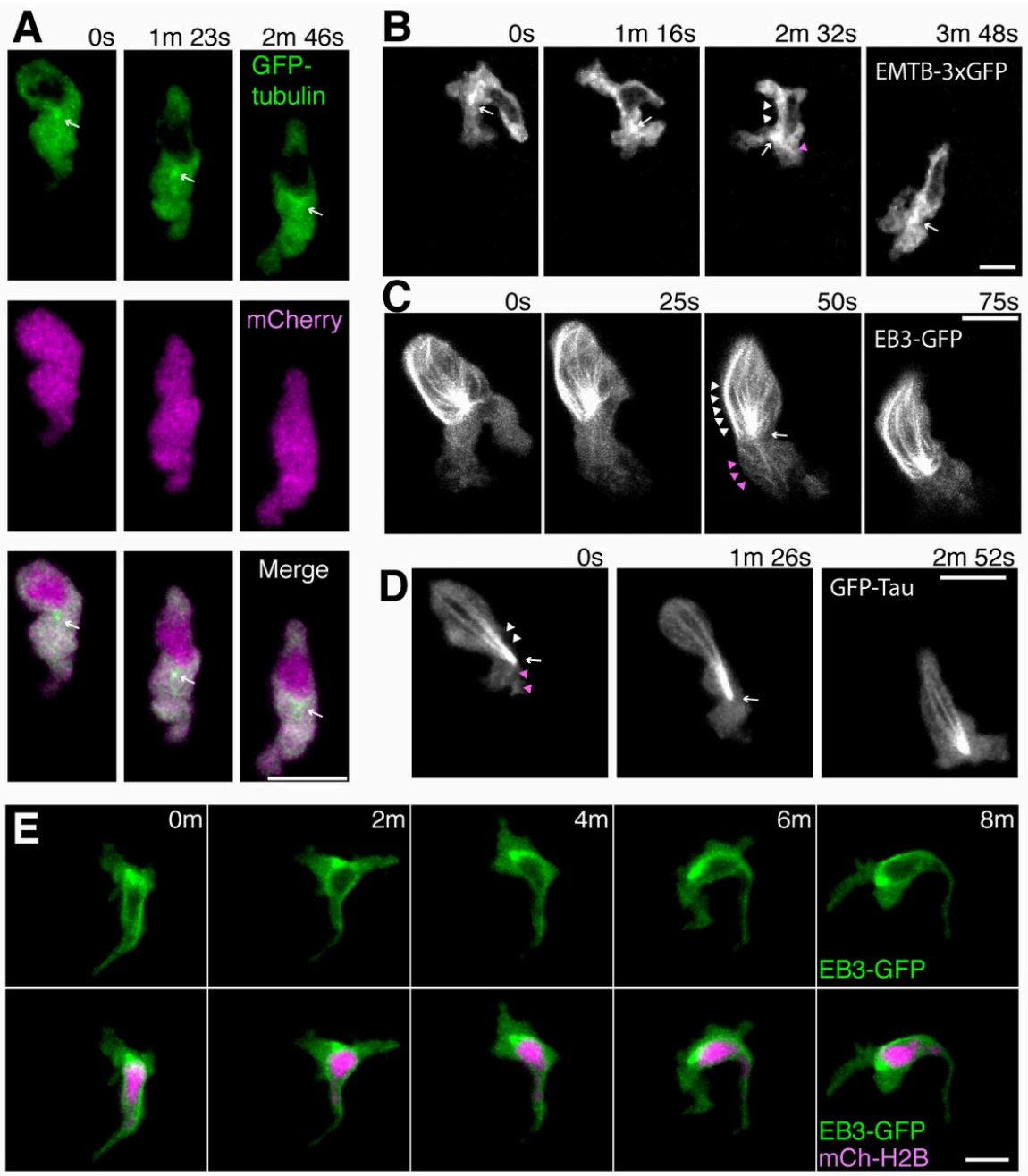
A
0s
1m 23s
2m 46s
GFP-tubulin
mCherry
Merge
B
0s
1m 16s
2m 32s
3m 48s
EMTB-3xGFP
C
0s
25s
50s
75s
EB3-GFP
D
0s
1m 26s
2m 52s
GFP-Tau
E
0m
2m
4m
6m
8m
EB3-GFP
EB3-GFP
mCh-H2B

Fig. 2. The MTOC is localized in front of the nucleus during neutrophil motility in live zebrafish. (A) Time-lapse imaging of a neutrophil expressing γtubulin-GFP. Arrows indicate the MTOC in front of the nucleus. (B) Simultaneous imaging of tubulin-GFP and a nucleus probe mCherry-histone H2B in the same cell with A. Data are representative of more than three separate time-lapse movies. Scale bars: 10 μm. (Note: I contributed this figure.)

Fig. 2

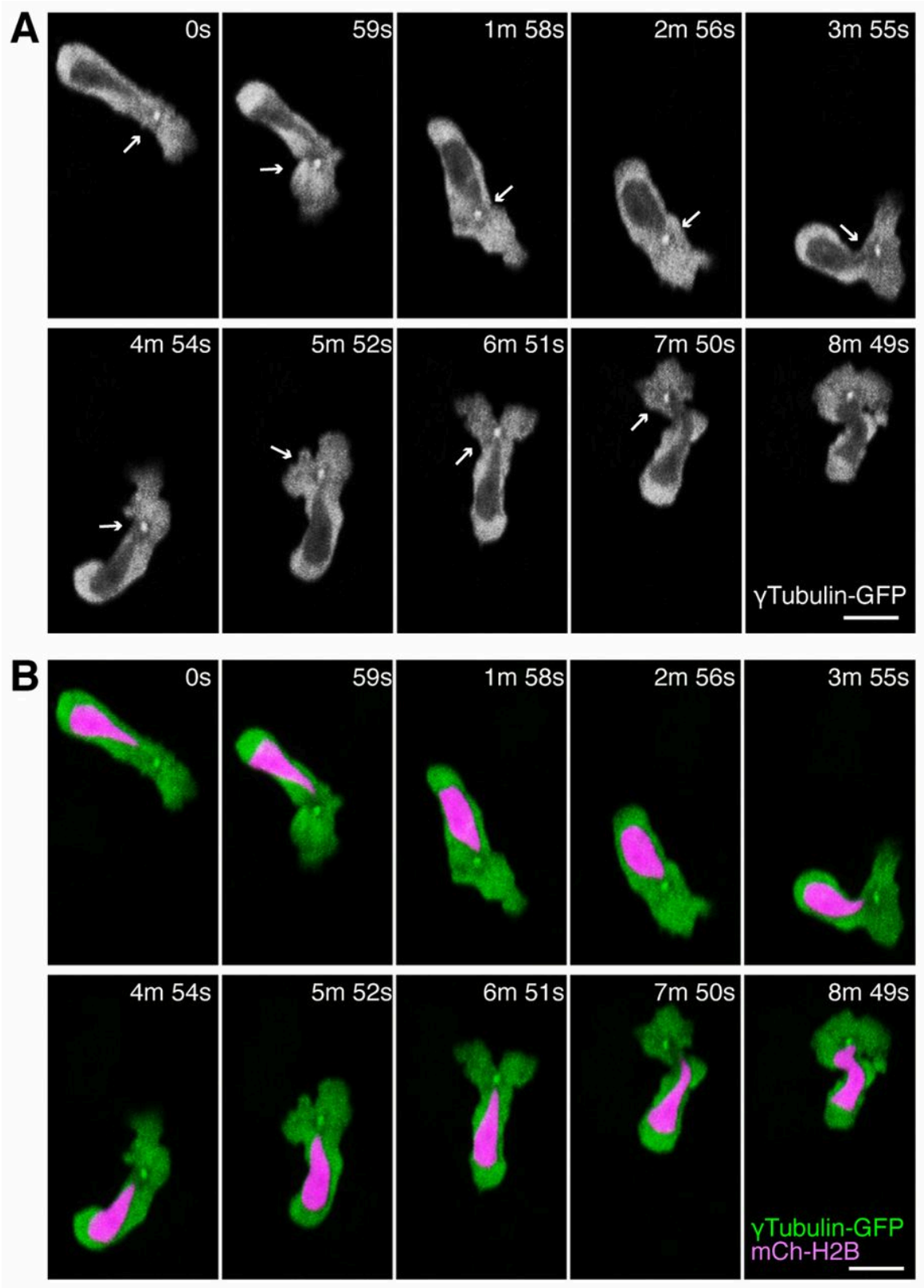
A
0s
59s
1m 58s
2m 56s
3m 55s
4m 54s
5m 52s
6m 51s
7m 50s
8m 49s
γTubulin-GFP
B
0s
59s
1m 58s
2m 56s
3m 55s
4m 54s
5m 52s
6m 51s
7m 50s
8m 49s
γTubulin-GFP
mCh-H2B

Fig. 3. Microtubule depolymerization impairs neutrophil wound attraction but enhances neutrophil motility and F-actin polarity. (A) Neutrophil recruitment to wounded fins at 30 minutes post wounding. Neutrophils were stained with Sudan Black. n=42 (DMSO), 22 (Noc 0.5 μM) and 22 (Noc 2 μM). (B–D) Microtubule depolymerization with nocodazole treatment enhances neutrophil 3D motility [(B), n=32 (DMSO), n=38 (Noc)], makes cells compact [(C), n=40 (DMSO), n=48 (Noc)] and induces a more round morphology [(D), n=40 (DMSO), n=48 (Noc)]. Tg(mpx:GFP-UtrCH) was used for live analysis. (E) Nocodazole treatment enhances polarity of F-actin dynamics in neutrophils. Rear localization of stable F-actin detected by GFP-UtrCH is particularly emphasized after microtubule depolymerization. Tg(mpx:GFP-UtrCH) was crossed with Tg(mpx:Lifeact-Ruby). *P<0.05, one-way ANOVA with Dunnett post-test (A) and two-tailed unpaired t-test (B–D). Data in A are representative of at least three separate experiments and three time-lapse movies were analyzed for data in B–D. Scale bar: 10 μm. (Note: I performed part of the experiments and analyses in Fig. 3A, B and E.)

Fig. 3

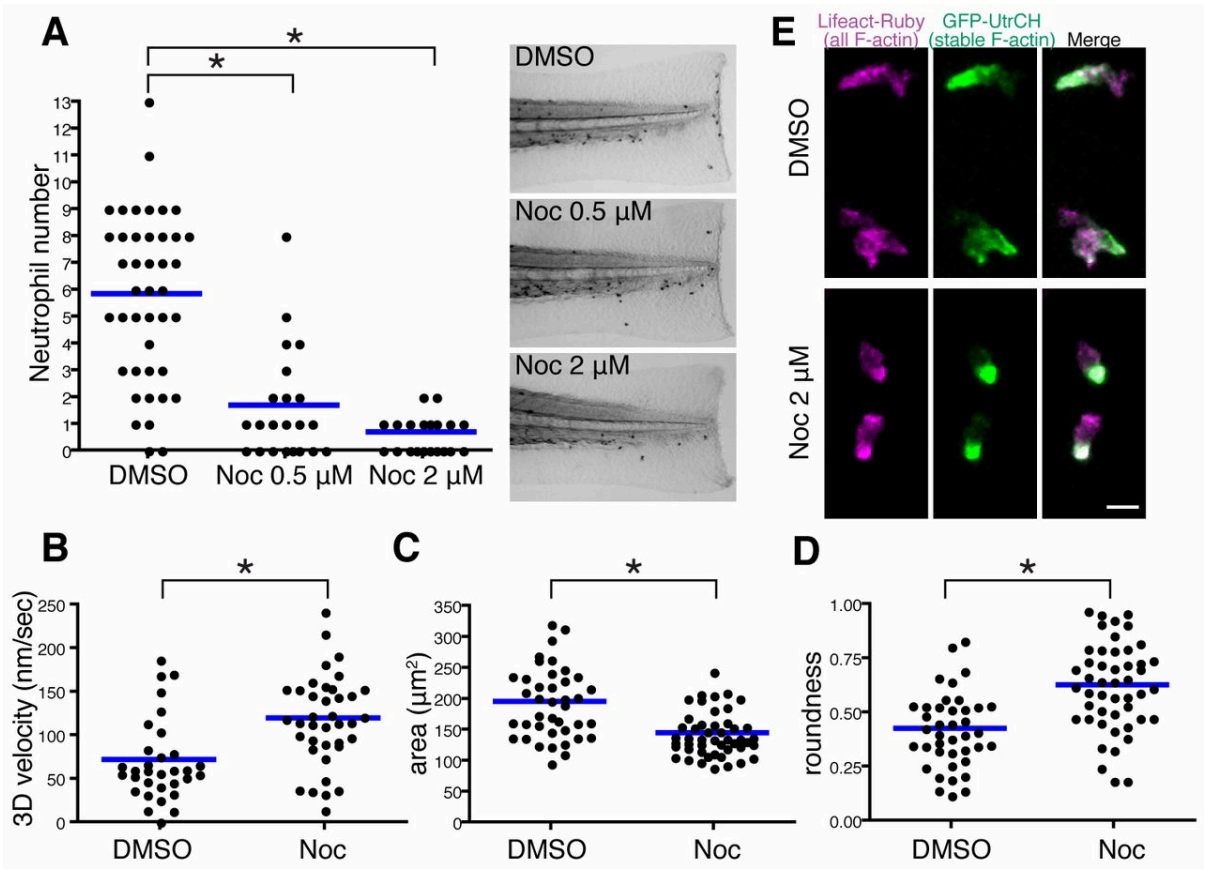
A
Neutrophil number
DMSO
Noc 0.5 µM
Noc 2 µM
B
3D velocity (nm/sec)
DMSO
Noc
C
area (µm²)
DMSO
Noc
D
roundness
DMSO
Noc
E
Lifeact-Ruby (all F-actin)
GFP-UtrCH (stable F-actin)
Merge
DMSO
Noc 2 µM

Fig. 4. Microtubule disassembly inhibits PI(3)K activation at the leading edge. (A) Time-lapse ratiometric imaging (PHAKT-GFP/mCherry) of PI(3,4,5)P3–PI(3,4)P2 dynamics during neutrophil random motility in the head. (B) Microtubule depolymerization inhibits localization of PI(3,4,5)P3–PI(3,4)P2 at the leading edge. Scale bars: 10 μm. (Note: I performed the initial experiments and analyses which were later repeated and lead to this figure in its final form.)

Fig. 4

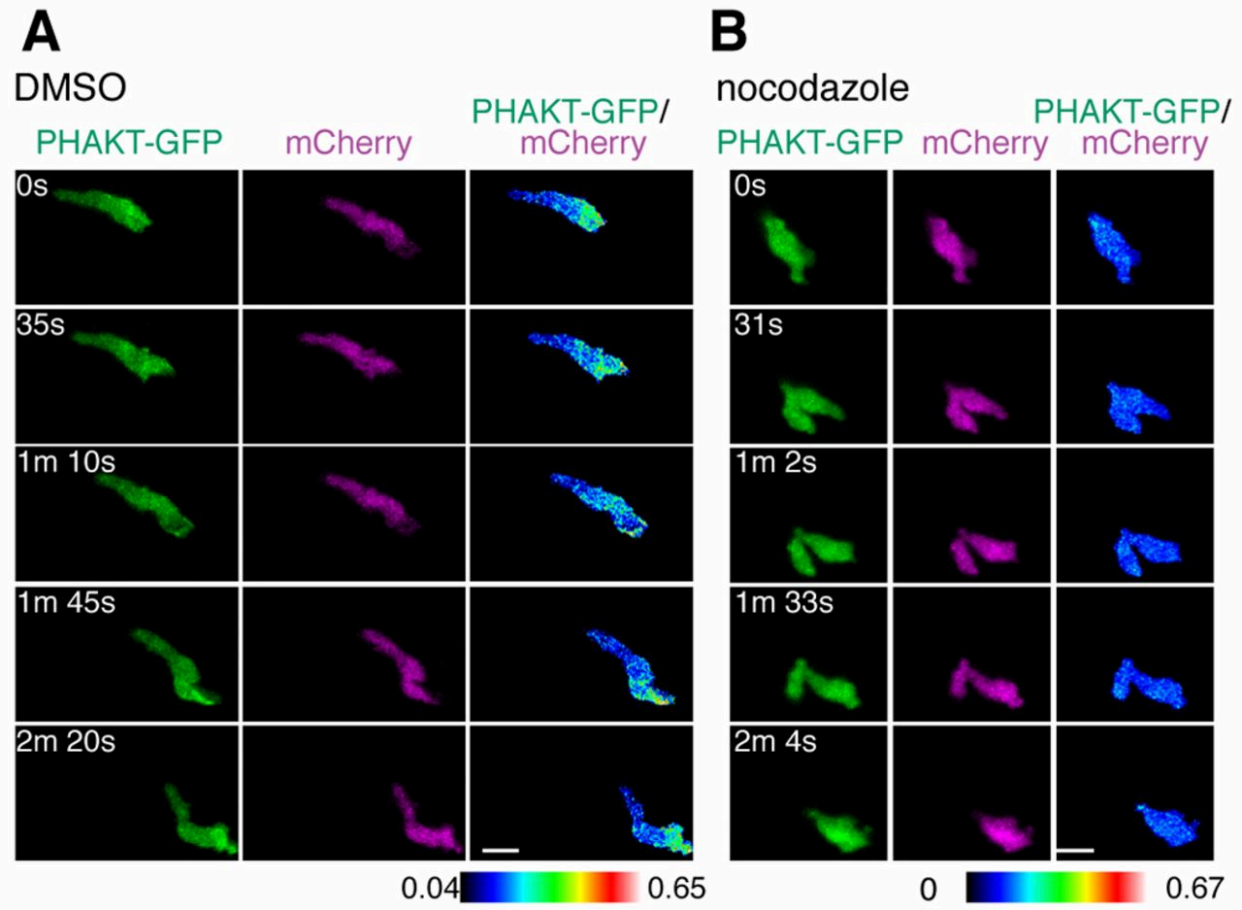
A
DMSO
PHAKT-GFP
mCherry
PHAKT-GFP/
mCherry
0s
35s
1m 10s
1m 45s
2m 20s
0.04
0.65
B
nocodazole
PHAKT-GFP
mCherry
PHAKT-GFP/
mCherry
0s
31s
1m 2s
1m 33s
2m 4s
0
0.67

Fig. 5. Microtubule disassembly induces neutrophil polarity and motility in a PI(3)K-independent manner. (A) Microtubule depolymerization with nocodazole reverses F-actin polarity defects caused by PI(3)K inhibition. (B) Microtubule disassembly reverses PI(3)K inhibition-induced migration arrest and enhances neutrophil motility compared with control. n=66 (DMSO), 64 (LY294002) and 48 (nocodazole, LY294002). *P<0.05, one-way ANOVA with Tukey post-test. Three time-lapse movies were analyzed for data for (B). Scale bar: 10 μm.

Fig. 5

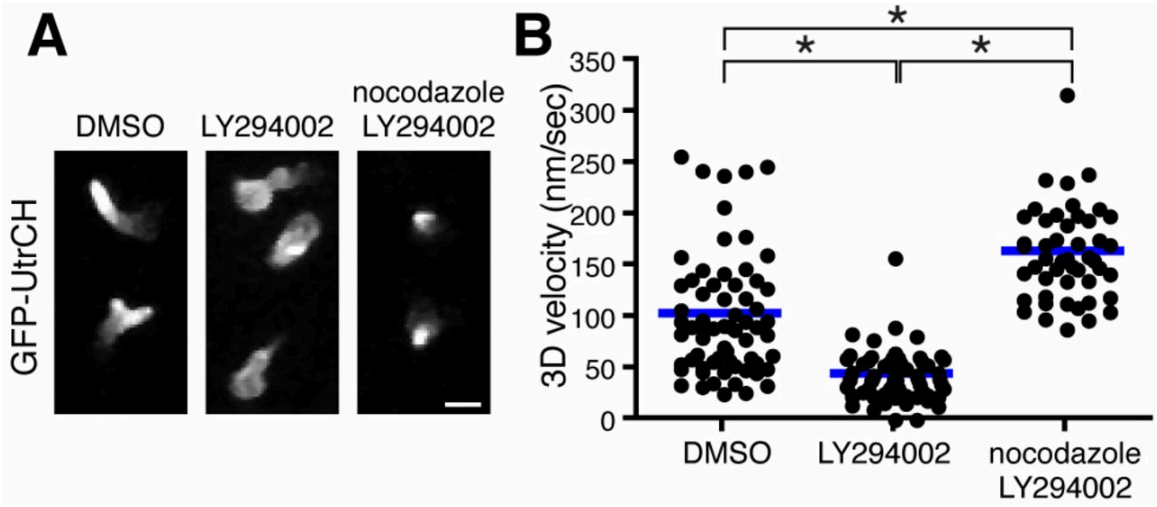
A
DMSO
LY294002
nocodazole
LY294002
GFP-UtrCH
B
3D velocity (nm/sec)
350
300
250
200
150
100
50
0
*
*
*
DMSO
LY294002
nocodazole
LY294002

Fig. 6. Rho regulates microtubule disassembly-mediated neutrophil motility. (A) Expression of a dominant negative RhoA T19N prevents microtubule depolymerization-induced neutrophil motility. Dendra2-Rho T19N was expressed in Tg(mpx:Lifeact-Ruby) and neutrophil motility was tracked for 30 minutes. (B) Nocodazole induces protrusion in Rho-inhibited cells. Data in A are representative of at least three time-lapse movies. Scale bars: 10 μm.

Fig. 6

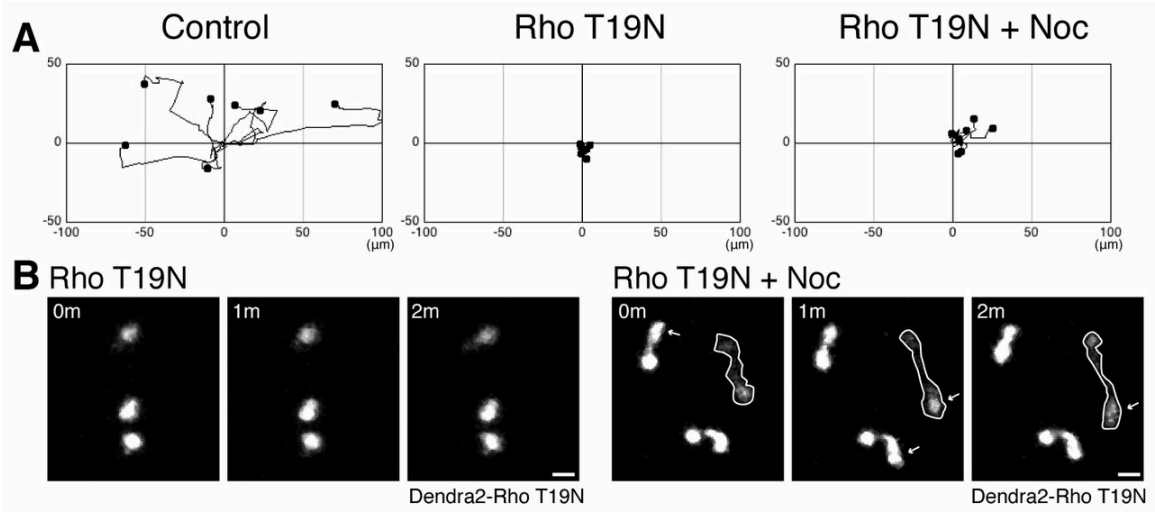
A
Control
Rho T19N
Rho T19N + Noc
50
0
-50
-100
-50
0
50
100
(μm)
B Rho T19N
Rho T19N + Noc
0m
1m
2m
Dendra2-Rho T19N
Dendra2-Rho T19N

Fig. 7. Rac regulates microtubule disassembly-mediated neutrophil motility. (A) rac2 MO inhibits microtubule depolymerization-induced neutrophil motility. Neutrophil motility was tracked for 30 minutes in Tg(mpx:GFP-UtrCH). (B) Rac2 knockdown makes neutrophils round, but nocodazole treatment makes Rac2-inhibited cells more round. n=53 (Control, DMSO), 52 (Control, Noc), 36 (rac2 MO, DMSO) and 44 (rac2 MO, Noc). (C) Rac2 knockdown makes neutrophils compact, but nocodazole treatment makes Rac2-inhibited cells more compact. n=54 (Control, DMSO), 52 (Control, Noc), 36 (rac2 MO, DMSO) and 44 (rac2 MO, Noc). (D) Transgenic neutrophil specific expression of dominant negative Rac2 D57N inhibits microtubule depolymerization-induced neutrophil motility. Neutrophil motility was tracked for 30 minutes in Tg(mpx:mCherry-2A-Rac2D57N). (E) Affinity precipitation assays with GST-RBD and GST-PBD to detect Rho-GTP and Rac-GTP, respectively (n=3). Microtubule disassembly directly activates Rac in addition to Rho in primary human neutrophils. Data in A and D are representative of at least three time-lapse movies. Three time-lapse movies were analyzed for data for B and C. Data in E are means ± s.e.m. of three separate experiments. *P<0.05, one-way ANOVA with Bonferroni post-test (B,C) and two-tailed paired t-test (E). (Note: I contributed Fig. 7D)

Fig. 7

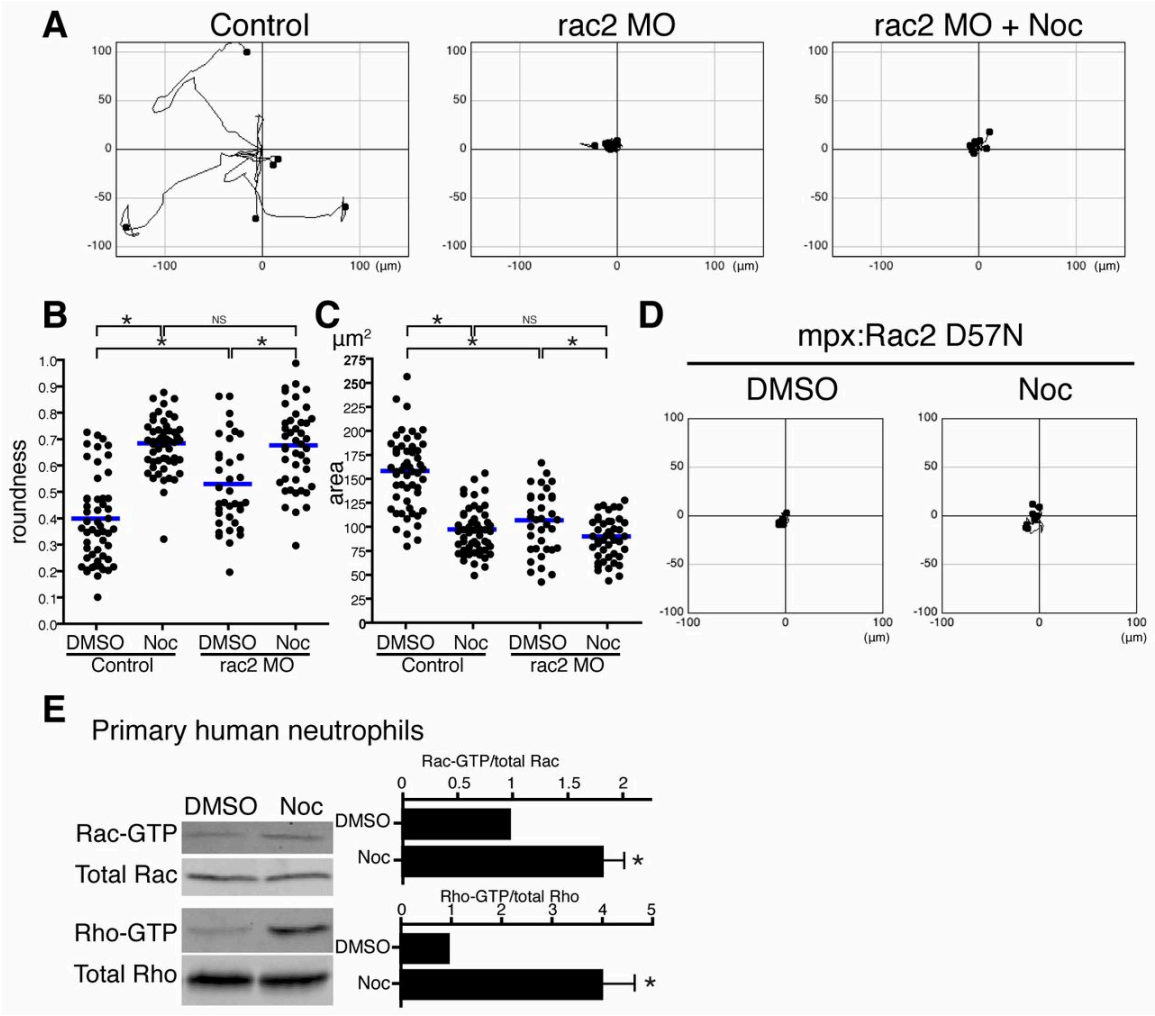
A
Control
rac2 MO
rac2 MO + Noc
100 (μm)
B
roundness
DMSO Noc DMSO Noc
Control
rac2 MO
C
μm²
area
NS
D
mpx:Rac2 D57N
DMSO
Noc
E
Primary human neutrophils
Rac-GTP/total Rac
DMSO Noc
Rac-GTP
Total Rac
Rho-GTP
Total Rho
Rho-GTP/total Rho

Fig. S1. The MTOC is mainly localized in front of the nucleus and occasionally on the side of the nucleus. Time-lapse imaging of a neutrophil expressing EB3-GFP and a nucleus probe mCherry-histone H2B. Arrows indicate localization of MTOC on the side of the nucleus. Scale bar: 10 mm. (Note: I contributed part of this figure by making the *lyz:mCherry-H2B* construct and performed some of the image analyses.)

Fig. S1

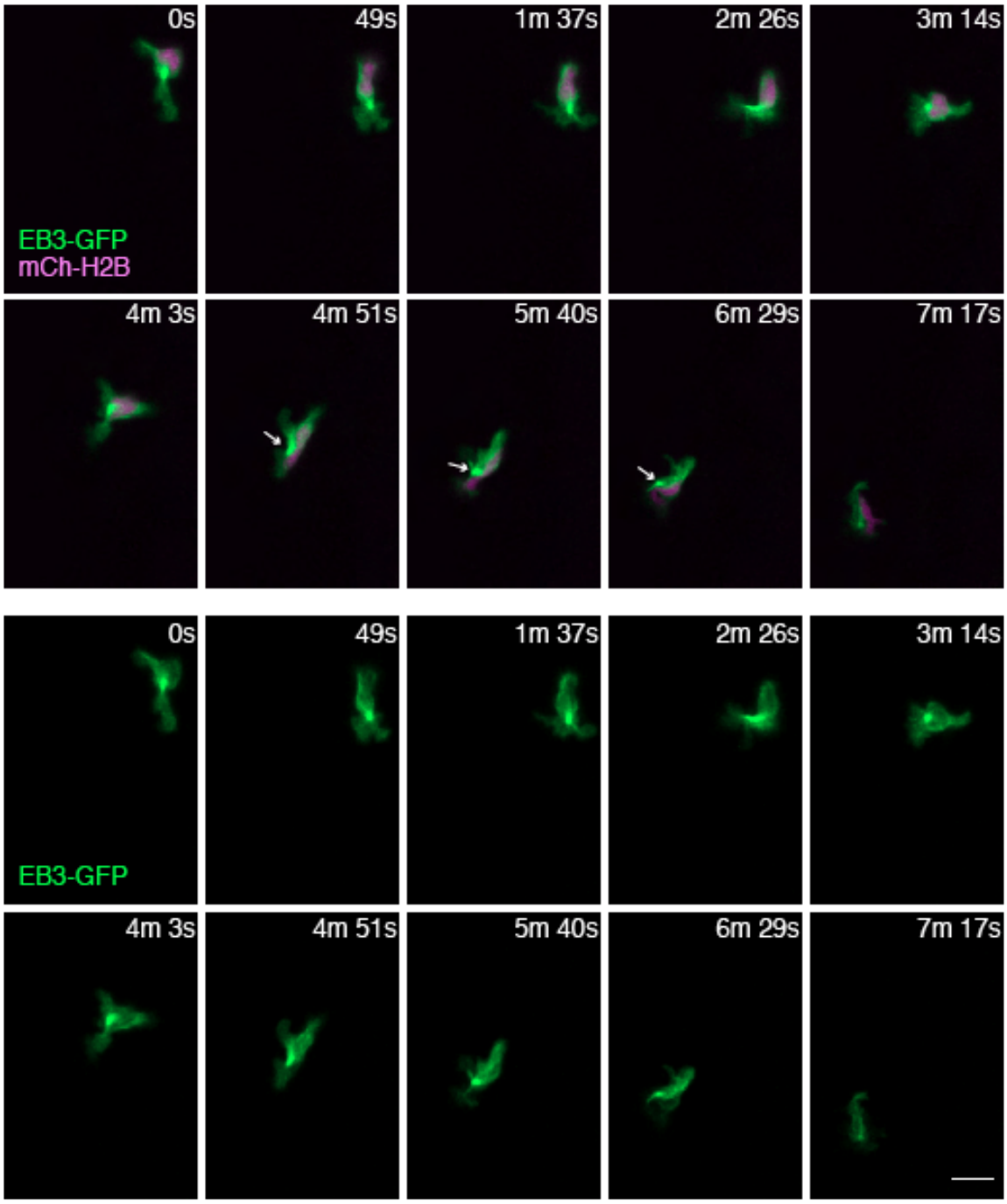
0s
49s
1m 37s
2m 26s
3m 14s
EB3-GFP
mCh-H2B
4m 3s
4m 51s
5m 40s
6m 29s
7m 17s
0s
49s
1m 37s
2m 26s
3m 14s
EB3-GFP
4m 3s
4m 51s
5m 40s
6m 29s
7m 17s

Movie 1. Time-lapse imaging of a neutrophil expressing GFP-tubulin (green) and mCherry (magenta).

Movie 2. Time-lapse imaging of a neutrophil expressing EMTB-3xGFP.

Movie 3. Two examples of time-lapse imaging of neutrophils expressing EB3-GFP.

Movie 4. Two examples of time-lapse imaging of neutrophils expressing EB3-GFP (green) and mCherry-H2B (magenta).

Movie 5. Time-lapse imaging of a neutrophil expressing GFP-Tau.

Movie 6. Time-lapse imaging of a neutrophil expressing gtubulin-GFP (green) and mCherry-H2B (red)

Movie 7. Time-lapse imaging of neutrophil random motility in the head (top: DMSO, bottom: nocodazole, green: GFP-UtrCH, magenta: Lifeact-Ruby).

Movie 8. Time-lapse imaging of neutrophils expressing PHAKT-GFP (green) and mCherry (magenta) in zebrafish treated with DMSO (first) or nocodazole (second).

Movie 9. Time-lapse imaging of neutrophils in tg(mpx:GFP-UtrCH) treated with DMSO, LY294002 then LY294002 and nocodazole.

Movie 10. Time-lapse imaging of neutrophils expressing Dendra2-Rho T19N in Tg(mpx:Lifeact-Ruby) treated with DMSO then nocodazole (green: Dendra2-Rho T19N, magenta: Lifeact-Ruby).

Movie 11. Time-lapse imaging of neutrophils expressing GFP-UtrCH in a rac2 morphant treated with DMSO (left) then nocodazole (right).

Movie 12. Time-lapse imaging of neutrophils expressing mCherry-2A-Rac2D57N in

Tg(mpx:mCherry-2A-Rac2D57N) treated with DMSO (left) then nocodazole (right).

Chapter 4

Heat shock modulates neutrophil motility in zebrafish

This Chapter was published in the following journal article:

Lam P.Y., Harvie E.A., and Huttenlocher A. (2013) Heat shock modulates neutrophil motility in zebrafish. *PLoS One*, Dec 19;8(12):e84436.

Abstract

Heat shock is a routine method used for inducible gene expression in animal models including zebrafish. Environmental temperature plays an important role in the immune system and infection progression of ectotherms. In this study, we analyzed the impact of short-term heat shock on neutrophil function using zebrafish (*Danio rerio*) as an animal model. Short-term heat shock decreased neutrophil recruitment to localized *Streptococcus iniae* infection and tail fin wounding. Heat shock also increased random neutrophil motility transiently and increased the number of circulating neutrophils. With the use of the translating ribosome affinity purification (TRAP) method for RNA isolation from specific cell types such as neutrophils, macrophages and epithelial cells, we found that heat shock induced the immediate expression of heat shock protein 70 (*hsp70*) and a prolonged expression of heat shock protein 27 (*hsp27*). Heat shock also induced cell stress as detected by the splicing of X-box binding protein 1 (*xbp1*) mRNA, a marker for endoplasmic reticulum (ER) stress. Exogenous expression of Hsp70, Hsp27 and spliced Xbp1 in neutrophils or epithelial cells did not reproduce the heat shock induced effects on neutrophil recruitment. The effect of heat shock on neutrophils is likely due to a combination of complex changes, including, but not limited to changes in gene expression. Our results indicate that routine heat shock can alter neutrophil function in zebrafish. The findings suggest that caution should be taken when employing a heat shock-dependent inducible system to study the innate immune response.

Introduction

Fever is an evolutionarily conserved response during infection. In ectotherms such as fish, where regulation of body temperature depends on external sources, behavioral fever is often displayed as a result of infection, manifested as an acute change in thermal preference. Examples of this can be found in largemouth blackbass and bluegill sunfish which prefer elevated water temperatures after injection with killed *Aeromonas hydrophila* (*A.h*) (Reynolds et al., 1976). Goldfish maintained at a febrile temperature had a higher survival rate after injection with live *A.h* (Covert and Reynolds, 1977). Rainbow trout show an increased preferred temperature and enhanced expression of inflammatory cytokine interleukin-1β after bacterial lipopolysaccharide (LPS) injection (Grans et al., 2012). Zebrafish also exhibit behavioral fever following viral infection, accompanied by upregulation of anti-viral genes (Boltana et al., 2013). Knowledge of what effect an elevated temperature has on immune cell function is limited. Several studies suggest that heat can affect neutrophil activation under some conditions. For example, heat exposure down-regulates TNFα signaling in suspended neutrophils but not in neutrophils interacting with fibronectin *in vitro* (Salanova et al., 2005). Heat inhibits LPS-induced neutrophil NF-κB activation in mice (Kettritz et al., 2006). The physiological and molecular consequences of elevated body temperature on immune cell function *in vivo* are not clear.

In addition to environmental temperature changes, short-term heat shock is a routine method for inducible gene expression with the use of heat shock protein promoters in various model organisms including mouse (Dietrich et al., 2000), zebrafish (Shoji and Sato-Maeda, 2008), *Drosophila* (Phelps and Brand, 1998) and

Caenorhabditis elegans (Bacaj and Shaham, 2007; Davis et al., 2008). Elevated temperature increases the expression of heat shock proteins (HSPs), which play important roles in innate and adaptive immunity (reviewed in (Colaco et al., 2013; Tsan and Gao, 2004; Tsan and Gao, 2009; Wallin et al., 2002)). Heat stress can also induce the unfolded protein response (UPR) and immune systems rely on intact UPR functions (reviewed in (Costa et al., 2011; Todd et al., 2008)). This study will address potential implications of the short-term heat shock procedure on neutrophil function.

In this paper, we focused on the effect of short-term temperature elevation on innate immune function using zebrafish (*Danio rerio*) as an animal model. The immune system of the zebrafish is highly conserved and has emerged as a powerful vertebrate disease model of both innate and adaptive immunity (reviewed in (Deng and Huttenlocher, 2012; Kanther and Rawls, 2010; Meeker and Trede, 2008)). Our data suggest that short-term heat shock affects innate immune function *in vivo* including a decrease in neutrophil recruitment to sites of infection and wound, and an increase in the mobilization of neutrophils into the circulation. This short-term heat shock, however, had no effect on larval survival with infection. Short-term heat shock increased neutrophil motility in a transient manner while the effect of heat shock on neutrophil wound response was long lasting. We showed that heat shock induced the expression of heat shock proteins such as Hsp70 and Hsp27 as well as the splicing of X-box binding protein 1 (*xbp1*) as part of the unfolded protein response. We adapted the translating ribosome affinity purification (TRAP) method for RNA isolation from specific cell types (Doyle et al., 2008; Heiman et al., 2008) in zebrafish and found that heat shock induced specific changes in gene expression in neutrophils, macrophages and

epithelial cells. Neutrophil specific over-expression of Hsp70, Hsp27 and spliced Xbp1 did not recapitulate the observed heat shock phenotypes. These findings suggest against a cell autonomous role for these specific heat shock-induced genes on neutrophil function. Our findings suggest that caution should be taken when using the heat shock procedure to study innate immune responses since heat shock alone can induce changes in neutrophil function.

Results and Discussion

Heat shock induces changes in the innate immune response

Zebrafish are normally maintained at 28.5°C. Heat shock (HS) was performed at 38-39°C for 1 hour in a water bath. To assess the effect of heat shock on immune cells, we performed the previously established methods of *Streptococcus iniae* (*S.i*) otic vesicle infections (Fig. 1A) (Harvie et al., 2012) and tail fin wound assays (Fig. 1B) (Lam et al., 2012) on zebrafish larvae at 3 days post fertilization (dpf). At this stage of development, adaptive immunity has not sufficiently matured (Lam et al., 2004; Willett et al., 1999), allowing for the direct study of innate immunity in isolation. Neutrophils, as the first responders to sites of infection or wounds (reviewed in (Lam and Huttenlocher, 2013)), are an important part of the innate immune response. Larvae were infected with *S.i* or injected with a PBS control in the otic vesicle and fixed at 2 hours post infection (hpi) for Sudan Black staining and quantification of neutrophil recruitment. There was a decrease in neutrophil recruitment to the site of *S.i.* otic infection in HS larvae compared to controls (Fig. 1C). Since it has been shown that tilapia are more susceptible to *S.i* infection at higher temperatures (Ndong et al., 2007), we then tested if short-term HS can affect the survival of zebrafish larvae after *S.i* infection. In our system, short-term HS for 1 hour did not alter survival 4 days post infection (Fig. 1D). HS also decreased neutrophil recruitment to the tail fin wound at 4 hours post wounding (hpw) when compared to controls (Fig. 1E). Since HS did not significantly change the total number of neutrophils (Fig. 1F), the effect was likely due to a change in neutrophil behavior after HS. Taken together, our results suggest that HS impairs neutrophil recruitment to sites of infection and tissue damage.

Heat shock affects neutrophil motility

It has previously been reported that isolated human neutrophils display an increase in motility at higher temperatures (Nahas et al., 1971). To further characterize the effects of heat shock, we analyzed the speed of neutrophils undergoing random motility in the head region of zebrafish larvae. We observed an increase in neutrophil speed immediately after HS followed by a return to baseline motility at 3 hours post heat shock (hpHS) (Fig. 2A). By contrast, the effect of HS on neutrophil wound recruitment was long lasting. When larvae were wounded at 3 hpHS and then assayed four hours later, there was a significant decrease in the number of neutrophils at the tail wound site at 4 hpw (Fig. 2B).

Heat shock increases neutrophil mobilization

Since HS impaired neutrophil wound recruitment without affecting global numbers of neutrophils (Fig. 1F), we next tested if we could detect a change in neutrophil distribution induced by HS. Previous work has established that neutrophils in zebrafish larvae reside outside the vasculature, in a region known as the caudal hematopoietic tissue (CHT) and only mobilize into the circulation upon infection (Deng et al., 2013), wounding (Yoo and Huttenlocher, 2011) or with leukocyte adhesion deficiency (Deng et al., 2011). Using the zebrafish transgenic lines (*Tg*(*mpx:dendra2*) or *Tg*(*mpx:mCherry*)), expressing fluorescent proteins specifically in neutrophils, we were able to perform live imaging of circulating neutrophils *in vivo*. We observed an increase in circulating neutrophils, particularly at 3 hpHS (Fig. 3A and 3B). This may indicate that

HS leads to either activation of the neutrophils or impaired retention of neutrophils within the CHT.

Heat shock induces changes in gene expression

We were interested in exploring the idea that heat shock-induced changes in gene expression might be responsible for the modification in neutrophil behavior. We looked at changes in gene expression immediately after HS and at 3 hpHS to assess the immediate-early and longer-term changes in gene expression. We focused on three candidate genes, *hsp70*, *hsp27* and the splicing of *xbp1*, due to their roles in immune function. Cell stress such as heat shock, infection, fever, inflammation, malignancy or autoimmunity can induce heat shock protein (HSP) synthesis (reviewed in (Wu and Tanguay, 2006)). HSP70 is involved in both innate and adaptive immunity and has been extensively reviewed (Borges et al., 2012; Srivastava, 2002; Stocki and Dickinson, 2012; Todryk et al., 2003; Tsan and Gao, 2004)). The role of HSP70 in inflammation is controversial. Recent studies suggest that it has pro-inflammatory functions (Senf et al., 2013) as well as anti-inflammatory functions (Vinokurov et al., 2012). HSP27 has been shown to function in different cellular processes such as protein folding, actin remodeling and in the reduction of oxidative stress (reviewed in (Vidyasagar et al., 2012)). HSP27 binds to the barbed end of actin filaments and inhibits actin polymerization (Benndorf et al., 1994; Miron et al., 1991; Schneider et al., 1998). HSP27 has also been shown to be important for cell motility in human cancer cells (Doshi et al., 2009). It has previously been reported that HSP27 regulates neutrophil chemotaxis,

however, this role is independent of its role in regulating actin reorganization (Jog et al., 2007). Although research on zebrafish Hsp27 is limited, it has been shown to have similar functions and to be regulated like mammalian HSP27 (Mao et al., 2005; Tucker and Shelden, 2009).

Upon ER stress induced unfolded protein response, the mRNA encoding the X-box-binding protein-1 (XBP1) is spliced by IRE1 to generate a more potent transcription factor XBP1S (Yoshida et al., 2001). XBP1 protects *Caenorhabditis elegans* during the activation of its innate immune response upon infection with pathogenic bacteria (Richardson et al., 2010). It has been shown that toll-like receptor activation leads to the production of spliced XBP1 in mouse macrophages, which is required for optimal production of proinflammatory cytokines (Martinon et al., 2010). XBP1 has also been linked to intestinal inflammation (Kaser et al., 2008). The splicing of *xbp1* in response to ER stress is conserved in zebrafish (Hu et al., 2007).

We found that heat shock induced a global increase in *hsp70* and *hsp27* expression as well as the splicing of x*bp1* (Fig. 4A). These specific heat shock proteins are normally expressed during development in certain tissue but not others. *hsp70*, for example, is normally expressed during lens development in zebrafish (Blechinger et al., 2002), while *hsp27* is normally expressed in skeletal and cardiac muscle tissues (Tucker et al., 2009). To assess changes in gene expression in specific cell types and to identify translationally active mRNAs from steady-state total mRNAs (Kudo et al., 2010), we adapted the translating ribosome affinity purification (TRAP) method that was previously developed for murine models (Doyle et al., 2008; Heiman et al., 2008). This method involves the expression of EGFP-tagged mouse ribosomal protein L10a in

defined cell populations, allowing characterization of actively translating genes in specific cell types. Since zebrafish L10a shares considerable homology with its mouse counterpart, we predicted the same construct could be employed for zebrafish TRAP. We generated three transgenic fish lines where EGFP-L10a is specifically expressed in neutrophils (lyz:TRAP), macrophages (mpeg1:TRAP) or epithelial cells (krt4:TRAP). The enriched mRNAs isolated from these transgenic lines were then analyzed. As expected, the lyz:TRAP and mpeg1:TRAP lines showed the expression of either the neutrophil marker (*mpx)* or macrophage marker (*mpeg1)*, respectively (Fig 4B). In the krt4:TRAP line, we detected the expression of the epithelial marker *krt4* but not the muscle marker *myoD* (Fig. 4C). We then used these transgenic lines to assess whether or not HS induced the expression of *hsp70*, *hsp27* and the splicing of *xbp1* specifically in these subsets of cells. Using the TRAP method, we observed that HS did indeed induce the expression of *hsp70* and *hsp27* in neutrophils, macrophages and epithelial cells (Fig. 4D). At 3 hpHS, expression of *hsp27* persisted while the expression of *hsp70* returned to baseline levels. Heat shock induced splicing of *xbp1* occurred in all three cell populations tested, but appears to be short lived since there was no *xbp1* splicing detectable at 3 hpHS (Fig. 4D).

The role of Hsp70, Hsp27 and spliced Xbp1 in neutrophil motility

In an attempt to determine if elevated levels of Hsp70, Hsp27 and spliced Xbp1 directly affect innate immune functions, we specifically expressed these proteins in neutrophils and/or epithelial cells. Expression of Hsp70 or spliced Xbp1 in neutrophils

and epithelial cells did not affect the neutrophil response to *S.i.* otic infection (Fig. 5A and 5C). Similar results were observed when Hsp27 was specifically expressed in neutrophils (Fig. 5B). We next asked if over-expression of Hsp70, Hsp27 or spliced Xbp1 individually in neutrophils or epithelial cells could reproduce the HS phenotypes. As seen in Fig. 5D-5H, this approach did not reproduce the HS phenotype of altering neutrophil recruitment. However, we cannot rule out the involvement of these genes and must consider that constitutive expression of HSPs and spliced Xbp1 may not faithfully recapitulate the short-term HS condition. Furthermore, the HS effects on neutrophil function may not be neutrophil cell autonomous. For example, it has been shown that elevated body temperatures can enhance LPS-induced proinflammatory cytokine TNFα production in macrophages (Lee et al., 2012). Similarly, the effect of heat shock on neutrophil function is likely due to a combination of differential gene expression within neutrophils as well as in other cell types that act to guide or influence the behavior of neutrophils.

Our results show that the effect of heat shock on the innate immune response should be taken into consideration when using heat shock as a tool for inducible gene expression. This is particularly important in the zebrafish field since heat shock is routinely used for temporal control of gene expression (Asakawa and Kawakami, 2008; Faucherre and Lopez-Schier, 2011; Halloran et al., 2000; Shoji and Sato-Maeda, 2008) and the Hsp70 promoter is commonly used in the zebrafish community. As the expression of *hsp27* persisted long after the initial heat shock, researchers may want to explore the use of the Hsp27 promoter for inducible gene expression in zebrafish, keeping in mind its endogenous tissue expression (Wu et al., 2008).

Conclusion

Our data suggest that short-term HS results in changes in neutrophil behavior including increased motility and mobilization but decreased response to infection and wounding. HS induces changes in gene expression including *hsp70* and *hsp27* and in the splicing of *xbp1*. These findings suggest that caution should be taken when employing a HS-dependent inducible system to study the innate immune system. The effect of long-term temperature increase on innate immunity will require further investigation.

Materials and Methods

Ethics Statement

All animal studies were approved by the University of Wisconsin – Madison Animal Care and Use Committee and performed in accordance with the guidelines.

Heat shock, tail fin wounding, otic vesicle injection and Sudan Black staining

Heat shock was performed in a water bath at 38-39°C for 1 hour. For tail fin wounding, larvae at 3 dpf were anesthetized using 0.2 mg/mL tricaine and wounded with a 33 gauge needle. Preparation of *Streptococcus iniae* and microinjection of bacteria into zebrafish larvae has been previously described (Harvie et al., 2012). 1 nl volume of 100 CFU of *S. iniae* wild-type strain 9117 (or a PBS control) was microinjected into the otic vesicle of larvae at 3 dpf. Larvae were then fixed at the time points indicated with 4% formaldehyde overnight at room temperature and stained with Sudan Black as described previously (Le Guyader et al., 2008).

Purification of mRNA from TRAP zebrafish larvae and RT-PCR

A protocol previously used for TRAP mRNA purification from mouse tissue (Heiman et al., 2008) was adapted for zebrafish larvae with slight modifications. Briefly, a glass dounce homogenizer was used to homogenize the larvae. Purified rabbit anti-GFP antibody (Invitrogen A11122) was used for immunoprecipitation. After immunoprecipitation and high-salt polysome buffer washing steps, RNA was purified using an RNeasy Mini Kit (Qiagen) with in-column DNase digestion. RT-PCR was performed using the OneStep RT-PCR Kit (Qiagen) according to the manufacturer's

instruction. Primers used to amplify *ef1α*, *mpx* (Mathias et al., 2009) and *xbp1* (Hu et al., 2007) have been described previously. The other primer sequences used in this study were as follow:

hsp27-F 5'-CGGATCCATGGCCGAGAGACGCATC-3'

hsp27-R 5'-TTATTTTGTGGTGCTGACGG-3'

hsp70-F 5'-CACCCAGCTATGTTGCCTTCAC-3'

hsp70-R 5'-CACCATGCGGTTGTCAAAGTCC-3'

krt4-F 5'-CTATGGAAGTGGTCTTGGTGGAGG-3'

krt4-R 5'-CCTGAAGAGCATCAACCTTGGC-3'

mpeg1-F 5'-CTTTAATTCAGAGCCACGGAGGAGC-3'

mpeg1 R 5'-GTAGACAACCCTAAGAAACCACAGG-3'

myoD-F 5'-CCTTGCTTCAACACCAACGACATG-3'

myoD-R 5'-GTCATAGCTGTTCCGTCTTCTCGTC-3'

PCR products were analyzed using 1% agarose electrophoresis with the exception of *xbp1* RT-PCR in which 8% polyacrylmide gel made in TAE buffer was used.

DNA injection

All DNA expression vectors contained the zebrafish lysozyme C (*lyz*) promoter for neutrophil expression (Kitaguchi et al., 2009; Lam et al., 2012), *mpeg1* promoter for macrophage expression (Harvie et al., 2012), or *krt4* promoter for epithelial cell expression (Chen et al., 2011; Yoo et al., 2012). To facilitate the production of multiple protein products from a single transgene, a viral 2A peptide linker sequence was used

(Provost et al., 2007). All expression vectors contain minimal Tol2 elements for efficient integration (Urasaki et al., 2006) and an SV40 polyadenylation sequence (Clontech Laboratories, Inc). The following constructs were generated: *lyz-EGFP-L10a, mpeg1-EGFP-L10a*, *krt4-EGFP-L10a, lyz-hsp27-2A-mCherry* (Zebrafish *hsp27* (ATCC 10809422, accession BC097148)), *lyz-hsp70-2A-EGFP* (Zebrafish *hsp70* (Open Biosystems Clone Id:6789418, accession BC056709)), *krt4-hsp70-2A-mCherry*, *lyz-xbp1-2A-EGFP* (Zebrafish spliced *xbp1* (Open Biosystems Clone Id:3816043, accession BC044134)) and *krt4-xbp1-2A-mCherry*. Expression of constructs was obtained by injecting 3 nL of solution containing 12.5 ng/μL of DNA plasmid and 17.5 ng/μL *in vitro* transcribed (Ambion) Tol2 transposase mRNA into the cytoplasm of one-cell stage embryo.

Live imaging and image quantification

Larvae at 3 dpf were anesthetized using 0.2 mg/mL tricaine and mounted on a glass-bottom dish with 1% low melt agarose for live imaging. Time-lapse fluorescence images were acquired using a confocal microscope (FluoView FV1000, Olympus) using a NA 0.75/20x objective. Z-stack images were collected for 30 minutes with 1 minute intervals. 3-dimentional tracking of neutrophils has been previously described (Lam et al., 2012). Quantification of circulating neutrophils has been previously described (Deng et al., 2013). Briefly, *Tg(mpx:mCherry)* or *Tg(mpx:dendra2)* were used and neutrophils that circulate through the posterior cardinal vein were scored in individual 3 minute movies with 3 second intervals using a Nikon SMZ-1500 zoom microscope equipped with epifluorescence and a CoolSnap ES camera (Roper Scientific, Duluth, GA).

Statistics

Experimental results were analyzed with Prism version 4 (GraphPad Software) statistical software. The resulting *P* values are included in the figure legends for each experiment.

Acknowledgments

We thank Julie M. Green for her support in the generation and maintenance of zebrafish lines.

Funding

Funding provided by National Institutes of Health [grant numbers GM074827 to A.H.].

References

Asakawa, K., and K. Kawakami. 2008. Targeted gene expression by the Gal4-UAS system in zebrafish. *Dev Growth Differ*. 50:391-9.

Bacaj, T., and S. Shaham. 2007. Temporal control of cell-specific transgene expression in Caenorhabditis elegans. *Genetics*. 176:2651-5.

Benndorf, R., K. Hayess, S. Ryazantsev, M. Wieske, J. Behlke, and G. Lutsch. 1994. Phosphorylation and supramolecular organization of murine small heat shock protein HSP25 abolish its actin polymerization-inhibiting activity. *J Biol Chem*. 269:20780-4.

Blechinger, S.R., T.G. Evans, P.T. Tang, J.Y. Kuwada, J.T. Warren, Jr., and P.H. Krone. 2002. The heat-inducible zebrafish hsp70 gene is expressed during normal lens development under non-stress conditions. *Mech Dev*. 112:213-5.

Boltana, S., S. Rey, N. Roher, R. Vargas, M. Huerta, F.A. Huntingford, F.W. Goetz, J. Moore, P. Garcia-Valtanen, A. Estepa, and S. Mackenzie. 2013. Behavioural fever is a synergic signal amplifying the innate immune response. *Proc Biol Sci*. 280:20131381.

Borges, T.J., L. Wieten, M.J. van Herwijnen, F. Broere, R. van der Zee, C. Bonorino, and W. van Eden. 2012. The anti-inflammatory mechanisms of Hsp70. *Front Immunol*. 3:95.

Chen, C.F., C.Y. Chu, T.H. Chen, S.J. Lee, C.N. Shen, and C.D. Hsiao. 2011. Establishment of a transgenic zebrafish line for superficial skin ablation and functional validation of apoptosis modulators in vivo. *PLoS One*. 6:e20654.

Colaco, C.A., C.R. Bailey, K.B. Walker, and J. Keeble. 2013. Heat shock proteins: stimulators of innate and acquired immunity. *Biomed Res Int*. 2013:461230.

Costa, C.Z., S.E. da Rosa, and M.M. de Camargo. 2011. The unfolded protein response: how protein folding became a restrictive aspect for innate immunity and B lymphocytes. *Scand J Immunol*. 73:436-48.

Covert, J.B., and W.W. Reynolds. 1977. Survival value of fever in fish. *Nature*. 267:43-5.

Davis, M.W., J.J. Morton, D. Carroll, and E.M. Jorgensen. 2008. Gene activation using FLP recombinase in C. elegans. *PLoS Genet*. 4:e1000028.

Deng, Q., and A. Huttenlocher. 2012. Leukocyte migration from a fish eye's view. *J Cell Sci*. 125:3949-56.

Deng, Q., M. Sarris, D.A. Bennin, J.M. Green, P. Herbomel, and A. Huttenlocher. 2013. Localized bacterial infection induces systemic activation of neutrophils through Cxcr2 signaling in zebrafish. *J Leukoc Biol*. 93:761-9.

Deng, Q., S.K. Yoo, P.J. Cavnar, J.M. Green, and A. Huttenlocher. 2011. Dual roles for Rac2 in neutrophil motility and active retention in zebrafish hematopoietic tissue. *Dev Cell*. 21:735-45.

Dietrich, P., I. Dragatsis, S. Xuan, S. Zeitlin, and A. Efstratiadis. 2000. Conditional mutagenesis in mice with heat shock promoter-driven cre transgenes. *Mamm Genome*. 11:196-205.

Doshi, B.M., L.E. Hightower, and J. Lee. 2009. The role of Hsp27 and actin in the regulation of movement in human cancer cells responding to heat shock. *Cell Stress Chaperones*. 14:445-57.

Doyle, J.P., J.D. Dougherty, M. Heiman, E.F. Schmidt, T.R. Stevens, G. Ma, S. Bupp, P. Shrestha, R.D. Shah, M.L. Doughty, S. Gong, P. Greengard, and N. Heintz. 2008. Application of a translational profiling approach for the comparative analysis of CNS cell types. *Cell*. 135:749-62.

Faucherre, A., and H. Lopez-Schier. 2011. Delaying Gal4-driven gene expression in the zebrafish with morpholinos and Gal80. *PLoS One*. 6:e16587.

Grans, A., M. Rosengren, L. Niklasson, and M. Axelsson. 2012. Behavioural fever boosts the inflammatory response in rainbow trout Oncorhynchus mykiss. *J Fish Biol*. 81:1111-7.

Halloran, M.C., M. Sato-Maeda, J.T. Warren, F. Su, Z. Lele, P.H. Krone, J.Y. Kuwada, and W. Shoji. 2000. Laser-induced gene expression in specific cells of transgenic zebrafish. *Development*. 127:1953-60.

Harvie, E.A., J.M. Green, M.N. Neely, and A. Huttenlocher. 2012. Innate immune response to Streptococcus iniae infection in zebrafish larvae. *Infect Immun*. 81:110-21.

Heiman, M., A. Schaefer, S. Gong, J.D. Peterson, M. Day, K.E. Ramsey, M. Suarez-Farinas, C. Schwarz, D.A. Stephan, D.J. Surmeier, P. Greengard, and N. Heintz. 2008. A translational profiling approach for the molecular characterization of CNS cell types. *Cell*. 135:738-48.

Hu, M.C., H.Y. Gong, G.H. Lin, S.Y. Hu, M.H. Chen, S.J. Huang, C.F. Liao, and J.L. Wu. 2007. XBP-1, a key regulator of unfolded protein response, activates transcription of IGF1 and Akt phosphorylation in zebrafish embryonic cell line. *Biochem Biophys Res Commun*. 359:778-83.

Jog, N.R., V.R. Jala, R.A. Ward, M.J. Rane, B. Haribabu, and K.R. McLeish. 2007. Heat shock protein 27 regulates neutrophil chemotaxis and exocytosis through two independent mechanisms. *J Immunol*. 178:2421-8.

Kanther, M., and J.F. Rawls. 2010. Host-microbe interactions in the developing zebrafish. *Curr Opin Immunol*. 22:10-9.

Kaser, A., A.H. Lee, A. Franke, J.N. Glickman, S. Zeissig, H. Tilg, E.E. Nieuwenhuis, D.E. Higgins, S. Schreiber, L.H. Glimcher, and R.S. Blumberg. 2008. XBP1 links ER stress to intestinal inflammation and confers genetic risk for human inflammatory bowel disease. *Cell*. 134:743-56.

Kettritz, R., M. Choi, B. Salanova, M. Wellner, S. Rolle, and F.C. Luft. 2006. Fever-like temperatures affect neutrophil NF-kappaB signaling, apoptosis, and ANCA-antigen expression. *J Am Soc Nephrol*. 17:1345-53.

Kitaguchi, T., K. Kawakami, and A. Kawahara. 2009. Transcriptional regulation of a myeloid-lineage specific gene lysozyme C during zebrafish myelopoiesis. *Mech Dev*. 126:314-23.

Kudo, K., Y. Xi, Y. Wang, B. Song, E. Chu, J. Ju, and J.J. Russo. 2010. Translational control analysis by translationally active RNA capture/microarray analysis (TrIP-Chip). *Nucleic Acids Res*. 38:e104.

Lam, P.Y., and A. Huttenlocher. 2013. Interstitial leukocyte migration in vivo. *Curr Opin Cell Biol*. 25:650-8.

Lam, P.Y., S.K. Yoo, J.M. Green, and A. Huttenlocher. 2012. The SH2-domain-containing inositol 5-phosphatase (SHIP) limits the motility of neutrophils and their recruitment to wounds in zebrafish. *J Cell Sci*. 125:4973-8.

Lam, S.H., H.L. Chua, Z. Gong, T.J. Lam, and Y.M. Sin. 2004. Development and maturation of the immune system in zebrafish, Danio rerio: a gene expression profiling, in situ hybridization and immunological study. *Dev Comp Immunol*. 28:9-28.

Le Guyader, D., M.J. Redd, E. Colucci-Guyon, E. Murayama, K. Kissa, V. Briolat, E. Mordelet, A. Zapata, H. Shinomiya, and P. Herbomel. 2008. Origins and unconventional behavior of neutrophils in developing zebrafish. *Blood*. 111:132-41.

Lee, C.T., L. Zhong, T.A. Mace, and E.A. Repasky. 2012. Elevation in body temperature to fever range enhances and prolongs subsequent responsiveness of macrophages to endotoxin challenge. *PLoS One*. 7:e30077.

Mao, L., A.L. Bryantsev, M.B. Chechenova, and E.A. Shelden. 2005. Cloning, characterization, and heat stress-induced redistribution of a protein homologous to human hsp27 in the zebrafish Danio rerio. *Exp Cell Res*. 306:230-41.

Martinon, F., X. Chen, A.H. Lee, and L.H. Glimcher. 2010. TLR activation of the transcription factor XBP1 regulates innate immune responses in macrophages. *Nat Immunol*. 11:411-8.

Mathias, J.R., M.E. Dodd, K.B. Walters, S.K. Yoo, E.A. Ranheim, and A. Huttenlocher. 2009. Characterization of zebrafish larval inflammatory macrophages. *Dev Comp Immunol*. 33:1212-7.

Meeker, N.D., and N.S. Trede. 2008. Immunology and zebrafish: spawning new models of human disease. *Dev Comp Immunol*. 32:745-57.

Miron, T., K. Vancompernolle, J. Vandekerckhove, M. Wilchek, and B. Geiger. 1991. A 25-kD inhibitor of actin polymerization is a low molecular mass heat shock protein. *J Cell Biol*. 114:255-61.

Nahas, G.G., M.L. Tannieres, and J.F. Lennon. 1971. Direct measurement of leukocyte motility: effects of pH and temperature. *Proc Soc Exp Biol Med*. 138:350-2.

Ndong, D., Y.Y. Chen, Y.H. Lin, B. Vaseeharan, and J.C. Chen. 2007. The immune response of tilapia Oreochromis mossambicus and its susceptibility to Streptococcus iniae under stress in low and high temperatures. *Fish Shellfish Immunol*. 22:686-94.

Phelps, C.B., and A.H. Brand. 1998. Ectopic gene expression in Drosophila using GAL4 system. *Methods*. 14:367-79.

Provost, E., J. Rhee, and S.D. Leach. 2007. Viral 2A peptides allow expression of multiple proteins from a single ORF in transgenic zebrafish embryos. *Genesis*. 45:625-9.

Reynolds, W.W., M.E. Casterlin, and J.B. Covert. 1976. Behavioural fever in teleost fishes. *Nature*. 259:41-2.

Richardson, C.E., T. Kooistra, and D.H. Kim. 2010. An essential role for XBP-1 in host protection against immune activation in C. elegans. *Nature*. 463:1092-5.

Salanova, B., M. Choi, S. Rolle, M. Wellner, C. Scheidereit, F.C. Luft, and R. Kettritz. 2005. The effect of fever-like temperatures on neutrophil signaling. *FASEB J*. 19:816-8.

Schneider, G.B., H. Hamano, and L.F. Cooper. 1998. In vivo evaluation of hsp27 as an inhibitor of actin polymerization: hsp27 limits actin stress fiber and focal adhesion formation after heat shock. *J Cell Physiol*. 177:575-84.

Senf, S.M., T.M. Howard, B. Ahn, L.F. Ferreira, and A.R. Judge. 2013. Loss of the inducible Hsp70 delays the inflammatory response to skeletal muscle injury and severely impairs muscle regeneration. *PLoS One*. 8:e62687.

Shoji, W., and M. Sato-Maeda. 2008. Application of heat shock promoter in transgenic zebrafish. *Dev Growth Differ*. 50:401-6.

Srivastava, P. 2002. Roles of heat-shock proteins in innate and adaptive immunity. *Nat Rev Immunol*. 2:185-94.

Stocki, P., and A.M. Dickinson. 2012. The immunosuppressive activity of heat shock protein 70. *Autoimmune Dis*. 2012:617213.

Todd, D.J., A.H. Lee, and L.H. Glimcher. 2008. The endoplasmic reticulum stress response in immunity and autoimmunity. *Nat Rev Immunol*. 8:663-74.

Todryk, S.M., M.J. Gough, and A.G. Pockley. 2003. Facets of heat shock protein 70 show immunotherapeutic potential. *Immunology*. 110:1-9.

Tsan, M.F., and B. Gao. 2004. Heat shock protein and innate immunity. *Cell Mol Immunol*. 1:274-9.

Tsan, M.F., and B. Gao. 2009. Heat shock proteins and immune system. *J Leukoc Biol*. 85:905-10.

Tucker, N.R., and E.A. Shelden. 2009. Hsp27 associates with the titin filament system in heat-shocked zebrafish cardiomyocytes. *Exp Cell Res*. 315:3176-86.

Tucker, N.R., A. Ustyugov, A.L. Bryantsev, M.E. Konkel, and E.A. Shelden. 2009. Hsp27 is persistently expressed in zebrafish skeletal and cardiac muscle tissues but dispensable for their morphogenesis. *Cell Stress Chaperones*. 14:521-33.

Urasaki, A., G. Morvan, and K. Kawakami. 2006. Functional dissection of the Tol2 transposable element identified the minimal cis-sequence and a highly repetitive sequence in the subterminal region essential for transposition. *Genetics*. 174:639-49.

Vidyasagar, A., N.A. Wilson, and A. Djamali. 2012. Heat shock protein 27 (HSP27): biomarker of disease and therapeutic target. *Fibrogenesis Tissue Repair*. 5:7.

Vinokurov, M., V. Ostrov, M. Yurinskaya, D. Garbuz, A. Murashev, O. Antonova, and M. Evgen'ev. 2012. Recombinant human Hsp70 protects against lipoteichoic acid-induced inflammation manifestations at the cellular and organismal levels. *Cell Stress Chaperones*. 17:89-101.

Wallin, R.P., A. Lundqvist, S.H. More, A. von Bonin, R. Kiessling, and H.G. Ljunggren. 2002. Heat-shock proteins as activators of the innate immune system. *Trends Immunol*. 23:130-5.

Willett, C.E., A. Cortes, A. Zuasti, and A.G. Zapata. 1999. Early hematopoiesis and developing lymphoid organs in the zebrafish. *Dev Dyn*. 214:323-36.

Wu, T., and R.M. Tanguay. 2006. Antibodies against heat shock proteins in environmental stresses and diseases: friend or foe? *Cell Stress Chaperones*. 11:1-12.

Wu, Y.L., X. Pan, S.P. Mudumana, H. Wang, P.W. Kee, and Z. Gong. 2008. Development of a heat shock inducible gfp transgenic zebrafish line by using the zebrafish hsp27 promoter. *Gene*. 408:85-94.

Yoo, S.K., C.M. Freisinger, D.C. LeBert, and A. Huttenlocher. 2012. Early redox, Src family kinase, and calcium signaling integrate wound responses and tissue regeneration in zebrafish. *J Cell Biol*. 199:225-34.

Yoo, S.K., and A. Huttenlocher. 2011. Spatiotemporal photolabeling of neutrophil trafficking during inflammation in live zebrafish. *J Leukoc Biol*. 89:661-7.

Yoshida, H., T. Matsui, A. Yamamoto, T. Okada, and K. Mori. 2001. XBP1 mRNA is induced by ATF6 and spliced by IRE1 in response to ER stress to produce a highly active transcription factor. *Cell*. 107:881-91.

Fig. 1. Heat shock effects on neutrophil recruitment. (A) Schematic illustration of the experimental setup for otic vesicle infection shown in C. (B) Schematic illustration of the experimental setup for tail fin wounding shown in E. The red rectangle indicates heat shock at 38-39°C for 1 hour. Grey circles indicate the time point for neutrophil counting. (C) Quantification of neutrophils at the otic vesicle (yellow dotted line) in control (cntl) and heat shocked (HS) larvae at 2 hours post infection (2 hpi). Larvae were injected with 100 CFU of *Streptococcus iniae* (*S.i*) into the otic vesicle (ear) at 3 days post fertilization (dpf). HS larvae showed decreased neutrophil recruitment compared with controls. ***P*<0.01 (two-tailed, unpaired t-test). (Right panel) Representative images of Sudan Black-stained larvae. Lateral view of the head of larvae at 2 hpi. (D) Survival of control (cntl) and heat shocked (HS) larvae infected with *S.i.* in the ear over time. Control and HS larvae showed a similar survival rate. dpi; days post infection. (E) Quantification of neutrophils at wounds in control (cntl) and heat shocked (HS) larvae at 1 and 4 hour post wounding (hpw). HS larvae showed fewer neutrophils at wounds at 4 hpw compared with controls. *****P*<0.0001; ns, not significant (two-tailed, unpaired t-test). (Right panel) Representative images of Sudan Black-stained larvae. Lateral view of the tail fin of larvae at 3 dpf. (F) Quantification of neutrophils in whole larvae for control (cntl), heat shocked (HS) and 3 hours post heat shocked (3 hpHS) larvae. (Right panel) Representative images of Sudan Black-stained larvae. Data are representative of at least three experiments.

Fig. 1

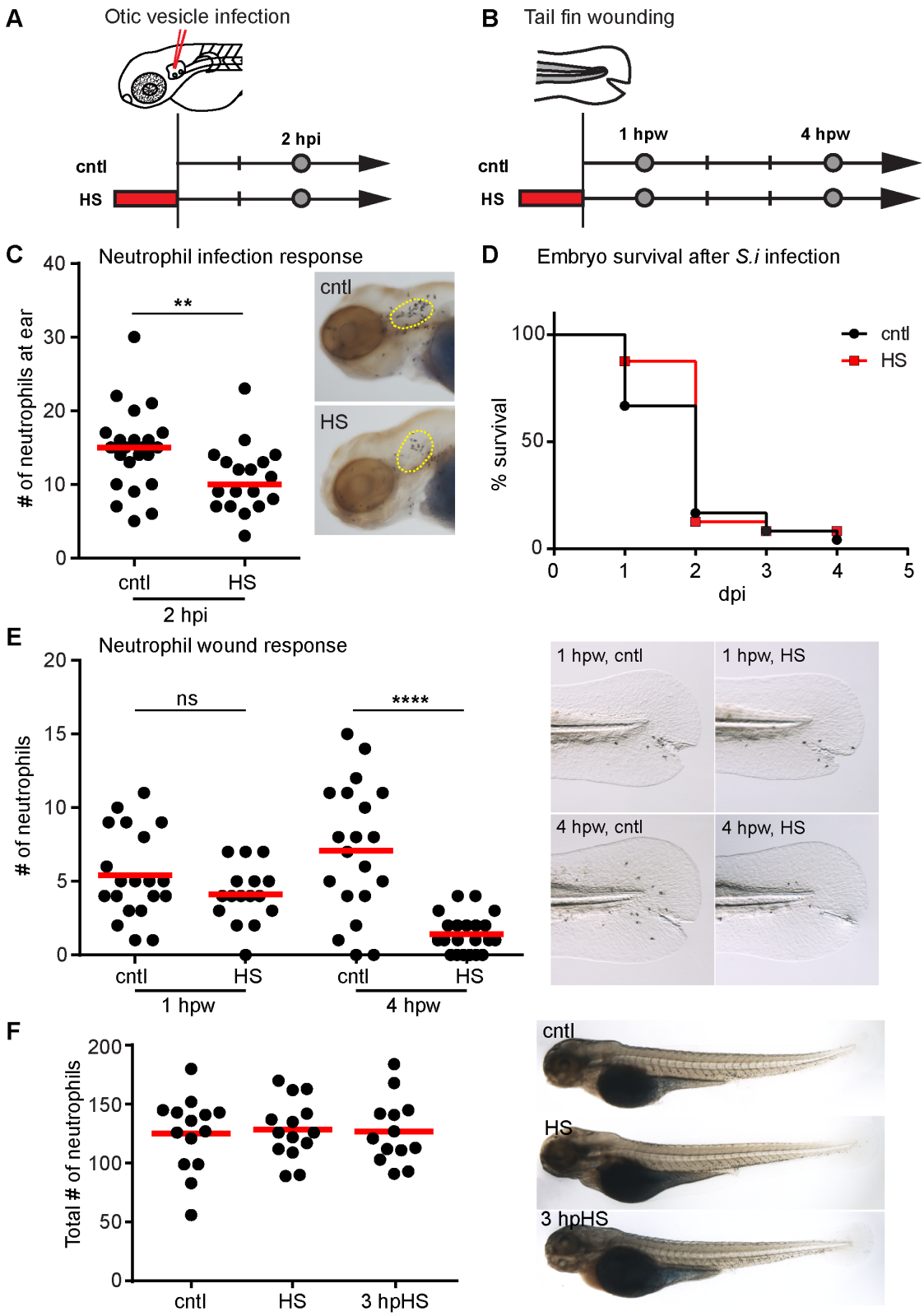
A
Otic vesicle infection
2 hpi
cntl
HS
B
Tail fin wounding
1 hpw
4 hpw
cntl
HS
C
Neutrophil infection response
# of neutrophils at ear
**
cntl
HS
2 hpi
D
Embryo survival after S.i infection
% survival
dpi
cntl
HS
E
Neutrophil wound response
# of neutrophils
ns
****
cntl
HS
1 hpw
4 hpw
1 hpw, cntl
1 hpw, HS
4 hpw, cntl
4 hpw, HS
F
Total # of neutrophils
cntl
HS
3 hpHS

Fig. 2. Heat shock induces transient changes in neutrophil random motility and sustained effects on recruitment to wounds. (A) (Top) Schematic illustration of the experimental setup for quantification of neutrophil speed. The red rectangles indicate heat shock at 38-39°C for 1 hour. Arrows indicate the time point for neutrophil live imaging in the same larva before heat shock (cntl), right after heat shock (HS) and at 3 hours post heat shock (3 hpHS). (Bottom) Scatter plot showing the mean speed of *Tg(mpx:dendra2*) neutrophils at time points indicated. Neutrophils were tracked in 3 dimensions (3D) using Image J software and the MTrackJ plugin. HS larvae showed increased neutrophil speed compared with controls. At 3 hpHS, the speed of neutrophils went back to control levels. ***P*<0.01; ns, not significant (one way ANOVA with Dunn's multiple comparison test). (B) (Top) Schematic illustration of the experimental setup for tail fin wounding. Larvae were wounded without heat shock (cntl), right after heat shock (HS) or at 3 hours post heat shock (3 hpHS). Larvae were then fixed at 4 hours post wounding (hpw) for quantification of neutrophils (grey circles). (Bottom) Quantification of neutrophils at tail fin wounds at 4 hpw. The effect of HS on neutrophil wound response persisted even when the wound was induced at 3 hpHS. *****P*<0.0001 (one way ANOVA with Dunn's multiple comparison test). Data are representative of at least three experiments.

Fig. 2

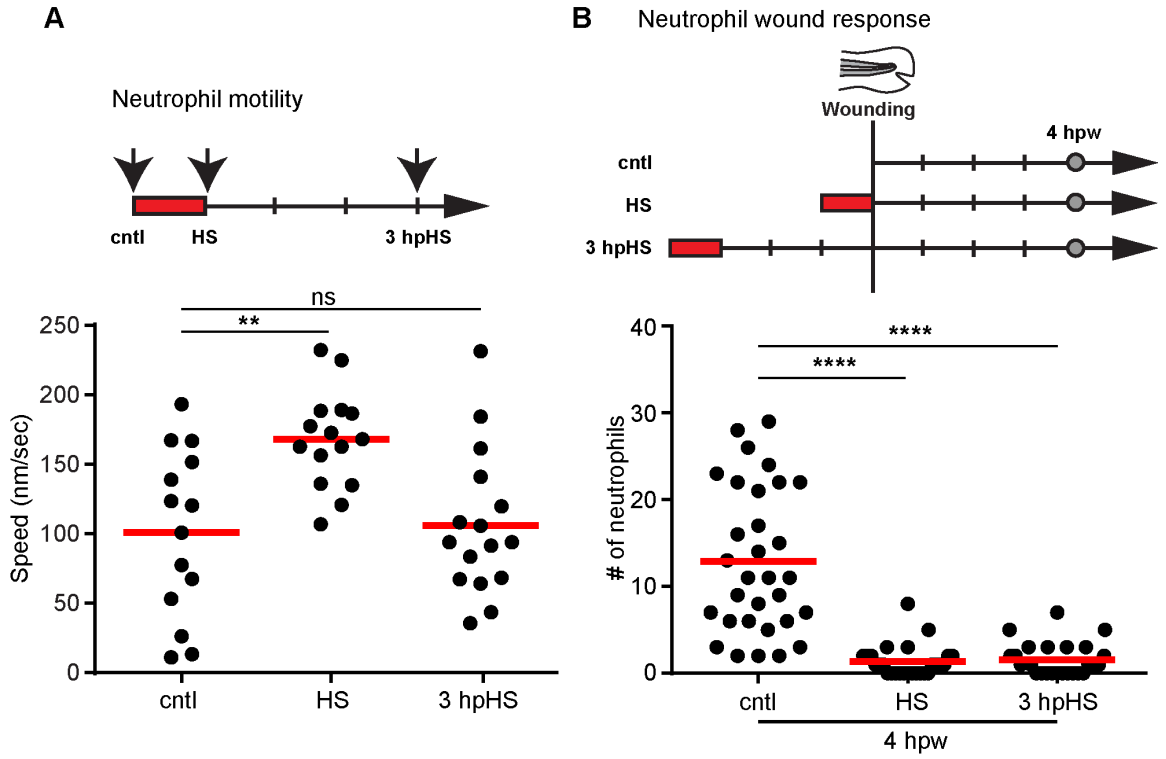
A
Neutrophil motility
cntl
HS
3 hpHS
ns
**
Speed (nm/sec)
250
200
150
100
50
0
cntl
HS
3 hpHS
B
Neutrophil wound response
Wounding
4 hpw
cntl
HS
3 hpHS
****
****
# of neutrophils
40
30
20
10
0
cntl
HS
3 hpHS
4 hpw

Fig. 3. Heat shock induces neutrophil mobilization. (A) Quantification of circulating neutrophils in larvae at 3 dpf. There was an increase in circulating neutrophils at 3 hpHS. $^{**}P<0.01$; ns, not significant (one way ANOVA with Dunn's multiple comparison test). (B) (Left panel) Yellow box indicates area where kymograph was generated. Fluorescent signal in boxed region was stacked vertically into a one-dimensional line at each time point. Scale bar = 100 μm. (Right panel) Kymograph of 3 minute movies with a 3 second interval indicating the presence or absence of circulating neutrophils is shown. Data are representative of at least three experiments.

Fig. 3

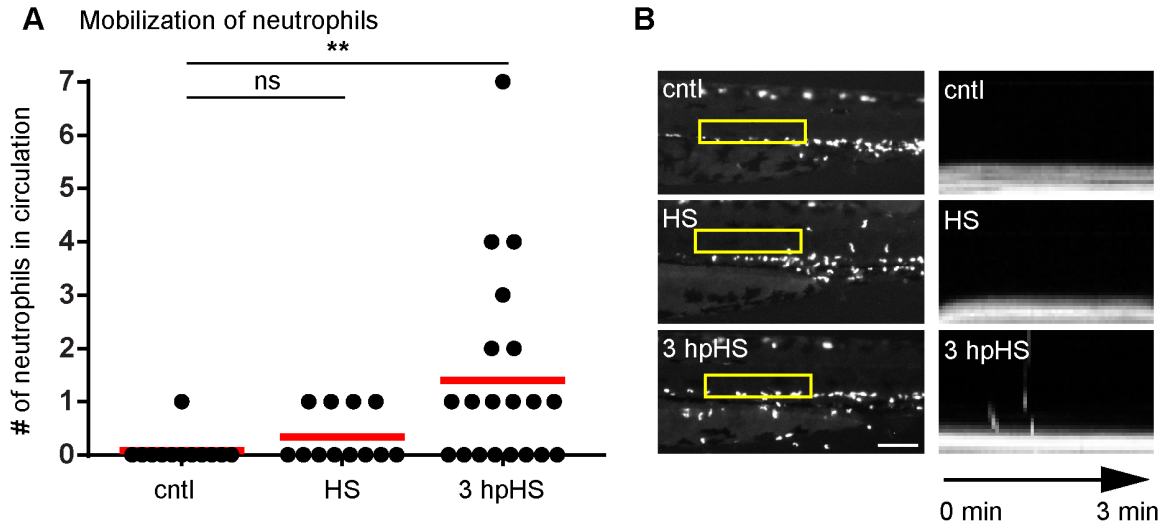
A
Mobilization of neutrophils
**
ns
# of neutrophils in circulation
0
1
2
3
4
5
6
7
cntl
HS
3 hpHS
B
cntl
HS
3 hpHS
cntl
HS
3 hpHS
0 min
3 min

Fig. 4. Heat shock induces changes in gene expression. (A) RT-PCR analysis of *hsp70*, *hsp27* and splicing of *xbp1* (p, pre-sliced; s, spliced) in control (cntl) or heat shock (HS) larvae. (B-C) RT-PCR analysis of the enrichment of RNA from neutrophils (lyz:TRAP), macrophages (mpeg1:TRAP) or epithelial cells (krt4:TRAP) from *Tg*(*lyz:EGFP-L10a*), *Tg*(*mpeg1:EGFP-L10a*) or *Tg*(*krt4:EGFP-L10a*) larvae, respectively. Whole larvae RNA (WT) or translating ribosome affinity purification (TRAP) RNA was used and specific markers for neutrophils (*mpx*), macrophages (*mpeg1*), epithelial cells (*krt4*) and muscle cells (*myoD*) were tested. (D) Heat shock (HS) induced expression of *hsp70*, *hsp27* and splicing of *xbp1* (p, pre-sliced; s, spliced) in neutrophils (lyz:TRAP), macrophages (mpeg1:TRAP) and epithelial cells (krt4:TRAP). Expression of *hsp27* persisted at 3 hours post heat shock (3 hpHS) while expression of *hsp70* and splicing of *xbp1* returned to control levels at 3 hpHS. Data are representative of at least two experiments.

Fig. 4

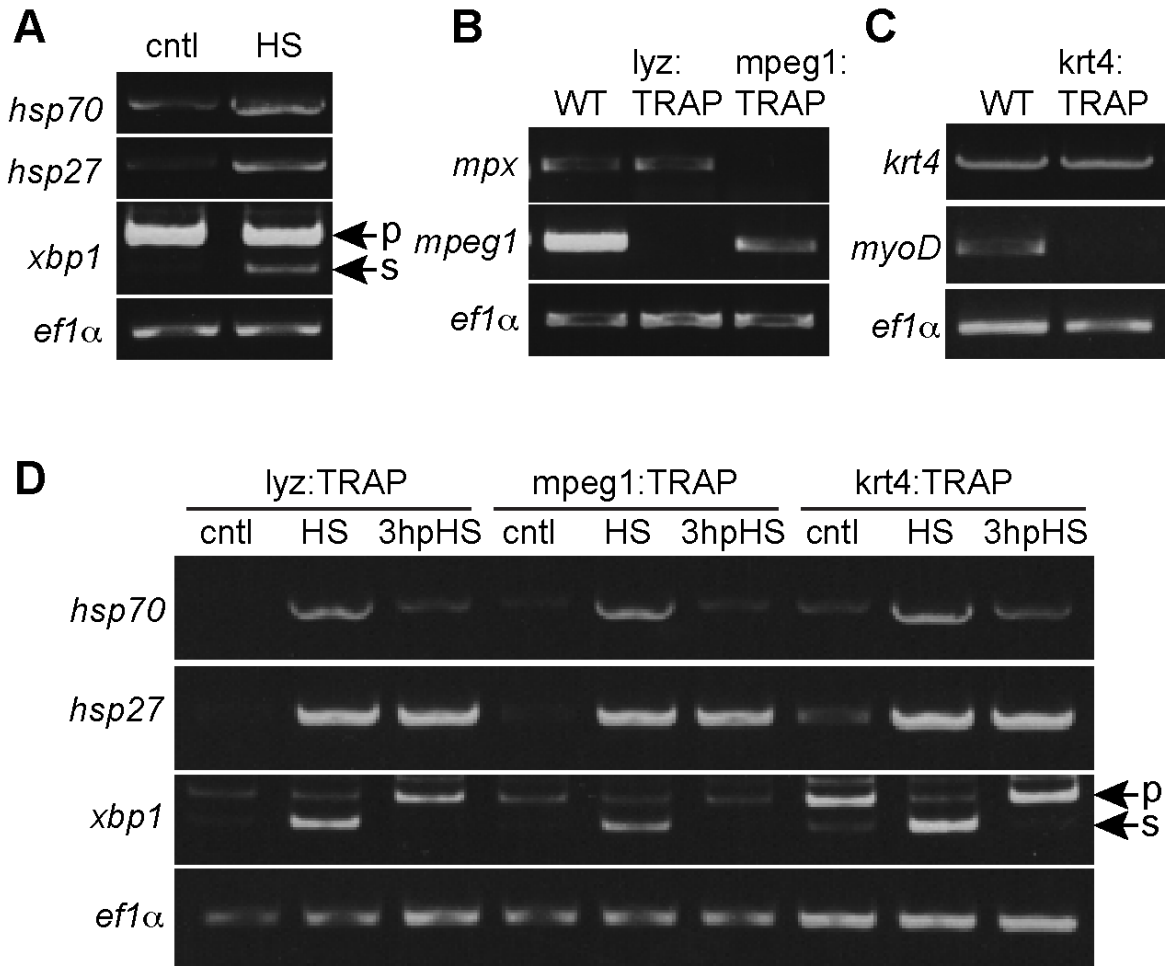
A
cntl
HS
hsp70
hsp27
xbp1
ef1α
p
s
B
WT
lyz: TRAP
mpeg1: TRAP
mpx
mpeg1
ef1α
C
WT
krt4: TRAP
krt4
myoD
ef1α
D
lyz:TRAP
mpeg1:TRAP
krt4:TRAP
cntl
HS
3hpHS
hsp70
hsp27
xbp1
ef1α
p
s

Fig. 5. Expression of Hsp27, Hsp70 or spliced Xbp1 in neutrophils or epithelial cells does not alter neutrophil recruitment. (A-C) Quantification of neutrophils at the otic vesicle (ear) of larvae at 2 hours post infection (hpi) with 100 CFU *S.i.* ear infection. Experiments were performed on the larvae of transgenic lines *Tg*(*lyz:hsp70-2A-EGFP*) x *Tg*(*krt4:hsp70-2A-mCherry*) (A), *Tg*(*lyz:hsp27-2A-mCherry*) (B) or *Tg*(*lyz:xbp1s-2A-EGFP*) x *Tg*(*krt4:xbp1s-2A-mCherry*) (C) at 3 dpf. Controls (cntl) were siblings with no transgene expression. Expression of Hsp27, Hsp70 and spliced Xbp1 (Xbp1s) did not have a significant effect on neutrophil recruitment to ear infection. (D-H) Quantification of neutrophils at tail fin wounds at 4 hpw. Experiments were performed on *Tg*(*lyz:hsp70-2A-EGFP*) (D), *Tg*(*krt4:hsp70-2A-mCherry*) (E), *Tg(lyz:hsp27-2A-mCherry*) (F), *Tg*(*lyz:xbp1s-2A-EGFP*) (G) or *Tg*(*krt4:xbp1s-2A-mCherry*) (H) larvae at 3 dpf. Controls (cntl) were siblings with no transgene expression. Expression of Hsp27, Hsp70 and spliced Xbp1 (Xbp1s) did not have a significant effect on neutrophil numbers at the wound at 4 hpw. Data are representative of at least two experiments.

Fig. 5

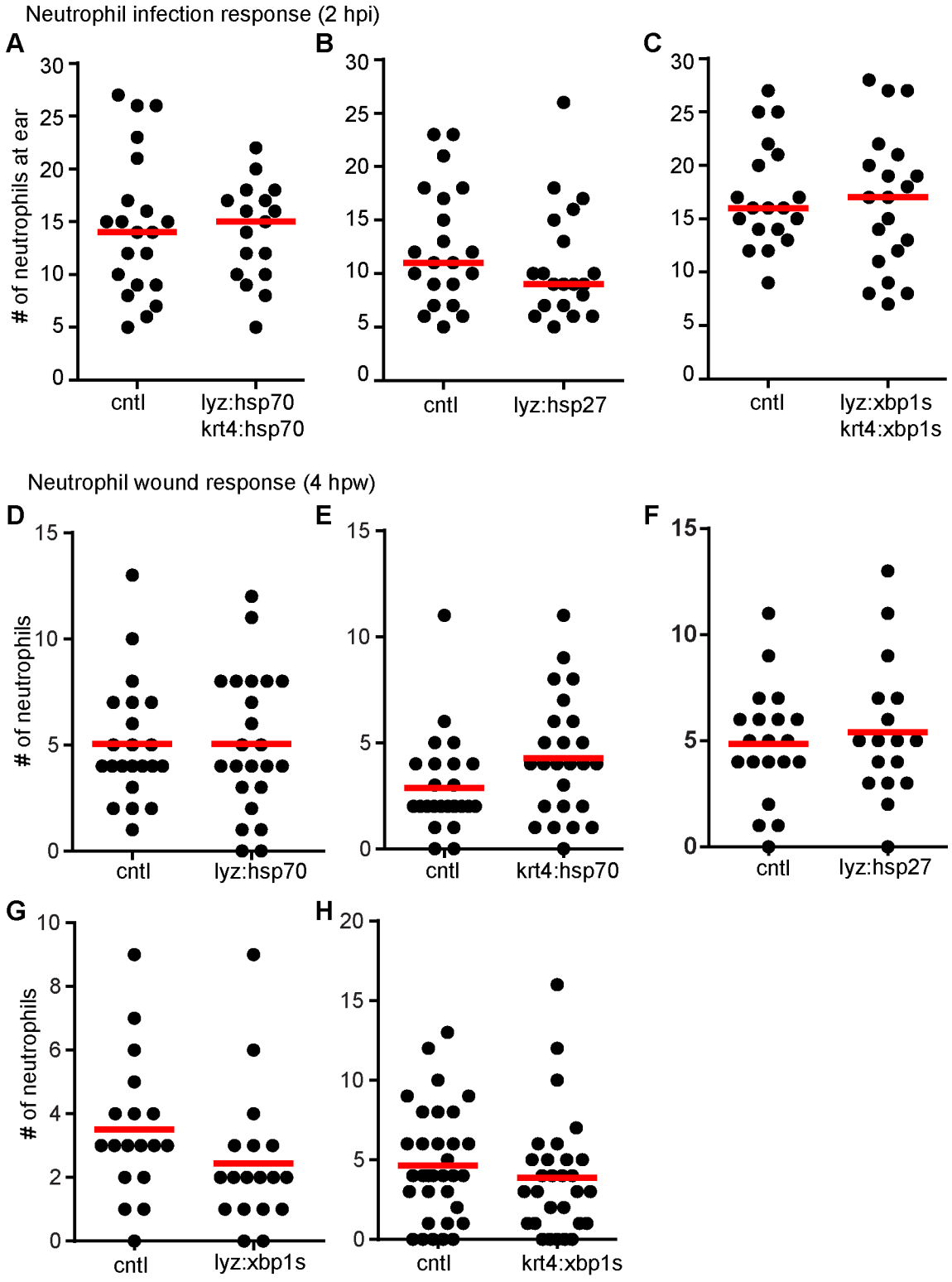
Neutrophil infection response (2 hpi)
A
B
C
# of neutrophils at ear
cntl
lyz:hsp70
krt4:hsp70
lyz:hsp27
lyz:xbp1s
krt4:xbp1s
Neutrophil wound response (4 hpw)
D
E
F
# of neutrophils
lyz:hsp70
krt4:hsp70
lyz:hsp27
G
H
lyz:xbp1s
krt4:xbp1s

Chapter 5

Conclusions and future directions

Rapid leukocyte motility is essential for immunity and host defense. There has been progress in understanding the molecular signals that regulate leukocyte motility both *in vitro* and *in vivo*. However, a gap remains in understanding how complex signals are prioritized to result in directed migration, which is critical for both adaptive and innate immune function. My dissertation research has provided insights into the cell signaling and cytoskeletal regulation of neutrophil interstitial migration *in vivo*. In particular, I elucidate that SHIP and microtubules act as two negative regulators of neutrophil motility. SHIP regulates neutrophil motility through modulating PI3K signaling. Proper microtubule dynamics maintain proper neutrophil polarity and directional motility at least partly by regulating Rac and Rho activity. In addition, I show that the short-term heat shock method commonly used for inducible gene expression in animal models can affect neutrophil function. Here, I will address the broader applications and implications in each of these areas and suggest future studies that may be followed as a result of my research findings.

SHIP and disease treatment implications

SHIP has been implicated as an important regulator of human disease status such as cancer, inflammatory disease, diabetes, atherosclerosis, and Alzheimer's disease (reviewed in (Viernes et al., 2014)). SHIP converts the phosphatidylinositol 3-kinase (PI3K) product PI(3,4,5)P3 to PI(3,4)P2 and therefore modulates the PI3K/Akt/mTOR signaling pathway which is often dysregulated in the disease state. Identifying inhibitors for PI3K is complicated by the numerous PI3K isoforms (reviewed

in (Blunt and Ward, 2012; Viernes et al., 2014)). Furthermore, the development of inhibitors for PI3Kγ, an isoform expressed in hematopoietic cell lineage, has been rather unsuccessful (Blunt and Ward, 2012). SHIP is therefore an alternative target to modulate PI3K signaling particularly in the immune system (Blunt and Ward, 2012; Viernes et al., 2014). In addition, SHIP may have dual roles in PI3K signaling as its product PI(3,4)P2 can activate downstream effectors of PI3K, as well as act as an independent signaling molecule (reviewed in (Blunt and Ward, 2012)). There has been considerable interest in identifying both antagonists and agonists of SHIP as potential therapeutic agents where modulating PI3K/Akt/mTOR signaling pathways may be beneficial (Viernes et al., 2014). In fact, a small molecule SHIP1 activator (AQX-1125) is already undergoing clinical trails (Stenton et al., 2013; Stenton et al., 2011). My thesis research has provided insights into the endogenous function of SHIPs in inhibiting normal neutrophil motility through modulating PI3K signaling. These findings highlight a potential use of the zebrafish for disease modeling in which PI3K signaling is dysregulated with a specific focus on determining whether or not SHIP can modulate disease status and progression. Characterizing the role of SHIP in modulating disease status in an *in vivo* experimental system is essential for accelerating the potential use of SHIP modulators as novel disease therapies. In addition, the zebrafish has proven to be a powerful platform for high throughput small molecule screening to indentify new chemical tools and drug leads (reviewed in (Tamplin et al., 2012; Taylor et al., 2010; Zhang and Yeh, 2012)). In my thesis work, I utilized zebrafish larval tail fin wounding assays to assess the role of SHIPs in neutrophil function and behavior. Neutrophil wound recruitment involves many signaling molecules, both from the injured tissue as

well as from the neutrophils themselves (Lam et al., 2012; Liu et al., 2014; McDonald et al., 2010; Niethammer et al., 2009; Stark et al., 2013; Yoo et al., 2012; Yoo et al., 2011). However, a thorough search of the literature reveals that SHIP is the only negative regulator of neutrophil wound response, as knockdown of SHIP results in an increase in neutrophil wound recruitment. This suggests that zebrafish tail fin wounding assays can potentially be used as a screening tool to identify inhibitors of SHIP.

Role of microtubules and neutrophils chemotaxis

Recent studies have advanced our understanding of how external cues are translated into intracellular signaling pathways that regulate leukocyte polarity, directional sensing and motility in three-dimensional spaces (reviewed in (Lam and Huttenlocher, 2013; Weninger et al., 2014)). Despite substantial progress in identifying mechanisms that initiate neutrophil wound attraction (Deng et al., 2012; McDonald et al., 2010; Niethammer et al., 2009; Yoo et al., 2011), exactly how neutrophil directional motility is regulated in live animals and 3D environments is not well defined. During an amoeboid mode of migration, cells undergo cycles of pseudopod generation and selection, as well as the retraction of the cell rear (reviewed in (Andrew and Insall, 2007; Insall, 2010)). Understanding the mechanism of neutrophil pseudopod selection will provide insight into the regulation of cell directional migration.

My work has shown that MTs play an important role in neutrophil polarity and directional migration *in vivo*. The microtubule organizing center (MTOC), where microtubule formation begins, is always maintained in front of the nucleus towards the

leading edge (Chapter 3). Investigating the regulation of MTs or the MTOC on neutrophil directional migration has been challenging, primarily due to the difficulties of direct imaging of MTs using traditional MT binding bioprobes, as well as the highly motile nature of neutrophil migration. In Appendix I, I have summarized various genetic and pharmacological approaches that I have used to elucidate MTs and MTOC positioning in regulating neutrophil migration *in vivo*. In particular, further imaging analyses suggest that the MTOC seems to always be positioned towards the pseudopod that is being selected and maintained, but not towards the retracted pseudopod (Appendix I Fig. 4A). Interestingly, nocodazole induced MT depolymerization results in disposition of the MTOC where it is no longer maintained in the front of the nucleus in migrating neutrophils *in vivo* (Appendix I Fig. 5). Under this condition, directional migration of neutrophils is also impaired. It is possible that microtubules are involved in pseudopod selection and therefore regulate directional motility. The cell autonomous function of MTOC position or microtubule integrity in pseudopod selection during directed cell migration remains to be tested. Molecular or genetic tools that interfere with proper MTOC positioning will be instrumental in testing this hypothesis. Further analysis is required to address the following question: What is the sub-cellular localization and dynamics of MTs in migrating neutrophils *in vivo*? How is the positioning of the MTOC in a migrating neutrophil being achieved? Is MTOC positioning adjacent to or in close proximity of a pseudopod sufficient and required for its stabilization? Does pseudopod retraction require depolymerization of local MTs? Lastly, is the regulation of macrophage pseudopod selection similar to that of neutrophils? Further details are discussed in Appendix I.

Heat Shock and innate immune response

In Chapter 5, I illustrated that the short-term heat shock method traditionally used for inducible gene expression has effects on innate immune cell function. Although heat shock induced changes in gene expression profile and neutrophil wound response, along with a transient increase in neutrophil motility, it did not affect the overall survival of zebrafish larvae upon *Streptococcus iniae* (*S.i*) otic vesicle infection. These results suggest that the heat shock innate immune cell phenotype is transient and that short-term heat shock does not provide any beneficial effect for larvae upon pathogenic bacterial infection (such as *S.i*). In mammals, it has been long debated whether or not a fever is a beneficial response towards an infection. There is evidence that fish exhibit behavioral fever upon infection and in some cases elevated temperature increases survival (Boltana et al., 2013; Covert and Reynolds, 1977; Grans et al., 2012; Reynolds et al., 1976). My research focused on short-term heat shock as it is relevant to a broader application of the heat shock method commonly used in the zebrafish community. The mechanism that underlies the heat shock neutrophil phenotype is complicated and not easily understood. It involves the expression of heat shock proteins such as Hsp70 and Hsp27, as well as the induction of at least one endoplasmic reticulum cell stress pathway, displayed by the expression of spliced Xbp1. We were able to observe and measure these responses in short-term heat-shocked larvae. However, recreating these conditions separately, and in the absence of heat shock, specifically to neutrophils or epithelial cells did not recapitulate the neutrophil heat shock phenotype. Further investigation is needed to identify the crucial underlying signaling changes that occur in response to short-term heat shock and which regulate immune

cell functions. Additionally, future interrogation of this process should include consideration of changes that are due to the increase in enzyme kinetics at higher temperatures. Furthermore, it will be informative to gain an understanding of the effect that long-term temperature elevation has on larval survival after infection.

Conclusions

Advances in multi-photon vital imaging technology and new model systems such as the zebrafish, have made it possible to study interstitial migration with higher resolution *in vivo*. What is becoming increasingly clear, however, is that although much of the knowledge acquired from *in vitro* studies can apply to the *in vivo* environment, not all mechanisms are similar. Therefore, future challenges will be to apply and combine both *in vitro* and *in vivo* analyses to increase our understanding of leukocyte interstitial migration and how responses are prioritized to competing extracellular cues and result in directional migration.

References

Andrew, N., and R.H. Insall. 2007. Chemotaxis in shallow gradients is mediated independently of PtdIns 3-kinase by biased choices between random protrusions. *Nat Cell Biol*. 9:193-200.

Blunt, M.D., and S.G. Ward. 2012. Pharmacological targeting of phosphoinositide lipid kinases and phosphatases in the immune system: success, disappointment, and new opportunities. *Front Immunol*. 3:226.

Boltana, S., S. Rey, N. Roher, R. Vargas, M. Huerta, F.A. Huntingford, F.W. Goetz, J. Moore, P. Garcia-Valtanen, A. Estepa, and S. Mackenzie. 2013. Behavioural fever is a synergic signal amplifying the innate immune response. *Proc Biol Sci*. 280:20131381.

Covert, J.B., and W.W. Reynolds. 1977. Survival value of fever in fish. *Nature*. 267:43-5.

Deng, Q., E.A. Harvie, and A. Huttenlocher. 2012. Distinct signalling mechanisms mediate neutrophil attraction to bacterial infection and tissue injury. *Cell Microbiol*. 14:517-28.

Grans, A., M. Rosengren, L. Niklasson, and M. Axelsson. 2012. Behavioural fever boosts the inflammatory response in rainbow trout Oncorhynchus mykiss. *J Fish Biol*. 81:1111-7.

Insall, R.H. 2010. Understanding eukaryotic chemotaxis: a pseudopod-centred view. *Nat Rev Mol Cell Biol*. 11:453-8.

Lam, P.Y., and A. Huttenlocher. 2013. Interstitial leukocyte migration in vivo. *Curr Opin Cell Biol*.

Lam, P.Y., S.K. Yoo, J.M. Green, and A. Huttenlocher. 2012. The SH2-domain-containing inositol 5-phosphatase (SHIP) limits the motility of neutrophils and their recruitment to wounds in zebrafish. *J Cell Sci*. 125:4973-8.

Liu, M., K. Chen, T. Yoshimura, Y. Liu, W. Gong, Y. Le, J.L. Gao, J. Zhao, J.M. Wang, and A. Wang. 2014. Formylpeptide receptors mediate rapid neutrophil mobilization to accelerate wound healing. *PLoS One*. 9:e90613.

McDonald, B., K. Pittman, G.B. Menezes, S.A. Hirota, I. Slaba, C.C. Waterhouse, P.L. Beck, D.A. Muruve, and P. Kubes. 2010. Intravascular danger signals guide neutrophils to sites of sterile inflammation. *Science*. 330:362-6.

Niethammer, P., C. Grabher, A.T. Look, and T.J. Mitchison. 2009. A tissue-scale gradient of hydrogen peroxide mediates rapid wound detection in zebrafish. *Nature*. 459:996-9.

Reynolds, W.W., M.E. Casterlin, and J.B. Covert. 1976. Behavioural fever in teleost fishes. *Nature*. 259:41-2.

Stark, K., A. Eckart, S. Haidari, A. Tirniceriu, M. Lorenz, M.L. von Bruhl, F. Gartner, A.G. Khandoga, K.R. Legate, R. Pless, I. Hepper, K. Lauber, B. Walzog, and S. Massberg. 2013. Capillary and arteriolar pericytes attract innate leukocytes exiting through venules and 'instruct' them with pattern-recognition and motility programs. *Nat Immunol*. 14:41-51.

Stenton, G.R., L.F. Mackenzie, P. Tam, J.L. Cross, C. Harwig, J. Raymond, J. Toews, D. Chernoff, T. MacRury, and C. Szabo. 2013. Characterization of AQX-1125, a small-molecule SHIP1 activator: Part 2. Efficacy studies in allergic and pulmonary inflammation models in vivo. *Br J Pharmacol*. 168:1519-29.

Stenton, G.R., L.F. Mackenzie, P. Tam, J.L. Cross, C. Harwig, J. Raymond, J. Toews, J. Wu, N. Ogden, T. MacRury, and C. Szabo. 2011. Characterization of AQX-1125, a small-molecule SHIP1 activator: Part 1. Effects on inflammatory cell activation and chemotaxis in vitro and pharmacokinetic characterization in vivo. *Br J Pharmacol*. 168:1506-18.

Tamplin, O.J., R.M. White, L. Jing, C.K. Kaufman, S.A. Lacadie, P. Li, A.M. Taylor, and L.I. Zon. 2012. Small molecule screening in zebrafish: swimming in potential drug therapies. *Wiley Interdiscip Rev Dev Biol*. 1:459-68.

Taylor, K.L., N.J. Grant, N.D. Temperley, and E.E. Patton. 2010. Small molecule screening in zebrafish: an in vivo approach to identifying new chemical tools and drug leads. *Cell Commun Signal*. 8:11.

Viernes, D.R., L.B. Choi, W.G. Kerr, and J.D. Chisholm. 2014. Discovery and development of small molecule SHIP phosphatase modulators. *Med Res Rev*. 34:795-824.

Weninger, W., M. Biro, and R. Jain. 2014. Leukocyte migration in the interstitial space of non-lymphoid organs. *Nat Rev Immunol*. 14:232-46.

Yoo, S.K., P.Y. Lam, M.R. Eichelberg, L. Zasadil, W.M. Bement, and A. Huttenlocher. 2012. The role of microtubules in neutrophil polarity and migration in live zebrafish. *J Cell Sci*. 125:5702-10.

Yoo, S.K., T.W. Starnes, Q. Deng, and A. Huttenlocher. 2011. Lyn is a redox sensor that mediates leukocyte wound attraction in vivo. *Nature*.

Zhang, Y., and J.R. Yeh. 2012. In vivo chemical screening for modulators of hematopoiesis and hematological diseases. *Adv Hematol*. 2012:851674.

Appendix I

Characterization of neutrophil pseudopod selection

Abstract

Neutrophil migration involves cycles of pseudopod generation, bifurcation, selection and retraction, as well as the retraction of the cell rear. This allows neutrophils to directionally migrate. In this chapter, I further characterize the cytoskeleton regulation of neutrophil directional motility. In particular, I will focus on the process of pseudopod selection and retraction. Preliminary data suggest that there is accumulation of stable F-actin and myosin light chain in the retracting pseudopod, pointing to the involvement of actomyosin contractility during pseudopod retraction. Further, F-actin dots are observed close to the cell surface during slow neutrophil motility but not when neutrophils are actively migrating. Microtubules (MTs) and the position of microtubule organizing center (MTOC) position are also involved in neutrophil migration. Preliminary data suggest that there is a positive correlation among the position of MTOC, pseudopod selection and cell speed. Further investigation is required to elucidate the mechanism by which MTs and the MTOC regulate neutrophil pseudopod selection and directional motility.

Introduction

The rapid single-cell migration used by leukocytes is classically known as ‘amoeboid’ migration. The term ‘amoeboid’ is based on a changing cell morphology, but can encompass different modes of locomotion (reviewed in (Lammermann and Sixt, 2009; Nourshargh et al., 2010)). During an amoeboid mode of migration under shallow chemotactic gradients, cells undergo cycles of pseudopod generation, bifurcation, selection and retraction, as well as the retraction of the cell rear (reviewed in (Andrew and Insall, 2007; Insall, 2010)). In the current paradigm for cell migration, actin filaments polymerize at front of the cell and control cell protrusion, whereas non-muscle myosin II activation in the rear results in retraction of the cell’s rear [reviewed in (Pollard and Borisy, 2003; Vicente-Manzanares et al., 2009)]. Substantial progress has been made in identifying mechanisms that initiate neutrophil wound attraction (Deng et al., 2012; McDonald et al., 2010; Niethammer et al., 2009; Yoo et al., 2011). However, the mechanism regulating pseudopod selection and therefore directional migration is not entirely clear.

Microtubules (MTs) are arranged asymmetrically during neutrophil polarization and migration (Eddy et al., 2002; Peris et al., 2009). It has been suggested in previous studies that MTs are required for preferential stabilization of appropriate pseudopods in amoebae (Ueda and Ogihara, 1994). Microtubules in neutrophils have been shown to suppress polarity and enhance directional migration *in vitro* (Niggli, 2003; Xu et al., 2005). However, the exact mechanism for how microtubule asymmetry regulates cell polarization and directional migration is less well understood. In clinical practice, colchicine (an anti-inflammatory drug) is used for treating autoinflammatory diseases

such as acute gout and familial Mediterranean fever (Molad, 2002). One of the biological functions of colchicine is to inhibit microtubule polymerization by binding to tubulin, but the exact mechanism of its effect on limiting inflammation is not known.

I have previously shown that MTs play an important role in neutrophil polarity and directional migration *in vivo*. The microtubule organizing center (MTOC) from which MTs emerge, is always maintained in front of the nucleus towards the leading edge (presented in Chapter 3). It is thought that the reorientation of the MTOC in migrating cells confers polarity (Prigozhina and Waterman-Storer, 2004). Others reported that the reorientation of the MTOC ***directs*** migration in fibroblasts and astrocytes (Etienne-Manneville and Hall, 2001; Gomes et al., 2005). On the contrary, it has been shown *in vitro*, that the MTOC of the neutrophil-like dHL-60 cell line ***follows*** the pseudopod and does not direct its orientation (Xu *et al.*, 2005). Interestingly, the MTOC strongly predicts the direction of polarity in dHL-60 cells (Xu et al., 2007). However, how MTs regulate directional migration remains unclear. The cell autonomous function of the MTOC's position or MT integrity in pseudopod selection during directed cell migration remains to be tested.

In this chapter, I will further characterize F-actin dynamics and actomyosin contraction during the process of pseudodpod retraction. I will also present data on the role of MTs and the MTOC in neutrophil steering.

Preliminary results and discussion

F-actin dynamics and actomyosin contraction during neutrophil pseudopod retraction

In order to visualize F-actin dynamic in neutrophils *in vivo*, I expressed two F-actin binding probes specifically in neutrophils of zebrafish larvae using the *mpx* promoter: Lifeact fused to Ruby, which detects all F-actin (Riedl et al., 2008); and the calponin homology domain of utrophin (UtrCH) fused to GFP, which detects more stable F-actin (Burkel et al., 2007). Dynamic F-actin, as indicated by the presence of Lifeact but not UtrCH signal, is observed in the protruding pseudopod of migrating neutrophils. Stable F-actin, as indicated by the presence of UtrCH signal, accumulates in the retracting pseudopod as well as in the rear of neutrophils (Fig. 1; left panels). Line-scan measurement in the retracting pseudopod indicates that the signal of stable F-actin relative to all F-actin increases as the pseudopod retracts (Fig 1; right panel).

In order to address the relationship of actomyosin localization and pseudopod retraction, time series ratiometric imaging comparing the signal from myosin regulatory light chain (MRLC) to that of Lifeact (F-actin) was performed. Ratiometric imaging analysis did not yield any correlation between the accumulation of MRLC and pseudopod retraction (data not shown). This may be due to the intrinsic difference between the localization of F-actin and MRLC in the cell (F-actin localization is highly cortical while MRLC is mostly cytosolic and there may also be unbound MRLC protein in the cell body). In order to solve this problem and have a better understanding of the dynamics of actomyosin during neutrophil migration, ratiometric imaging of MRLC to a volume marker, mCherry, was performed. As expected, there is a strong MRLC/mCherry signal in the rear of neutrophils indicating the actomyosin structure for

tail retraction. Interestingly, ratiometric and kymograph analysis suggests that there is an increase in MRLC signal in pseudopods during the phase of pseudopod retraction. This strong MRLC signal is absent in the protruding pseudopod (Fig. 2A-C). Further experiments are needed to refine the exact timing of MRLC accumulation in the pseudopod retraction process. Additionally, it will be informative to perform image analysis of MRLC in combination with a membrane marker in neutrophils *in vivo,* in order to further characterize the spatial and temporal localization of MRLC relative to the very edge of the pseudopod.

An additional phenomenon was observed during imaging of GFP-UtrCH or Lifeact-Ruby in neutrophils *in vivo* – F-actin dots. These F-actin dots appear mostly in the rear of neutrophils during migration (Fig. 3Ai) and increase in number when neutrophil motility decreases or stops (Fig. 3Aii). Most of these F-actin dots are observed close to the cell surface (Fig. 3B). Focal adhesions (FAs) and podosomes are the two known structures with an actin core that are commonly found in motile cells (Linder and Kopp, 2005). Both FAs and podosomes are intimately involved in cell motility, with podosomes specifically implicated in cell invasion. Proteins that are found in both FAs and podosomes include; vinculin, paxillin and Arp2/3 etc (Linder and Kopp, 2005). A preliminary investigation using transient overexpression of fluorescently tagged vinculin and paxillin in neutrophils *in vivo* did not reveal any dot-like structures (data not shown). In an attempt to elucidate the nature of these F-actin dots in neutrophils, several pertinent observations were considered. With respect to focal adhesions, FAs are often connected to actin stress fibers (Hotulainen and Lappalainen, 2006). In neutrophils, no stress fibers attached to punctate actin dots have ever been

observed. It has been shown that nocodazole prevents microtubules from elongating and subsequently triggers the enlargement of FAs (Ezratty *et al.*, 2005). In a series of experiments, I observe that nocodazole induced a reduction of F-actin dots in neutrophils (Fig. 3Aiii). In addition, actomyosin contraction downstream of the RhoA-Rho kinase can mediate podosome dissolution and FA formation (van Helden *et al.*, 2008). Inhibition of Rho kinase by the inhibitor rockout did not inhibit the formation of these actin structures (data not shown). Taken together, these observations suggest that the F-actin dots observed in neutrophils may not in fact be FAs.

Research dealing with podosomes is equally intriguing. Rho GTPases are involved in podosome localization and assembly in dentritic cells (Burns *et al.*, 2001). Previous work in the Huttenlaocher lab has shown that expression of dominant negative Rac2 (D57N) impairs neutrophil motility and polarity (Deng et al., 2011). Building on these findings, I expressed Rac2(D57N) in neutrophils and observed a significant increase in F-actin dot structures. Inhibition of Src by PP2 or inhibition of PLCγ by U73122 both result in impaired podosome formation *in vitro* (Boateng *et al.*, 2012; Wang *et al.*, 2009). When I treated zebrafish larvae with PP2 or U73122, F-actin dots were still observed in neutrophils *in vivo* (data not shown). Furthermore, podosomes can be inhibited when NADPH oxidase (NOX) is inhibited using the chemical DPI (diphenyleneiodonium) (Diaz *et al.*, 2009). All Nox family enzymes require $p22^{phox}$ for catalytic activity (Ambasta *et al.*, 2004). When I treated zebrafish embryos with either DPI or with a $p22^{phox}$ morpholino (Niethammer et al., 2009) to knockdown its expression, neutrophils still displayed the formation of F-actin dots (data not shown). WASP (Wiskott-Aldrich Syndrome protein) activates actin polymerization by binding to

the Arp2/3 complex and is required for podosome formation (Burns *et al.*, 2001; Linder *et al.*, 1999). A mutation in human WASP (I294T) results in increased levels of F-actin and abnormal podosome clustering (Ancliff *et al.*, 2006). By overexpressing the equivalent zebrafish WASP mutation (I277T) in neutrophils, I observed a decrease in the polarization of stable F-actin but no obvious changes in F-actin dots (data not shown). Taken together, my data suggest that these F-actin dots may not be podosomes.

It must be considered that the F-actin dots observed in neutrophils may be both FAs and podosome or neither. In support of the later, integrins are part of both the FA and podosome structure. It has been shown that integrins are NOT required for leukocyte migration in 3D interstitial tissues (Lammermann *et al.*, 2008), the type of movement we are observing in the zebrafish model. Podosomes are a common structure in leukocytes including; monocytes, macrophages and dentritic cells (reviewed in (Dovas and Cox, 2011)). To date, there are no reports of podosomes in neutrophils *in vivo* and only a single report suggesting the presence of podosomes in the front of neutrophils *in vitro* (Szczur *et al.*, 2006). Further investigation is needed to definitively ascertain whether or not podosomes or FAs are indeed present in neutrophils and, furthermore, what function these actin structures have in neutrophils *in vivo*.

MTOC positioning during neutrophil motility

Neutrophil specific expression of γtubulin-GFP allows visualization of the MTOC in neutrophils *in vivo*. Image analyses suggest that the MTOC seems to always be positioned towards the pseudopod that is being selected and maintained, but not

towards the retracted pseudopod (Fig. 4A). As pseudopods can be generated in the opposite direction to the location of MTOC (Fig. 4B), it suggests that MTOC translocation is not necessary for pseudopod formation but mediates stabilization. As shown previously, the MTOC is maintained in front of the nucleus in neutrophils during migration *in vivo* (Fig. 5A). Further analysis to characterize the relationship among the position of the MTOC, pseudopod maintenance and speed of neutrophil migration was carried out. This was achieved by measuring the MTOC angle and the speed of the neutrophil migration. The MTOC angle is determined by measuring the angle between the line drawn from the MTOC to the cell centroid and the line drawn from the cell centroid to the dominant pseudopod - determined from the next frame of serial image capture (Fig. 5B). Preliminary data suggest that there is an inverse relationship between the MTOC angle and the speed of neutrophil (Fig. 5C). This suggests that when the MTOC is aligned with the dominant pseudopod, neutrophils migrate faster. When the MTOC is not aligned with the dominant pseudopod, neutrophils migrate slower. This shows a positive correlation between MTOC position and the dominant pseudopod, which may promote neutrophils to migrate more efficiently. Interestingly, nocodazole induced MT depolymerization results in the disposition of the MTOC where it is no longer maintained in the front of the nucleus in migrating neutrophil *in vivo* (Fig. 5A). Under these conditions, directional migration of neutrophils is also impaired. The inverse relationship between MTOC angle and speed is also altered compared to control (Fig. 5D). The causal relationship between MTOC position and directional migration, however, is not addressed in this analysis.

It has been an ongoing challenge to address the function of MTs and the MTOC in pseudopod selection. Glycogen synthase kinase 3 (GSK3) has been shown to regulate MTOC position in some cell types such as astrocytes (reviewed in (Sun et al., 2009)). In an attempt to modulate MTOC position in neutrophils, embryos were treated with LiCl to inhibit GSK3. Preliminary data suggest that inhibition of GSK3 using LiCl did not change the frequency of pseudopod generation in neutrophils (Fig. 6A). However, embryos treated with LiCl exhibited *de novo* pseudopod generation. This is in contrast to NaCl treated controls where new pseudopods are mainly generated from the bifurcation of an existing pseudopod (Fig. 6B). The caveat of this experiment is that GSK3 also plays a role in actin cytoskeleton reorganization (Tang et al., 2011), making interpretation of the phenotype complicated as proper actin polymerization is also required for pseudopod generation. Other approaches considered for the manipulation of MTOC position included photoactivation of Rac to induce pseudopod generation and laser ablation of the MTOC itself. However, these have proven to be very technically challenging since neutrophils are highly motile *in vivo* and precise laser targeting for a long period of time may not be feasible. Also considered was the use of an *in vitro* setup using differentiated PLB cells, a neutrophil like cell line, in a 3D environment. However, the MTOC position in these cells, does not faithfully recapitulate *in vivo* observations (data not shown). As a result, further detailed analysis using an *in vitro* setup is not currently warranted.

Genetic manipulation, such as neutrophil specific expression of proteins that regulate MT dynamics, would be useful in addressing the remaining questions. For example, overexpression of Nek2 or catalytically inactive Nek2 (K37R) has been shown

to disrupt MTOC organization (Fry et al., 1998). However, overexpression of Nek2 or Nek2(K37R) in neutrophils did not result in obvious disorganization of the MTOC as visualized by γTubulin localization (data not shown). Attachment of MTs to cortical regions is important for cell polarization. Expression of the carboxyl-terminal of IQGAP1 (IQGAP(CT)), an effector of Rac1 and Cdc42, has been shown to delocalize CLIP-170 from the tips of MTs and alters the MT array (Fukata et al., 2002). When IQGAP(CT) is overexpressed in neutrophils *in vivo* using a neutrophil specific promoter, it did not result in any obvious changes in neutrophil morphology (data not shown). Expression of IQGAP(CT) in neutrophils also did not affect directional migration, as determined by tail fin wounding assay on stable F1 *Tg(lyz-IQGAP(CT)-2A-mCherry)* transgenic larvae (data not shown). It must be noted that although the human IQGAP1 has a high degree of homology with zebrafish IQGAP, especially in the carboxyl-terminal, it is possible that the human ortholog does not perform the same function in zebrafish. It is also possible that this IQGAP-CLIP-170 pathway arose later in evolution and may not be involved in MT organization in zebrafish neutrophils.

p21-activated kinase (PAK) is another genetic candidate that may be utilized to manipulate MTs. PAK is a serine/threonine kinase that is activated by Cdc42 or Rac (Knaus et al., 1995; Manser et al., 1994). PAK phosphorylates stathmin and inactivates its microtubule catastrophe promoting activity (Daub et al., 2001; Wittmann et al., 2004). Since activation of Rac can induce pseudopod formation in neutrophils (Yoo et al., 2010), PAK is an ideal candidate to study the process of pseudopod selection, directional migration and the importance of regulating Rho GTPase activity and microtubule dynamics. I constructed plasmids containing different Pak mutations, a

kinase active form that cannot bind to Pix (Pak2a-CA) (Liu et al., 2007) and a dominant negative Pak2a (aa1-218) (Pak2a-DN) based on sequence homology with human PAK2 (human NP_002568.2, aa 1-225) (Martin et al., 1995; Royal et al., 2000) (Fig. 7A). These constructs were used to address the requirement of intact MTs and MTOC positioning in psuedopod selection. The expression of these transgenes is driven by the lysozyme C promoter for neutrophil specific expression in zebrafish larvae. Pak2a-CA expression in neutrophils induced cell rounding (Fig. 7C) and impaired neutrophil motility. Expression of Pak2a-DN, on the other hand, resulted in altered neutrophil morphology with more pseudopod branching, thinner pseudopods. On some occasions neutrophils failed to completely retract their pseudopods, leading to partial cellular fragmentation (Fig. 7D). F-actin polarity of neutrophils remained intact (Fig. 7D). This Pak2a-DN induced hyper pseudopod phenotype is unexpected and suggests Pak2a might have an inhibitory effect on pseudopod generation. Further characterization is required to address its possible role in pseudopod formation. In an attempt to dissect Pak2a function, I have tried to knockdown Pak2a using a published morpholino sequence (Buchner et al., 2007). Unfortunately, it had no effect in knocking down the Pak2a mRNA in my hands, as determined by RT-PCR using published primers (data not shown). Nevertheless, the Pak2a-DN approach can be used as a tool to analyze MTOC position and pseudopod selection. Interestingly, even during excessive pseudopod formation resulting from Pak2a-DN expression, γtubulin-GFP visualization of the MTOC shows that it maintained its localization in the dominant pseudopod (Fig. 8). Further experiments are required to determine if neutrophil directional migration is

affected under similar conditions and if Pak2a-DN expression affects MT dynamics in neutrophils.

It is intriguing to observe such dynamic and orchestrated MTOC positioning during neutrophil migration. A number of new questions arise from these observations: What is the nature of the MT localization and dynamics in migrating neutrophils *in vivo*? How is MTOC positioning achieved and what are the main players involved? Does MTOC positioning adjacent to a pseudopod sufficient and required for pseudopod stabilization? Does pseudopod retraction require depolymerization of local MTs? Is there a crosstalk mechanism between actin and MTs in neutrophils to govern proper directional migration? Lastly, is the regulation of macrophage pseudopod selection similar to that of neutrophils? Answers to these questions will be aided with the development of more amenable tools and more intensive investigation using relevant *in vivo* models such as the zebrafish.

Materials and Methods

DNA and RNA injection

All DNA expression vectors contain either the zebrafish myeloperoxidase (*mpx*) promoter or lysozyme C (*lyz*) promoter for neutrophil expression (Kitaguchi *et al.*, 2009; Mathias *et al.*, 2006), minimal Tol2 elements for efficient integration (Urasaki *et al.*, 2006), and an SV40 polyadenylation sequence (Clontech Laboratories, Inc.). Constructs with each of the following in the backbone were constructed: EGFP-MRLC (BC004994), IQGAP(CT)-2A-EGFP (IQGAP aa1547-1657; NP_003861), γTubulin-GFP (Yoo et al., 2012), Pak2a-DN-2A-mCherry (Pak2a aa1-218) (Liu et al., 2007) and Pak2a-CA-2A-mCherry (Pak2a T395E/R189G/P190A) (Liu et al., 2007).

Image acquisition and analysis

For live imaging, embryos at 2-3 dpf were anesthetized using 0.2 mg/mL tricaine and mounted under a glass cover slip in a glass-bottom dish. To prevent pigment formation, embryos were maintained in embryo media containing 0.2 mM N-phenylthiourea (PTU). All images except Fig. 1 were acquired using a Spinning disk confocal microscope (Yokogawa CSU-X) with confocal scanhead on a Zeiss Observer Z.1 inverted microscope (NA1.3/60× water immersion objective). A Photometrics Evolve EMCCD camera was used to acquire the images. Z-series images were acquired using a 0.4 µM step size and 300 EM gain. Maximum intensity projection images were made using the Zen 2011 (blue edition) software (Carl Zeiss). Images in Fig. 1 were acquired using a spinning disk confocal microscope (Yokogawa CSU-X) confocal scanhead on a Nikon Eclipse Ti inverted microscope equipped with a NA 1.2/60x water immersion objective. A Photometrics CoolSNAP HQ_2 CCD camera was used to acquire the digital

images. Z-series images were acquired using a 0.4 µm step size and binning set at 2. For ratio image analysis, movie files were first exported to ZVI file using the Zen software. The ZVI files were then imported to AxioVision SE64 Rel. 4.8 software for ratio analysis using the Physiology module. All images were acquired on randomly migrating neutrophils in the head region of zebrafish larvae. MTOC angle and line scan analysis was performed using Fiji.

Pharmalogical treatments

All treatments were performed at 3 dpf in E3 with 0.5% DMSO except for LiCl and NaCl treatments. *Tg(mpx:GFP-UtrCH) x Tg(mpx:Lifeact-Ruby)* zebrafish larvae were pretreated with the following compounds before imaging: 2 µM nocodazole for 0.5 h to induce microtubule depolymerization; 0.3M LiCl for 1.5 h to inhibit GSK3; 0.3M NaCl for 1.5 h as a control for LiCl treatment; 100 µM Rockout for 2 h to inhibit Rho kinase; 20 µM PP2 for 1 h to inhibit Src kinase; 1 µM U73122 for 1 h to inhibit PLC; and 100 µM DPI for 1 h to inhibit NOX.

.

References

Ambasta, R.K., P. Kumar, K.K. Griendling, H.H. Schmidt, R. Busse, and R.P. Brandes. 2004. Direct interaction of the novel Nox proteins with p22phox is required for the formation of a functionally active NADPH oxidase. *J Biol Chem*. 279:45935-41.

Ancliff, P.J., M.P. Blundell, G.O. Cory, Y. Calle, A. Worth, H. Kempski, S. Burns, G.E. Jones, J. Sinclair, C. Kinnon, I.M. Hann, R.E. Gale, D.C. Linch, and A.J. Thrasher. 2006. Two novel activating mutations in the Wiskott-Aldrich syndrome protein result in congenital neutropenia. *Blood*. 108:2182-9.

Andrew, N., and R.H. Insall. 2007. Chemotaxis in shallow gradients is mediated independently of PtdIns 3-kinase by biased choices between random protrusions. *Nat Cell Biol*. 9:193-200.

Boateng, L.R., C.L. Cortesio, and A. Huttenlocher. 2012. Src-mediated phosphorylation of mammalian Abp1 (DBNL) regulates podosome rosette formation in transformed fibroblasts. *J Cell Sci*. 125:1329-41.

Buchner, D.A., F. Su, J.S. Yamaoka, M. Kamei, J.A. Shavit, L.K. Barthel, B. McGee, J.D. Amigo, S. Kim, A.W. Hanosh, P. Jagadeeswaran, D. Goldman, N.D. Lawson, P.A. Raymond, B.M. Weinstein, D. Ginsburg, and S.E. Lyons. 2007. pak2a mutations cause cerebral hemorrhage in redhead zebrafish. *Proc Natl Acad Sci U S A*. 104:13996-4001.

Burkel, B.M., G. von Dassow, and W.M. Bement. 2007. Versatile fluorescent probes for actin filaments based on the actin-binding domain of utrophin. *Cell Motil Cytoskeleton*. 64:822-32.

Burns, S., A.J. Thrasher, M.P. Blundell, L. Machesky, and G.E. Jones. 2001. Configuration of human dendritic cell cytoskeleton by Rho GTPases, the WAS protein, and differentiation. *Blood*. 98:1142-9.

Daub, H., K. Gevaert, J. Vandekerckhove, A. Sobel, and A. Hall. 2001. Rac/Cdc42 and p65PAK regulate the microtubule-destabilizing protein stathmin through phosphorylation at serine 16. *J Biol Chem*. 276:1677-80.

Deng, Q., E.A. Harvie, and A. Huttenlocher. 2012. Distinct signalling mechanisms mediate neutrophil attraction to bacterial infection and tissue injury. *Cell Microbiol*. 14:517-28.

Deng, Q., S.K. Yoo, P.J. Cavnar, J.M. Green, and A. Huttenlocher. 2011. Dual roles for Rac2 in neutrophil motility and active retention in zebrafish hematopoietic tissue. *Dev Cell*. 21:735-45.

Diaz, B., G. Shani, I. Pass, D. Anderson, M. Quintavalle, and S.A. Courtneidge. 2009. Tks5-dependent, nox-mediated generation of reactive oxygen species is necessary for invadopodia formation. *Sci Signal*. 2:ra53.

Dovas, A., and D. Cox. 2011. Signaling networks regulating leukocyte podosome dynamics and function. *Cell Signal*. 23:1225-34.

Eddy, R.J., L.M. Pierini, and F.R. Maxfield. 2002. Microtubule asymmetry during neutrophil polarization and migration. *Mol Biol Cell*. 13:4470-83.

Etienne-Manneville, S., and A. Hall. 2001. Integrin-mediated activation of Cdc42 controls cell polarity in migrating astrocytes through PKCzeta. *Cell*. 106:489-98.

Ezratty, E.J., M.A. Partridge, and G.G. Gundersen. 2005. Microtubule-induced focal adhesion disassembly is mediated by dynamin and focal adhesion kinase. *Nat Cell Biol*. 7:581-90.

Fry, A.M., P. Meraldi, and E.A. Nigg. 1998. A centrosomal function for the human Nek2 protein kinase, a member of the NIMA family of cell cycle regulators. *EMBO J*. 17:470-81.

Fukata, M., T. Watanabe, J. Noritake, M. Nakagawa, M. Yamaga, S. Kuroda, Y. Matsuura, A. Iwamatsu, F. Perez, and K. Kaibuchi. 2002. Rac1 and Cdc42 capture microtubules through IQGAP1 and CLIP-170. *Cell*. 109:873-85.

Gomes, E.R., S. Jani, and G.G. Gundersen. 2005. Nuclear movement regulated by Cdc42, MRCK, myosin, and actin flow establishes MTOC polarization in migrating cells. *Cell*. 121:451-63.

Hotulainen, P., and P. Lappalainen. 2006. Stress fibers are generated by two distinct actin assembly mechanisms in motile cells. *J Cell Biol*. 173:383-94.

Insall, R.H. 2010. Understanding eukaryotic chemotaxis: a pseudopod-centred view. *Nat Rev Mol Cell Biol*. 11:453-8.

Kitaguchi, T., K. Kawakami, and A. Kawahara. 2009. Transcriptional regulation of a myeloid-lineage specific gene lysozyme C during zebrafish myelopoiesis. *Mech Dev*. 126:314-23.

Knaus, U.G., S. Morris, H.J. Dong, J. Chernoff, and G.M. Bokoch. 1995. Regulation of human leukocyte p21-activated kinases through G protein--coupled receptors. *Science*. 269:221-3.

Lammermann, T., B.L. Bader, S.J. Monkley, T. Worbs, R. Wedlich-Soldner, K. Hirsch, M. Keller, R. Forster, D.R. Critchley, R. Fassler, and M. Sixt. 2008. Rapid leukocyte migration by integrin-independent flowing and squeezing. *Nature*. 453:51-5.

Lammermann, T., and M. Sixt. 2009. Mechanical modes of 'amoeboid' cell migration. *Curr Opin Cell Biol*. 21:636-44.

Linder, S., and P. Kopp. 2005. Podosomes at a glance. *J Cell Sci*. 118:2079-82.

Linder, S., D. Nelson, M. Weiss, and M. Aepfelbacher. 1999. Wiskott-Aldrich syndrome protein regulates podosomes in primary human macrophages. *Proc Natl Acad Sci U S A*. 96:9648-53.

Liu, J., S.D. Fraser, P.W. Faloon, E.L. Rollins, J. Vom Berg, O. Starovic-Subota, A.L. Laliberte, J.N. Chen, F.C. Serluca, and S.J. Childs. 2007. A betaPix Pak2a signaling pathway regulates cerebral vascular stability in zebrafish. *Proc Natl Acad Sci U S A*. 104:13990-5.

Manser, E., T. Leung, H. Salihuddin, Z.S. Zhao, and L. Lim. 1994. A brain serine/threonine protein kinase activated by Cdc42 and Rac1. *Nature*. 367:40-6.

Martin, G.A., G. Bollag, F. McCormick, and A. Abo. 1995. A novel serine kinase activated by rac1/CDC42Hs-dependent autophosphorylation is related to PAK65 and STE20. *EMBO J*. 14:4385.

Mathias, J.R., B.J. Perrin, T.X. Liu, J. Kanki, A.T. Look, and A. Huttenlocher. 2006. Resolution of inflammation by retrograde chemotaxis of neutrophils in transgenic zebrafish. *J Leukoc Biol*. 80:1281-8.

McDonald, B., K. Pittman, G.B. Menezes, S.A. Hirota, I. Slaba, C.C. Waterhouse, P.L. Beck, D.A. Muruve, and P. Kubes. 2010. Intravascular danger signals guide neutrophils to sites of sterile inflammation. *Science*. 330:362-6.

Molad, Y. 2002. Update on colchicine and its mechanism of action. *Curr Rheumatol Rep*. 4:252-6.

Niethammer, P., C. Grabher, A.T. Look, and T.J. Mitchison. 2009. A tissue-scale gradient of hydrogen peroxide mediates rapid wound detection in zebrafish. *Nature*. 459:996-9.

Niggli, V. 2003. Microtubule-disruption-induced and chemotactic-peptide-induced migration of human neutrophils: implications for differential sets of signalling pathways. *J Cell Sci*. 116:813-22.

Nourshargh, S., P.L. Hordijk, and M. Sixt. 2010. Breaching multiple barriers: leukocyte motility through venular walls and the interstitium. *Nat Rev Mol Cell Biol*. 11:366-78.

Peris, L., M. Wagenbach, L. Lafanechere, J. Brocard, A.T. Moore, F. Kozielski, D. Job, L. Wordeman, and A. Andrieux. 2009. Motor-dependent microtubule disassembly driven by tubulin tyrosination. *J Cell Biol*. 185:1159-66.

Pollard, T.D., and G.G. Borisy. 2003. Cellular motility driven by assembly and disassembly of actin filaments. *Cell*. 112:453-65.

Prigozhina, N.L., and C.M. Waterman-Storer. 2004. Protein kinase D-mediated anterograde membrane trafficking is required for fibroblast motility. *Curr Biol*. 14:88-98.

Riedl, J., A.H. Crevenna, K. Kessenbrock, J.H. Yu, D. Neukirchen, M. Bista, F. Bradke, D. Jenne, T.A. Holak, Z. Werb, M. Sixt, and R. Wedlich-Soldner. 2008. Lifeact: a versatile marker to visualize F-actin. *Nat Methods*. 5:605-7.

Royal, I., N. Lamarche-Vane, L. Lamorte, K. Kaibuchi, and M. Park. 2000. Activation of cdc42, rac, PAK, and rho-kinase in response to hepatocyte growth factor differentially regulates epithelial cell colony spreading and dissociation. *Mol Biol Cell*. 11:1709-25.

Sun, T., M. Rodriguez, and L. Kim. 2009. Glycogen synthase kinase 3 in the world of cell migration. *Dev Growth Differ*. 51:735-42.

Szczur, K., H. Xu, S. Atkinson, Y. Zheng, and M.D. Filippi. 2006. Rho GTPase CDC42 regulates directionality and random movement via distinct MAPK pathways in neutrophils. *Blood*. 108:4205-13.

Tang, W., Y. Zhang, W. Xu, T.K. Harden, J. Sondek, L. Sun, L. Li, and D. Wu. 2011. A PLCbeta/PI3Kgamma-GSK3 signaling pathway regulates cofilin phosphatase slingshot2 and neutrophil polarization and chemotaxis. *Dev Cell*. 21:1038-50.

Ueda, M., and S. Ogihara. 1994. Microtubules are required in amoeba chemotaxis for preferential stabilization of appropriate pseudopods. *J Cell Sci*. 107 (Pt 8):2071-9.

Urasaki, A., G. Morvan, and K. Kawakami. 2006. Functional dissection of the Tol2 transposable element identified the minimal cis-sequence and a highly repetitive sequence in the subterminal region essential for transposition. *Genetics*. 174:639-49.

van Helden, S.F., M.M. Oud, B. Joosten, N. Peterse, C.G. Figdor, and F.N. van Leeuwen. 2008. PGE2-mediated podosome loss in dendritic cells is dependent on actomyosin contraction downstream of the RhoA-Rho-kinase axis. *J Cell Sci*. 121:1096-106.

Vicente-Manzanares, M., X. Ma, R.S. Adelstein, and A.R. Horwitz. 2009. Non-muscle myosin II takes centre stage in cell adhesion and migration. *Nat Rev Mol Cell Biol*. 10:778-90.

Wang, J., Y. Taba, J. Pang, G. Yin, C. Yan, and B.C. Berk. 2009. GIT1 mediates VEGF-induced podosome formation in endothelial cells: critical role for PLCgamma. *Arterioscler Thromb Vasc Biol*. 29:202-8.

Wittmann, T., G.M. Bokoch, and C.M. Waterman-Storer. 2004. Regulation of microtubule destabilizing activity of Op18/stathmin downstream of Rac1. *J Biol Chem*. 279:6196-203.

Xu, J., A. Van Keymeulen, N.M. Wakida, P. Carlton, M.W. Berns, and H.R. Bourne. 2007. Polarity reveals intrinsic cell chirality. *Proc Natl Acad Sci U S A*. 104:9296-300.

Xu, J., F. Wang, A. Van Keymeulen, M. Rentel, and H.R. Bourne. 2005. Neutrophil microtubules suppress polarity and enhance directional migration. *Proc Natl Acad Sci U S A*. 102:6884-9.

Yoo, S.K., Q. Deng, P.J. Cavnar, Y.I. Wu, K.M. Hahn, and A. Huttenlocher. 2010. Differential regulation of protrusion and polarity by PI3K during neutrophil motility in live zebrafish. *Dev Cell*. 18:226-36.

Yoo, S.K., P.Y. Lam, M.R. Eichelberg, L. Zasadil, W.M. Bement, and A. Huttenlocher. 2012. The role of microtubules in neutrophil polarity and migration in live zebrafish. *J Cell Sci*. 125:5702-10.

Yoo, S.K., T.W. Starnes, Q. Deng, and A. Huttenlocher. 2011. Lyn is a redox sensor that mediates leukocyte wound attraction in vivo. *Nature*.

Fig 1. Stable F-actin accumulates in the retracting pseudopod in neutrophils *in vivo*. (Left panels) Time series sequential confocal imaging of all F-actin (Lifeact-Ruby) in red, stable F-actin (GFP-UtrCH) in green, and a merged image of these two signals (Overlay). (Right panel) Line-scan measurement of Lifeact-Ruby and GFP-UtrCH signal in the retracting pseudodpod as indicated by the dotted line in the overlay images. Scale bar = 10 μm.

Fig. 1

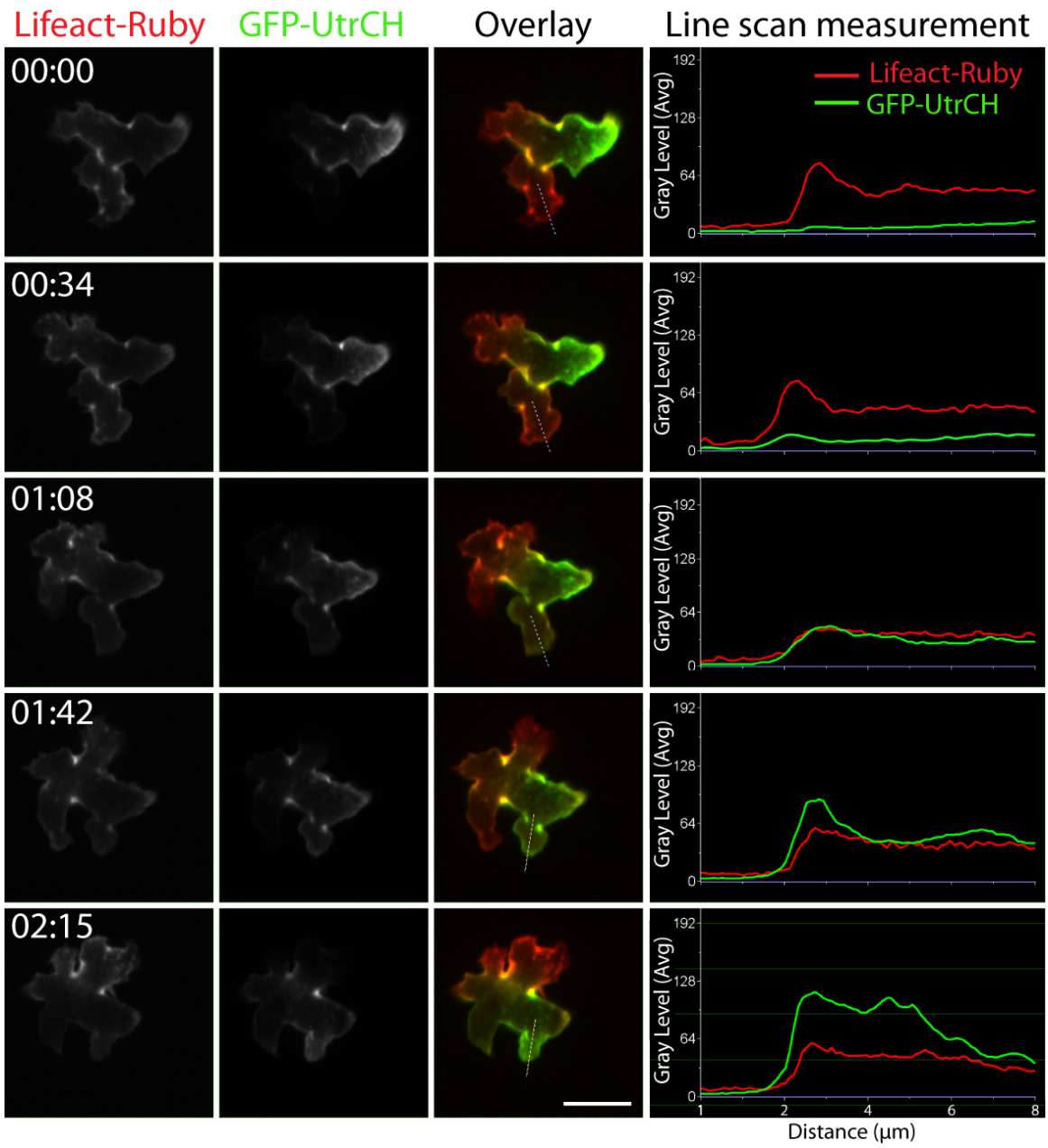
Lifeact-Ruby
GFP-UtrCH
Overlay
Line scan measurement
00:00
00:34
01:08
01:42
02:15
Lifeact-Ruby
GFP-UtrCH
Gray Level (Avg)
192
128
64
0
1
2
4
6
8
Distance (μm)

Fig 2. Myosin regulatory light chain (MRLC) accumulates in the retracting pseudopod in neutrophils *in vivo*. (A) A time series of ratiometric images taken of myosin regulatory light chain (MRLC) signal compared to a volumetric control (mCherry) in neutrophils. The white line indicates the location of the kymographic measurement. (B) Kymograph on MRLC/mCherry ratio of a pseudopod undergoing protrusion and retraction. (C) Bar graph showing the ratio of MRLC to mCherry in the same pseudopod during protrusion and retraction. The color of individual bars corresponds to that in (A).

Fig. 2

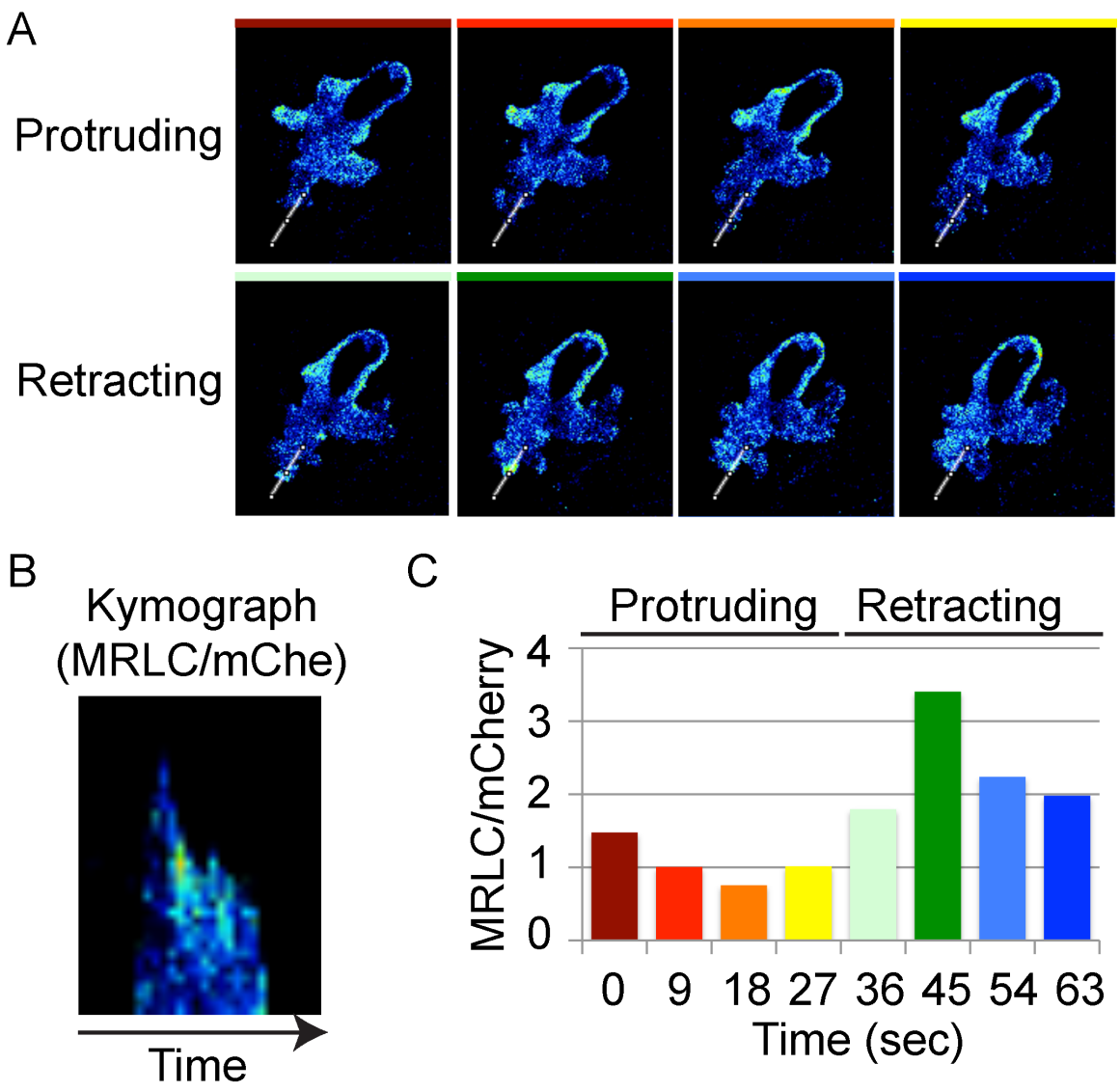
A
Protruding
Retracting
B
Kymograph
(MRLC/mChe)
Time
C
Protruding
Retracting
MRLC/mCherry
0
1
2
3
4
0
9
18
27
36
45
54
63
Time (sec)

Fig. 3. F-actin dots in neutrophils *in vivo*. (A) Maximum intensity projection of a neutrophil expression GFP-UtrCH and Lifeact-Ruby. (Ai-ii) The same neutrophil during relatively fast (Ai) and slow migration (Aii). (Aiii) Zebrafish larvae were treated with nocodazole (Noc) to induce MTs depolymerization. (B) Maximum intensity projection (MIP) and single confocal plane at 0.4 μm Z-step of a neutrophil expressing GFP-UtrCH and Lifeact-Ruby.

Fig. 3

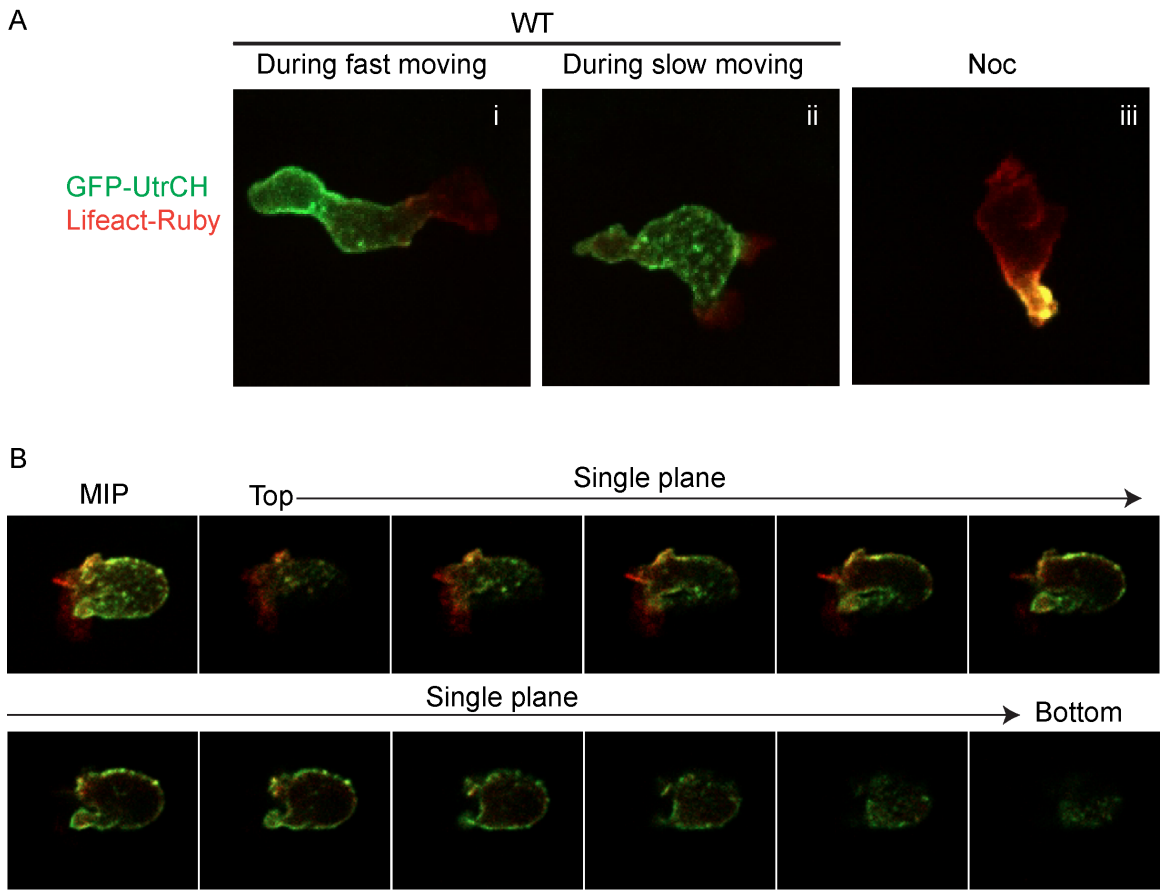
A
WT
During fast moving
During slow moving
Noc
i
ii
iii
GFP-UtrCH
Lifeact-Ruby
B
MIP
Top
Single plane
Single plane
Bottom

Fig. 4. Relationship between the position of the MTOC and pseodopods. (A-B) Time series maximum intensity projection of a neutrophil expressing γtubulin-GFP. White arrows indicate the location of the MTOC. Red arrows indicate the dominant pseudopod that is being maintained. Red arrowheads indicate the pseudopod that is being retracted. Red doted arrows indicate the direction of cell migration. (A) The MTOC is positioned in the pseudopod that is being maintained. (B) A new pseudopod is generated on the side of cell opposite to the initial position of MTOC, suggesting the generation of pseudopods can be independent of MTOC position.

Fig. 4

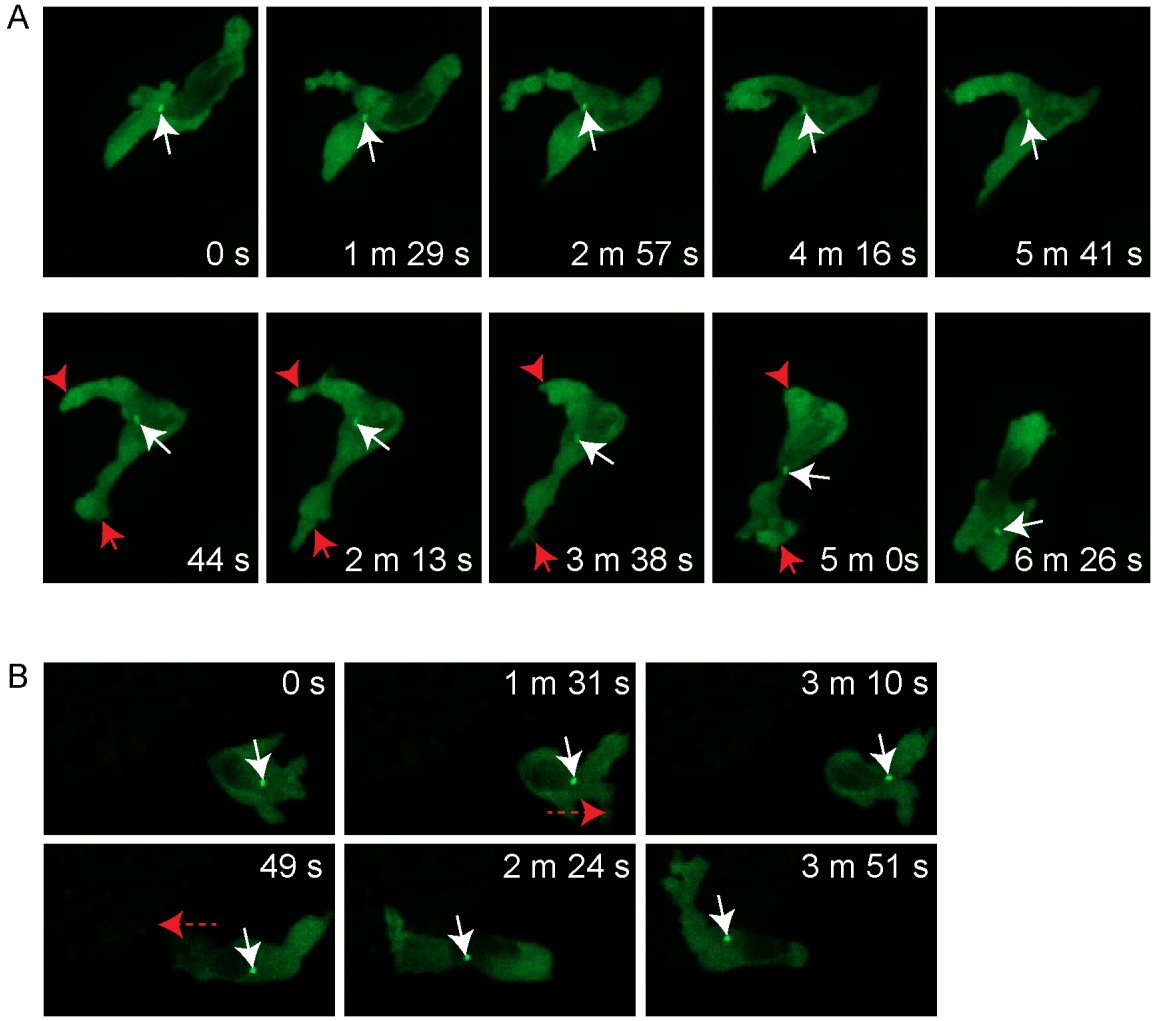
A
0 s
1 m 29 s
2 m 57 s
4 m 16 s
5 m 41 s
44 s
2 m 13 s
3 m 38 s
5 m 0s
6 m 26 s
B
0 s
1 m 31 s
3 m 10 s
49 s
2 m 24 s
3 m 51 s

Fig. 5. MTOC position during neutrophil migration *in vivo*. (A) Time series maximum intensity projection of a neutrophil expressing γtubulin-GFP and a nucleus probe mCherry-histone H2B in control (WT) or nocodazole (Noc) treated zebrafish larvae. Arrows indicate the MTOC in front of the nucleus. Scale bars, 10 μm. (B) Schematic drawing showing the analysis of MTOC angle, which is the angle between the line drawn from the MTOC to the cell centroid and the line drawn from the cell centroid to the dominant pseudopod determined by the next time point. (C-D) Correlation of MTOC angle to the speed of neutrophil migration in control (C) or in nocodazole treated zebrafish larvae (D).

Fig. 5

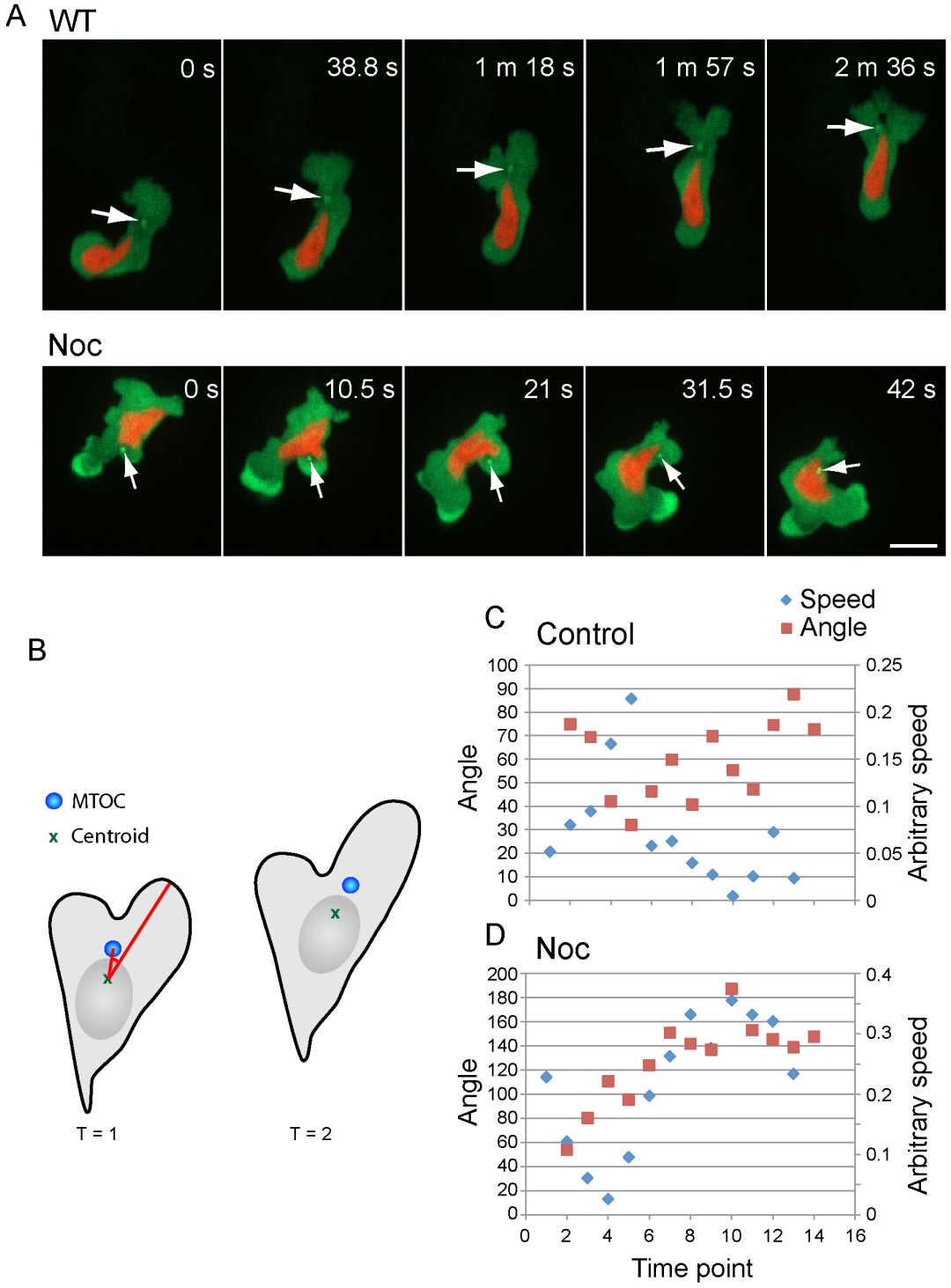
A
WT
0 s
38.8 s
1 m 18 s
1 m 57 s
2 m 36 s
Noc
0 s
10.5 s
21 s
31.5 s
42 s
B
MTOC
Centroid
T = 1
T = 2
C
Control
Speed
Angle
Arbitrary speed
D
Noc
Angle
Arbitrary speed
Time point

Fig. 6. Inhibition of GSK3 results in an altered pseudopod generation phenotype. Zebrafish larvae were treated with 0.3M LiCl to inhibit GSK3 or 0.3M NaCl as control for 1.5 h. Confocal time lapse movies were acquired every 30 sec for 30 min. (A) Frequency of pseudopod generation is calculated by dividing the number of pseudopods generated by time in minutes. (B) The ratio of the number of pseudopods generated *de novo* to pseudopod generated by bifurcation of an existing pseudopod.

Fig. 6

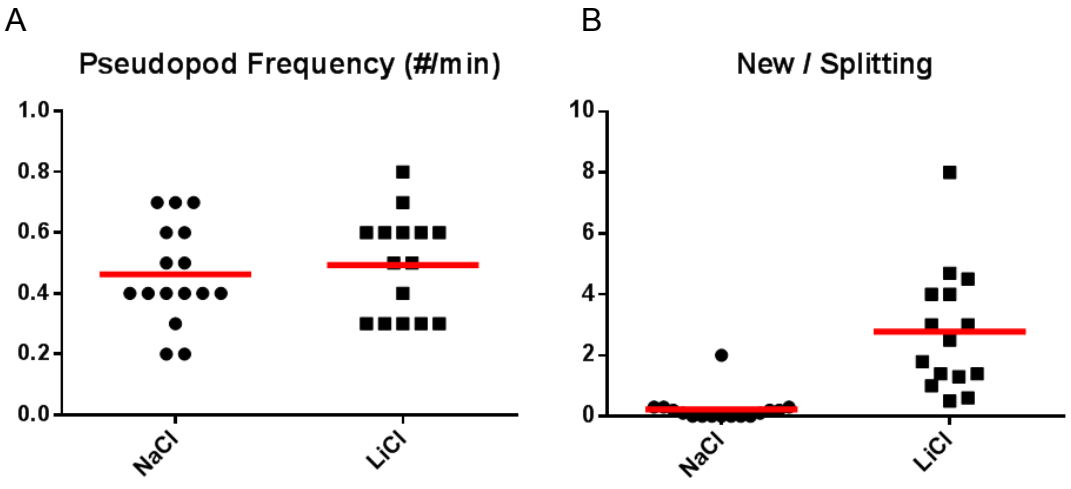
A
Pseudopod Frequency (#/min)
1.0
0.8
0.6
0.4
0.2
0.0
NaCl
LiCl
B
New / Splitting
10
8
6
4
2
0
NaCl
LiCl

Fig. 7. Morphology of neutrophils *in vivo* expressing different forms of Pak2a. (A) Schematic drawing showing the different domains in constitutive active (CA) and dominant negative (DN) Pak2a. CRIB, Cdc42/Rac1 interacting binding; AID, autoinhibitory domain; PR, proline rich domain. (B-D) A neutrophil expressing Lifeact-Ruby (red) and GFP-UtrCH (green) that labels all F-actin and stable F-actin, respectively. (B-D) Neutrophils expressing Lifeact-Ruby and GFP-UtrCH (B) or Pak2a-CA (C) or Pak2a-DN (D). Scale bar, 10μm.

Fig. 7

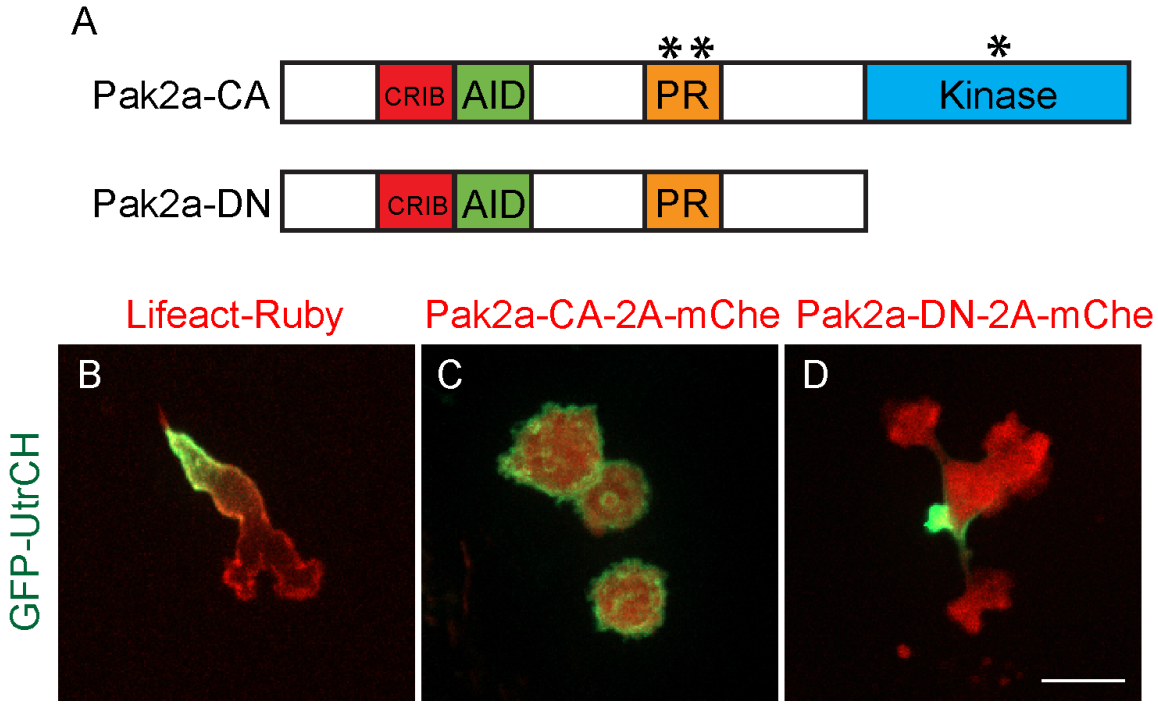
A
Pak2a-CA
CRIB
AID
PR
Kinase
Pak2a-DN
CRIB
AID
PR
Lifeact-Ruby
Pak2a-CA-2A-mChe
Pak2a-DN-2A-mChe
GFP-UtrCH
B
C
D

Fig. 8. Pak2a-DN expression and MTOC position. Time series maximum intensity projection of a neutrophil expressing γtubulin-GFP and Pak2a-DN-2A mCherry. White arrows indicate position of MTOC.

Fig. 8

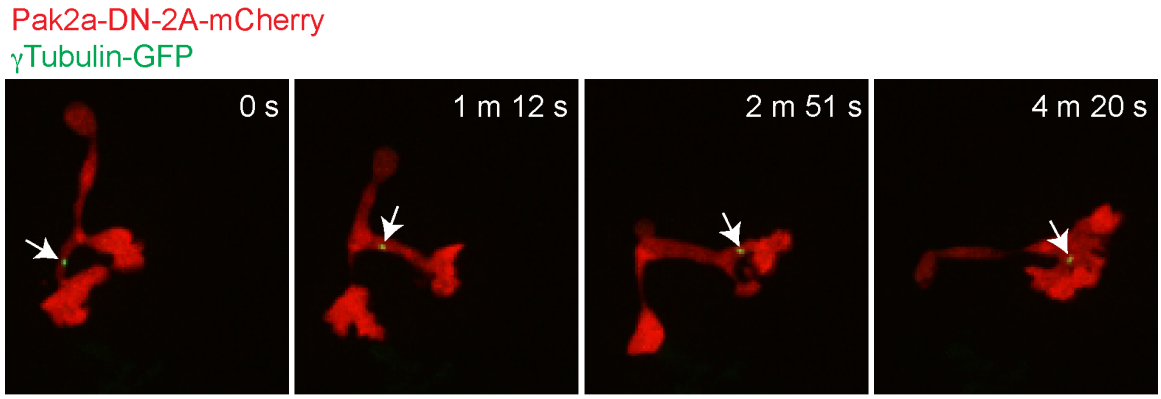

Appendix II

Interstitial leukocyte migration *in vivo*

This Chapter was published in the following journal article:

Lam P.Y. and Huttenlocher A. (2013) Interstitial leukocyte migration *in vivo*. *Current Opinion in Cell Biology*, Oct;25(5):650-8.

Abstract

Rapid leukocyte motility is essential for immunity and host defense. There has been progress in understanding the molecular signals that regulate leukocyte motility both *in vitro* and *in vivo*. However, a gap remains in understanding how complex signals are prioritized to result in directed migration, which is critical for both adaptive and innate immune function. Here we focus on interstitial migration and how external cues are translated into intracellular signaling pathways that regulate leukocyte polarity, directional sensing and motility in three-dimensional spaces.

Introduction

The trafficking of leukocytes into peripheral tissues and lymphoid organs is critical for both innate and adaptive immune function and has been extensively reviewed [1-3]. A key step in this process is the interstitial motility of leukocytes within three-dimensional (3D) spaces, which can be either random or directed. Interstitial motility involves cycles of motility and arrest that is orchestrated by a complex hierarchy of external cues that are translated into changes in intracellular signaling. This function is evolutionarily conserved as demonstrated by the chemotactic interstitial migration of *Drosophila* hemocytes (immunosurveillance cells) to sites of tissue damage and infection (reviewed in [4]).

The rapid single-cell migration of leukocytes is classically known as ‘amoeboid’ migration. The term ‘amoeboid’ is based on a changing cell morphology, but can encompass different modes of locomotion (reviewed in [5,6]). Pseudopod driven gliding motility is the major mode of locomotion. During this mode of motility, actin polymerization below the leading plasma membrane generates forces for membrane extension. This is coupled with actomyosin contraction in the cell’s rear, which detaches the cell and propels the cell body forward. Leukocytes can also display a blebbing type of migration under some conditions where actomyosin contraction generates hydrostatic pressure to form bleb-based protrusions.

Migration in 3D

Efficient leukocyte migration through interstitial tissues is a key component of the normal function of the cells of the innate and adaptive immune system. The patrolling

function of leukocytes requires cells to maneuver rapidly through complex matrix environments at speeds of up to 20–30 μm per minute. The type of protrusions formed by different leukocytes can be quite distinct, as demonstrated by neutrophils and macrophages migrating *in vivo* (Figure 1a and b). Neutrophils project small pseudopodia that often bifurcate, while macrophages frequently extend long, thin filopodia-like protrusions in many directions as they maneuver through the interstitium toward damaged tissues within zebrafish embryos (Figure 1c-e). T cells, on the other hand, often migrate randomly in their surveillance of lymph nodes in mice, with extension of small pseudopodia at the leading edge [7]. The mechanisms that regulate the generation and maintenance of amoeboid pseudopodia and biased selection are under intense investigation both *in vitro* and *in vivo* (reviewed in [8,9]).

Leukocyte amoeboid motility, in general, occurs in the absence of strong adhesive interactions with surrounding cells or tissues (reviewed in [10]), although leukocyte arrest often requires integrin-mediated adhesion, in particular during transendothelial migration (reviewed in [11]). Integrin-mediated adhesion is essential for migration on two-dimensional surfaces. However, integrins can be dispensable for leukocyte migration in interstitial tissues [12] or in 3D collagen lattices [13]. The idea that movement within confined spaces can be integrin-independent was paradigm shifting and highlights the key role for adhesion in limiting leukocyte migration speed and mediating leukocyte arrest rather than an essential role in motility under many *in vivo* conditions.

Interstitial environments contain both soluble and tissue-bound cues that help guide leukocytes to migrate or mediate cell arrest. Here, we review the key steps in

interstitial leukocyte migration including sensing of environmental cues and the intracellular signaling mechanisms that orchestrate leukocyte motility and cell arrest (Figure 2a and b).

Cell signaling underlying leukocyte motility

Chemoattractants transmit signals through heterotrimeric G-protein-coupled receptors (GPCRs) [14], which activate a plethora of effectors [15,16]. One of the key effectors is the class Ib phosphatydylinositol-3-kinase (PI(3)K) (Figure 2c). Although the role of PI(3)K during *in vitro* chemotaxis is controversial, PI(3)Kγ is required for cell polarity and motility *in vivo* [17-19]. PI(3)K promotes Rac-mediated actin polymerization at the leading edge and generates F-actin anteroposterior polarity (dynamic F-actin at the leading edge and stable F-actin at the rear; Figure 2c and f). Inhibition of PI(3)K results in impaired F-actin polarity and neutrophil recruitment to both wounds and infection in zebrafish [17,20]. The importance of PI(3)K signaling is further illustrated by studies showing that the modulation of PI(3)K signaling can result in an inflammation phenotype. The PI(3)K products PI(3,4,5)P3-PI(3,4)P2 are localized to the leading edge of zebrafish neutrophils *in vivo* [17,21]. PI(3,4,5)P3 can be hydrolyzed to PI(3,4)P2 by SH2-domain-containing inositol 5-phosphatases (SHIP). SHIP limits myeloid cell motility through the modulation of PI(3)K signaling *in vitro* [22] and *in vivo* in zebrafish [21]. In addition, SHIP knockout mice show increased myeloid infiltration into vital organs [23,24]. Taken together, the modulation of PI(3,4,5)P3 levels through SHIP can negatively regulate cell motility.

Small GTPases are another class of key effectors downstream of GPCR signaling (reviewed in [25]). They function as molecular switches and play a critical role in the generation and maintenance of cell polarity and motility [25,26]). We will focus on some recent *in vivo* findings highlighting the role of different small GTPases (i.e., Ras and Rho subfamily) in leukocyte interstitial motility. The Ras subfamily Rap1 GTPase is important for leukocyte migration *in vivo* (Figure 2d). Interstitial motility of B and T cells in the mouse lymph node is dependent on a Rap1 effector molecule RAPL (Rap1-GTP binding protein) [27]. The complex of RAPL and GTP-bound Rap1 activate the serine-threonine kinase Mst1 (Ste20-like kinase) [28] and Mst1 is required for T-cell and B-cell motility within lymph nodes [29].

The Rho subfamily GTPases including Rac, Cdc42 and Rho are also critical for leukocyte interstitial migration (Figure 2e and f). In agreement with *in vitro* studies [30,31], Rac is required for neutrophil polarity and motility in zebrafish [32]. Rac2 depletion results in impaired neutrophil motility to wounds. In addition, dominant negative Rac2 expression in neutrophils impairs PI(3,4,5)P3-PI(3,4)P2 polarization and pseudopod formation [32]. Local activation of Rac can mediate protrusion, induce the polarity of F-actin dynamics, activate PI(3)K signaling and is sufficient to direct neutrophil migration in zebrafish [17]**.** In mature dendritic cells (DCs), Rac1 and Rac2 deletion in mice also impairs migration to lymph nodes [33]. It is becoming increasingly clear that both Rac and PI(3)K are required for leukocyte interstitial motility through a positive feedback loop.

Cdc42 regulates pseudopod stability [30] and controls neutrophil polarity and migration *in vitro* via crosstalk between WASp, CD11b and microtubules [34]. Although

Cdc42 deficient DCs retain the ability to sense chemotactic cues and form protrusions, these protrusion are temporally and spatially dysregulated resulting in impaired interstitial migration in mice [35] (Figure 2c). The Cdc42 GEF, DOCK8, regulates interstitial DC migration in mice at least partly by controlling Cdc42 activity. DOCK8 deficiency impairs Cdc42 activation at the leading edge and results in defective migration [36]. The accumulating evidence suggests that Cdc42 activity maintains pseudopod protrusion.

Rho regulates cell polarity and helps propel the cell forward (Figure 2f). Expression of constitutively active Rho or dominant-negative RhoA impairs neutrophil F-actin polarity in zebrafish [17]. Inhibition of the Rho effector, Rho-associated protein kinase (ROCK), impairs neutrophil migration in zebrafish [17] and DC migration within the interstitium in mice [37]. Overall, Rho GTPases play an important role in leukocyte motility through the regulation of cell protrusion and retraction.

Mitogen-activated protein kinases (MAPKs) are other downstream effectors of GPCR signaling [38,39] that regulate leukocyte interstitial migration *in vivo* (Figure 2d). Understanding the role of MAPKs has been difficult, partly, due to some conflicting results. An *in vivo* study using mice reports that p38 positively regulates neutrophil interstitial chemotaxis to a keratinocyte-derived cytokine [40]. However, in zebrafish, p38 has been reported to negatively regulate myeloid cell migration, or may be dispensable [41,42]. In zebrafish, ERK has been shown to be required for neutrophil recruitment [43] but is dispensable for macrophage recruitment to wounds [42]. The requirement of JNK in leukocyte migration *in vivo* is also controversial [41,42]. These

discrepancies may be due to different regulatory roles played by MAPKs depending on the *in vivo* conditions, and will be questions for future investigation.

The role of microtubules in interstitial motility

Microtubules suppress the polarity and motility of many leukocytes *in vitro* [44,45] and *in vivo* [46,47]. Depolymerization of microtubules using nocodazole enhances neutrophil polarity and motility but impairs directional migration in zebrafish [46]. In macrophages, microtubule depolymerization does not affect migration speed in zebrafish, although directional migration is impaired [47]. It is known that microtubules regulate Rho GTPase activity (Figure 2e). Microtubule depolymerization can activate RhoA *in vitro* partly through the release of microtubule associated Rho GEF [44,48,49]. Both microtubule polymerization and depolymerization activate Rac *in vitro* [46,50]. It is probably that the dysregulation of Rho and Rac activity upon microtubule depolymerization contributes to impaired directional motility *in vivo*. These observations suggest that the interconnected relationship between microtubules and the Rho GTPases plays a role in regulating leukocyte directional motility. In addition, microtubules may regulate PI(3)K signaling (Figure 2e) which is required for leukocyte polarization and motility [17]. It has been shown that microtubule depolymerization inhibits PI(3)K activation at the leading edge of neutrophils in zebrafish [46]. These observations highlight the essential role for microtubules in leukocyte directional motility *in vivo*.

Directional sensing and interstitial migration

Leukocyte gradient sensing and subsequent biased migration are necessary steps in directed migration. Directional migration can be guided by soluble or tissue-bound chemoattractant signals (Table 1). These directional cues can work separately or, in some cases, in concert.

Injured epithelial cells generate hydrogen peroxide (H_2O_2) through an NADPH oxidase (DUOX), which mediates rapid neutrophil wound detection in zebrafish [51]. Similarly, H_2O_2 is generated by oncogene-transformed cells, and this also mediates neutrophil and macrophage recruitment in zebrafish [52]. These observations suggest that H_2O_2 serves as an important signal for leukocyte detection of tissue damage. Recently, a Src family kinase (Lyn), was identified as a redox sensor that neutrophils use to detect the H_2O_2 gradients in injured tissues in zebrafish [43]. H_2O_2 directly oxidizes and activates Lyn. Activation of Lyn, in turn, leads to the phosphorylation and activation of the MAPK Erk but not p38 or JNK [43]. Interestingly, H_2O_2 is not required for neutrophils to detect localized bacterial infections in zebrafish, since inhibition of H_2O_2 production does not inhibit neutrophil recruitment to localized *Pseudomonas aeruginosa* or *Streptococcus iniae* infection [20].

Other cytokines are up-regulated with wounding or infection, including Tumor Necrosis Factor (TNF) expression in zebrafish [53,54]. The adaptor protein FAN (Factor associated with neutral sphingomyelinase activity) binds to the TNF receptor and plays a role in leukocyte interstitial directed migration in response to wounds and bacterial infections in zebrafish. FAN knockdown results in disorganized pseudopod generation in leukocytes, leading to impaired navigational capacity [55]. FAN mediates TNF-induced

Cdc42 activation and actin reorganization *in vitro* [56]. WASP is one of the effectors of Cdc42, and WASP depletion impairs neutrophil and macrophage wound responses in zebrafish, similar to FAN knockdown [57].

In a zebrafish infection model, zCxcl8 (also known as IL-8) expression is induced upon local *Escherichia coli* infection. A zCxcl8 tissue-bound gradient is established by binding to heparan sulfate proteoglycans on the tissue surface. This zCxcl8 gradient mediates neutrophil directional bias by altering the relationship between cell speed and directionality [58]. DCs have been shown to use a similar strategy for interstitial migration in mice. The chemokine CCL21 generated on the lymphatic endothelium forms a tissue-bound gradient, which guides DCs to migrate from dermal tissue into afferent lymphatic vessels [59]. Antigen-engaged B cells in mice also sense the increasing CCL21 gradients from the follicle zone to the B-zone-T-zone boundary for directional migration, where early B-cell-T-cell interactions occur. This CCL21 gradient and its G-protein coupled receptor CCR7 are required for B cell directional migration [60].

The hierarchy and integration of signaling that govern leukocyte chemotaxis *in vivo* is further illustrated in several sterile inflammation models in which inflammation occurs in the absence of any microorganisms. In a sterile skin inflammation model in mice, a three-step cascade of neutrophil responses can occur with initial scouting neutrophils followed by waves of arriving neutrophils (amplification phase) and subsequently stabilization of neutrophils at injured tissues. The involvement of GPCRs in initial recruitment is followed by a role for cyclic ADP ribose in the amplification phase [61]. In another mouse sterile skin inflammation model, pericytes that wrap around the

capillaries regulate leukocyte interstitial migration through their effects on leukocyte responsiveness to interstitial migratory cues and their effector functions [62]. Upon local sterile inflammation, proteoglycan $NG2^+$ pericytes increase ICAM-1 expression and secrete the chemoattractant macrophage migration-inhibitory factor (MIF) that increases myeloid cell migration. It is suggested that the $NG2^+$ pericytes form a 'highway' for the rapid migration of extravasted leukocytes. By contrast, in a hepatic sterile inflammation mouse model, leukocyte chemotaxis is guided within an intravascular 'highway' instead of the extravascular space mediated by pericytes [63]. In this model, a multi-step process of directional cues guide neutrophils to sites of sterile inflammation with neutrophil chemotaxis in the vasculature directed by macrophage inflammatory protein 2 (MIP-2) gradients. Closer to the tissue injury, formyl peptides released from necrotic cells serve as end-target chemoattractants. Different insults, therefore, can trigger distinct signaling cascades that mediate leukocyte recruitment. It appears that leukocytes can utilize a variety of chemotactic signaling pathways for directional migration in response to tissue damage that is context dependent.

The requirement for proteases in interstitial leukocyte motility is less clear. In 3D collagen matrices, the tyrosine-kinase collagen receptor discoidin domain receptor 2 regulates neutrophil chemotaxis through the induction of metalloproteinase secretion and the subsequent generation of collagen-derived chemotactic peptides [64]. It has been shown that knockdown of Mmp13 metalloproteinase decreases macrophage wound recruitment in zebrafish, indicating that protease activity is required for proper leukocyte interstitial migration [42]. In addition, migrating neutrophils in zebrafish can

deform the collagen matrix, suggesting the involvement of proteases in interstitial migration [65].

Interstitial leukocyte arrest

Localized leukocyte arrest is also a key component of interstitial leukocyte function. It limits leukocyte motility to regions where the effector immune function is needed. This is perhaps best demonstrated in the context of sequestered zones of leukocyte function in lymph nodes that are guided by specific chemokine signatures (reviewed in [66]). Leukocyte arrest/immobilization appears to be an active process that is mediated by specific chemokines and downstream effector pathways (Figure 2a). In support of this idea, there has been extensive work showing an essential role for calcium signaling in T cell arrest, including developing T cells in 3D mouse thymic tissues [67] through intracellular Ca^{2+} flux mediated by calcium release-activated calcium (CRAC) channels, such as Orai (reviewed in [68]). Evidence suggests that intracellular calcium influx through CRAC channels also mediates neutrophil arrest (reviewed in [69]), probably downstream of chemokine signaling. During tissue injury in zebrafish, the chemokine Cxcl8 has been implicated in mediating neutrophil retention [58]. Deficiencies in Cxcl8 result in decreased neutrophil retention at sites of infection. CXCR4-Rac2 signaling is also required for neutrophil retention in hematopoietic tissues in zebrafish [32]. Lack of Rac2 function results in decreased neutrophil motility but increased neutrophil release into the circulation, suggesting that retention is an active process mediated by Rac signaling. Stromal cell-derived factor 1 (SDF1, CXCL12) has also been implicated in the retention of leukocytes in hematopoietic tissue in zebrafish

[70]. These observations suggest that leukocyte arrest in interstitial tissues, including wounds and hematopoietic tissues, is an active process. The regulation of leukocyte mobility versus arrest allows leukocytes to perform proper immune functions at the right place and at the right time, and is a fundamental part of leukocyte directional decision making during leukocyte interstitial motility.

Conclusion

Advances in multi-photon vital imaging technology and new model systems such as the zebrafish, have made it possible to study interstitial migration with higher resolution *in vivo*. What is becoming increasingly clear, however, is that although much of the knowledge acquired from *in vitro* studies can apply to the *in vivo* environment, not all mechanisms are similar. Therefore, future challenges will be to apply and combine both *in vitro* and *in vivo* analyses to increase our understanding of leukocyte interstitial migration and how responses are prioritized to competing extracellular cues.

Acknowledgements

This work was supported by the National Institutes of Health [grant number GM074827] to AH. We thank our lab members for their critical comments on the manuscript.

References and recommended reading

Papers of particular interest, published within the period of review, have been highlighted as:

* of special interest

** of outstanding interest

1. Stein JV, Nombela-Arrieta C: **Chemokine control of lymphocyte trafficking: a general overview**. *Immunology* 2005, **116**:1-12.

2. Notarangelo LD, Badolato R: **Leukocyte trafficking in primary immunodeficiencies**. *J Leukoc Biol* 2009, **85**:335-343.

3. Rot A, von Andrian UH: **Chemokines in innate and adaptive host defense: basic chemokinese grammar for immune cells**. *Annu Rev Immunol* 2004, **22**:891-928.

4. Fauvarque MO, Williams MJ: **Drosophila cellular immunity: a story of migration and adhesion**. *J Cell Sci* 2011, **124**:1373-1382.

5. Lammermann T, Sixt M: **Mechanical modes of 'amoeboid' cell migration**. *Curr Opin Cell Biol* 2009, **21**:636-644.

6. Nourshargh S, Hordijk PL, Sixt M: **Breaching multiple barriers: leukocyte motility through venular walls and the interstitium**. *Nat Rev Mol Cell Biol* 2010, **11**:366-378.

7. Friedman RS, Jacobelli J, Krummel MF: **Mechanisms of T cell motility and arrest: deciphering the relationship between intra- and extracellular determinants**. *Semin Immunol* 2005, **17**:387-399.

8. Insall RH: **Understanding eukaryotic chemotaxis: a pseudopod-centred view**. *Nat Rev Mol Cell Biol* 2010, **11**:453-458.

9. Van Haastert PJ: **Chemotaxis: insights from the extending pseudopod**. *J Cell Sci* 2010, **123**:3031-3037.

10. Schmidt S, Friedl P: **Interstitial cell migration: integrin-dependent and alternative adhesion mechanisms**. *Cell Tissue Res* 2010, **339**:83-92.

11. Vestweber D: **Novel insights into leukocyte extravasation**. *Curr Opin Hematol* 2012, **19**:212-217.

*12. Lammermann T, Bader BL, Monkley SJ, Worbs T, Wedlich-Soldner R, Hirsch K, Keller M, Forster R, Critchley DR, Fassler R, et al.: **Rapid leukocyte migration by integrin-independent flowing and squeezing**. *Nature* 2008, **453**:51-55.

This study is the first to show that integrins are required in 2D but not during interstitial migration. DCs depleted of all integrin receptors can still migrate in interstitial tissues.

13. Friedl P, Entschladen F, Conrad C, Niggemann B, Zanker KS: **CD4+ T lymphocytes migrating in three-dimensional collagen lattices lack focal adhesions and utilize beta1 integrin-independent strategies for polarization, interaction with collagen fibers and locomotion**. *Eur J Immunol* 1998, **28**:2331-2343.

14. Janetopoulos C, Jin T, Devreotes P: **Receptor-mediated activation of heterotrimeric G-proteins in living cells**. *Science* 2001, **291**:2408-2411.

15. Kimmel AR, Parent CA: **The signal to move: D. discoideum go orienteering**. *Science* 2003, **300**:1525-1527.

16. Bhattacharya M, Babwah AV, Ferguson SS: **Small GTP-binding protein-coupled receptors**. *Biochem Soc Trans* 2004, **32**:1040-1044.

17. Yoo SK, Deng Q, Cavnar PJ, Wu YI, Hahn KM, Huttenlocher A: **Differential regulation of protrusion and polarity by PI3K during neutrophil motility in live zebrafish**. *Dev Cell* 2010, **18**:226-236.

18. Sasaki T, Irie-Sasaki J, Jones RG, Oliveira-dos-Santos AJ, Stanford WL, Bolon B, Wakeham A, Itie A, Bouchard D, Kozieradzki I, et al.: **Function of PI3Kgamma in thymocyte development, T cell activation, and neutrophil migration**. *Science* 2000, **287**:1040-1046.

19. Hirsch E, Katanaev VL, Garlanda C, Azzolino O, Pirola L, Silengo L, Sozzani S, Mantovani A, Altruda F, Wymann MP: **Central role for G protein-coupled phosphoinositide 3-kinase gamma in inflammation**. *Science* 2000, **287**:1049-1053.

20. Deng Q, Harvie EA, Huttenlocher A: **Distinct signalling mechanisms mediate neutrophil attraction to bacterial infection and tissue injury**. *Cell Microbiol* 2012, **14**:517-528.

21. Lam PY, Yoo SK, Green JM, Huttenlocher A: **The SH2-domain-containing inositol 5-phosphatase (SHIP) limits the motility of neutrophils and their recruitment to wounds in zebrafish**. *J Cell Sci* 2012, **125**:4973-4978.

22. Vedham V, Phee H, Coggeshall KM: **Vav activation and function as a rac guanine nucleotide exchange factor in macrophage colony-stimulating factor-induced macrophage chemotaxis**. *Mol Cell Biol* 2005, **25**:4211-4220.

23. Liu Q, Sasaki T, Kozieradzki I, Wakeham A, Itie A, Dumont DJ, Penninger JM: **SHIP is a negative regulator of growth factor receptor-mediated PKB/Akt activation and myeloid cell survival**. *Genes Dev* 1999, **13**:786-791.

24. Helgason CD, Damen JE, Rosten P, Grewal R, Sorensen P, Chappel SM, Borowski A, Jirik F, Krystal G, Humphries RK: **Targeted disruption of SHIP leads to hemopoietic perturbations, lung pathology, and a shortened life span**. *Genes Dev* 1998, **12**:1610-1620.

25. Charest PG, Firtel RA: **Big roles for small GTPases in the control of directed cell movement**. *Biochem J* 2007, **401**:377-390.

26. Parent CA: **Making all the right moves: chemotaxis in neutrophils and Dictyostelium**. *Curr Opin Cell Biol* 2004, **16**:4-13.

27. Ebisuno Y, Katagiri K, Katakai T, Ueda Y, Nemoto T, Inada H, Nabekura J, Okada T, Kannagi R, Tanaka T, et al.: **Rap1 controls lymphocyte adhesion cascade and interstitial migration within lymph nodes in RAPL-dependent and -independent manners**. *Blood* 2010, **115**:804-814.

28. Katagiri K, Imamura M, Kinashi T: **Spatiotemporal regulation of the kinase Mst1 by binding protein RAPL is critical for lymphocyte polarity and adhesion**. *Nat Immunol* 2006, **7**:919-928.

29. Katagiri K, Katakai T, Ebisuno Y, Ueda Y, Okada T, Kinashi T: **Mst1 controls lymphocyte trafficking and interstitial motility within lymph nodes**. *EMBO J* 2009, **28**:1319-1331.

30. Srinivasan S, Wang F, Glavas S, Ott A, Hofmann F, Aktories K, Kalman D, Bourne HR: **Rac and Cdc42 play distinct roles in regulating PI(3,4,5)P3 and polarity during neutrophil chemotaxis**. *J Cell Biol* 2003, **160**:375-385.

31. Sun CX, Downey GP, Zhu F, Koh AL, Thang H, Glogauer M: **Rac1 is the small GTPase responsible for regulating the neutrophil chemotaxis compass**. *Blood* 2004, **104**:3758-3765.

32. Deng Q, Yoo SK, Cavnar PJ, Green JM, Huttenlocher A: **Dual roles for Rac2 in neutrophil motility and active retention in zebrafish hematopoietic tissue**. *Dev Cell* 2011, **21**:735-745.

33. Benvenuti F, Hugues S, Walmsley M, Ruf S, Fetler L, Popoff M, Tybulewicz VL, Amigorena S: **Requirement of Rac1 and Rac2 expression by mature dendritic cells for T cell priming**. *Science* 2004, **305**:1150-1153.

34. Kumar S, Xu J, Perkins C, Guo F, Snapper S, Finkelman FD, Zheng Y, Filippi MD: **Cdc42 regulates neutrophil migration via crosstalk between WASp, CD11b, and microtubules**. *Blood* 2012, **120**:3563-3574.

35. Lammermann T, Renkawitz J, Wu X, Hirsch K, Brakebusch C, Sixt M: **Cdc42-dependent leading edge coordination is essential for interstitial dendritic cell migration**. *Blood* 2009, **113**:5703-5710.

36. Harada Y, Tanaka Y, Terasawa M, Pieczyk M, Habiro K, Katakai T, Hanawa-Suetsugu K, Kukimoto-Niino M, Nishizaki T, Shirouzu M, et al.: **DOCK8 is a Cdc42 activator critical for interstitial dendritic cell migration during immune responses**. *Blood* 2012, **119**:4451-4461.

37. Nitschke M, Aebischer D, Abadier M, Haener S, Lucic M, Vigl B, Luche H, Fehling HJ, Biehlmaier O, Lyck R, et al.: **Differential requirement for ROCK in dendritic cell migration within lymphatic capillaries in steady-state and inflammation**. *Blood* 2012, **120**:2249-2258.

38. Aomatsu K, Kato T, Fujita H, Hato F, Oshitani N, Kamata N, Tamura T, Arakawa T, Kitagawa S: **Toll-like receptor agonists stimulate human neutrophil migration via activation of mitogen-activated protein kinases**. *Immunology* 2008, **123**:171-180.

39. Lopez-Ilasaca M: **Signaling from G-protein-coupled receptors to mitogen-activated protein (MAP)-kinase cascades**. *Biochem Pharmacol* 1998, **56**:269-277.

40. Cara DC, Kaur J, Forster M, McCafferty DM, Kubes P: **Role of p38 mitogen-activated protein kinase in chemokine-induced emigration and chemotaxis in vivo**. *J Immunol* 2001, **167**:6552-6558.

41. Taylor HB, Liepe J, Barthen C, Bugeon L, Huvet M, Kirk PD, Brown SB, Lamb JR, Stumpf MP, Dallman MJ: **P38 and JNK have opposing effects on persistence of in vivo leukocyte migration in zebrafish**. *Immunol Cell Biol* 2012, **91**:60-69.

42. Zhang Y, Bai XT, Zhu KY, Jin Y, Deng M, Le HY, Fu YF, Chen Y, Zhu J, Look AT, et al.: **In vivo interstitial migration of primitive macrophages mediated by JNK-matrix metalloproteinase 13 signaling in response to acute injury**. *J Immunol* 2008, **181**:2155-2164.

43. Yoo SK, Starnes TW, Deng Q, Huttenlocher A: **Lyn is a redox sensor that mediates leukocyte wound attraction in vivo. *Nature* 2011, **480**:109-112.

The recruitment of leukocytes to wounds is mediated by a gradient of hydrogen peroxide (Niethammer et al). This study in zebrafish identifies the Src family kinase Lyn as a redox sensor that mediates initial neutrophil recruitment to wounds.

44. Niggli V: **Microtubule-disruption-induced and chemotactic-peptide-induced migration of human neutrophils: implications for differential sets of signalling pathways**. *J Cell Sci* 2003, **116**:813-822.

45. Xu J, Wang F, Van Keymeulen A, Rentel M, Bourne HR: **Neutrophil microtubules suppress polarity and enhance directional migration**. *Proc Natl Acad Sci U S A* 2005, **102**:6884-6889.

46. Yoo SK, Lam PY, Eichelberg MR, Zasadil L, Bement WM, Huttenlocher A: **The role of microtubules in neutrophil polarity and migration in live zebrafish**. *J Cell Sci* 2012, **125**:5702-5710.

47. Redd MJ, Kelly G, Dunn G, Way M, Martin P: **Imaging macrophage chemotaxis in vivo: studies of microtubule function in zebrafish wound inflammation**. *Cell Motil Cytoskeleton* 2006, **63**:415-422.

48. Krendel M, Zenke FT, Bokoch GM: **Nucleotide exchange factor GEF-H1 mediates cross-talk between microtubules and the actin cytoskeleton**. *Nat Cell Biol* 2002, **4**:294-301.

49. Chang YC, Nalbant P, Birkenfeld J, Chang ZF, Bokoch GM: **GEF-H1 couples nocodazole-induced microtubule disassembly to cell contractility via RhoA**. *Mol Biol Cell* 2008, **19**:2147-2153.

50. Waterman-Storer CM, Worthylake RA, Liu BP, Burridge K, Salmon ED: **Microtubule growth activates Rac1 to promote lamellipodial protrusion in fibroblasts**. *Nat Cell Biol* 1999, **1**:45-50.

51. Niethammer P, Grabher C, Look AT, Mitchison TJ: **A tissue-scale gradient of hydrogen peroxide mediates rapid wound detection in zebrafish. *Nature* 2009, **459**:996-999.

This study in zebrafish is the first observation of hydrogen peroxide as a paracrine signal to induce leukocyte recruitment.

*52. Feng Y, Santoriello C, Mione M, Hurlstone A, Martin P: **Live imaging of innate immune cell sensing of transformed cells in zebrafish larvae: parallels between tumor initiation and wound inflammation**. *PLoS Biol* 2010, **8**:1-19.

This study demonstrated parallels between leukocyte recruitment to wounds and transformed cells. Similar to the hydrogen peroxide-induced neutrophil recruitment to wounds (Niethammer et al), hydrogen peroxide mediates neutrophil recruitment to transformed cells.

53. Pressley ME, Phelan PE, 3rd, Witten PE, Mellon MT, Kim CH: **Pathogenesis and inflammatory response to Edwardsiella tarda infection in the zebrafish**. *Dev Comp Immunol* 2005, **29**:501-513.

54. Li L, Yan B, Shi YQ, Zhang WQ, Wen ZL: **Live imaging reveals differing roles of macrophages and neutrophils during zebrafish tail fin regeneration**. *J Biol Chem* 2012, **287**:25353-25360.

55. Boecke A, Sieger D, Neacsu CD, Kashkar H, Kronke M: **Factor associated with neutral sphingomyelinase activity mediates navigational capacity of**

leukocytes responding to wounds and infection: live imaging studies in zebrafish larvae. *J Immunol* 2012, **189**:1559-1566.

56. Haubert D, Gharib N, Rivero F, Wiegmann K, Hosel M, Kronke M, Kashkar H: **PtdIns(4,5)P-restricted plasma membrane localization of FAN is involved in TNF-induced actin reorganization**. *EMBO J* 2007, **26**:3308-3321.

57. Cvejic A, Hall C, Bak-Maier M, Flores MV, Crosier P, Redd MJ, Martin P: **Analysis of WASp function during the wound inflammatory response--live-imaging studies in zebrafish larvae**. *J Cell Sci* 2008, **121**:3196-3206.

58. Sarris M, Masson JB, Maurin D, Van der Aa LM, Boudinot P, Lortat-Jacob H, Herbomel P: **Inflammatory Chemokines Direct and Restrict Leukocyte Migration within Live Tissues as Glycan-Bound Gradients. *Curr Biol* 2012, **22**:2375-2382.

This study in zebrafish shows that a zCxcl8 tissue-bound gradient established upon local bacterial infection mediates neutrophil recruitment and retention at sites of infection. This paper together with (Weber et al) demonstrated a functional haptotactic gradient *in vivo* for leukocyte directed migration.

59. Weber M, Hauschild R, Schwarz J, Moussion C, de Vries I, Legler DF, Luther SA, Bollenbach T, Sixt M: **Interstitial dendritic cell guidance by haptotactic chemokine gradients. *Science* 2013, **339**:328-332.

This study in mice demonstrated that tissue-bound chemokine CCL21 gradients produced by lymphatic endothelium guide dendritic cell directional migration to

the lymphatic vessels. This paper together with (Sarris et al) demonstrated a functional haptotactic gradient *in vivo* for leukocyte directed migration.

60. Okada T, Miller MJ, Parker I, Krummel MF, Neighbors M, Hartley SB, O'Garra A, Cahalan MD, Cyster JG: **Antigen-engaged B cells undergo chemotaxis toward the T zone and form motile conjugates with helper T cells**. *PLoS Biol* 2005, **3**:1047-1061.

*61. Ng LG, Qin JS, Roediger B, Wang Y, Jain R, Cavanagh LL, Smith AL, Jones CA, de Veer M, Grimbaldeston MA, et al.: **Visualizing the neutrophil response to sterile tissue injury in mouse dermis reveals a three-phase cascade of events**. *J Invest Dermatol* 2011, **131**:2058-2068.

This study utilizes intravital multiphoton microscopy to uncover the three-step cascade of neutrophil attraction (scouting, amplification and stabilization phase) in response to sterile tissue injury.

*62. Stark K, Eckart A, Haidari S, Tirniceriu A, Lorenz M, von Bruhl ML, Gartner F, Khandoga AG, Legate KR, Pless R, et al.: **Capillary and arteriolar pericytes attract innate leukocytes exiting through venules and 'instruct' them with pattern-recognition and motility programs**. *Nat Immunol* 2013, **14**:41-51.

This study uses a local sterile skin inflammation model to show that proteoglycan $NG2^+$ pericytes increase ICAM-1 expression and secrete the chemoattractant MIF (macrophage migration-inhibitory factor) leading to increased myeloid cell migration. The contact of $NG2^+$ pericytes and myeloid cells drives the increased expression of Toll-like receptors, integrins and matrix metalloproteinases in myeloid cells. As a result, myeloid cells become more efficient in directional

migration through interstitial space along capillaries and arterioles toward the inflammatory foci.

*63. McDonald B, Pittman K, Menezes GB, Hirota SA, Slaba I, Waterhouse CC, Beck PL, Muruve DA, Kubes P: **Intravascular danger signals guide neutrophils to sites of sterile inflammation**. *Science* 2010, **330**:362-366.

This study uses a local hepatic sterile inflammation model to show that neutrophils migrate into the necrotic site through the vasculature instead of transmigrating out of the vasculature and migrating through the shorter interstitial path. Neutrophil chemotaxis is directed by a macrophage inflammatory protein 2 (MIP-2) and formyl peptides released from necrotic cells. Interestingly, ATP released from necrotic cells does not serve as a chemotactic signal.

*64. Afonso PV, McCann CP, Kapnick SM, Parent CA: **Discoidin domain receptor 2 regulates neutrophil chemotaxis in 3D collagen matrices**. *Blood* 2012, **121**:1644-1650.

This study shows that the discoidin domain receptor 2 (DDR2) mediates persistence of 3D neutrophil motility through increased metalloproteinase secretion and generation of collagen-derived chemotactic peptide gradients, independent of its adhesive function.

65. He S, Lamers GE, Beenakker JW, Cui C, Ghotra VP, Danen EH, Meijer AH, Spaink HP, Snaar-Jagalska BE: **Neutrophil-mediated experimental metastasis is enhanced by VEGFR inhibition in a zebrafish xenograft model**. *J Pathol* 2012, **227**:431-445.

66. von Andrian UH, Mempel TR: **Homing and cellular traffic in lymph nodes**. *Nat Rev Immunol* 2003, **3**:867-878.

67. Bhakta NR, Oh DY, Lewis RS: **Calcium oscillations regulate thymocyte motility during positive selection in the three-dimensional thymic environment**. *Nat Immunol* 2005, **6**:143-151.

68. Shaw PJ, Qu B, Hoth M, Feske S: **Molecular regulation of CRAC channels and their role in lymphocyte function**. *Cell Mol Life Sci* 2012.

69. Dixit N, Simon SI: **Chemokines, selectins and intracellular calcium flux: temporal and spatial cues for leukocyte arrest**. *Front Immunol* 2012, **3**:188.

70. Walters KB, Green JM, Surfus JC, Yoo SK, Huttenlocher A: **Live imaging of neutrophil motility in a zebrafish model of WHIM syndrome**. *Blood* 2010, **116**:2803-2811.

71. Deng Q, Sarris M, Bennin DA, Green JM, Herbomel P, Huttenlocher A: **Localized bacterial infection induces systemic activation of neutrophils through Cxcr2 signaling in zebrafish**. *J Leukoc Biol* 2013, **93**:761-769.

72. Friedl P, Weigelin B: **Interstitial leukocyte migration and immune function**. *Nat Immunol* 2008, **9**:960-969.

Table 1 Signaling molecules (soluble or tissue-bound) mediate leukocyte directed migration *in vivo*.

Table 1

Tissue/ Type of injury	Signaling Molecule	Mode of function	Distance from injury/ Destination	Leukocyte	Receptor/ Direct downstream target	Outcome	Ref.
Epithelium injury	H_2O_2	Signal peaks at ~20 min after wounding	Extends to ~100 to 200 μm from wound	Neutrophils	Lyn	Initial recruitment to tissue damage	[51] [43]
	(TNF)	--	--	Neutrophils, Macrophages	FAN	Directed interstitial migration	[55]
	(Purine nucleotides)	--	--	Neutrophils	cADPR production	Amplification phase of recruitment	[61]
Oncogene-transformed cells	H_2O_2	Stochastic and transient	In transformed cells and their immediately neighboring cells	Neutrophils, Macrophages	--	Leukocyte recruitment	[52]
Normal lymphatic endothelium	CCL21	Tissue-bound gradient	≤ 90 μm from lymphatic vessel	DCs	CCR7	Directed migration from dermal interstitium into afferent lymphatic vessels	[59]
Normal lymph nodes	CCL21	Tissue-bound gradient	Increasing gradient from follicle region to the B/T boundary	B cells	CCR7	Migration from follicle zone to the B/T boundary	[60]
Sterile skin inflammation	ICAM-1	Cell surface protein	On $NG2^+$ pericytes	Monocytes, Neutrophils, Macrophages	--	Increases chemotaxis	[62]
	MIF	Secreted by $NG2^+$ pericytes	On $NG2^+$ pericytes	Monocytes, Neutrophils, Macrophages	--	Increases chemotaxis	[62]
Sterile hepatic inflammation	MIP-2	Intravascular gradient	Decreasing gradient from ~150 μm to 650 μm from the injury border	Neutrophils	CXCR2	Directed intravascular migration	[63]
	Formyl peptides	Released from necrotic cells	Within ~150 μm around the injury	Neutrophils	FPR1	Serves as end-target chemoattractant	[63]
Local bacterial infection	(TNF)	--	--	Neutrophils/ Macrophages	FAN	Directed interstitial migration	[55]
	Cxcl8	Tissue-bound gradient	≤ 50 μm from the producing cells	Neutrophils	--	Mediates directional bias and restricts cell motility near the source	[58]
	Cxcl8	--	Systemic	Neutrophils	Cxcr2	Neutrophil mobilization from hematopoietic tissue and recruitment to infection sites	[71]

cADPR, cyclic ADP ribose
DCs, dendritic cells
FAN, Factor associated with neutral sphingomyelinase activity
FPR1, formyl-peptide receptor 1
H_2O_2, hydrogen peroxide
ICAM-1, intercellular adhesion molecule 1
MIF, macrophage migration-inhibitory factor
MIP-2, macrophage inflammatory protein 2, the closest IL-8 homologue in the mouse
TNF-R1, p55 TNF receptor

Figure 1. Neutrophil and macrophage distribution, morphology and response to wounding in zebrafish embryo at 3 days post fertilization. (a) Neutrophils distribute mainly in the mesenchymal tissue in the head region (yellow box) and in the caudal hematopoietic tissue (white box). (Inset in (a)) A typical migrating neutrophil has multiple pseudopodia (arrow heads) and a uropod (arrow). Scale bar = 20 μm. (b) Macrophages distribute in the whole embryo with no clear tissue localization. (Inset in (b)) A typical migrating macrophage shows multiple spindly protrusions. Scale bar = 20 μm. (c) Time series image of neutrophils (red; lifeact-Ruby) and macrophages (green; dendra) migrating to tail fin wound. Neutrophils have arrived at the wound at 0.5 hours post wounding (hpw) and macrophages arrived at later time points. Scale bar = 50 μm. Time series image of a neutrophil (d) or a macrophage (e) migrating from left to right toward the wound. Scale bar = 20 μm.

Figure 1

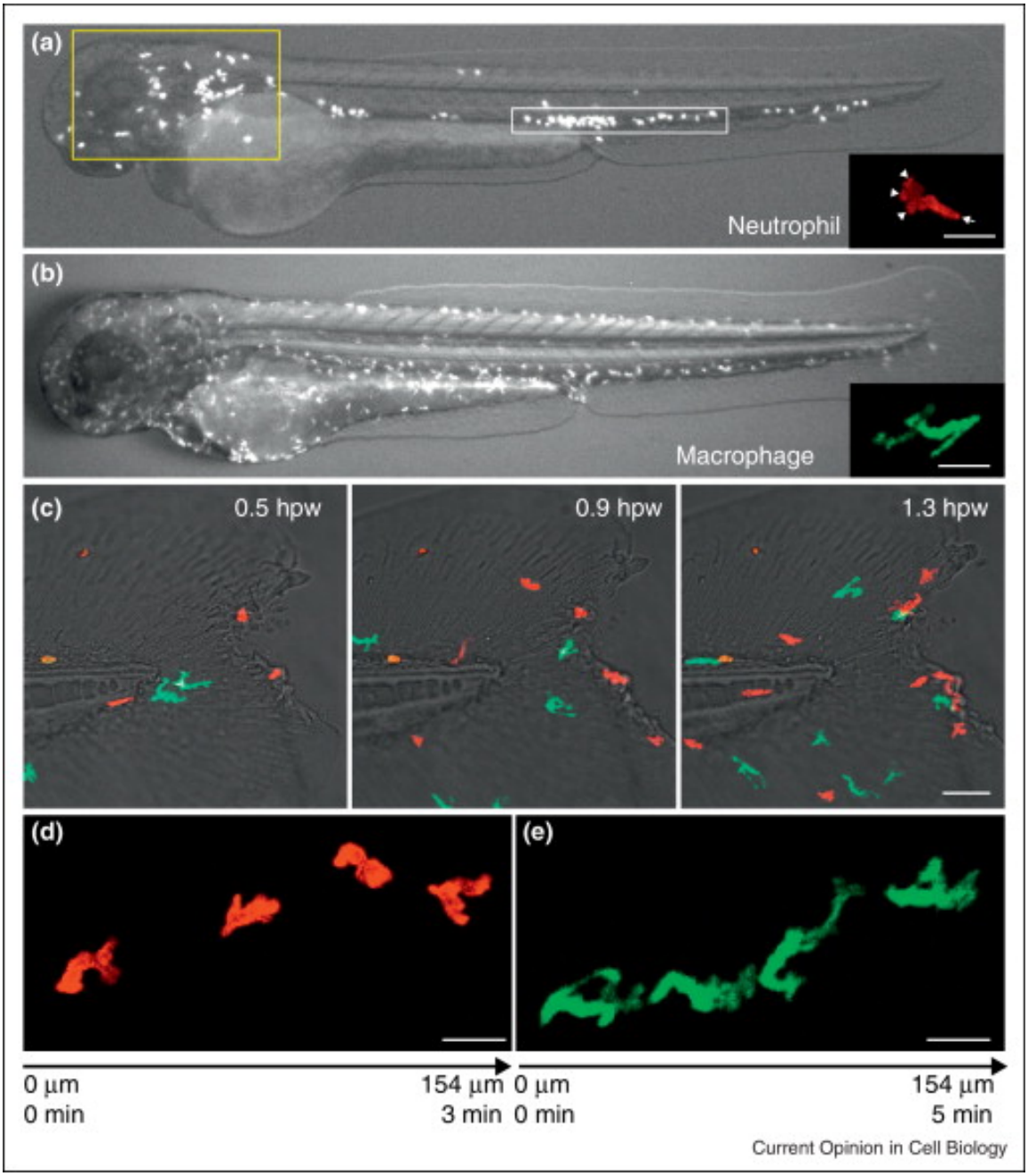
(a)
Neutrophil
(b)
Macrophage
(c)
0.5 hpw
0.9 hpw
1.3 hpw
(d)
(e)
0 µm
0 min
154 µm
3 min
0 µm
0 min
154 µm
5 min
Current Opinion in Cell Biology

Figure 2. Cell signaling and morphology in leukocyte interstitial migration *in vivo*. Detailed in vitro findings are reviewed elsewhere [72]. Here, we highlight the *in vivo* data. (a) A round and non-polarized morphology of leukocytes during arrest. (b) A polarized, amoeboid morphology during directed or random motility. (c) Signaling events and cytoskeletal structure at the leading edge. Positive feedback between PI(3)K and Rac supports the formation of the leading edge while Cdc42 regulates the actin flow and stability of protrusions. SHIP hydrolyzes the PI(3)K product PIP3 into PIP2 and limits leukocyte motility. (d) GPCR can also activate the small GTPase Rap1; Rap1-RAPL-Mst1 signaling probably contributes to both integrin-dependent and independent leukocyte migration. The regulation of MAPKs on overall leukocyte motility is less clear. (e) Microtubules regulate Rac, Rho and PI(3)K activities, and thus leukocyte motility. (f) Signaling events and cytoskeletal structure at the uropod. Stable filamentous actin present in the uropod mediates retraction. CK, chemokines; GPCR, G-protein coupled receptor; MAPKs, Mitogen-activated protein kinases including p38, ERK and JNK; PIP2, PI(3,4)P2; PIP3, PI(3,4,5)P3; ROCK, Rho effector Rho-associated protein kinase; SDF1, stromal cell-derived factor 1 (or CXCL12); SHIP, SH2 domain-containing inositol 5'-phosphatase.

Figure 2

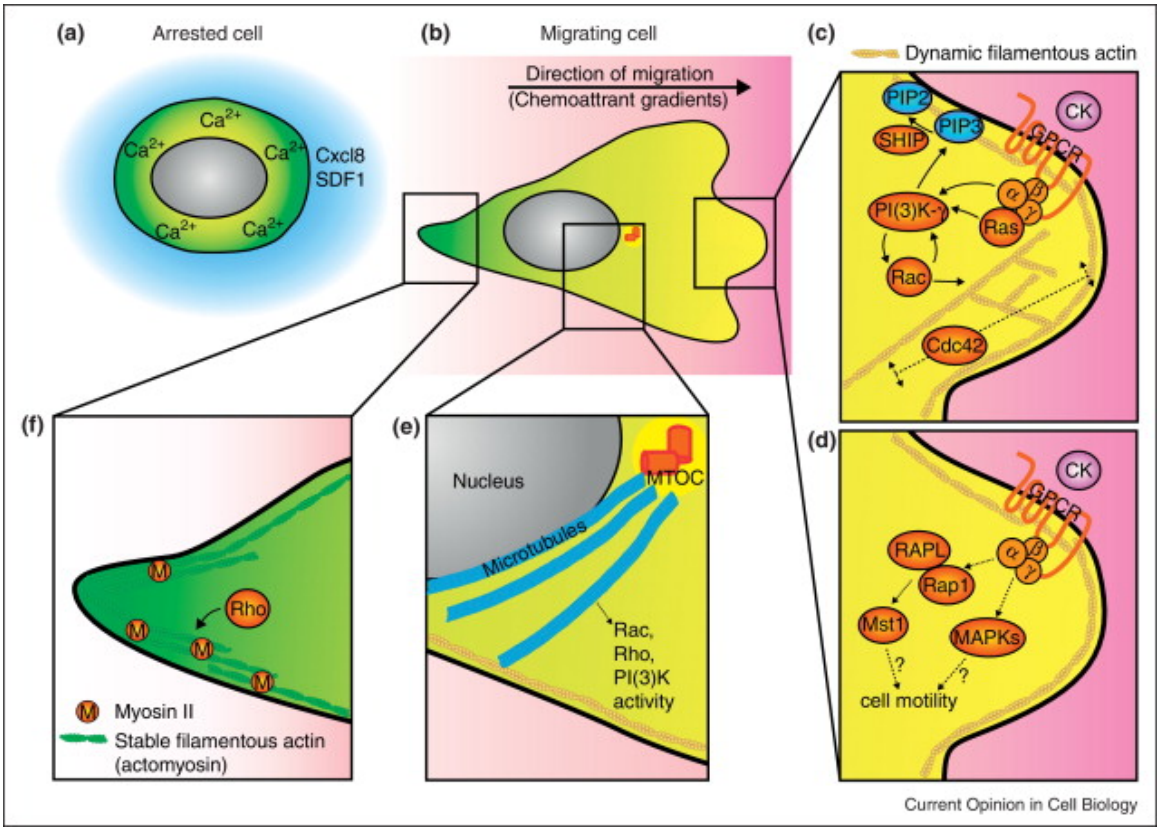
(a)
Arrested cell
Ca2+
Cxcl8
SDF1
(b)
Migrating cell
Direction of migration
(Chemoattrant gradients)
(c)
Dynamic filamentous actin
PIP2
PIP3
SHIP
CK
GPCR
PI(3)K-γ
Ras
Rac
Cdc42
(d)
CK
GPCR
RAPL
Rap1
Mst1
MAPKs
cell motility
(e)
Nucleus
MTOC
Microtubules
Rac,
Rho,
PI(3)K
activity
(f)
Rho
Myosin II
Stable filamentous actin
(actomyosin)
Current Opinion in Cell Biology

Appendix III

Spinning disk confocal imaging of neutrophil migration in zebrafish

This Chapter was published in the following journal article:

Lam P.Y., Fischer R.S., Shin W.D., Waterman C.M., and Huttenlocher A. (2014) Spinning disk confocal imaging of neutrophil migration in zebrafish. *Methods in Molecular Biology*, 1124:219-33.

Summary

Live-cell imaging techniques have been substantially improved due to advances in confocal microscopy instrumentation coupled with ultrasensitive detectors. The spinning disk confocal system is capable of generating images of fluorescent live samples with broad dynamic range and high temporal and spatial resolution. The ability to acquire fluorescent images of living cells *in vivo* on a millisecond timescale allows the dissection of biological processes that have not previously been visualized in a physiologically relevant context. *In vivo* imaging of rapidly moving cells such as neutrophils can be technically challenging. In this chapter, we describe the practical aspects of imaging neutrophils in zebrafish embryos using spinning disk confocal microscopy. Similar setups can also be applied to image other motile cell types and signaling processes in translucent animals or tissues.

1. Introduction

The zebrafish (*Danio rerio*) immune system is remarkably similar to its mammalian counterpart and it has therefore gained tremendous popularity as a vertebrate disease model of both innate and adaptive immunity (reviewed in (Deng and Huttenlocher, 2012; Meeker and Trede, 2008)). Zebrafish embryos are largely translucent for the first few days of development, allowing for noninvasive *in vivo* imaging and studies of cell behavior in a physiologically relevant context.

Here, we describe methods for *in vivo* live imaging of neutrophils in zebrafish embryos. Neutrophil imaging is usually performed at 2 to 3 days post fertilization (dpf). At this stage of development, adaptive immunity has not sufficiently matured, allowing the direct study of innate immunity in isolation. Neutrophils at this stage are considered to be fully functional, as they can directionally migrate (chemotaxis) to wounds or infections and perform immune functions to fight off pathogens. In addition, neutrophils migrate spontaneously (random migration) in the interstitial tissue within the head region (reviewed in (Deng and Huttenlocher, 2012)). The ability to image both neutrophil chemotaxis and random motility in the same organism allows for the dissection of the molecular regulators required for basic motility and directional sensing. One thing to note is that neutrophils at this developmental stage are not terminally differentiated, since they retain the ability to undergo cell division under some conditions and possess an elongated nucleus instead of the multi-lobulated nucleus observed in human neutrophils.

This protocol describes the use of spinning disk confocal microscopy (SDCM) for live imaging of genetically encoded fluorescent reporters expressed in zebrafish embryos.

The benefits of imaging using SDCM over conventional single-point laser scanning confocal microscopy (LSM) including acquisition speed, detection efficiency, resolution, reduced photobleaching, and improved signal-to-noise ratio, both *in vitro* and *in vivo,* has been discussed elsewhere (Fischer et al., 2011; Graf et al., 2005; Wang et al., 2005). One common concern regarding high-speed imaging is the trade-off between speed and resolution. In our experience, acquiring a Z-stack time series using an SDCM system with optimal camera setup offers improved temporal and spatial resolution as compared to laser scanning confocal microscopy (**Fig. 1**). One of the major differences between the acquisition speed of the LSM and SDCM is that the former collects signals from the specimen one pixel at a time through a single pinhole. The speed of the LSM thus depends on the line frequency of the scanner, which is limited by the galvanometer mirrors that move the laser beams, along with the number of lines needed for the field of view imaged. However, because the galvanometer speed is fixed, the limitation on image acquisition speed in practice is the dwell time for each XY position (pixel) to produce sufficient signal over background. The detector for LSM is typically a photomultiplier tube (PMT). Although PMTs have a huge capacity for amplification of signal, they also have relatively low quantum efficiency (~10-15% is typical depending on wavelength). Thus, in order to increase speed for a given signal, one must increase excitation laser power, which can result in faster photobleaching and/or increased phototoxicity with LSM (Fischer et al., 2011). In addition, PMT amplification applies to both signal and noise, thus reducing the overall SNR in LSM images.

In contrast to point scanning with an LSM, a spinning disk confocal utilizes a rotating Nipkow disk with thousands of pinholes arranged in a series of nested spirals to

simultaneously illuminate and collect signals from the entire specimen field, thus leading to significantly faster frame rates than LSM systems. Perhaps more significantly, SDCM systems use a charge-coupled device (CCD) camera or camera as a detector, which have both higher quantum efficiencies (~60%) and lower noise than PMTs, resulting in significantly higher SNR and increased sensitivity (Murray et al., 2007; Salmon and Waters, 2011). Due to the improved SNR and sensitivity, SDCM imaging has the added advantage of requiring lower levels of excitation laser light, leading to less photobleaching and/or phototoxicity of the imaged samples. In recent years, electron multiplying CCDs (EMCCDs) have been introduced that have even greater quantum efficiency (~90%) and low-noise signal amplification resulting in exceptionally high SNR and sensitivity.

When imaging any live specimen by fluorescence microscopy, high expression of fluorescent fusion proteins can produce cytotoxicity or unintended phenotypic effects, including developmental defects in zebrafish. However, live cells expressing fluorescent fusion proteins expressed at approximately endogenous levels of the target protein are often very dim. With samples in which a fluorescent signal is relatively weak, the enhanced sensitivity of SDCM is clearly advantageous. In addition, low fluorescence emission intensity can be compensated for by using longer exposure time; however, this too will decrease the speed advantages of using a SDCM. Further improvements in sensitivity and SNR can be gained through pixel binning, at the cost of lateral resolution. For example, 2X2 binning will increase the SNR by a factor of four, but reduce the lateral resolution by 50%. An EMCCD camera can sometimes abrogate the need for

pixel binning, but it should be noted that native pixel sizes vary with camera type (*see* **Note 1** and **18**).

A major advantage of using SDCM for live, fast motile cell imaging lays in the image quality, which arises from the aforementioned high SNR due to the use of CCD and EMCCD camera technologies. One notable downside of SDCM for intravital imaging is pinhole cross talk, which can degrade image quality. This effect is particularly problematic with specimens that have high light scattering properties (Fischer et al., 2011). Newer model spinning disk heads with greater pinhole spacing can mitigate this problem to some degree. Another potential downside of standard SDCM systems relative to LSM is that they do not have the inherent ability to select a region of interest (ROI) for high power illumination as is required in photobleaching or photoactivation experiments. However, ROI illumination can be achieved via separate illumination paths. Despite these potential drawbacks, SDCM is a powerful system for high-speed three-dimensional imaging of fast-moving cells like neutrophils.

In the following sections, we provide protocols for performing live spinning disk confocal microscopy of transgenic zebrafish expressing fluorescent-tagged proteins in neutrophils. This includes protocols for optimizing neutrophil-specific protein expression, preparation of transgenic fish for imaging, microscope setup, and image acquisition.

2. Materials

2.1 Zebrafish embryos

1. Zebrafish husbandry according to The Zebrafish Book (Westerfield, 2000). Available online http://zfin.org/zf_info/zfbook/zfbk.html. Accessed 14 February 2013.

2.2 Microscope supplies & components

This is just a reference of the setup we use to acquire the images presented in the figures (**Fig. 2 and 3**). Other vendors also provide similar systems.

1. Inverted microscope (Zeiss Observer Z1) (*see* **Note 2**)
2. Spinning disk (Yokogawa CSU X1) (*see* **Note 3**)
3. EMCCD camera (Photometrics Evolve 512 EMCCD) (*see* **Note 1 and 18**)
4. Objective (LCI Plan-Neofluar 63x/1.3 Imm Corr DIC M27; water or glycerine immersion) (*see* **Note 4**)
5. Immersion medium (Carl Zeiss Immersol W 2010; distilled water is also suitable for short-term imaging; see **Note 5**)
6. Heating stage/heating chamber (PECON Incubator P, compact S1 and Heating Insert P S1; heating is optional depending on room setup and stage of embryo)
7. Scanning stage with Z-piezo (*see* **Note 6)**
8. Multi laser module (laser unit 488 / 20 mW (OPSL laser) and 561 nm / 20 mW (DPSS laser)) (*see* **Note 7)**
9. Emission filter (BP 525/50 DMR 25; FF02-617/73-25) (*see* **Note 8**)
10. Vibration isolation table (Newport Vision IsoStation)
11. Glass bottom petri dish (*see* **Note 9**)

12. Zen 2011 (Carl Zeiss) image acquisition software

2.3 Buffers and other reagents (Image Acquisition Components)

1. 60x E3: To make 1L, add 17.2g NaCl, 0.17.2g NaCl, 2.9g $CaCl_2$ and 4.9g $MgSO_4$, Fill to 1L with reverse osmosis (RO) water. Adjust pH to 7.2 with NaOH.
2. 1xE3: Dilute 60x E3 with RO water to 1X. Add 0.1% methylene blue.
3. E3/PTU: 0.003% 1-phenyl-2-thiourea in1x E3.
4. 20x Tricaine: 400 mg tricaine (MS-222) powder, 97.9 ml RO water, ~2.1 ml 1 M Tris (pH 9). Adjust pH to ~7. Store at 4°C.
5. 1x Tricaine: Dilute 20x Tricaine to 1x in E3/PTU
6. Water bath at 42°C.
7. Prepare 0.75--1% low melting point agarose (L.M.A.) in E3 solution for embryo mounting. Microwave to melt the L.M.A. The solution remains fluid at 37°C but quickly hardens when cooled. Maintain the melted L.M.A. in a 42°C water bath.

2.4 Image Processing Components

Image acquisition software usually contains some image viewing and/or imaging analysis functions. Additional commonly used software includes but is not limited to the following:

1. ImageJ (free software; http://rsbweb.nih.gov/ij. Accessed 14 February 2013).
2. FIJI (free software; http://fiji.sc. Accessed 14 February 2013).

3. FluoRender (free software; http://www.sci.utah.edu/software/127-fluorender.html. Accessed 14 February 2013).
4. Bitplane Imaris (http://www.bitplane.com/go/products/imaris. Accessed 14 February 2013).
5. MetaMorph (http://www.moleculardevices.com/products/software/meta-imaging-series/metamorph.html. Accessed 14 February 2013).
6. Volocity (http://www.perkinelmer.com/pages/020/cellularimaging/products/volocity.xhtml. Accessed 14 February 2013)

3. Methods

3.1 Neutrophil-specific protein expression

For imaging purposes, transient mosaic expression is usually sufficient. However, in the case where high levels of expression of the transgene affect neutrophil function, generation of a transgenic line may be desired, as gene expression can be lower and specific transgenic lines with low copy number of the transgene can be identified (*see* **Note 10**). Preparation of transient expression or transgenic zebrafish embryos that express the gene of interest in a neutrophil-specific manner requires the use of a neutrophil-specific promoter such as the myeloperoxidase (*mpx*) (Mathias et al., 2006; Renshaw et al., 2006) or the lysozyme C (*lyz*) promoter (Hall et al., 2007; Lam et al., 2012) (*see* **Note 11**):

1. Construction of plasmid: Use DNA expression vectors containing minimal Tol2 elements for efficient integration (Urasaki et al., 2006) flanking either *mpx* or *lyz* promoter, the gene of interest and an SV40 polyadenylation sequence (Clonetech Laboratories Inc.).
2. Preparation of plasmid DNA: Transformation of plasmid into regular cloning competent cells, e.g., *E. coli* DH5α is sufficient with the exception of plasmids containing the *mpx* promoter (*see* **Note 12**). DNA extraction and purification is achieved using a commercially available miniprep kit (Promega Wizard *Plus* SV Minipreps DNA purification system) (*see* **Note 13**).
3. Preparation of Tol2 transposase mRNA: transposase is prepared by *in vitro* transcription (Ambion mMESSAGE mMACHINE) followed by column purification (Qiagen-RNeasy Mini Kit).

4. Microinjection of zebrafish embryos is a pretty standard routine procedure. Different laboratories will have slightly different setups. For basic setup information and injection procedures, please refer to The Zebrafish Book (Westerfield, 2000) and a video demonstration published elsewhere (Rosen et al., 2009).
5. Expression of construct is obtained by injection of 3 nL of 12.5 ng/μL DNA plasmid with 17.5 ng/μL Tol2 transposase mRNA into the cytoplasm of one-cell stage embryos.

3.2 Preparation of 35-mm glass bottom petri dish.

Embryos will stick to polystyrene and glass surfaces without coating and this will create unwanted wounds on the embryos. Submerge the 35-mm glass bottom Petri dish (*see* **Note 9**) in 1% BSA or 1% skim milk for 10 minutes. Rinse several times with RO water and air dry before use.

3.3 Preparation of samples

Imaging is usually performed at 2--3 days post fertilization (dpf). To prevent pigmentation, exchange regular media with E3 containing 0.003% 1-phenyl-2-thiourea (PTU) as early as 15 hours post fertilization and no later than 1 dpf before pigment starts appearing. Keep the embryos in the E3/PTU medium throughout. Before imaging, remove chorion using ultrafine forceps if embryos are still unhatched. Mounting of an embryo in L.M.A. which will stabilize the embryo and prevent movement is required for

high-magnification imaging, since even the slightest movement by an embryo will affect image quality. Proceed to the mounting procedures as follow:

1. Put embryos in 0.2 mg/mL tricaine in E3/PTU for 1 minute.
2. Transfer 1-2 embryos onto a glass bottom Petri dish using a plastic or glass transfer pipette. Remove as much E3 as possible without drying out the embryo using a P100 pipette or transfer pipette. Any exposure of the embryo to air is enough to create injury on the epithelium and may affect neutrophil behavior.
3. Add in ~80 µL of the melted L.M.A. directly onto the drop of liquid containing the embryo. In order to achieve an even consistency of the L.M.A. around the embryo, remove the L.M.A. and add in new L.M.A.. Repeat the removal and addition of L.M.A. steps again and let it settle. Embryos usually lay down on the bottom of the plate laterally at this stage and are ideal for imaging. Otherwise, adjust the angle of the embryo before the L.M.A. hardens. Wait for approximately 5 minutes at room temperature to ensure that the L.M.A. has hardened (*see* **Note 14**).
4. Slowly add in 2--4 mL E3/PTU with tricaine. Check if embryos are still attached to the bottom and have not floated. If floating occurs, perform the mounting steps again.

3.4 Microscopy, Image Acquisition and analysis

Imaging is performed at the desired developmental stage, typically at 2--3 dpf. Imaging of spontaneous neutrophil motility is performed in the head region. The typical average speed of neutrophils undergoing random motility that we have observed is

between 80--130 nm/s. Directional migration can be performed with different stimulants, i.e., tail fin or ventral fin wounding using a needle or surgical scalpel (Lam et al., 2012; Yoo and Huttenlocher, 2011), $CuSO_4$ induced neuromast damage (d'Alencon et al.), and LTB4 injection (Tobin et al.) or incubation (Yoo et al., 2011) etc. Common applications include imaging the dynamics of the cytoskeleton such as F-actin (**Fig. 2**); subcellular localization of organelles such as the microtubule organizing center and the nucleus (**Fig. 3**); subcellular localization of proteins; subcellular localization of signaling molecules and protein activity using various bioprobes and ratio analysis; and morphological and tracking analysis during cell trafficking, etc.

Different SDCM setups and image acquisition programs can be used. Here, we describe a general inverted microscope setup and the acquisition parameters to be considered before image acquisition. There is no fixed parameter for each acquisition as every sample is different and adjustments are often required to determine the optimal settings. The key is the balance between the speed of acquisition, phototoxicity and image SNR. The following is a general procedure of setting up a Z-stack time series for single or multiple channel image acquisition:

1. Turn on heating stage and set at 28.5 ˚C.
2. Apply a small drop of immersion medium on the objective (*see* **Note 5)**.
3. Secure the glass bottom Petri dish with samples on the microscope stage. Make sure that the dish is seated flat and firmly in the stage, as this will minimize focus drift during imaging. If stage clips are present, clip the sample in tightly.
4. Locate target cell using eyepiece (*see* **Note 15**).
5. Choose a suitable emission filter for acquisition (*see* **Note 16**).

6. Adjust laser power to as low as possible while still obtaining a good SNR image, especially for long time imaging (*see* **Note 17)**.
7. Adjust optimal exposure time (usually around 50--100 msec) and EM gain (around 300--500 for Evolve EMCCD) (*see* **Note 18**). Note that exposure time and laser power will be interdependent. In general, lower laser power at the cost of longer exposure times will result in less phototoxocity and photobleaching, assuming that the time resolution for Z-stack collection is not limiting for the experiment.
8. Set spinning disk revolution speed to maximum (*see* **Note 19**).
9. Set the Z-range with a little buffer distance above and below the cell's initial position, as the cell is actively migrating in a three-dimensional tissue.
10. Set the step size for Z-acquisition (*see* **Note 20**).
11. Set time interval and total duration of the acquisition (*see* **Note 21**).
12. Set the mode of acquisition as all channels per Z-slice (*see* **Note 22**).
13. Start acquiring image.
14. Common post-acquisition image analysis programs include but not limited to freeware like ImageJ/Fiji and FluoRender or commercially available Bitplane Imaris, Volocity, and MetaMorph. Each program has a different capacity and details of such are out of the scope of this chapter.

4. Notes

1. Photometrics Evolve 512 EMCCD and CoolSNAP HQ2 CCD are the common high-performance cameras of choice for SDCM. Sensitivity and resolution are the main criteria for choosing a suitable camera. Evolve EMCCD offers a higher sensitivity but a relatively big 16 μm x 16 μm pixel size. CoolSNAP HQ2 has a 6.45 μm x 6.45 μm pixel size; however, binning may be needed for image acquisition to reduce illumination intensity and exposure time needed. It is highly recommended to have a demonstration of different cameras to find out which one is better suited for your specific application. For our applications, we selected the Evolve EMCCD taking into consideration the speed of neutrophil migration and fluorescent levels of live cells (also *see* **Note 18**). One thing to note is that because the Evolve EMCCD is very sensitive, it can pick up cosmic ray signals stochastically that appear sporadically as very bright transient dots/comets within the image (Groom, 2002). These transient dots/comets are very bright and are easily distinguishable from the real signal generated by fluorescent protein expression.
2. The inverted microscope stand provides a stable base for minimizing vibration as well as providing long-term stability for time-lapse imaging. As most microscope models will have manual parts, automation of the stand is not necessary for spinning disk confocal image acquisition. Motorized components of the stand conveniently allow for fast and seamless switching between preconfigured settings for sample viewing and image acquisition.

The stand should include a filter-cube turret to allow switching between different dichromatic mirrors for specimen viewing and image acquisition, a multi-position objective lens nose piece for switching between magnifications, transilluminator for phase/DIC imaging/viewing, and an epi-illuminator for wide-field excitation of the sample for viewing. Having multiple imaging ports provides flexibility for introducing illumination, mounting digital cameras, and sample observation. Incorporating electronic shutters in the transillumination and epifluorescence illumination path will help to minimize photobleaching and phototoxicity when imaging/viewing the sample.

3. The Yokogawa CSU X1 spinning disk confocal unit is a dual-disk scan head design that consists of a disk with microlenses that are in conjugate with the pinholes of the Nipkow disk. This has several advantages for high temporal and spatial resolution live cell imaging over other spinning disk confocal systems. Single Nipkow disk systems only transmit 5% of the incident illumination, whereas the microlenses in the second disk of the Yokogawa CSU X1 increase the illumination efficiency theoretically up to 40%. Slit-scanning systems do not reject out-of-focus fluorescence along the axis of the slit and thus suffer from higher backgrounds. Compared to previous models (CSU 10, CSU 22), the CSU X1 has increased illumination throughput and improved beam expanding optics providing flatter field of illumination. The CSU X1 is available as a manual or motorized version and has a wide range of configurations such as 2 camera port and bright field bypass module. For

our application, we chose the basic manual version with 6 position electronic emission filter wheel.

4. Imaging deep in the sample and far away from the coverslip with an oil immersion objective can suffer from optical artifacts such as spherical aberration. Utilizing a high NA water immersion objective with a correction collar can minimize these induced spherical aberrations caused by mismatched refractive indices of the sample and immersion medium. In addition, the correction collar not only allows one to compensate for coverslip thickness variations but also changes in refractive medium due to temperature.
5. For extended time-lapse imaging experiments, Carl Zeiss Immersol W 2010 instead of distilled water is used as a water objective immersion medium. This reduces evaporation of the immersion medium and allows uninterrupted long-term imaging.
6. A piezoelectric Z-stage allows higher Z-focusing speeds than a stepper- or servomotor-driven Z-stage. In our experience, it can cut down on the time for a Z-stack acquisition by nearly half. As an alternative, a piezoelectric-driven objective lens mount can be used. Note that piezo devices have much smaller focus range limits (typically 100 μm, some as high as 300 μm) compared to motor-driven devices (tens of millimeters).
7. Developments in diode lasers and diode-pumped solid state (DPSS) lasers have made them a cost-effective alternative to gas lasers. They are small and quiet, have low heat loads and large range of wavelength selection, and don’t

require bulky water coolers. Most microscope manufacturers provide fiber-coupled laser combiners to deliver the laser beam, which use an acousto-optic tunable filter (AOTF) or TTL modulation to quickly select, shutter, and modulate the wavelength power. When choosing from the wide selection of available laser lines, the wavelength should optimally excite the fluorescent protein. Common laser wavelengths used for exciting fluorophores are 405 nm for DAPI, 442 nm for CFP, 488 nm for GFP, 514 nm for YFP, 561 nm for RFP, and 647 nm for Cy5. In addition, when considering power selection of individual lines, it should be noted that for fiber-coupled laser combiners, 40-60% of the illumination power (wavelength dependent) is loss due to fiber coupling efficiency. For our application, 20 mW has proven to be sufficient for live zebrafish imaging (also *see* **Note 17**).

8. Individual band-pass emission filters, denoted by the center wavelength and bandwidth, should be chosen based on the spectral properties of the fluorophore. When selecting band-pass filters, it is important that the bandwidth be wide enough for efficient emission collection of the fluorophore, as well as provides sufficient blocking to eliminate the excitation source and signal from other fluorescent channels. For our filters, we chose a center wavelength of 525 nm with a 50 nm bandwidth (BP 525/50 DMR 25) and a 617 nm center wavelength with a 73 nm bandwidth (FF02-617/73-25). Manufacturers, such as Chroma Technology Corp and Semrock, Inc., can provide suggestions for filter selection based on the fluorophore spectral properties.

9. Glass bottom dishes are commercially available, but an inexpensive and relatively easy alternative is to make them in house. Drill a 16-18 mm hole in the center of a 35-mm tissue culture dish bottom. Apply a thin layer of Norland Optical Adhesive 68 on the outside surface around the hole. Place a 22-mm round #1 coverslip on top of the adhesive and press down slightly. The adhesive is cured by UV light. Overnight exposure of UV light in a tissue culture hood or approximately 1 hour on a UV transilluminator is sufficient to cure the adhesive.
10. To make a transgenic line, injected embryos displaying mosaic transgene expression are raised to sexual maturity (as early as 2.5 months). F_0 founders are screened by outcrossing with wild-type zebrafish and checked for transgene expression in the neutrophils in the F_1 embryos at 2--3 dpf. The positive F_1 transgenic progeny can then be used for imaging or propagation of the transgenic line.
11. Since the *mpx* promoter is much larger than that of the *lyz* promoter (8 Kb vs. 4.1 Kb, respectively), it is easier to express larger transgenes (i.e., >3 Kb) driven under the *lyz* promoter in our experience. The *mpx* promoter drives gene expression mainly in neutrophils, although there may be very low levels of expression in macrophages as well (Mathias et al., 2006). The *lyz* promoter drives gene expression in neutrophils at later stages (≥ 2 dpf) (Lam et al., 2012). However, in earlier stage embryos (i.e., 1dpf), expression can be seen in primitive macrophages (Zhang et al., 2008).

12. Cloning with the *mpx* promoter is better achieved using bacterial strains specific for unstable DNA inserts, e.g., Stbl3 (Invitrogen).
13. Not all DNA extraction and purification procedures/kits produces high enough DNA quality for microinjection. Injecting poor quality DNA will result in embryo death. For small amounts of DNA preparation, the Promega Wizard *Plus* SV Minipreps DNA purification system yields good DNA quality in our experience.
14. A small amount of L.M.A. just covering the embryo is enough for securing the position of the embryo on the glass bottom dish. The water tension of a small drop of L.M.A. helps hold the embryo close to the bottom of the dish. A larger volume of L.M.A. may result in an agarose gap between the embryo and the glass bottom, which is not obvious under low-power magnification. As higher magnification and higher NA objectives usually have a shorter working distance, this may make a substantial difference in image quality.
15. Ideally, find neutrophils that are close to the objective lens (i.e., not deep into the embryo) and have a normal morphology, i.e., elongated cell shape and display pseudopod formation. Rounding of neutrophils is a common sign of abnormality due to transgene overexpression. If neutrophils have multiple fluorescent proteins expressed, find neutrophils that have similar fluorescent intensity of both fluorophores.
16. When performing ratio image analysis or imaging more than one fluorescence channel, caution should be taken to check for bleed-through between fluorescence channels. If this happens, separate single band-pass emission filters in an electronic filter wheel should be used instead of a multiband

emission. Although the time needed for the filter wheels to switch between filters limits the acquisition speed of multicolor images on a single camera, sequential acquisition of different channels is necessary to produce an accurate co-localization and/or ratio quantitative analysis. It is recommended to acquire the longest wavelength emission probe first to avoid possible bleed-through (also *see* **Note 22**). Careful control of total signal for each channel is also important in limiting the contribution of cross talk. In addition, the intensity of fluorescence emission varies from one channel to another, in order to acquire two channels with comparable exposure time and signal intensity, it is best to adjust laser power without introducing excessive phototoxicity.

17. We usually use ≤ 30% laser power with our laser unit for imaging experiments. Too high of a laser intensity will result in unhealthy neutrophils or even cell death (also *see* **Note 7**). Ideally, set the initial maximum signal to 50% of the dynamic range of the camera bit depth. Fiber optic coupling efficiency and final output power at the objective will vary depending on the microscope setup, so empirical testing or direct power measurements should be done to optimize imaging quality and embryo health.
18. EM gain technology multiplies the charge signal from each pixel on a CCD array to a level above the read noise. Therefore, EMCCD cameras can further improve image acquisition speed by reducing the exposure time needed compared to a CCD camera. It can also reduce the amount of excitation illumination needed that may cause photobleaching and phototoxicity of the

cell and therefore can extend the possible imaging time of the sample. This is important when performing long-term time-lapse acquisition, especially with Z-stack acquisition of each time point. However, the cost of EMCCD cameras is much higher than traditional CCD cameras. If an EMCCD camera is used, adjust EM gain settings, preferably to the camera optimal setting. Increasing EM gain will increase signal intensity but may introduce noise at the same time. In the case where a bright field image is needed, EM gain for bright field acquisition can be reduced to zero to decrease graininess. Alternatively, 2X2 binning on a CCD camera with small pixel sizes (e.g., 6.45 μm in the case of the Photometrics HQ2) will improve its sensitivity but will still lack the signal amplification afforded by an EMCCD.

19. In practice, it is best to synchronize the spinning disk speed and camera exposure time so that the pinholes traverse an integral number of frame crossings during exposure. When the disk speed is not optimal, striped patterns can be observed especially for shorter exposure times (smaller than 50 msec). As it takes time for the spinning disk to change its speed, the disk speed should be set constant throughout the acquisition. For this reason, it is best to set similar exposure times for different channels during multiple channel acquisition.
20. Ideally, as a minimum requirement, a Nyquist theorem satisfying step size is preferred, which is equal to half the Z resolution (depth of field/optical depth). This is determined by the objective used and any additional magnification in the light path, as well as the wavelength of excitation used. As an example,

for the microscope setup and objective that we use (LCI Plan-Neofluar 63x/1.3 Imm Corr DIC M27), we usually set the step size as 0.4 μm.

21. In general, 0.5 to 1 minute intervals for a duration of 30 minutes using a 20x objective is sufficient for imaging neutrophil long distance migration. Allowing the specimen to experience maximal “dark periods” (no laser exposure) during the collection will generally result in less phototoxic effects over longer imaging times. For imaging neutrophil pseudopod dynamics, acquire images for ≥10 minutes continuously at maximal speed or at minimum with a time interval of 10 to 30 seconds using a 60x objective.
22. Caution should be taken in choosing to acquire all channels per Z-slice or whole Z-stack per channel. It is recommended to use all channels per Z-slice, as it will acquire an image of each channel for each Z-plane sequentially, resulting in a more accurate temporal comparison between channels. However, switching between filters for each Z-plane will increase the overhead time.

Acknowledgement

Dr. Benjamin Ng (Carl Zeiss) has provided valuable advice on the SDCM setup. This work was supported by the National Institutes of Health [grant number GM074827] to A. H. and the Hong Kong Croucher Foundation, Joint Universities Summer Teaching Laboratory (JUSTL) program to P-Y.L.

References

d'Alencon, C.A., O.A. Pena, C. Wittmann, V.E. Gallardo, R.A. Jones, F. Loosli, U. Liebel, C. Grabher, and M.L. Allende. A high-throughput chemically induced inflammation assay in zebrafish. *BMC Biol*. 8:151.

Deng, Q., and A. Huttenlocher. 2012. Leukocyte migration from a fish eye's view. *J Cell Sci*. 125:3949-56.

Fischer, R.S., Y. Wu, P. Kanchanawong, H. Shroff, and C.M. Waterman. 2011. Microscopy in 3D: a biologist's toolbox. *Trends Cell Biol*. 21:682-91.

Graf, R., J. Rietdorf, and T. Zimmermann. 2005. Live cell spinning disk microscopy. *Adv Biochem Eng Biotechnol*. 95:57-75.

Groom, D. 2002. Cosmic rays and other nonsense in astronomical CCD imagers. *Experimental Astronomy*:45-55.

Hall, C., M.V. Flores, T. Storm, K. Crosier, and P. Crosier. 2007. The zebrafish lysozyme C promoter drives myeloid-specific expression in transgenic fish. *BMC Dev Biol*. 7:42.

Lam, P.Y., S.K. Yoo, J.M. Green, and A. Huttenlocher. 2012. The SH2-domain-containing inositol 5-phosphatase (SHIP) limits the motility of neutrophils and their recruitment to wounds in zebrafish. *J Cell Sci*. 125:4973-8.

Mathias, J.R., B.J. Perrin, T.X. Liu, J. Kanki, A.T. Look, and A. Huttenlocher. 2006. Resolution of inflammation by retrograde chemotaxis of neutrophils in transgenic zebrafish. *J Leukoc Biol*. 80:1281-8.

Meeker, N.D., and N.S. Trede. 2008. Immunology and zebrafish: spawning new models of human disease. *Dev Comp Immunol*. 32:745-57.

Murray, J.M., P.L. Appleton, J.R. Swedlow, and J.C. Waters. 2007. Evaluating performance in three-dimensional fluorescence microscopy. *J Microsc*. 228:390-405.

Renshaw, S.A., C.A. Loynes, D.M. Trushell, S. Elworthy, P.W. Ingham, and M.K. Whyte. 2006. A transgenic zebrafish model of neutrophilic inflammation. *Blood*. 108:3976-8.

Rosen, J.N., M.F. Sweeney, and J.D. Mably. 2009. Microinjection of zebrafish embryos to analyze gene function. *J Vis Exp*.

Salmon, W.C., and J.C. Waters. 2011. CCD cameras for fluorescence imaging of living cells. *Cold Spring Harb Protoc*. 2011:790-802.

Tobin, D.M., J.C. Vary, Jr., J.P. Ray, G.S. Walsh, S.J. Dunstan, N.D. Bang, D.A. Hagge, S. Khadge, M.C. King, T.R. Hawn, C.B. Moens, and L. Ramakrishnan. The lta4h locus modulates susceptibility to mycobacterial infection in zebrafish and humans. *Cell*. 140:717-30.

Urasaki, A., G. Morvan, and K. Kawakami. 2006. Functional dissection of the Tol2 transposable element identified the minimal cis-sequence and a highly repetitive sequence in the subterminal region essential for transposition. *Genetics*. 174:639-49.

Wang, E., C.M. Babbey, and K.W. Dunn. 2005. Performance comparison between the high-speed Yokogawa spinning disc confocal system and single-point scanning confocal systems. *J Microsc*. 218:148-59.

Westerfield, M. 2000. *The zebrafish book. A guide for the laboratory use of zebrafish (Danio rerio). 4th ed., Univ. of Oregon Press, Eugene.*

Yoo, S.K., and A. Huttenlocher. 2011. Spatiotemporal photolabeling of neutrophil trafficking during inflammation in live zebrafish. *J Leukoc Biol*. 89:661-7.

Yoo, S.K., T.W. Starnes, Q. Deng, and A. Huttenlocher. 2011. Lyn is a redox sensor that mediates leukocyte wound attraction in vivo. *Nature*.

Zhang, Y., X.T. Bai, K.Y. Zhu, Y. Jin, M. Deng, H.Y. Le, Y.F. Fu, Y. Chen, J. Zhu, A.T. Look, J. Kanki, Z. Chen, S.J. Chen, and T.X. Liu. 2008. In vivo interstitial migration of primitive macrophages mediated by JNK-matrix metalloproteinase 13 signaling in response to acute injury. *J Immunol*. 181:2155-64.

Fig. 1. Comparison of laser scanning confocal (LSM) and spinning disk confocal (SDCM) on *in vivo* neutrophil imaging. Maximum intensity projection image of a neutrophil expressing GFP-UtrCH (green) and Lifeact-Ruby (magenta), which labels stable F-actin and all F-actin, respectively. (A-B) Image acquired using an LSM (Olympus). Olympus LUMFL 60x/ 1.1NA Water objective (A) or Olympus PlanApo N 60x/ 1.45NA Oil objective (B) was used with S.U. 200, optimal step size and 3.8x zoom in. (C-D) Image acquired using SDCM (Zeiss). LCI Plan-Neofluar 63x/ 1.3NA Water objective (C) or Plan Apo 63x/ 1.4NA Oil objective (D) was used with 300 EM gain, 55 msec exposure for both channels and 0.4 μm step size. SDCM images showed superior image quality compared to that of the LSM images. The difference between using an oil objective with a higher NA than the water objective is less significant. Scale bar: 10 μm.

Fig. 1

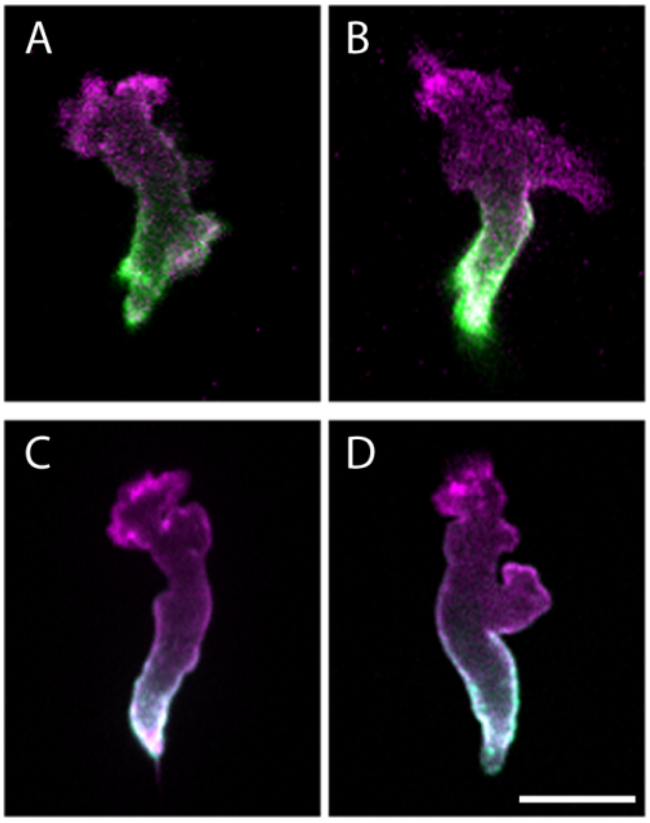

Fig. 2. Spinning disk confocal imaging of F-actin cytoskeleton dynamics. Time-lapse maximum intensity projection image of a neutrophil undergoing random motility in a zebrafish embryo *in vivo*. The neutrophil expresses GFP-UtrCH (green) and Lifeact-Ruby (red), which labels stable F-actin and all F-actin, respectively. A SDCM equipped with an EMCCD camera was used for the acquisition. LCI Plan-Neofluar 63x/1.3 Water objective; 300 EM gain; 55 msec exposure (GFP-UtrCH), 36 msec exposure (Lifeact-Ruby); emission filter BP 525/50 and FF02-617/73-25; 0.4 μm step size. Acquisition was made as fast as possible and consecutive images are shown in the panel. Scale bar: 10 μm.

Fig. 2

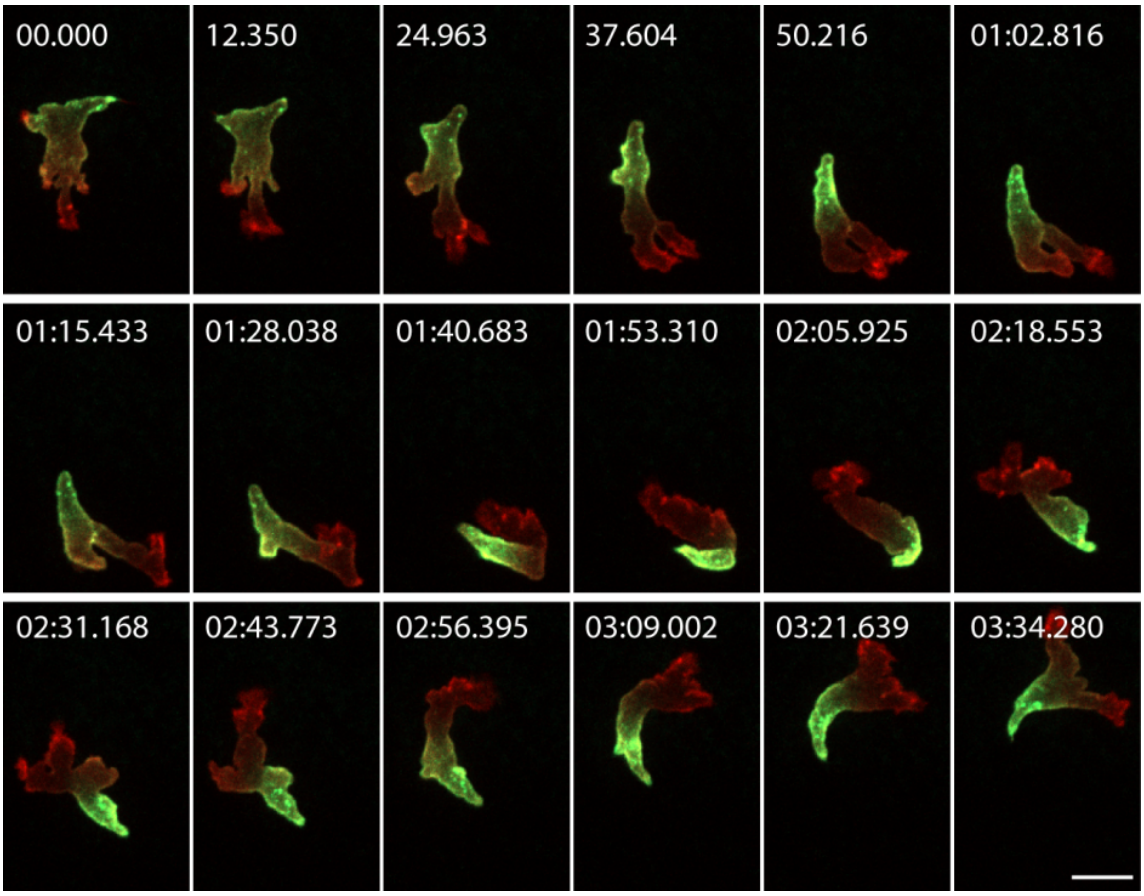
00.000
12.350
24.963
37.604
50.216
01:02.816
01:15.433
01:28.038
01:40.683
01:53.310
02:05.925
02:18.553
02:31.168
02:43.773
02:56.395
03:09.002
03:21.639
03:34.280

Fig. 3. Spinning disk confocal imaging of organelle subcellular localization. Time-lapse maximum intensity projection image of a neutrophil expressing γtubulin-GFP (green) and a nuclear probe, mCherry-histone H2B (red). The Microtubule Organizing Center (MTOC-arrow) is localized in front of the nucleus during neutrophil motility *in vivo*. Scale bar: 10 μm.

Fig. 3

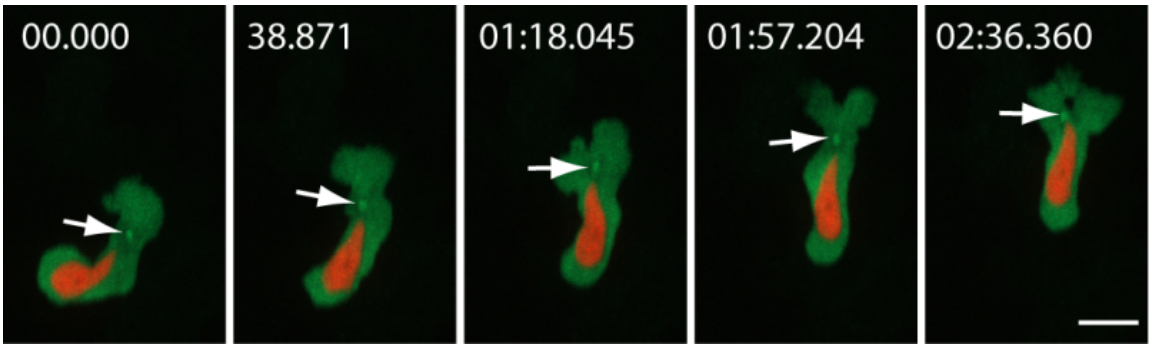

Appendix IV

In vivo imaging and characterization of actin microridges

Abstract

Actin microridges form labyrinth like patterns on superficial epithelial cells across animal species. This highly organized assembly has been implicated in mucus retention and in the mechanical structure of mucosal surfaces, however the mechanisms that regulate actin microridges remain largely unknown. Here we characterize the composition and dynamics of actin microridges on the surface of zebrafish larvae using live imaging. Microridges contain phospho-tyrosine, cortactin and VASP, but not focal adhesion kinase. Time-lapse imaging reveals dynamic changes in the length and branching of microridges in intact animals. Transient perturbation of the microridge pattern occurs before cell division with rapid re-assembly during and after cytokinesis. Microridge assembly is maintained with constitutive activation of Rho or inhibition of myosin II activity. However, expression of dominant negative RhoA or Rac alters microridge organization, with an increase in distance between microridges. Latrunculin A treatment and photoconversion experiments suggest that the F-actin filaments are actively treadmilling in microridges. Accordingly, inhibition of Arp2/3 or PI3K signaling impairs microridge structure and length. Taken together, actin microridges in zebrafish represent a tractable *in vivo* model to probe pattern formation and dissect Arp2/3-mediated actin dynamics *in vivo*.

Introduction

Superficial epithelial cells make labyrinth like patterns known as actin microridges. Microridges are observed on mucosal surfaces across animal species, including the human uterine epithelium (Thie et al., 1998), post-menopausal fallopian tubes (Correr et al., 2006), rat kidney collecting ducts (Rice et al., 2013), the cornea of multiple species (Collin and Collin, 2000; Simmich et al., 2012; Uppal et al., 2013); and the surface epithelium of zebrafish larvae (Li et al., 2011; Villava et al., 2007). The ubiquitous presence and remarkable organization of microridges across animal species suggest an important function. It is generally thought that microridges help with mucus retention (Sperry and Wassersug, 1976) and they have been hypothesized to provide rigidity and plasticity to surface epithelial cells (Sharma et al., 2005; Uehara et al., 1991). However, the signaling pathways that regulate microridge structure remain largely unknown. Previous studies using transmission electron microscopy and atomic force microscopy of epithelial cells *in vitro*, have shown that microridges contain filamentous actin (F-actin) bundles (Bereither-Hahn et al., 1979; Sharma et al., 2005; Uehara et al., 1991). Microridges form only in the most superficial confluent layer of the epithelial cells *in vitro* (Sharma et al., 2005) and are not observed in single epithelial cells (Doyle and Lee, 2005; Wilson et al., 2010) suggesting that the presence of a monolayer or cell-cell contact is essential for their formation. In addition, proper lipid secretion and lamellar granule trafficking have been suggested to regulate microridge structure (Li et al., 2011). The nature of F-actin in microridges is unclear. Uehara et al. has previously shown by scanning electron microscopy that some epithelial cells are distended and have thicker microridges when treated with cytochalasin B (Uehara et al.,

1991). Sharma et al., on the other hand, has shown by fluorescence microscopy and cytochalasin B treatment that F-actin in microridges was more stable than F-actin in lamellipodia (Sharma et al., 2005). Here we define the composition and dynamics of actin microridges using real time imaging in intact zebrafish (*Danio rerio*) larvae. We found that Arp2/3 and PI3K are necessary for microridge length, but myosin II activity is dispensable. Both Rac and Rho activity regulate the distance between microridges. This work provides new insights into how actin microridges are regulated *in vivo*, and provides a platform to analyze pattern formation in a dynamic Arp2/3 driven actin network in live animals.

Results

Microridge structure and composition

To analyze microridge structure, we performed scanning electron microscopy (SEM) on zebrafish at different developmental stages and found that microridges appear as early as 12 hours post fertilization in epithelial cells that seem to have recently undergone cytokinesis (Figure S1Ai). At this stage of development, however, most cells do not form microridges (Figure S1Aii). By 1 day post fertilization (dpf), microridges are present on all epithelial surfaces examined, including the cornea, yolk and trunk region (Figure 1A, Figure S1B). Microridges generally become more prominent as larvae develop, with the exception of the cornea where microridges diminish by 4-5 dpf (Figure S1B). Interestingly, microridges reappear on the cornea in adults (Figure S1C).

Previous studies have shown that microridges contain F-actin bundles (Bereither-Hahn et al., 1979; Sharma et al., 2005; Uehara et al., 1991). We were interested in testing if there is a polarity of F-actin dynamics in microridges. One example of such F-actin polarity has been reported in motile neutrophils in zebrafish larvae, where more dynamic F-actin is at the cell front and stabilized F-actin is at the uropod (Yoo et al., 2010). We expressed two F-actin binding probes specifically in epithelial cells of zebrafish larvae using the *krt4* promoter: Lifeact fused to Ruby, which detects all F-actin (Riedl et al., 2008); and the calponin homology domain of utrophin (UtrCH) fused to GFP, which detects more stable F-actin (Burkel et al., 2007). Confocal analysis showed that Lifeact and UtrCH labeled F-actin colocalize in microridges (Figure 1B), suggesting that there is no obvious polarity of F-actin dynamics in microridges.

Focal adhesions (FAs) are well-studied actin containing structures on the cell cortex where F-actin bundles anchor and connect to the extracellular matrix. The formation of these F-actin bundles is tightly regulated in part by actin regulatory proteins that localize to FAs (reviewed in (Burridge and Chrzanowska-Wodnicka, 1996; Burridge et al., 1997; Gilmore and Burridge, 1996; Petit and Thiery, 2000; Ridley et al., 2003). We next performed immunofluorescent staining and expressed fluorescently tagged proteins to identify the actin regulatory proteins that localize to microridges. We found that tyrosine phosphorylated proteins (Figure 1C) and cortactin (Figure 1D) colocalize with F-actin in microridges. By contrast, focal adhesion kinase (FAK) localizes to cell-cell contact sites but not to microridges (Figure 1E). Vasodilator-stimulated phosphoprotein (VASP) is associated with FAs and is thought to have an important role in F-actin assembly (Holt et al., 1998). Using fluorescently tagged VASP expressed in epithelial cells, we performed live dual imaging of VASP and Lifeact-Ruby labeled F-actin. VASP colocalizes with Lifeact at microridges. Interestingly, there are puncta labeled only with Lifeact but not VASP along the microridges and occasionally at the tips of filaments (Figure 1F; see movie S1). The localization of tyrosine phosphorylated proteins, cortactin and VASP, but not FAK, in microridges suggests that the highly organized F-actin bundles in microridges may have mechanisms of regulation that are similar to focal adhesions, stress fibers or other actin structures, like invadopodia.

Microridge dynamics *in vivo*

Microridges form highly organized patterns *in vivo*. We next wanted to determine if these organized F-actin structures are dynamic using real time imaging of F-actin

bioprobes in intact animals. A previous study using phase contrast imaging on keratocytes *in vitro* revealed that microridges are dynamic within monolayers (Sharma et al., 2005). However, the keratocytes in monolayers are also mobile (Sharma et al., 2005), while epithelial cells in zebrafish larvae are relatively stationary. To achieve fast, high-resolution image acquisition of microridges within a three-dimensional live animal, we expressed GFP-UtrCH specifically in epithelial cells in zebrafish larvae to visualize F-actin in microridges. Confocal time-lapse imaging showed that microridges are constantly shifting in position through bending, merging and breaking (Figure 2A-2C; see movie S2 and S3), consistent with *in vitro* observations (Sharma et al., 2005). These findings suggest that although microridges maintain a highly ordered structure, the microridge pattern is dynamic *in vivo*.

To determine if cell perturbations alter microridge structure, we visualized actin microridges during cytokinesis and after wounding using confocal live imaging of epithelial cells expressing GFP-UtrCH. Interestingly, microridges are reduced to sparse, small foci of actin prior to cytokinesis (Figure 3A; see movie S4). Before the appearance of the cleavage furrow, microridges are shorter and more punctate (Figure 3Ai, ii), and then gradually diminish with a near homogeneous distribution of GFP-UtrCH right before the cleavage furrow forms (Figure 3Aiii). During cleavage furrow formation, microridges first reappear as dots (Figure 3Aiv, v) and then progress to form longer structures as cleavage furrow formation progresses. Shortly after cytokinesis, F-actin re-assembles to form the organized microridge pattern (Figure 3Avi). The neighboring epithelial cells also undergo changes in cell shape without the disappearance of microridges. It is interesting that microridges on superficial epithelial cells are constantly

changing although the overall pattern is maintained over time.

Activation of Rho is essential during cytokinesis in eukaryotic cells and is a key regulator of the actin cytoskeleton (reviewed in (Piekny et al., 2005)). We therefore tested if an increase in Rho activity was sufficient to alter microridge structure by expressing constitutively active Rho (Rho Q63L) in epithelial cells of zebrafish larvae. Epithelial cells on zebrafish larvae are usually polygonal and flat (Figure 3Bi). Rho Q63L expression induces cell rounding and apical protrusions from the cell surface (Figure 3Bii). However, microridges are still present despite the change in cell shape, even with cell rounding, suggesting that the F-actin bundles are likely associated with the cortical actin network. Taken together, these findings suggest that an increase in Rho activity and cell shape change alone is not a significant determinant of microridge architecture.

We next determined if microridges change during wound closure. Multicellular epithelial wound closure in embryos is often mediated by the formation of a contractile actomyosin purse string at wound edges (Brock et al., 1996; Clark et al., 2009; Martin and Lewis, 1992), which requires Rho activation (Brock et al., 1996; Clark et al., 2009). To test how wounding alters microridge structure, we performed single cell laser ablation on zebrafish larvae that express GFP-UtrCH in epithelial cells (Figure 3Ci). Confocal live imaging showed that microridges are present in the responding epithelial cells during cell contraction and wound closure (Figure 3Cii, iii). The presence of microridges following wounding further confirms the finding that an increase in Rho activity is not sufficient to induce microridge disassembly. However, with wounding we observed rearrangement in the orientation of microridges at the wound edge. Live imaging revealed that microridges bend, break and rearrange after the laser wound, but

maintain their overall structure (Figure 3C; see movie S5). Further investigation will be required to address whether the change in microridge orientation in these responding epithelial cells is due to changes in cell signaling or is due to the physical changes involved in wound closure. Taken together, these findings suggest that the overall structure of microridges may be relatively independent of changes in cellular tension, in contrast to focal adhesions and stress fibers.

Regulation of microridge architecture

To further investigate the role of motors and cellular tension on microridges, we tested the effects of myosin II inhibition. Previous studies have supported an essential role for myosin II activity in stress fiber formation and the regulation of focal adhesions (reviewed in (Petit and Thiery, 2000)). To determine the role of myosin II in microridges, we analyzed microridge length in the same cell from intact zebrafish larvae before and after treatment with blebbistatin. Measuring microridge length in the same cell helped to control for the variation in microridges between different cells. Myosin II inhibition has no effect on the length or overall organization of microridges compared to control (Figure 4A). To further test the possible role of myosin activity in microridges, we performed immunofluorescent staining using an antibody that recognizes phospho-myosin light chain (pMLC). pMLC is detected in muscle fibers under the epithelium as expected (data not shown), but surprisingly, is not detected in microridges (Figure S2). These findings suggest that myosin II activity is dispensable for the maintenance of microridges.

To further probe the role of actomyosin contractility in microridge structure, we

expressed dominant negative RhoA (RhoA T19N) in epithelial cells. We found that microridges are still present in cells expressing RhoA T19N (Figure 4B). However, there is a wider distance between these microridges (Figure 4C), which correlates with an increase in cell area (Figure 4D). One caveat is that we could not measure microridge length in the same cell before and after Rho inhibition, since RhoA T19N is driven constitutively from the *krt4* promoter. Further experiments will be needed to address how RhoA modulates cell size and the distance between microridges. Rac is another small Rho GTPase that regulates actin polymerization. We tested the involvement of Rac in microridge architecture by expressing a dominant negative form of Rac (Rac2 D57N), which inhibits both endogenous Rac1 and Rac2 (Deng et al., 2011), in epithelial cells using the *krt4* promoter. Microridges persist even with the constitutive expression of Rac2 D57N (Figure 4E). However, we observed an increase in the distance between microridges (Figure 4F) with no significant change in the average cell size (Figure 4G). Our data suggest that both Rho and Rac are involved in the regulation of microridge organization.

F-actin is treadmilling in microridges

It is unclear how microridges are both highly dynamic yet maintain an intrinsic organization that remains stable, even after perturbations like wounding. In order to study F-actin dynamic in microridges, we inhibited F-actin polymerization using Latrunculin A (LatA). Microridge length in the same cell before and after treatment was visualized, measured and quantified using GFP-UtrCH localization and confocal microscopy. LatA treatment results in shorter microridges and fewer microridges as

compared to DMSO controls (Figure 5Ai-ii). The surface topology of this microridge phenotype was further confirmed using SEM (Figure 5Aiii). In contrast to the *in vitro* studies (Sharma et al., 2005), this suggests that F-actin in microridges is actively treadmilling and that actin polymerization is required to maintain microridge structure. Our findings are consistent with an earlier *in vivo* study using carp epithelium (Uehara et al., 1991).

Previously reported transmission electron microscopy images of carp epithelial microridges show branching of F-actin filaments in microridges (Uehara et al., 1991). This is reminiscent of Arp2/3 mediated actin assemblies *in vitro*. To determine if Arp2/3 regulates microridges, Arp2/3 was inhibited using CK-666. We found a dramatic change in microridge architecture in the presence of Arp2/3 inhibition, with substantially shorter microridges compared to control inhibitor (Figure 5Bi-ii). Similar to the LatA experiment, SEM analysis confirmed that the surface topology closely resembles the underlying actin microridge pattern (Figure 5Biii). To further identify signaling pathways that regulate microridge structure, we tested the effects of PI3K inhibition, since PI3K has been implicated in dynamic F-actin at the leading edge of motile cells *in vivo* (Yoo et al., 2010). PI3K inhibition using LY294002 impairs microridge length compared to control (Figure 5Ci-iii). Our results suggest that F-actin in microridges is actively treadmilling and that Arp2/3 and PI3K regulate actin microridge structure.

To further test the dynamics of F-actin in microridges we examined the turnover of mEos-tagged actin after photoconversion in epithelial cells *in vivo*. mEos is irreversibly converted from green to red fluorescent emission upon 405 nm laser excitation. A small region of the microridge was photoconverted and time-lapse images

were acquired after photoconversion. The signal from the photo-converted actin in the microridge rapidly diffuses and weakens after a few minutes (Figure S3, see movie S6). This suggests that actin is actively depolymerizating in microridges. When a larger region of the microridges was photoconverted, the non-converted microridges region shows incorporation of photoconverted actin within a few minutes (Figure 6, see movie S7). As photoconversion also occurs in the pool of un-incorporated actin-mEos in the cytosol, this observation suggests that the incorporation of actin into microridges is very rapid. As a control, mEos alone was expressed in epithelial cells. Under these conditions, no microridge pattern was observed (Figure S4), confirming the specificity of the actin-mEos photoconversion in microridges. Overall, our findings suggest that F-actin in microridges is highly dynamic.

Discussion

Microridges have been observed on epithelial cells of the mucosal epithelium across animal species from fish to humans. The mechanisms that regulate the formation and maintenance of microridges remain largely unknown. Here for the first time, we characterize the dynamics of actin microridges in intact animals using live imaging. We found that actin microridges form a dynamic Arp2/3-dependent F-actin network in superficial epithelial cells of live zebrafish that is amenable to high-resolution live imaging. We also found that inhibition of myosin II does not significantly affect actin microridge length. Moreover, expression of dominant negative RhoA or Rac affects the distance between microridges but not their overall organization. These findings, together with the observation that microridges bend *in vivo*, suggest that significant tension is not necessary to maintain their structure. As proper actin polymerization is essential for the microridge structure, we speculate that other actin regulators are likely involved in the formation and maintenance of actin microridges.

The reduction of microridges that occurs before cytokinesis is intriguing. It has been proposed that cell protrusions can serve as a membrane reservoir for other cellular processes (reviewed in (Figard and Sokac, 2014)). One example is during *Drosophila* cellularization, where microvilli flatten out during cleavage furrow ingression to fuel cell-surface growth (Figard et al., 2013). Unlike microvilli during *Drosophila* cellularization, it is not clear whether microridges provide a membrane reservoir during epithelial cell cytokinesis. Microridges shorten and become drastically reduced before an obvious cleavage furrow is formed and before a change in cell shape is observed during cytokinesis. This suggests that the disappearance of microridges precedes the

change in membrane tension generated by the cleavage furrow and the need for extra plasma membrane. Interestingly, the reappearance of microrridges and actin puncta coincides with cleavage furrow ingression. This further suggests that microridge formation can occur in the presence of high cell membrane tension. These observations suggest that in addition to positive signaling through Arp2/3 and PI3K, there are likely inhibitory signaling pathways that negatively regulate microridge structure. Understanding how microridges change during cytokinesis should provide valuable insight into the regulation of microridge architecture.

It is interesting that the change in tension and cell shape that occurs during wound closure affects microridge arrangement but not its overall structure. To our knowledge, microridge rearrangement has not been described previously in other wound healing models, but this may be due to the difference in model systems (Abreu-Blanco et al., 2012; Brock et al., 1996; Clark et al., 2009; Li et al., 2013; Martin and Lewis, 1992). Since both wound closure and cytokinesis require localized actin polymerization, the maintenance of microridges during these processes suggests that microridges do not simply function as a reservoir for actin. As microridges are ubiquitously present on mucosal surfaces across species, further investigation will be needed to understand microridge rearrangements on different epithelial surfaces following wounding. In addition, we have observed that microridges on the cornea diminish starting at 4-5 dpf (Figure S1B) but are then re-established in adults (Figure S1C). This has not previously been reported during cornea development (Zhao et al., 2006), and will provide an additional area for future investigation.

Alan Turing proposed that organized patterns, like microridges, arise from an interaction between two molecules that diffuse at different rates (Turing, 1990). This reaction-diffusion model or 'Turing model' mathematically predicts how spatial patterns develop autonomously and has been used as a framework for understanding biological pattern formation (reviewed in (Kondo and Miura, 2010)). Using Turing theory, the interaction between two morphogens, such as an activator and an inhibitor, can result in a labyrinth of color patterns (Miyazawa et al., 2010) that appears to be very similar to the microridge pattern in epithelial cells. Analogous to the unique nature of markings seen on animals within a species with respect to the exact position of each spot or stripe, microridge patterns appear to be different among individual epithelial cells within the same animal. In addition, the overall microridge pattern is distinguishable across species (Collin and Collin, 2000; Correr et al., 2006; Gamal et al., 2012; Gardner and Scott, 1976; Hafez et al., 2013; Li et al., 2011; Rice et al., 2013; Simmich et al., 2012; Thie et al., 1998; Uppal et al., 2013; Villava et al., 2007; Wong and Wong, 2000; Yashpal et al., 2006; Yashpal et al., 2009). However, unlike a stationary animal color pattern, the change in microridge pattern over time suggests a dynamic change in morphogen-like interactions within individual cells. We speculate that the subcellular pattern of microridges might be another biological example of the Turing mechanism. In this study, we have found that Arp2/3 and PI3K activity are positive regulators of microridge length. Rac and Rho both play a role in establishing the distance between microridges with the caveat that Rho activity also affects cell size. The molecular events involved in forming microridges, including the diffusion efficiency of the above listed

regulators, their interactions, and other yet-identified activators/inhibitors requires further exploration.

In summary, our findings have provided new insights into the dynamics and regulation of microridges *in vivo*. This work may open up exciting avenues for probing the regulation of Arp2/3 dependent actin networks and pattern formation in an intact animal. It also provides a physiologically relevant context for investigating the regulation and function of microridges. A challenge for future investigation will be to use this system to test the “Turing” model in an *in vivo* tissue to uncover the elaborate signaling networks needed to maintain these beautiful actin-based structures present on surface epithelia.

Material and Methods

Ethics Statement

This study was carried out in strict accordance with the recommendations in the Guide for the Care and Use of Laboratory Animals of the National Institutes of Health. The protocol was approved by the University of Wisconsin – Madison Animal Care and Use Committee (Protocol number: M01570-0-02-13).

Zebrafish line

Wild-type AB zebrafish (*Danio rerio*) were maintained and raised, as described previously (Westerfield, 1995). Embryos were kept at 28.5°C in E3 solution.

DNA injection

All DNA expression vectors contained the zebrafish *krt4* promoter for epithelial cell expression (Chen et al., 2011; Yoo et al., 2012). All expression vectors contain minimal Tol2 elements for efficient integration (Urasaki et al., 2006) and an SV40 polyadenylation sequence (Clontech Laboratories, Inc). The following constructs were generated: *krt4-Lifeact-Ruby*, *krt4-GFP-UtrCH*, *krt4-EGFP-VASP* (XM_005173679.1), *krt4-Rho Q63L-mCherry* (Yoo et al., 2010), *krt4-Dendra-RhoA T19N* (Yoo et al., 2010), *krt4-mCherry-2A-Rac2 D57N* (Deng et al., 2011), *krt4-mEos* and *krt4-actin-mEos* (Kanchanawong et al., 2010). Expression of constructs was obtained by injecting 3 nL of solution containing 3-3.6 ng/μL of DNA plasmid and 8.7 ng/μL *in vitro* transcribed (Ambion) Tol2 transposase mRNA into the cytoplasm of one-cell stage embryos.

Scanning Electron Microscopy

Zebrafish larvae or dissected adult eyes were fixed at the indicated times in EM fix (1.5% glutaraldehyde; 1% paraformaldehyde; 70 mM $NaPO_4$; 3% sucrose). Specimen were then rinsed in 0.1 M Cacodylate buffer, postfixed in 1% OsO_4, rinsed again in 0.1 M Cacodylate buffer then dehydrated in a graded series of ethanol dilutions to 100% ethanol. Samples were then critically dried using liquid CO_2 as the substitution medium (EMS 850 Critical Point Dryer), then adhered to aluminum specimen mounts (Ted Pella) using carbon conductive cement (Plano GMBH). A Cressington 108 auto Sputter Coater (Ted Pella) was used to gold coat the samples. Imaging was carried out using a Zeiss Sigma HDVP Electron Microscope.

Immunohistochemistry and imaging

2.5 dpf larvae were fixed with 1.5% formaldehyde in 0.1 M Pipes, 1 mM $MgSO_4$, and 2 mM EGTA overnight at 4°C. Larvae were then washed in PBS and incubated in methanol at -20°C overnight. Larvae were rehydrated in a graded series of methanol in PBS containing 0.2% Triton X-100 (PBSTx) and incubated with 0.15 M glycine in PBS for 10 min at room temperature. Larvae were then washed with PBSTx several time and blocked in PBSTx containing 1% BSA for 1 hour at room temperature and then with primary antibody at 4°C overnight. Following several washes in PBSTx, larvae were incubated with secondary antibody at 4°C overnight. We used the following primary antibodies: mouse anti-phosphotyrosine antibody, clone 4G10 (EMD Millipore 05-321) at 1:50 dilution; mouse anti-cortactin antibody, clone 4F11 (Millipore 05-180) at 1:100 dilution; rabbit anti-FAK (Cell Signaling #3285) at 1:50 dilution; rabbit anti-Myosin Light

Chain Antibody, phospho-specific (Ser19) (EMD Millipore AB3381) at 1:50 dilution. For secondary antibody, anti-rabbit or anti-mouse DyLight 549–conjugated IgG antibodies (Jackson ImmunoResearch Laboratories, Inc.) at 1:250 dilution was used.

All images were acquired using a spinning disk confocal microscope (Yokogawa CSU-X) with a confocal scanhead on a Zeiss Observer Z.1 inverted microscope (NA1.3/60X water immersion objective) at 28.5°C. A Photometrics Evolve EMCCD camera was used to acquire the images. Z-series images were acquired using a 0.4 μM step size and 300 EM gain. Maximum intensity projection images were made using the Zen 2012 (blue edition) software (Carl Zeiss). For imaging before and after pharmacological treatments, larvae were anesthetized with 0.2 mg/mL tricaine in E3 and placed on a glass-bottom dish for imaging. For time-lapse imaging, larvae were mounted on a glass-bottom dish with 1% low-melting point agarose and covered with E3 containing tricaine. Carl Zeiss Immersol W 2010 immersion medium was used to reduce evaporation of the immersion medium and allow uninterrupted long-term imaging.

Laser ablation and photoconversion

Larvae at 2.5 dpf were mounted on a glass-bottom dish with 1% low-melting point agarose. A Z-stack image of the targeted ablation and surrounding area in the trunk was acquired using the spinning disk confocal system before laser ablation. Laser ablation was performed using a laser scanning confocal microscope (FluoView FV1000, Olympus) with a NA1.3/40X oil objective. A 405 nm diode laser at maximal power was used, focusing on a small circular area of an epithelial cell (diameter ~1 μm) for 3-4

minutes. Larvae were then transferred to the spinning disk system immediately for Z-stack time-lapse image acquisition. Photoconversion of actin-mEos was performed using the same microscope setup as laser ablation, except that the 405 nm laser was set at 3%, focusing on an area as indicated for 2 seconds. Images were acquired on the same Olympus laser scanning confocal microscope before and after photoconversion.

Pharmacological treatments and microridge measurements

All pharmacological treatments were performed in zebrafish larvae at 2.5 dpf. 0.5% DMSO was used as controls except for CK-666 treatment. To inhibit myosin II, a 25 mM stock of Blebbistatin (Sigma B0560) was made in DMSO. Larvae were treated with 25 μM Blebbistatin (Bleb) for 1 hour. To inhibit actin polymerization, a 10 mM Latrunculin A (Fisher Scientific NC9114335) stock was made in DMSO. Larvae were treated with 1 μM Latrunculin A for 30 minutes. To inhibit Arp2/3, a 100 mM stock of CK-666 (Sigma SML0006) was made in DMSO. Larvae were treated with 200 μM CK-666 for 1 hour. 200 μM CK-689 (EMD Millipore 182517) used as an inactive control of CK-666. To inhibit PI3K, a 65 mM stock of LY294002 (EMD Millipore 440202) was made in DMSO. Larvae were treated with 130 μM LY294002 for 1 hour.

Measurement of microridge length: GFP-UtrCH was transiently expressed in epithelial cells to allow for clear visualization of microridges. Confocal Z-stack images of the same cell in the lateral side of the mid-trunk region were taken before and after pharmacological or control treatments. Maximum intensity projection images were generated using the Zen 2012 (blue edition) software (Carl Zeiss). The length of microridges in the same cell before and after treatments was measured using FIJI

"Freehand Line" tool. 8-15 microridge length measurements were made per cell. Percentage change of length was calculated by dividing the average length of microridges in the same cell after treatment to that before treatment. All the inhibitor treatments were performed at least 3 separate times. Each experiment was performed on at least 3 larvae, with microridge measurements on 3-4 cells per larva.

Distance between microridges was measured manually using FIJI "Straight Line" tool. Lifeact-Ruby or GFP-UtrCH was transiently expressed in the epithelial cells of zebrafish larvae to allow for clear visualization of microridges. Confocal images were acquired at 2.5 dpf. To calculate the average distance between microridges, ten random measurements of the distance between two adjacent microridges were made per cell. Area of epithelial cells was measure manually using FIJI "Freehand selections" tool.

Statistics

Experimental results were analyzed with Prism version (GraphPad Software) statistical software. The resulting *P* values are included in the figure legends for each experiment.

Acknowledgements

We would like to thank the insightful discussion with Dr. William M. Bement at the University of Wisconsin-Madison as well as members from the Madison zebrafish group meeting. The *Tol2-krt4-EGFP-VASP* construct was subcloned from construct provided by Dr. Robert S Fischer from the National Heart, Lung, and Blood Institute at National Institutes of Health.

References

Abreu-Blanco, M.T., J.M. Verboon, R. Liu, J.J. Watts, and S.M. Parkhurst. 2012. Drosophila embryos close epithelial wounds using a combination of cellular protrusions and an actomyosin purse string. *J Cell Sci*. 125:5984-97.

Bereither-Hahn, J., M. Osborn, K. Weber, and M. Voth. 1979. Filament organization and formation of microridges at the surface of fish epidermis. *Journal of ultrastructure research*. 69:15.

Brock, J., K. Midwinter, J. Lewis, and P. Martin. 1996. Healing of incisional wounds in the embryonic chick wing bud: characterization of the actin purse-string and demonstration of a requirement for Rho activation. *J Cell Biol*. 135:1097-107.

Burkel, B.M., G. von Dassow, and W.M. Bement. 2007. Versatile fluorescent probes for actin filaments based on the actin-binding domain of utrophin. *Cell Motil Cytoskeleton*. 64:822-32.

Burridge, K., and M. Chrzanowska-Wodnicka. 1996. Focal adhesions, contractility, and signaling. *Annu Rev Cell Dev Biol*. 12:463-518.

Burridge, K., M. Chrzanowska-Wodnicka, and C. Zhong. 1997. Focal adhesion assembly. *Trends Cell Biol*. 7:342-7.

Chen, C.F., C.Y. Chu, T.H. Chen, S.J. Lee, C.N. Shen, and C.D. Hsiao. 2011. Establishment of a transgenic zebrafish line for superficial skin ablation and functional validation of apoptosis modulators in vivo. *PLoS One*. 6:e20654.

Clark, A.G., A.L. Miller, E. Vaughan, H.Y. Yu, R. Penkert, and W.M. Bement. 2009. Integration of single and multicellular wound responses. *Curr Biol*. 19:1389-95.

Collin, H.B., and S.P. Collin. 2000. The corneal surface of aquatic vertebrates: microstructures with optical and nutritional function? *Philos Trans R Soc Lond B Biol Sci*. 355:1171-6.

Correr, S., S. Makabe, R. Heyn, M. Relucenti, T. Naguro, and G. Familiari. 2006. Microplicae-like structures of the fallopian tube in postmenopausal women as shown by electron microscopy. *Histol Histopathol*. 21:219-26.

Deng, Q., S.K. Yoo, P.J. Cavnar, J.M. Green, and A. Huttenlocher. 2011. Dual roles for Rac2 in neutrophil motility and active retention in zebrafish hematopoietic tissue. *Dev Cell*. 21:735-45.

Doyle, A.D., and J. Lee. 2005. Cyclic changes in keratocyte speed and traction stress arise from Ca2+-dependent regulation of cell adhesiveness. *J Cell Sci*. 118:369-79.

Figard, L., and A.M. Sokac. 2014. A membrane reservoir at the cell surface: unfolding the plasma membrane to fuel cell shape change. *Bioarchitecture*. 4:39-46.

Figard, L., H. Xu, H.G. Garcia, I. Golding, and A.M. Sokac. 2013. The plasma membrane flattens out to fuel cell-surface growth during Drosophila cellularization. *Dev Cell*. 27:648-55.

Gamal, A.M., E.H. Elsheikh, and E.S. Nasr. 2012. Morphological adaptation of the buccal cavity in relation to feeding habits of the omnivorous fish *Clarias gariepinus*: A scanning electron microscopic study. *The Journal of Basic & Applied Zoology*. 65:8.

Gardner, I.C., and A. Scott. 1976. The surface structure of the ovine oesophagus. *Micron (1969)*. 7:6.

Gilmore, A.P., and K. Burridge. 1996. Molecular mechanisms for focal adhesion assembly through regulation of protein-protein interactions. *Structure*. 4:647-51.

Hafez, E.A.A.E., D.M. Mokhtar, A.S. Abou-Elhamd, and A.H.S. Hassan. 2013. Comparative Histomorphological Studies on Oesophagus of Catfish and Grass Carp. *Journal of Histology*. 2013:10.

Holt, M.R., D.R. Critchley, and N.P. Brindle. 1998. The focal adhesion phosphoprotein, VASP. *Int J Biochem Cell Biol*. 30:307-11.

Kanchanawong, P., G. Shtengel, A.M. Pasapera, E.B. Ramko, M.W. Davidson, H.F. Hess, and C.M. Waterman. 2010. Nanoscale architecture of integrin-based cell adhesions. *Nature*. 468:580-4.

Kondo, S., and T. Miura. 2010. Reaction-diffusion model as a framework for understanding biological pattern formation. *Science*. 329:1616-20.

Li, J., S. Zhang, X. Soto, S. Woolner, and E. Amaya. 2013. ERK and phosphoinositide 3-kinase temporally coordinate different modes of actin-based motility during embryonic wound healing. *J Cell Sci*. 126:5005-17.

Li, Q., M. Frank, M. Akiyama, H. Shimizu, S.Y. Ho, C. Thisse, B. Thisse, E. Sprecher, and J. Uitto. 2011. Abca12-mediated lipid transport and Snap29-dependent trafficking of lamellar granules are crucial for epidermal morphogenesis in a zebrafish model of ichthyosis. *Dis Model Mech*. 4:777-85.

Martin, P., and J. Lewis. 1992. Actin cables and epidermal movement in embryonic wound healing. *Nature*. 360:179-83.

Miyazawa, S., M. Okamoto, and S. Kondo. 2010. Blending of animal colour patterns by hybridization. *Nat Commun*. 1:66.

Petit, V., and J.P. Thiery. 2000. Focal adhesions: structure and dynamics. *Biol Cell*. 92:477-94.

Piekny, A., M. Werner, and M. Glotzer. 2005. Cytokinesis: welcome to the Rho zone. *Trends Cell Biol*. 15:651-8.

Rice, W.L., A.N. Van Hoek, T.G. Paunescu, C. Huynh, B. Goetze, B. Singh, L. Scipioni, L.A. Stern, and D. Brown. 2013. High resolution helium ion scanning microscopy of the rat kidney. *PLoS One*. 8:e57051.

Ridley, A.J., M.A. Schwartz, K. Burridge, R.A. Firtel, M.H. Ginsberg, G. Borisy, J.T. Parsons, and A.R. Horwitz. 2003. Cell migration: integrating signals from front to back. *Science*. 302:1704-9.

Riedl, J., A.H. Crevenna, K. Kessenbrock, J.H. Yu, D. Neukirchen, M. Bista, F. Bradke, D. Jenne, T.A. Holak, Z. Werb, M. Sixt, and R. Wedlich-Soldner. 2008. Lifeact: a versatile marker to visualize F-actin. *Nat Methods*. 5:605-7.

Sharma, A., K.I. Anderson, and D.J. Muller. 2005. Actin microridges characterized by laser scanning confocal and atomic force microscopy. *FEBS Lett*. 579:2001-8.

Simmich, J., S.E. Temple, and S.P. Collin. 2012. A fish eye out of water: epithelial surface projections on aerial and aquatic corneas of the 'four-eyed fish' Anableps anableps. *Clin Exp Optom*. 95:140-5.

Sperry, D.G., and R.J. Wassersug. 1976. A proposed function for microridges on epithelial cells. *Anat Rec*. 185:253-7.

Thie, M., R. Rospel, W. Dettmann, M. Benoit, M. Ludwig, E.H. Gaub, and H.W. Denker. 1998. Interactions between trophoblast and uterine epithelium: monitoring of adhesive forces. *Human Reproduction*. 13:9.

Turing, A.M. 1990. The chemical basis of morphogenesis. 1953. *Bull Math Biol*. 52:153-97; discussion 119-52.

Uehara, K., M. Miyoshi, and S. Miyoshi. 1991. Cytoskeleton in microridges of the oral mucosal epithelium in the carp, Cyprinus carpio. *Anat Rec*. 230:164-8.

Uppal, R.K., M.S. Johal, and M.L. Sharma. 2013. Toxicological effects and recovery of the corneal epithelium in Cyprinus carpio communis Linn. exposed to monocrotophos: an scanning electron microscope study. *Vet Ophthalmol*.

Urasaki, A., G. Morvan, and K. Kawakami. 2006. Functional dissection of the Tol2 transposable element identified the minimal cis-sequence and a highly repetitive sequence in the subterminal region essential for transposition. *Genetics*. 174:639-49.

Villava, C.E., A. Arellano-Torres, R.E. Navarro, and E. Maldonado. 2007. Freeze-crack technique to study epidermal development in zebrafish using differential interference contrast microscopy and fluorescent markers. *Biotechniques*. 43:313-4, 316, 318-20 passim.

Westerfield, M. 1995. The Zebrafish Book. *Eugene: University of Oregon Press*.

Wilson, C.A., M.A. Tsuchida, G.M. Allen, E.L. Barnhart, K.T. Applegate, P.T. Yam, L. Ji, K. Keren, G. Danuser, and J.A. Theriot. 2010. Myosin II contributes to cell-scale actin network treadmilling through network disassembly. *Nature*. 465:373-7.

Wong, C.K., and M.H. Wong. 2000. Morphological and biochemical changes in the gills of Tilapia (Oreochromis mossambicus) to ambient cadmium exposure. *Aquat Toxicol*. 48:517-527.

Yashpal, M., U. Kumari, S. Mittal, and M.A. K. 2006. Surface architecture of the mouth cavity of a carnivorous fish Rita rita (Hamilton, 1822) (Siluriformes, Bagridae). *Belg J Zool*. 136:8.

Yashpal, M., U. Kumari, S. Mittal, and A.K. Mittal. 2009. Morphological specializations of the buccal cavity in relation to the food and feeding habit of a carp Cirrhinus mrigala: a scanning electron microscopic investigation. *J Morphol*. 270:714-28.

Yoo, S.K., Q. Deng, P.J. Cavnar, Y.I. Wu, K.M. Hahn, and A. Huttenlocher. 2010. Differential regulation of protrusion and polarity by PI3K during neutrophil motility in live zebrafish. *Dev Cell*. 18:226-36.

Yoo, S.K., C.M. Freisinger, D.C. LeBert, and A. Huttenlocher. 2012. Early redox, Src family kinase, and calcium signaling integrate wound responses and tissue regeneration in zebrafish. *J Cell Biol*. 199:225-34.

Zhao, X.C., R.W. Yee, E. Norcom, H. Burgess, A.S. Avanesov, J.P. Barrish, and J. Malicki. 2006. The zebrafish cornea: structure and development. *Invest Ophthalmol Vis Sci*. 47:4341-8.

Fig. 1. Microridge structure and composition. (A) Scanning electron microscopy on zebrafish larvae at 2 days post fertilization (dpf) in the area of the trunk. Scale bar, 5 μm. (B) Single plane confocal images of epithelial cells expressing actin bioprobes Lifeact-Ruby and GFP-UtrCH, which label all F-actin and stable F-actin, respectively. Signal from Lifeact-Ruby and GFP-UtrCH colocalize. Scale bar, 10 μm. (C-E) *Tg(krt4-GFP-UtrCH)* larvae at 2.5 dpf were fixed and immunostaining was performed using anti-phosphotyrosine antibody 4G10 (C), anti-cortactin antibody (D) or anti-FAK antibody (E). Scale bar, 10 μm. (F) Single plane confocal images of epithelial cells expressing actin bioprobe Lifeact-Ruby and EGFP-VASP. VASP localizes to a subset of Lifeact labeled microridges (see movie S1). Arrows indicate regions of Lifeact labeling that did not colocalize with VASP. Scale bar, 5 μm.

Fig. 1

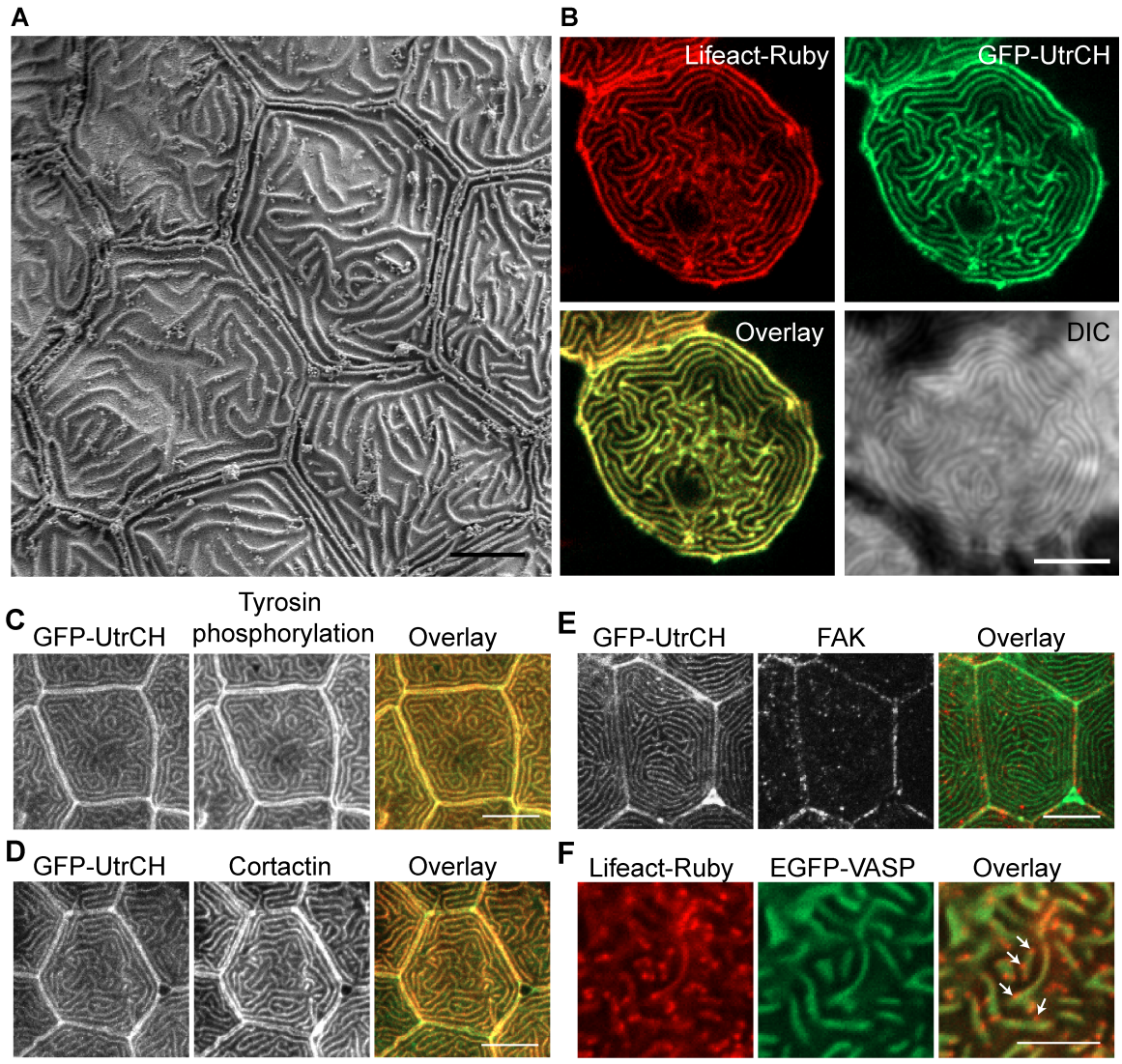
A
B
Lifeact-Ruby
GFP-UtrCH
Overlay
DIC
C
GFP-UtrCH
Tyrosin phosphorylation
Overlay
D
GFP-UtrCH
Cortactin
Overlay
E
GFP-UtrCH
FAK
Overlay
F
Lifeact-Ruby
EGFP-VASP
Overlay

Fig. 2. Microridges are dynamic *in vivo*. GFP-UtrCH was transiently expressed in epithelial cells in zebrafish larvae at 2.5 dpf. (A) Maximum intensity projection of confocal images showing changes in microridge pattern over time (see movie S2). Scale bar, 10 μm. (B) Overlay of microridge pattern in the same cell at time points indicated. Microridges are color-coated to indicate patterns from different time points. (C) Time-lapse maximum intensity projection images showing how microridge patterns rapidly change by bending (red arrow), breaking (red arrowhead) and connecting (green arrowhead) (see movie S3). (Top panel) Images acquired every 2 minutes are shown. (Bottom panel) Duplication of the top panel with two adjacent microridges labeled with pseudo-color to aid in the visualization of microridge dynamics. Scale bar, 5 μm.

Fig. 2

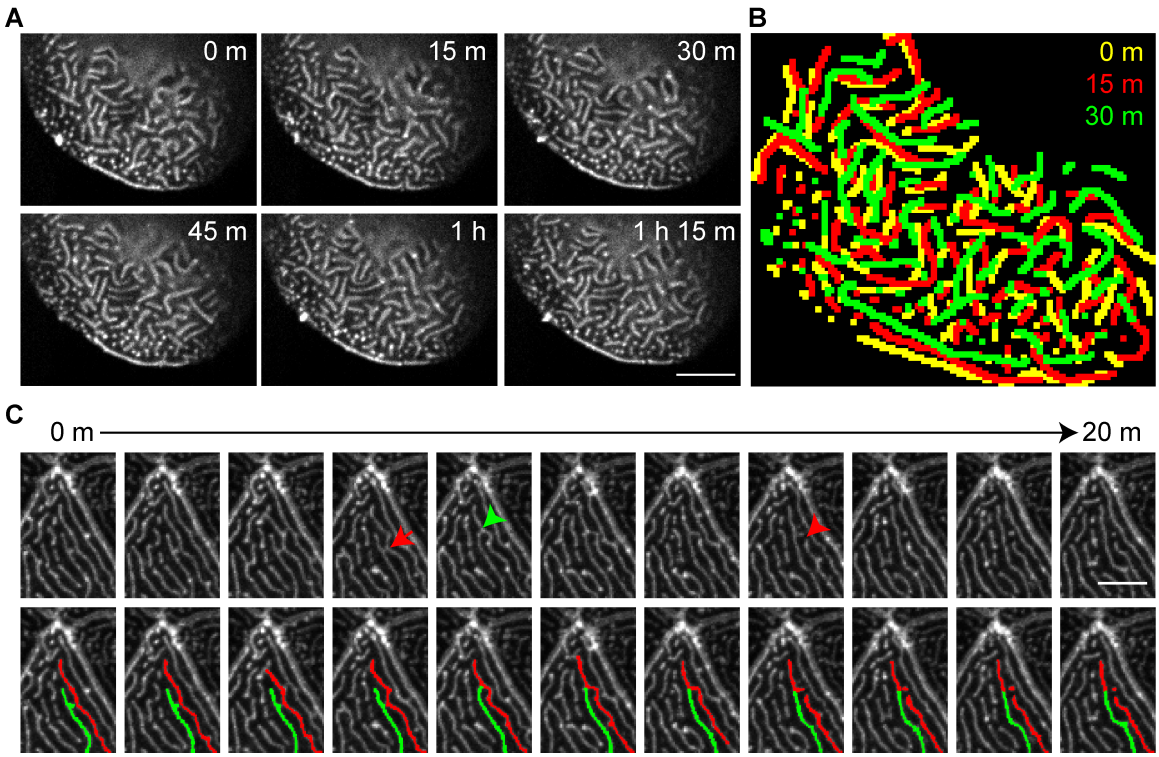

Fig. 3. Microridge organization during cytokinesis and wounding. (A) Time-lapse maximum intensity projection images show changes in microridge pattern during cytokinesis at 30 hours post fertilization (see movie S4). Mosaic transient expression of GFP-UtrCH in epithelial cells allows visualization of microridges. Microridges gradually became shorter before cytokinesis (i and ii). Microridges transiently disappear (iii; in cells labeled with green asterisk) shortly before the appearance of the cleavage furrow (iv and v; arrows); reappear quickly during cleavage furrow formation (iv and v; in cells labeled with red star); and then gradually become longer after cytokinesis (vi; arrowheads). Data are representative of 6 individual cells from 3 zebrafish larvae. Scale bar, 10 μm. (B) Maximum intensity projection of epithelial cells expressing GFP-UtrCH alone (i) or with constitutive active Rho (Rho Q63L-mCherry; ii) in zebrafish larvae at 2.5 dpf. Active Rho expression in epithelial cells results in cell rounding and apical protrusion but microridges are maintained. YZ, maximum intensity projection on the YZ axis. Data are representative of 63 individual cells in 21 larvae from three separate experiments. Scale bar, 10 μm. (C) Rearrangement of microridges during epithelial wound healing *in vivo*. Laser cell ablation was performed on a single cell (red asterisk) in a zebrafish larva at 2.5 dpf that transiently expresses GFP-UtrCH in epithelial cells. Maximum intensity projection images before (i) and after laser ablation (ii and iii) show the change in microridge pattern and cell shape in the epithelial cells (green asterisk) adjacent to the wound (see movie S5). Data are representative of 5 individual experiments. Scale bar, 10 μm.

Fig. 3

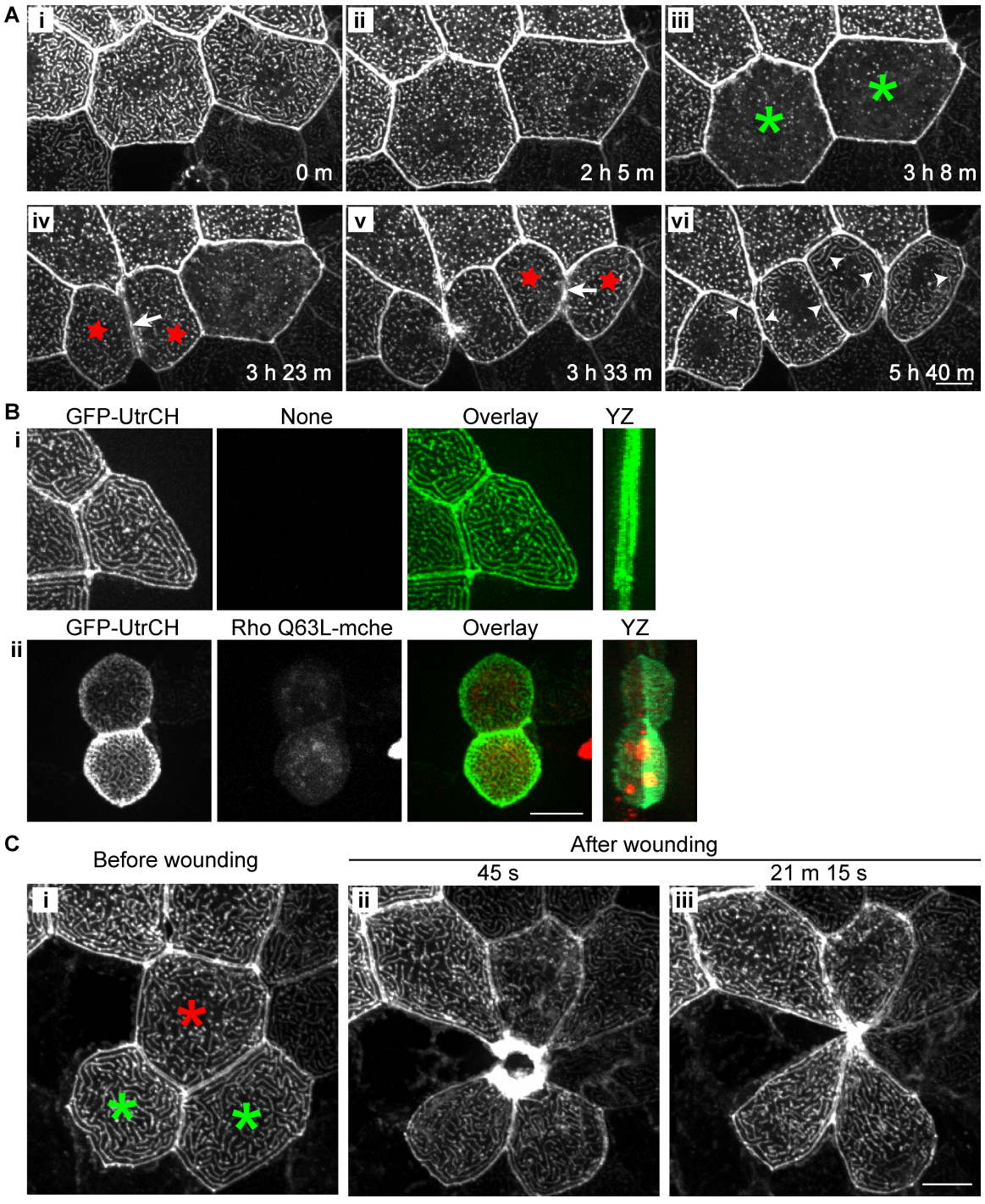
A
i
0 m
ii
2 h 5 m
iii
3 h 8 m
iv
3 h 23 m
v
3 h 33 m
vi
5 h 40 m
B
GFP-UtrCH
None
Overlay
YZ
i
GFP-UtrCH
Rho Q63L-mche
Overlay
YZ
ii
C
Before wounding
After wounding
45 s
21 m 15 s
i
ii
iii

Fig. 4. Rho GTPases regulate microridge organization. (A) Larvae at 2.5 dpf were treated with 25 μM Blebbistatin (Bleb) for 1 h to inhibit myosin II. 0.5% DMSO was used as a control. The length of microridges in the same cell before and after treatment was measured. Each data point represents the percentage change of the average microridge length in an individual cell after treatment. Data are representative of at least three different experiments. Each experiment was performed on at least 3 larvae, with measurements performed on 3-4 cells per larva. For details of the methods and analysis, refer to the Methods and Materials section. Efficacy of blebbistatin was confirmed by changes in neutrophil morphology and motility after treatment (data not shown). ns, not significant (two-tailed, unpaired *t*-test). (Right panel) Representative confocal images of GFP-UtrCH labeled microridges before and after treatment. Scale bar, 10 μm. (B) Maximum intensity projection of epithelial cells expressing Lifeact-Ruby alone (i) or with dominant negative RhoA (Dendra-RhoA T19N) (ii) in zebrafish larvae at 2.5 dpf. Scale bar, 10 μm. Average distance between microridges (C) and cell area (D) in control or Dendra-RhoA T19N expressing epithelial cells were measured and compared. Each data point represents the value from one cell. Data are collected from more than ten individual larva for each group from 3 separate experiments. **** $P<0.0001$ (two-tailed, unpaired *t*-test). (E) Maximum intensity projection of epithelial cells expressing GFP-UtrCH alone (i) or with dominant negative Rac2 (mCherry-2A-Rac2 D57N) (ii) in zebrafish larvae at 2.5 dpf. Scale bar, 10 μm. Average distance between microridges (F) and cell area (G) in control or mCherry-2A-Rac2 D57N expressing epithelial cells were measured and compared. Each data point represents the value from one cell. Data are collected from more than twelve individual larva for

each group from 3 separate experiments. For details of the methods and analysis refer to the Methods and Materials section. **** $P<0.0001$; ns, not significant (two-tailed, unpaired *t*-test).

Fig. 4

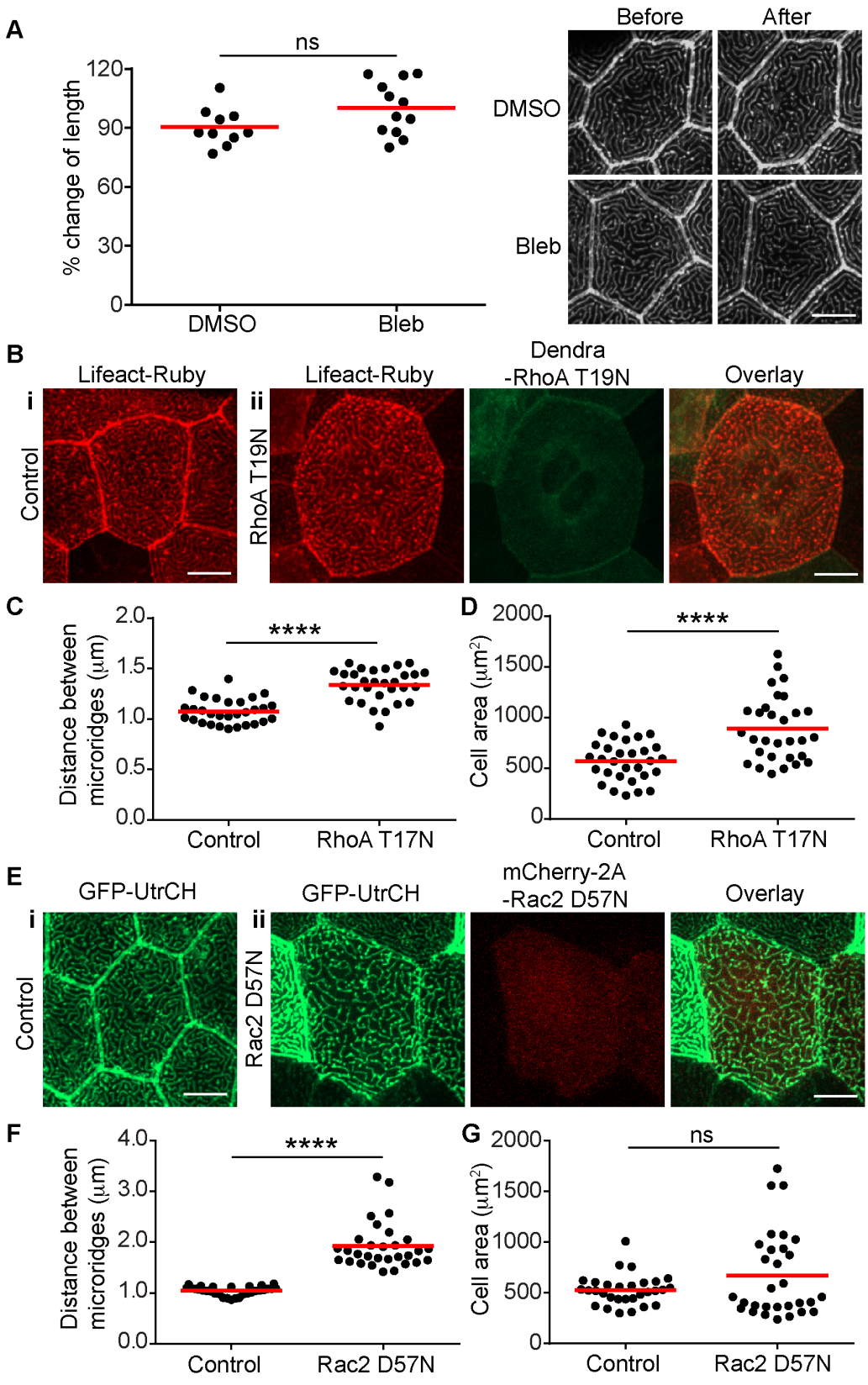
A
ns
% change of length
120
90
60
30
0
DMSO
Bleb
Before
After
DMSO
Bleb
B
Lifeact-Ruby
Lifeact-Ruby
Dendra
-RhoA T19N
Overlay
i
ii
Control
RhoA T19N
C
****
Distance between microridges (μm)
2.0
1.5
1.0
0.5
0.0
Control
RhoA T17N
D
****
Cell area (μm²)
2000
1500
1000
500
0
Control
RhoA T17N
E
GFP-UtrCH
GFP-UtrCH
mCherry-2A
-Rac2 D57N
Overlay
i
ii
Control
Rac2 D57N
F
****
Distance between microridges (μm)
4.0
3.0
2.0
1.0
0.0
Control
Rac2 D57N
G
ns
Cell area (μm²)
2000
1500
1000
500
0
Control
Rac2 D57N

Fig. 5. Microridges are actively treadmilling. Inhibition of actin polymerization using Latrunculin A (LatA) (A) or inhibition of Arp2/3 using CK-666 (B) resulted in shortened microridges. Larvae at 2.5 dpf were treated with 1 μM LatA or 0.5% DMSO as controls for 30 minutes, or with 200 μM CK-666 or its inactive analogue CK-689 for 1 hour. (C) PI3K kinase activity is involved in maintaining microridge length. Larvae at 2.5 dpf were treated with 130 μM LY294002 for 1 hour to inhibit PI3K. 0.5% DMSO was used as a control. (Ai, Bi and Ci) The length of microridges in the same cell before and after treatment was measured and compared. Each data point represents the percentage change of average microridge length in one cell after treatment. Data are representative of at least three separate experiments. Each experiment was performed on at least 3 larvae, with microridge measurements on 3-4 cells per larva. For details of the methods and analysis refer to the Methods and Materials section. ** $P<0.01$; *** $P<0.001$ (two-tailed, unpaired *t*-test). (Aii, Bii and Cii) Representative confocal images of GFP-UtrCH labeled microridges before and after the respective treatments. Scale bar, 10 μm. (Aii, Bii and Ciii) Representative scanning electron microscopy images of zebrafish larvae with the respective treatments. Scale bar, 10 μm

Fig. 5

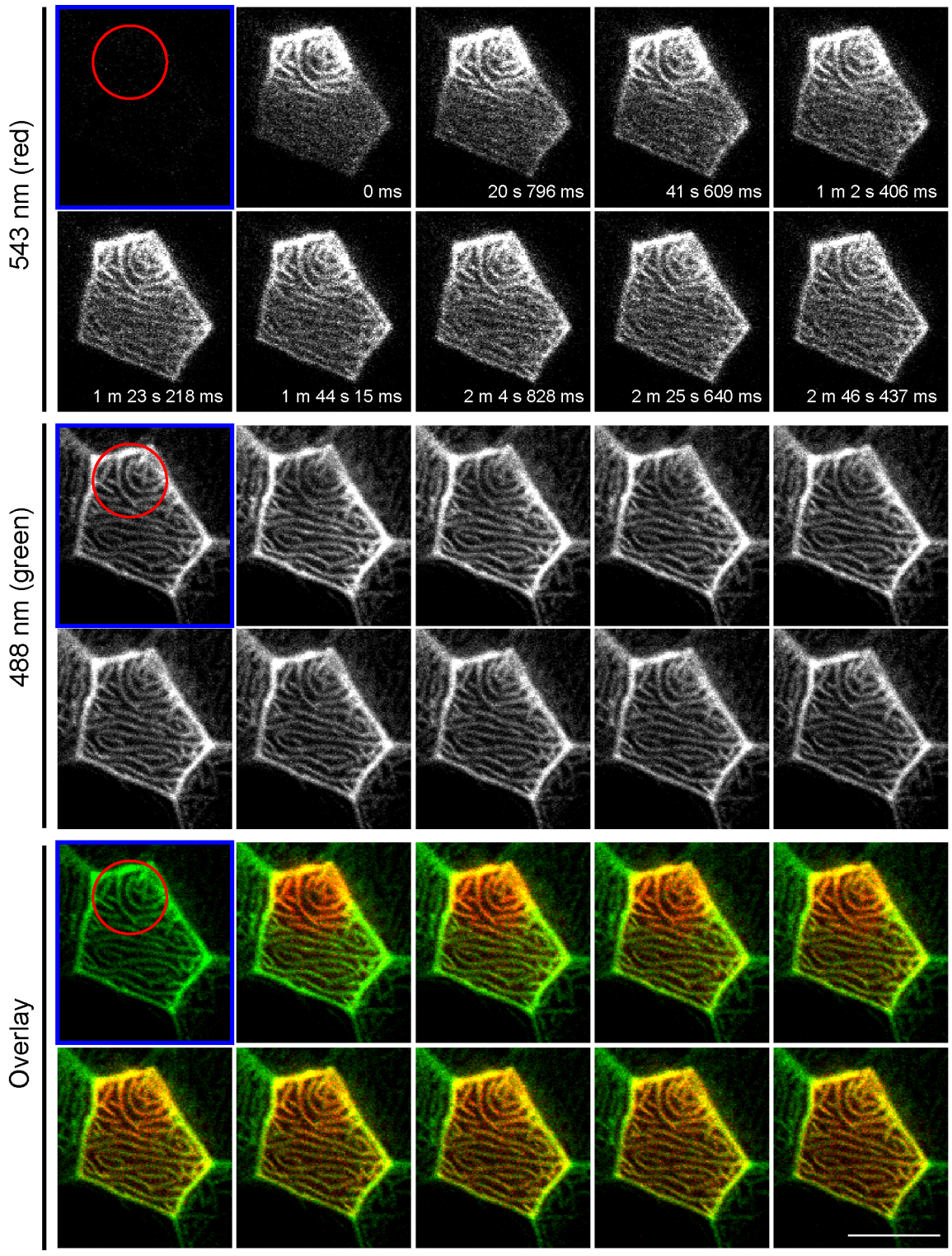
543 nm (red)
488 nm (green)
Overlay
0 ms
20 s 796 ms
41 s 609 ms
1 m 2 s 406 ms
1 m 23 s 218 ms
1 m 44 s 15 ms
2 m 4 s 828 ms
2 m 25 s 640 ms
2 m 46 s 437 ms

Fig. 6. F-actin in microridges is highly dynamic. Photoconversion of actin-mEos was performed on 3 dpf larvae by focusing on a sub-region (red circle) of an epithelial cell displaying microridges *in vivo* and time-lapse images were taken before (labeled with blue frame) and after photoconversion. Upon photoconversion, mEos-actin is irreversibly converted from emitting a green to a red fluorescent signal. For details of photoconversion refer to Materials and Methods. Single plane of confocal image of red channel, green channel and overlay of the two are shown. Data are representative of 9 individual cells. Scale bar, 10 μm. See movie S7.

Fig. 6

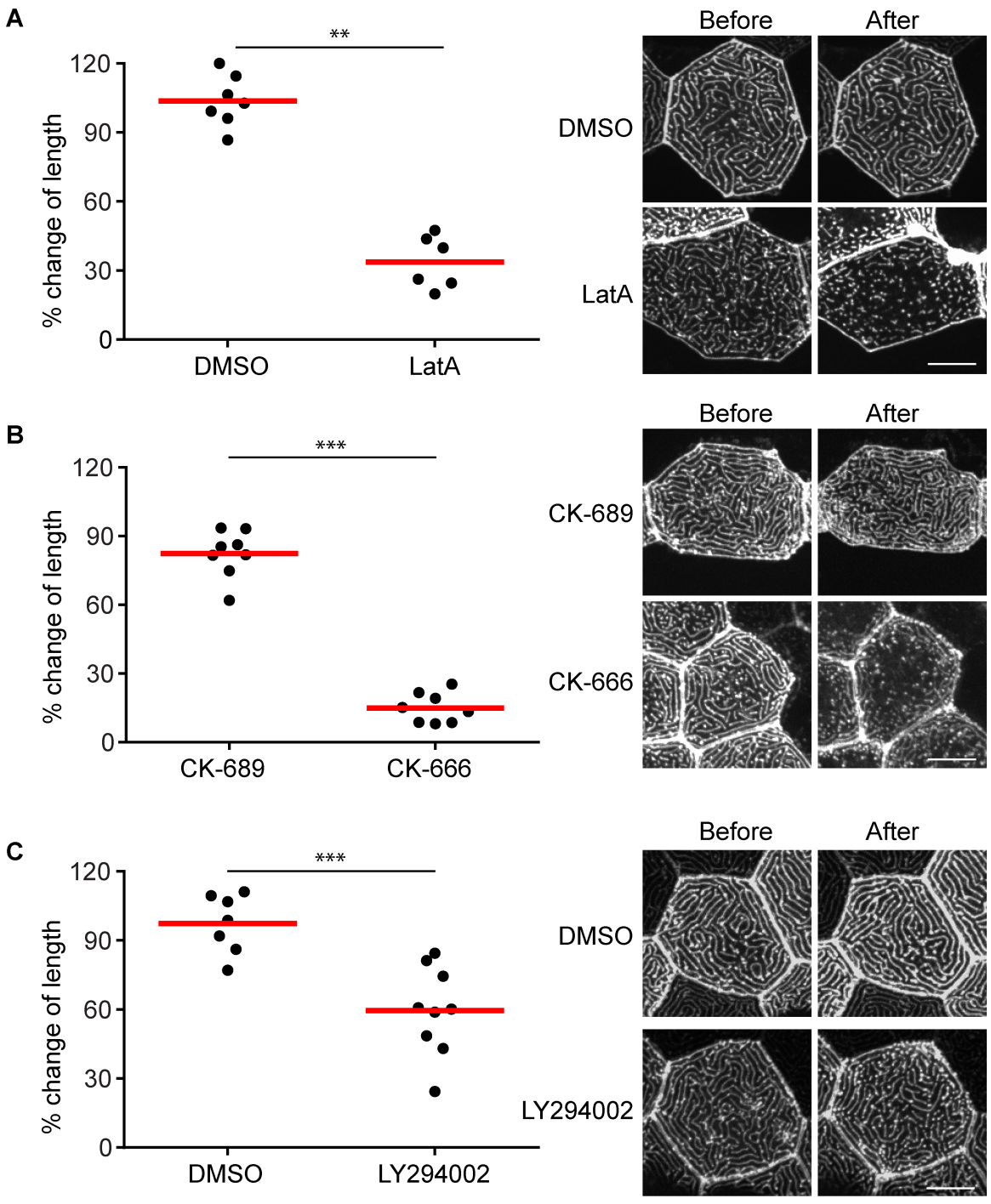
A
**
120
90
60
30
0
% change of length
DMSO
LatA
Before
After
DMSO
LatA
B
***
120
90
60
30
0
% change of length
CK-689
CK-666
Before
After
CK-689
CK-666
C
***
120
90
60
30
0
% change of length
DMSO
LY294002
Before
After
DMSO
LY294002

Fig. S1. Microridge structure during zebrafish development. (Ai – Aii) Scanning electron microscopy images on zebrafish embryo at 12 hour post fertilization (hpf). (Ai) Microridges were observed in epithelial cells that appeared to have recently undergone cytokinesis. Arrows indicate example of microridges. (B) SEM images at 1 - 5 and 9 day post fertilization (dpf) on the cornea, yolk and trunk region of zebrafish larvae. (C) SEM images of cornea at adult stage. Scale bar, 5 μm.

Fig. S1

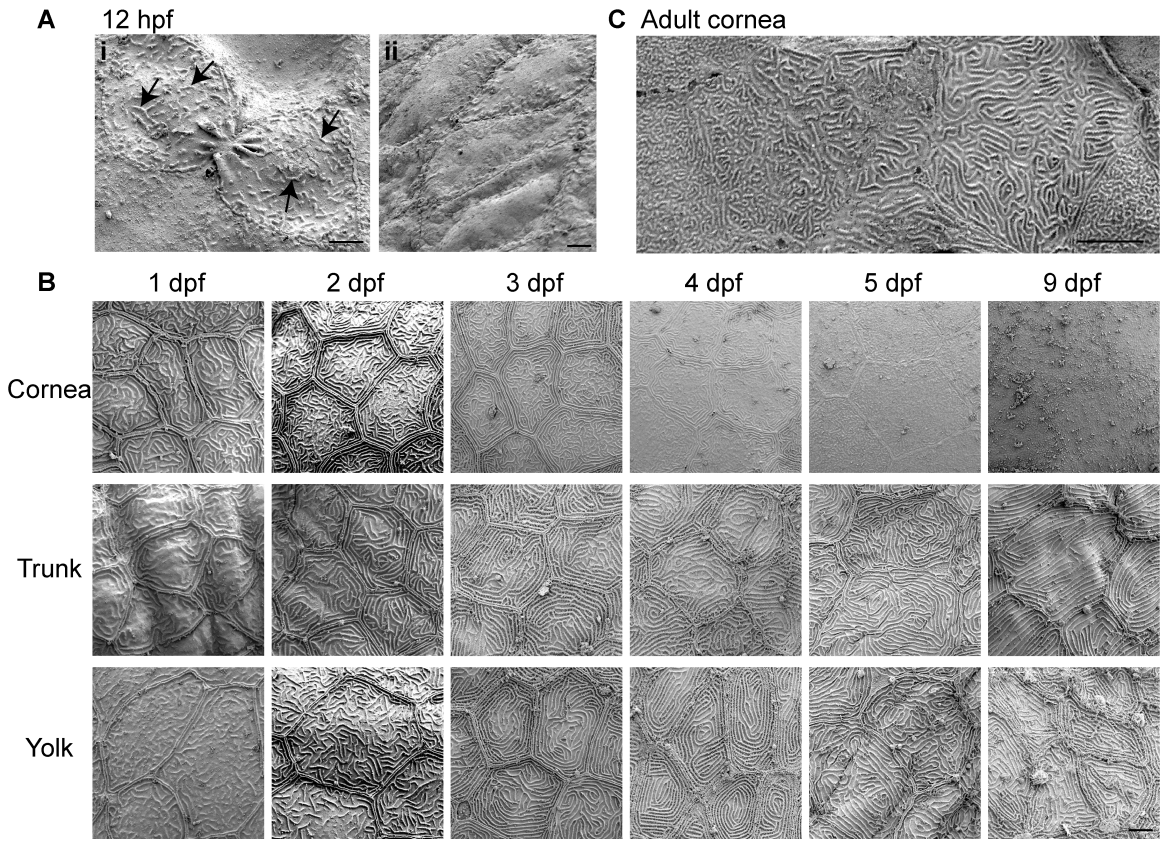
A
12 hpf
i
ii
C
Adult cornea
B
1 dpf
2 dpf
3 dpf
4 dpf
5 dpf
9 dpf
Cornea
Trunk
Yolk

Fig. S2. Phospho-Myosin Light Chain antibody staining. Maximum intensity projection of confocal images show phospho-Myosin Light Chain (pMLC) antibody staining in *Tg(krt4:GFP-UtrCH)* larvae at 2.5 dpf. Scale bar, 10 μm.

Fig. S2

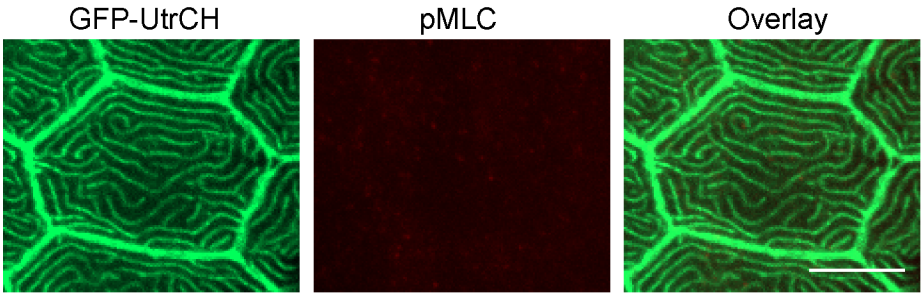

Fig. S3. F-actin in microridges is highly dynamic. Photoconversion of actin-mEos was performed on 3 dpf larvae by focusing on a small region of an epithelial cell containing microridges (red circle) and acquiring time-lapse images before (labeled with blue frame) and after photoconversion. Upon photoconversion, mEos-actin is irreversibly converted from exhibiting green to red fluorescent emission. Data are representative of 15 individual cells. For details of photoconversion refer to Materials and Methods. Single plane of confocal image of red channel, green channel and overlay of the two are shown. Scale bar, 10 μm. See movie S6.

Fig. S3

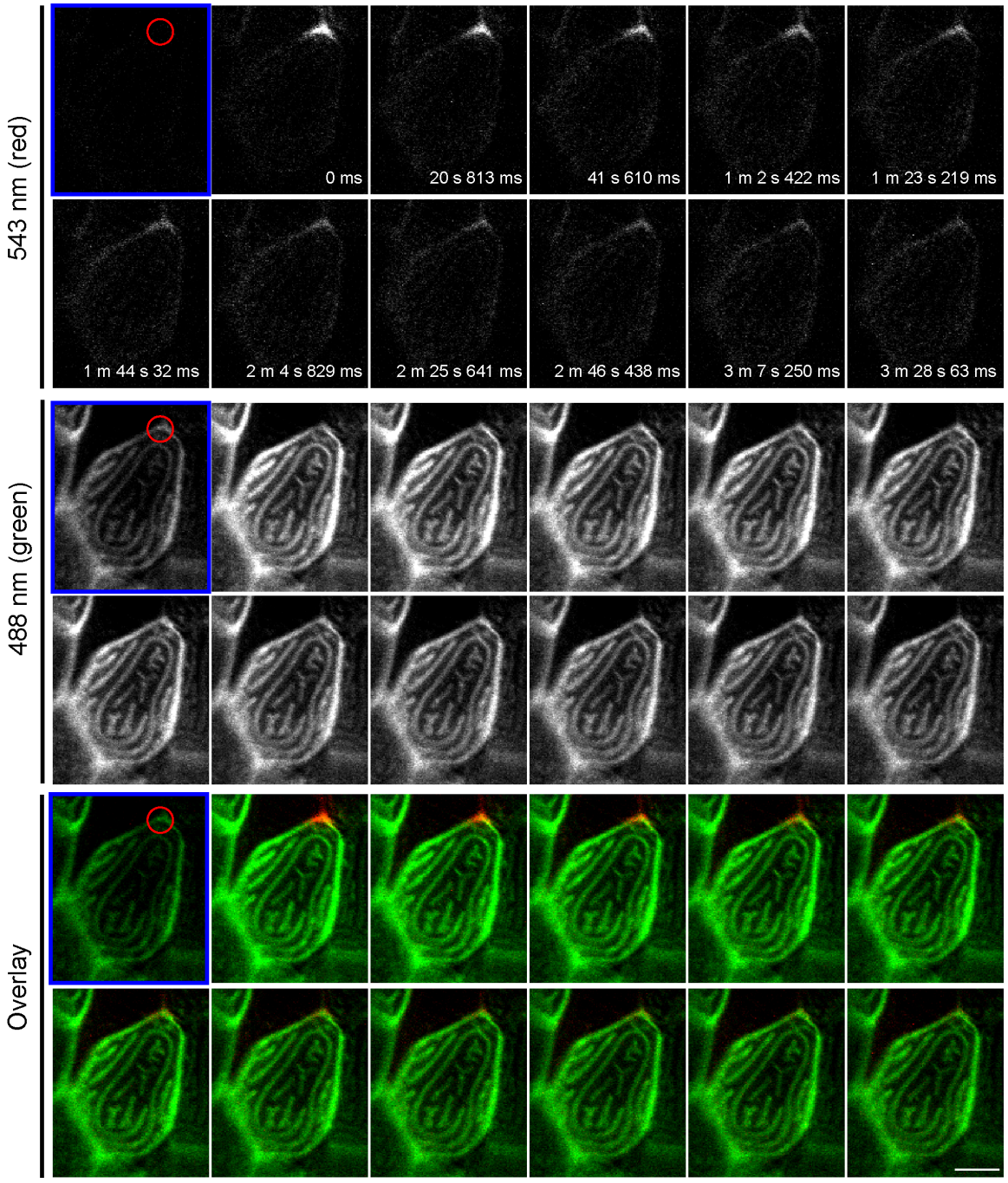
543 nm (red)
488 nm (green)
Overlay
0 ms
20 s 813 ms
41 s 610 ms
1 m 2 s 422 ms
1 m 23 s 219 ms
1 m 44 s 32 ms
2 m 4 s 829 ms
2 m 25 s 641 ms
2 m 46 s 438 ms
3 m 7 s 250 ms
3 m 28 s 63 ms

Fig. S4. mEos expression in epithelial cells *in vivo*. Krt4-mEos was transiently expressed in epithelial cell. Single Z-plane of DIC or mEos at 1.9 μm step size was shown. Scale bar, 10 μm.

Fig. S4

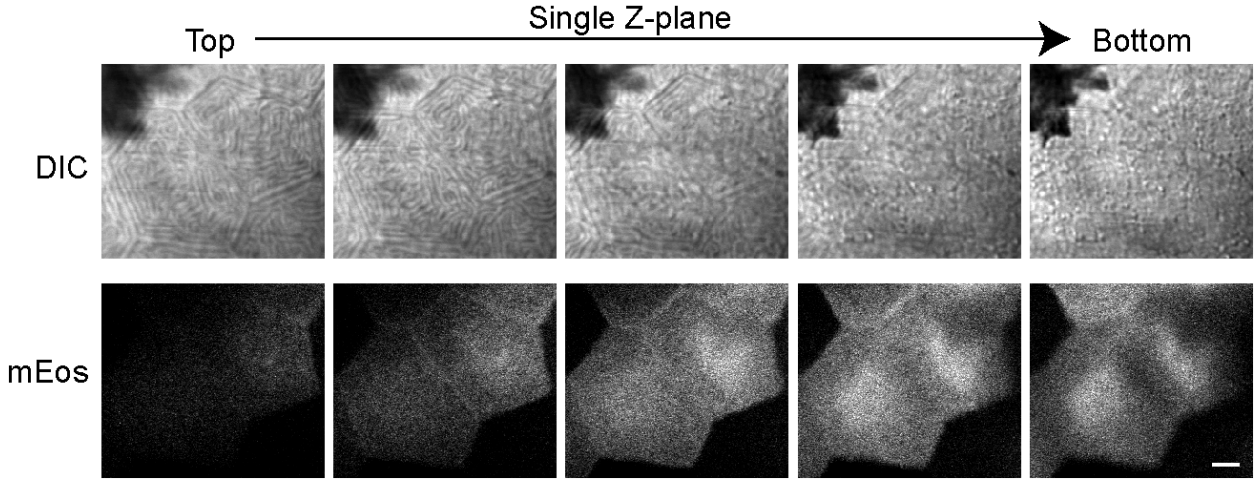

Movie S1. Live imaging of VASP and F-actin *in vivo*. Lifeact-Ruby (left panel) and EGFP-VASP (middle panel) were transiently expressed in epithelial cells in zebrafish larvae at 2.5 dpf. (Right panel) Overlay of Lifeact-Ruby and EGFP-VASP. Images were acquired using a spinning disk confocal microscope. Images were taken every 15 seconds for 14 minutes and 45 seconds.

Movie S2. Microridges are dynamic *in vivo*. GFP-UtrCH was transiently expressed in epithelial cells in zebrafish larvae at 2.5 dpf. Images were acquired using a spinning disk confocal microscope. Images were taken every 15 minutes for 1 hour 45 minutes.

Movie S3. Microridges are dynamic *in vivo*. GFP-UtrCH was transiently expressed in epithelial cells in zebrafish larvae at 2.5 dpf. Images were acquired using a spinning disk confocal microscope. Images were taken every 1 minute for 20 minutes.

Movie S4. Change in microridge pattern during cytokinesis. GFP-UtrCH was transiently expressed in epithelial cells in zebrafish larvae at 2 dpf. Images were acquired using a spinning disk confocal microscope. Images were taken every 1 minute for 5 hour 46 minutes.

Movie S5. Change in microridge pattern during wound healing. GFP-UtrCH was transiently expressed in epithelial cells in zebrafish larvae at 2.5 dpf. Laser cell ablation was performed in a single cell (red asterisk) of zebrafish larvae transiently expressing GFP-UtrCH in epithelial cells. Images were acquired before and after laser wounding

using a spinning disk confocal microscope. Images were taken every 15 seconds for 21 minutes.

Movie S6. Photoconversion of actin-mEos in microridges. Actin-mEos was transiently expressed in epithelial cells in zebrafish larvae at 3 dpf. Photoconversion of actin-mEos was performed in a small region (red circle) of an epithelial cell displaying microridges *in vivo*. Time-lapse images were taken before and after photoconversion. Left panel, signal of actin-mEos before photoconversion; middle panel, signal of actin-mEos after photoconversion; right panel, overlay of the two channels. Images were taken every 21 seconds for 9 minutes 42 seconds.

Movie S7. Photoconversion of actin-mEos in microridges. Actin-mEos was transiently expressed in epithelial cells in zebrafish larvae at 3 dpf. Photoconversion of actin-mEos was performed in a region (red circle) of an epithelial cell displaying microridges *in vivo*. Time-lapse images were taken before and after photoconversion. Left panel, signal of actin-mEos before photoconversion; middle panel, signal of actin-mEos after photoconversion; right panel, overlay of the two channels. Images were taken every 21 seconds for 9 minutes 42 seconds.